Department of Earth Sciences
Institute of Geographic Sciences

Freie Universität Berlin

Modeling the Effect of Climate and Land Use Change on the Water Resources in Northern Ethiopia: the Case of Suluh River Basin

Dissertation to obtain the doctoral degree

Submitted by
Bizuneh Asfaw Abebe, M.Sc.

Supervisors:

Univ. Prof. Dr. Brigitta Schütt - Freie Universität Berlin
Jun.-Prof. Dr. Wiebke Bebermeier - Freie Universität Berlin

Date of the oral examination: 20.01.2014

This page is intentionally left blank.

Acknowledgments

I would like to thank my supervisor Prof. Dr. Brigitta Schütt for her support and invaluable advices throughout the research period. Her many fruitful suggestions and careful review of the draft have made the production of this thesis possible. It was a great pleasure for me to conduct this research under her supervision. I extend my deepest gratitude for my second supervisor Jun.-Prof. Dr. Wiebke Bebermeier for her invaluable comment and support to my effort.

This research work is financially supported from Engineering Capacity Building Program (ECBP) under the framework of university reform. I would like to express my great gratitude to all of them for making the fund available. Thanks are also to Deutscher Akademischer Austauschdienst (DAAD) for the scholarship and the supports I obtained. I would like to thank particularly my contact person madam Ada-Samira Osinski.

I am thankful to the hydrology section of Ministry of Water Resources, National Meteorological Services and Ethiopian Mapping Agency for the provision of stream flow, Meteorological data and topographical maps respectively. I gratefully acknowledge the use of facilities at Freie Universität Berlin, department of Earth Science and Mekelle University, Ethiopian Institute of Technology for allowing me to use the resources like vehicle and geotechnical laboratory facilities during my field work.

I would like to thank Dr.-Ing. Joachim Lengricht for the encouragements and administrative support during my field work in Ethiopia. I deeply acknowledge staff and PhD-students in the Department of Physical Geography (Freie Universität Berlin) providing me an excellent working environment. I wish to express my sincere thanks to Dr. Jan Krause for the unrestricted support and encouragements and many useful contributions in the field work and facilitation of administrative works in Berlin. Special thanks to Steffen Schneider and Anette Stumptner. My acknowledgment also extends particularly to Nicole Lamm as she offered me unlimited support in editing and formatting my final thesis work.

I thank to staff members of department of Civil Engineering Mekelle University for their support during my field and laboratory work. Special thanks to Dr. Haddush Goitom, Yonas Fitsum, Ahemd Umer, Zenebe Haile, Kenfe Mussie, Melaku Berhe and his family. My thanks also goes to Eskinder Gidey as he provided me unreserved support during image processing.

I would like to thank my dearest friend Abraha Adugna for sharing all the fun and sorrow during my stay in Berlin. Thanks to Dr. Adem Hiko, we had unforgettable time in Berlin. I would like to appreciate Eshetu Adugna for his unreserved support regarding administrative issues in Addis Ababa. Last but by no means least I would like to convey a heartfelt gratitude to my family and friends for their unfailing support. Special thanks to Gebreanania Gebru and Letebrehan G/Medhin and all my sisters and brothers. My wife Azeb Gebreanania has been the key figure throughout my career, providing a bedrock of both stability and encouragement. Words are not enough to express what this has meant to me. Adiyam Bizuneh and Reena Bizuneh you are the gifts of my life and such an extra motivation and strength.

Bizuneh Asfaw Abebe

Berlin, January 2014

Table of contents

List of figures

List of tables

List of abbreviations

AI	Aridity Index
AoI	Area of Interest
a.s.l.	Above Sea Level
CGCM3	Third version of the Canadian Coupled Global Climate Model
CCLM	COSMO model in CLimate Mode
	Climate
CoSAERT	Commission for Sustainable Agriculture and Environmental Rehabilitation in Tigray
DEM	Digital Elevation Model
DEPHA	Data Exchange Platform for the Horn of Africa
EMA	Ethiopia Mapping Agency
ECHAM	Model developed by Max-Planck-Institute for Meteorology
	ENSO
ENSO	El Niño/Southern Oscillation
ETM+	Enhanced Thematic Mapper Plus
ETo	Reference Evapotranpiration
FAO	Food and Agricultural Organization of the United Nations
GCM	General Circulation Model
GIS	Geographic Information System
GLCF	Global Land Cover Facility
GPS	Global Positioning System
HadCM3	Hadley Centre Coupled Model version 3
HEC-DSS	Hydrologic Engineering Centre Data Storage System
HEC-GeoHMS	Hydrologic Engineering Center-Geospatial Hydrologic Modeling System
HEC-HMS	Hydrologic Engineering Center-Hydrologic Modeling System
IFPRI	The International Food Policy Research Institute
IPCC	Intergovernmental Panel on Climate Change
ITCZ	Intertropical Convergence Zone
LARS-WG	Long Ashton Research Station Weather Generator
LULC	Land Use and Land Cover
MoWR	Ministry of Water Resource
MOVE.1	Maintenance Of Variance-Extension, type 1
MSS	Multi-spectral Scanner
NCEP	National Center for Environmental Prediction
NEDECO	Netherlands Engineering Consultants
NMSA	National Meteorology Service Agency
NMS	National Meteorological Service

REMO	REgional atmosphere MOdel
SWAT	Soil and Water Assessment Tool
SDSM	Statistical DownScaling Model
SMA	Soil Moisture Accounting
SRES	Special Report on Emission Scenarios
SRTM	Shuttle Radar Topographic Mission
TM	Thematic Mapper
USACE	United States Army Corps of Engineers
USDA	United States Department of Agriculture
UTM	Universal Transverse Mercator coordinate system
WAPCOS	Water and Power Consulting Services Ltd
WaSIM-ETH	Water balance Simulation Model
WBISPP	Woody Biomass Inventory and Strategic Planning Project
WetSpa	Water Energy Transfer in Soil Plant and Atmosphere

Abstract

The northern Ethiopian regions are known for water scarcity and vulnerability to desertification, furthermore they are subjected to climate variability both in time and space. The Suluh river basin, located in northern Ethiopia, has an areal coverage of around 964 km^2. It is characterized by semi-arid climate conditions, it is highly degraded and the rainfall varies with the season. Due to an ongoing destruction of natural resources during the last decades together with climate variability the availability and distribution of water resources in the basin is limited resulting in food insecurity and a diminshed socio-economic development. Therefore, this study focuses on the investigationof possible effects of land use/land cover dynamics and future climate changes on water resources in the Suluh river basin.

Different statistical methods were applied to analyze the historical climate data. For the mean monthly temperature increasing trends are documented whereas the annual precipitation remains constant in the last decades. Furthermore it is proven that the extension of the dry periods inbetween the rainy seasons extends. In addition field and laboratory analysis of soil samples were conducted to support the estimation of hydrologic parameters. Geomorphological mapping indicates that soil erosion, mass movements and construction works are the major geomorphological processes in the basin.

A physical based semi-distributed hydrological model (HEC-HMS) is applied to simulate hydrological processes in the Suluh basin as well as to simulate the impact of climate and land use/land cover changes. Model sensitivity analysis of the physical parameters, calibration and validation of the model were successfully carried out for daily and monthly time steps. The HEC-HMS Soil Moisture Accounting model was run for 1992 to 1996 for calibration and for 1997–1999 for validation purposes. The long term annual water balance of the basin is evaluated too. The model results reveal that 76.3% of the total precipitation is lost through evapotranspiration while 11% accounts for surface runoff, 6.3% for base flow and 6.4% are lost from the system to recharge the deep aquifer.

The land use change dynamics of the basin are observed for the time span 1972 to 2003.Three land use and land cover maps were developed based on aerial photographs and satellite images. For the two different periods 1972 to 1986 and 1986 to 2003 significant land use changes occurred. Almost all natural vegetation was transformated into cultivated land. Also it could be proven the land use change in the basin resulted in a decline in runoff of only 1.5%.

To analyze the possible impacts of future climate change on the water resources in the Suluh basin, climate projections for precipitation, minimum and maximum temperatures have been carried out, using downscaled predictors from two GCMs (HadCM3 and CGCM3) under SRES scenarios A2a and B2a. The mean annual minimum and maximum temperatures show an increasing trend between 2041 and 2099. Evaluating the annual precipitation a decrease between 2011 and 2040 and an increase between 2071 and 2099 can be emphasized. The impact of climate change on the water resources of the Suluh basin show that on an annual basis the water yield decrease up to 30.2% in the time period 2011 to 2040, and might increase up to 2.4% in the time period 2041 to 2070 and might increase again again up to 25.6% in the time period 2071 to 2099. Among the hydrological processes surface runoff is identified as the most sensitive parameter to the effects of climate change.

Chapter 1

1 Introduction

In the northern Ethiopian highlands water is a scare resource due to the arid and semi-arid climate and consequently a decisive factor for socio-economic development and food security. The rainfall here is highly variability in space and time. The rivers in such regions are characterized by long periods of low or no flow. Hence, the main subject of this research is the assessment, analysis and quantification of water resource availability through hydrological modeling and testing of the long term water balance of the Suluh river basin considering the effect of land use/land cover and climate change.

The capability to determine the catchment response to changes in climate and land use and land cover effect is the basis for the management of the available water resource. One of the main aims of this study is to estimate the level of climate change impact at the local scale. As a baseline study to understand the level of land use and land cover dynamics in the basin, it is the objective of this study to assess their direct and indirect effects on watershed hydrology in the study site. The two global phenomena, i.e. land use and land cover and climate change, have significant impact on watershed hydrology and are used to characterize the catchment response for the present and predicting future on the basis of rainfall-runoff relationship. It is well known that understanding of the geomorphologic processes of a catchment is important for many ecological and management issues because it is strongly related to catchment hydrology, land and soil degradation. Understanding of catchment processes with respect to climate and land use dynamics is a continuing need in the northern Ethiopian highlands, as it is the major problem threatening the availability of water resource. Rapid growth of population, excessive land and soil degradation of the region due to overgrazing, and expansion of cultivation land and hilly slope cultivations have a significant impact on the natural resources, mainly on water and land.

The key objective of this study is to understand the coupled effect of land use and land cover and climate change on the availability of water resources in the northern Ethiopian highlands, specifically in the Suluh river basin. A combination of field and laboratory investigations, the inclusion of remote sensing data (Landsat) and various climate modeling results (HadCM3, CGCM3) are used for impact assessments. To understand thoroughly the effects of spatial and temporal variation of both, climate and land land cover change, the semi-distributed hydrological model Hydraulic Engineering Centers Hydrological Modeling System (HEC-HMS) is applied. This is combined with Statistical DownScaling Methods (SDSM) for downscaling climate data. Land use and cover maps are based on satellite image analysis for the years 1972, 1986 and 2000.

More specifically, this study addresses the following distinct, but related issues:

- Understanding of the spatial and temporal variability of hydrological and climatic parameters in the study area.
- Developing of geomorphological maps for selected test sites to understand the geomorphological processes of the study site.
- Assessing and quantifying the land use and cover change dynamics of the basin.
- Downscaling GCM outputs climate data to the local watershed scale.
- Testing the applicability of semi-distributed hydrological model HEC-HMS to simulate runoff processes in the Suluh River basin.
- To assess land use/cover and climate change effects on water resources of the basin.

Chapter 2

2 State of the art

2.1 Effect of climate and land use and land cover change on water resource

2.1.1 Global level

Human activities, the driving forces for land cover and land use changes, due to the burning of fossil fuels and expansion of cultivated area are believed to increase the greenhouse gases concentrations in the atmosphere and then resulting change in climate (Coulibaly and Dibike, 2004). According to the report of the Intergovernmental Panel on Climate Change (IPCC), the mean annual global surface temperature has increased by about 0.3–0.6^{o}C since the late 19th century and it is anticipated to further increase by 1.0–3.5°C over the next 100 years (Houghton et al., 1996).

The cyclic interrelationships of land use and land cover and climate change significantly affect the water cycle. Deterioration of the global fresh water resources is the most challenging question and becomes the forefront scientific and political agenda in relation to global environmental changes in climate, land-use and bio-diversity (Montoya and Raffaelli, 2010; Miranda et al., 2011). The impacts of climate change on the accessibility and availability of freshwater along with natural resource degradation become the main cause of food insecurity all over the developing countries particularly in Sub-Saharan Africa (Ludi, 2009).

According to the World Bank (2010) climate change adds new challenges to the management of water resources. The increased rainfall variability will have a significant impact on the multidimensional use of water and its management, including greater uncertainty and an increase in extreme events such as floods and droughts (Yang et al., 2013).

Water resource variability, particularly rainfall variability, is a key constraint to rainfed agricultural production and economic growth in many developing countries (Hailu, 2003). Even though in some places the total amount of rain increases, rainfall variability is amplified as a result of climate change (McCartney and Smakhtin, 2010). Changes in rainfall characters will also increase variability in groundwater recharge and river flow, thus affecting all water sources (McCartney and Smakhtin, 2010). In consequence, agricultural production in many African countries and regions will be severely compromised by climate variability, resulting in food shortage (Parry et al., 2007). Due to the ever increasing demand in water resource most of the African transboundary river basins are under stress. Hence, it becomes a source of potential water conflicts (UNFCCC, 2007).

In sub-Saharan African countries, particularly the horn of Africa is subjected to droughts that lead to food insecurity. Out of 160 million people living in the Horn of Africa, more than 40% of the populations are repeatedly affedted by droughts (Ndaruzaniye, 2011). Interestingly, in this area flood and drought jointly occur within short period interval. Poor water resource management systems parallel with inadequate and insufficient capacities as well as a low level of technology cause a high vulnerability to climate change impact (UNESCO-WWAP, 2004). Particularly rural livelihoods of Sub-Saharan African

countries are dependent on natural resources; water, cultivated and grazing lands are crucial physical assets in their subsistence agricultural economy. Due to this case, any changes in land use, land cover and climate variability have a direct impact on food production and alternative economic activities. Climate change has and will continue to affect the hydrological cycle (Karl et al., 2009).

The magnitude of hydrologic extreme events increases with climate change. Coincidingly, the non-climate drivers cause in Sub-Saharan Africa country's significant impacts on the subsistence agricultural practice. Hence, adaptation to climate change and controlling its drivers is the key development issue (Anderson et al., 2010).

2.1.2 National level

During the past decades the increasing population growth in Ethiopia coupled with a traditional land and water resource management system put enormous pressure on the natural resources (Dubale, 2003). The Ethiopian population counted in 2012 over 85 million and had doubled since 1984 and is expected to double again until 2050 (IFRC, 2012). The high pressure on natural resources, the historical settlement in the highlands together with traditional farming system creates environmental instability in the area (FAO, 1986; Nyssen et al., 2004). Hurni et al. (2005) and Amsalu et al. (2007) assure that the enormous increment of population in the last century resulted in deforestation and intensification of land cultivation, as well as accelerated land degradation throughout the Ethiopean highlands. Similarly in northern Ethiopia population pressure was an important driver for the expansion of agricultural land in recent periods (Hadgu, 2008). According to the National Meteorological Service Agency (Abebe, 2007) the average annual minimum temperature over the country has been increasing by about 0.25^{o}C each decade since 1950 while average annual maximum temperature has been increasing by about 0.1^{o}C during the same period. The average annual rainfall of the country shows a very high variability over the past years even though the sum of annual average rainfall remains stable (Abebe, 2007). It is expected that the mean annual temperature will increase in the range of 1.7–2.1^{o}C by the year 2050 and 2.7–3.4^{o}C by the year 2080 in Ethiopia (Abebe, 2007). The future climate change scenario indicates adversely effects on water availability due to increasing rainfall variability, evapotranspiration and dry spell of the country (Ndaruzaniye, 2011).

The progressively changing land use and land cover pattern along with climate variability result in food insecurity and declining water availability, and cause erratic rainfall over the country finally leading to poverty and environmental damage (Abebe, 2007). In general, Ethiopia is blessed with a huge water resource potential with 80 to 90 percent of the water resources found locally in the four river basins Abay (Blue Nile), Tekeze, Baro Akobo and Omo Gibe in the western parts of Ethiopia, draining into the Nile basin. The population in these basins totals only 30 to 40% (MoWR, 2002). Hence, even without the effects of climate change the spatial variability of the available water resource causes problems of accessibility to water resource in the highly populated areas of the country.

Across the country rainfall is seasonally and annually highly variable (Donkor and Yilma, 1999). This variability subjects the country to frequent droughts and famines (Comenetz and Caviedes, 2002). The increase of population density leads to clear cutting, shrinking forests and grasslands, the expansion of cultivated areas and intensified land use resulting in an almost complete abandonment of the fallow

systems (Hurni et al., 2005). As a consequence, soil degradation and sediment loss heavily increased (Demelash and Stahr, 2010). Land degradation is serious in the highlands, contributing to low soil productivity and poor agricultural production. Soil erosion also causes downstream sedimentation, which can significantly decrease reservoir life (Schütt and Thiemann, 2001; Gebeyehu, 2003; Haregeweyn et al., 2005, 2006; Tamene et al., 2006).

On the other hand, poor water management policy on the national level and shortage of skilled manpower badly affect the development of the water sector (MoWR, 2002). Agriculture depends fundamentally on natural resources and has an important role for their conservation. The deteriorating land and water resources in Ethiopia present a concern to rural land users, and wider public awareness of environmental issues is bringing urgency to watershed management (Hailu, 2003; Alemayehu et al., 2009). Water depletion and land degradation are the result of increasing ecological imbalances. This caused the recurrent droughts and famines occurring every 3 to 5 years (Abebe, 2007; Abebe, 2010). Sustainable agriculture plays the pivotal role in poverty reduction efforts of the country (Hailu, 2003).

In addition, absences of extension services supported by applied research referring to the traditional agricultural practices, the country's available water resource are not efficiently utilized for the development of agricultural sector (Hailu, 2003).

To utilize water appropriately means to enhance the positive and minimize the negative impacts on the water resources (Bekele, 2003). Positively it can be used for drinking, irrigation, hydropower etc. Water can also negatively influence socio-economic development in the form of flood, erosion, sedimentation etc. To utilize water in a sustainable manner, it is necessary to understand the quantity and quality in space and time through hydrological model studies and research in relation to changing climate and land use and land cover, which are the drivers of negative effect of water (Legesse et al., 2010; Pechlivanidis et al., 2011).

Different researchers tried to indicate the severity of climate and land use and land cover change effects on water resource and environmental degradation. Among others Gebresamuel et al. (2010) indicate that cultivated land has expanded on the expense of forest and woodland and brought deleterious impacts on surface runoff in northern Ethiopia.

Different catchment specific studies also strengthen the idea. For Gerado watershed in northeastern Ethiopia (Asmamaw et al., 2011) and Debre-Mewi watershed in northwestern Ethiopia (Fisseha et al., 2011) it is documented that there is a trend of increasing cultivation land on the expense of natural forest, grazing land and woodland. High population growth, fuel wood demand and bad land and water management practices are the cause for land use and land cover change (Asmamaw et al., 2011). These led to further land degradation and more food insecurity among many farming households. Moreover, Bewket and Sterk (2003) observe for the Chemoga watershed (Blue Nile basin) that degradation due to the destruction of natural vegetation, extreme expansion of cultivated land and overgrazing have adverse impact in stream flow (Bewket and Sterk, 2005). Generally, Legesse et al. (2003) mention multiple triggers of change such as, demographic trends, climate variability, national policies, and macroeconomic activities which all affect alterations in land cover and land use, which in turn impact the hydrologic system.

2.1.3 Regional/local level

Natural resources management at national, regional and local levels is very fragmented due to the lack of strong coordination mechanism, both, at the federal and regional governing bodies. Furthermore, inadequacy of cross-sectorial links of ministries and line departments, poor linkage between local and international non-governmental agents and governmental offices, a lack of elaborated links of federal and regional sector offices involved in environment, the absence of research and development centers like institutions for water, climate change adaptation and low level of awareness of the community for environment etc. have major share for natural resource degradation in the country (Abebe, 2007).

Poor land use practices caused deforestation and overexploitation of natural resources in the northern Ethiopian highlands (Feoli et al., 2002). The Tigray region in northern Ethiopia is generally considered as the most degraded part of the country (Araya and Edwards, 2006). Deforestation in Ethiopia, particularly in Tigray regional state, has been a major cause for land degradation processes (Nyssen et al., 2009; Reubens, 2010). Deforestation was induced by the communities who expanded the agricultural lands, cultivated hill slopes, and had to fulfill the need of daily energy consumption (Feoli et al., 2002; Hadgu, 2008).

The issue of water security in Tigray is crucial. The region has been facing a massive crisis in water supply for domestic and irrigation purposes. Many traditional sources of water, such as springs and streams, have dried-up (Behailu and Haile, 2003). Surprisingly, the regional government has planned to alleviate the water scarcity problem through the construction of an extensive water harvesting scheme. Since 1981 the regional government is attempted to rehabilitate the natural environment through different soil and water conservation works. Later on an institution called 'Commission for Sustainable Agriculture and Environmental Rehabilitation in Tigray' (CoSAERT) was setup to undertake the construction of micro-dams. Since 1995, over 50 micro-dams have been built in the region and a good deal was achieved in economic, hydrologic and ecological terms (Tamene, 2005; Yazew, 2005).

In the areas where the water harvesting schemes were constructed, farmers are able to harvest crops at least twice a year (Behailu, 2002; Yazew, 2005). The micro-dams also provide locally drinking water for the population and their livestock. The newly built micro-dams lead to the development of new springs due to an increased ground water recharge (Woldearegay, 2002; Nedaw and Walraevens, 2009). However, the sustainability of the aforementioned benefits is equivocal as most of the reservoirs fail within a very short period of their planned life span. On top of the engineering related failures, hydrology and siltation are the most important problems facing the reservoirs (Tamene et al., 2006; Haregeweyn et al., 2006, 2008; Abdurahman, 2009). The siltation and hydrological problems are directly linked with upstream land use and land cover change and climate variability of the region.

Under these circumstances, along with the high population pressure, depleted natural resources and the arid climate conditions impede to ensure food security (Tesfay, 2011). Maintaining moisture stress and soil fertility are the challenges to alleviate the crop production in the area. Therefore, the assessment of water resources potential is necessary for regional water management, water allocation, effective utilization and economic planning, wherever the economy is highly depend on rainfed agriculture.

2.2 Modelling of land use and land cover and climate change effect

2.2.1 Overview of the hydrological model

Catchment models simulate the hydrologic processes by which rainfall is converted into stream flow. The catchment is the system being modeled; with rainfall corresponding to the input parameter and runoff characteristics being computed (Xu, 2009).

Due to the spatial and temporal variability of the parameters involved in the transformation of rainfall-runoff process, modeling catchment response to land use and land cover and climate change forcing can only be achieved with great difficulty (Lastoria, 2008; Lund et al., 2010). Catchment hydrologic models have been developed for different reasons and therefore have different forms (Xu, 2009). However, they are in general designed to meet one of the following two primary objectives: i) to understand the hydrologic phenomena operating in a catchment and how changes in the catchment may affect these phenomena and ii) to generate synthetic sequences of hydrologic data for facilitating design or forecasting purpose.

Rapid advances in computer technology, nowadays hydrological models vary greatly in their computational capabilities and enormous range in levels of sophistication including the input data requirements of the model (DeVries and Hromadka, 1993). Hydrological models have high importance to quantify the processes of the hydrological cycle in an entire catchment or parts of it and allow assessing the potential impacts of land use and land cover and climate change on the hydrological cycle. However, choosing a model of appropriate complexity is equally important to consider the ability of the model to perform the desired land use or climate change scenarios (Lund et al., 2010).

2.2.2 Classification of hydrologic models

Models documenting the physical processes like rainfall runoff relation are expressed either based on simple physical laws to link between input and output variables, or describing the basic processes involved in the runoff generation (Lastoria, 2008). Hydrologic models can be variously classified. One of the classification methods used by Nirmalakhandan (2002) distinguishes hydrologic models as (1) physical models, (2) empirical models and (3) mathematical models.

Physical models involve the real system by a geometrically and dynamically similar, scaled model and conducts experiments in it to make observations and compare them with real measurements. The empirical model, the so called black box model, is based on an inductive or data-driven approach, in which historical observed data are used to develop relationships between variables believed to be significant in the system studied (Xu, 2009). Statistical tools are often used in this process to ensure validity of the predictions for the real system (Xu, 2009). Mathematical models, the so called mechanistic models, are based on the deductive or knowledge-driven approach. Here, basic physical principles and theories along with simplified assumptions on the governing techniques are applied to derive information on the relation between input-output variables (Nirmalakhandan, 2002). Hence, based on the differential equations governing the system's behavior a complete description of the water cycle dynamics in the mathematical model can be achieved (Lastoria, 2008).

On the basis of spatial description, the hydrological models are broadly classified into two main categories: lumped models and spatially distributed models (Chow et al., 1988; Nirmalakhandan, 2002). According to Lastoria (2008) and Xu (2009) hydrological models are classified as lumped models, semi distributed and distributed models.

Lumped models do not consider the spatially varying character of drainage basin character and precipitation rather it considers the whole basin as one entity. It averages the output results at the outlet of the basin (Lastoria, 2008). Lumped conceptual models are characterized by a simple structure, minimum data requirements, fast set up and calibration and by easy use (Cunderlik, 2003).

In semi-distributed models spatial variation is partially allowed through dividing the basin into a number of smaller entities or sub-basins. They are more physically-based than lumped models and less demanding on input data than fully distributed models (Orellana et al., 2008). Semi-distributed continuous models are often used to evaluate monthly and annual water balance (Xu and Singh, 2004).

In distributed models spatial variability of processes, input, boundary conditions, watershed characteristics and output is defined by the user and is strictly dependent on the resolution of available data. Since the distributed models consider the spatially and temporally varying character of the data they provide the highest accuracy in the process of hydrological modeling (Cunderlik, 2003). Parameters of these models spatially vary at a given resolution and therefore require considerably more input data, often unavailable, than semi-distributed models and they have a direct physical interpretation (Pechlivanidis et al., 2011).

The time-variant models consider temporal varying rainfall input and control the temporal resolution and duration of hydrologic simulations (Chow et al., 1988). They correspond to event-driven models that are able to capture short-term-events (Lastoria, 2008).

An event model simulates a single storm event. The duration of the storm may range from a few hours to a few days. They are mostly applied where direct runoff is the dominating runoff component (Lastoria, 2008). Event models give less attention for moisture recovery between storm events hence, they are not appropriate for dry weather simulation. In contrast, a continuous model simulates longer periods to predict hydrologic response during and between storm events. Continuous models consider all runoff components. It is suited for the simulation of stream flow at all time scales (daily, monthly, or seasonal) (DeVries and Hromadka, 1993; Cunderlik, 2003). Based primarily on the capability of modeling the land use and land cover and climate change effects on water resources availability, the Hydrologic Engineering Center's Hydrological Modeling System (HEC-HMS) is capable to model rainfall-runoff relations in time and space (Feldman, 2000).

2.2.3 Application of HEC-HMS model

The Hydrologic Engineering Center Hydrologic Modeling System (HEC-HMS) is a semi-distributed physically based hydrologic model which is designed to simulate the rainfall-runoff processes particularly for dendritic watershed. The model has an integrated graphical user interface. The operation is seamless with a fast computational engine as well as data storing and reporting capability (Feldman, 2000). It is designed to be applicable in a wide range of geographic areas for solving the

widest possible range of problems. The model can be applied as well to small scale urban drainage basins as to to large scale river basins to simulate water supply and flood hydrographs (Feldman, 2000).

HEC-HMS (successor of HEC-1) is designed to simulate event-driven and continuous runoff over long periods of time, and to compute runoff using grid-cell depiction of the watershed (Scharffenberg and Fleming, 2006). HEC-HMS is comprised of a graphical user interface, integrated hydrologic analysis components, data storage and management capabilities, and graphics and reporting facilities (Scharffenberg, 2001). HEC-HMS uses a separate model to represent each component of the runoff process. Thus, it includes separate models to compute runoff volume, direct runoff (overland flow and interflow), base flow and channel flow (Feldman, 2000).

Deficit and constant loss and the five-layer Soil Moisture Accounting model can be used to simulate losses in complex infiltration and evapotranspiration environments (Feldman, 2000). Excess precipitation can be transformed into surface runoff by unit hydrograph methods. A variety of hydrologic routing methods are included for simulating flow in open channels (lag method, Muskingum method, modified Puls method, kinematic wave or Muskingum-Cunge method) and a total of four different base flow methods are provided. Some of the methods are designed primarily for simulating events while others are intended for continuous simulation (Feldman, 2000).

Since the model was developed over 30 years of continuous research and improvement made it widely applicable for rainfall-runoff modeling (Scharffenberg, 2001). The current version of the HEC-HMS model is a highly flexible package both in time and space and it is capable to model the effect of land use and climate change (Cunderlik, 2003).

The application of hydrological models becomes popular and indispensable to study the hydrological response of catchments to changing climate and land use. Different models are used to forecast effects of climate and land use change on hydrological process. HEC-HMS is the one to perform this task (Cunderlik and Simonovic, 2004). Many researchers so far applied the HEC-HMS event and continuous modeling approach in a wide range of geographical locations from semi-arid to humid regions. For example, Bashar and Zaki (2005) and Yimer et al. (2009) applied the HEC-HMS Soil Moisture Accounting (SMA) algorithm to analyze the long term water balance of the Blue Nile in the context of climate change. According to Dhar and Mazumdar (2009) the HEC-HMS Soil Moisture Accounting (SMA) model was applied to simulate the future water availability in the Natunhat Watershed, West Bengal under climate change scenarios. Similarly, the HEC-HMS continuous model was applied in different Indian watersheds for example by Meenu et al. (2012) and Roy and Mazumdar (2013) and for climate change impact assessment by Roy et al. (2013) for evaluating water availability. Abdurahman (2009) and Tulu (2010) applied an event based HEC-HMS approach to develop rainfall-runoff relations in northern Ethiopia to regionalize runoff coefficients.

Runoff generation from rainfall follows a non-linear relation due to the temporal and spatial variability of the input parameters (Habte et al., 2007). Hence, a proper understanding and modeling of the rainfall-runoff relationship at basin scale is essential for water resources availability and management studies and design activities such as flood control, management and planning of various water resource development projects etc. (Habte et al., 2007).

Chapter 3

3 Methodology

3.1 Soil sampling and soil analysis

Data on soils, land use and land cover are the baseline for watershed hydrological modeling. Most of the hydrological model parameters are usually derived from soil properties and land cover information. Often those data are acquired from different specialized institutions. Verification and countercheck is important prior to model application. An appropriate field data collection methodology plays an important role to acquire data for watershed based hydrological modes.

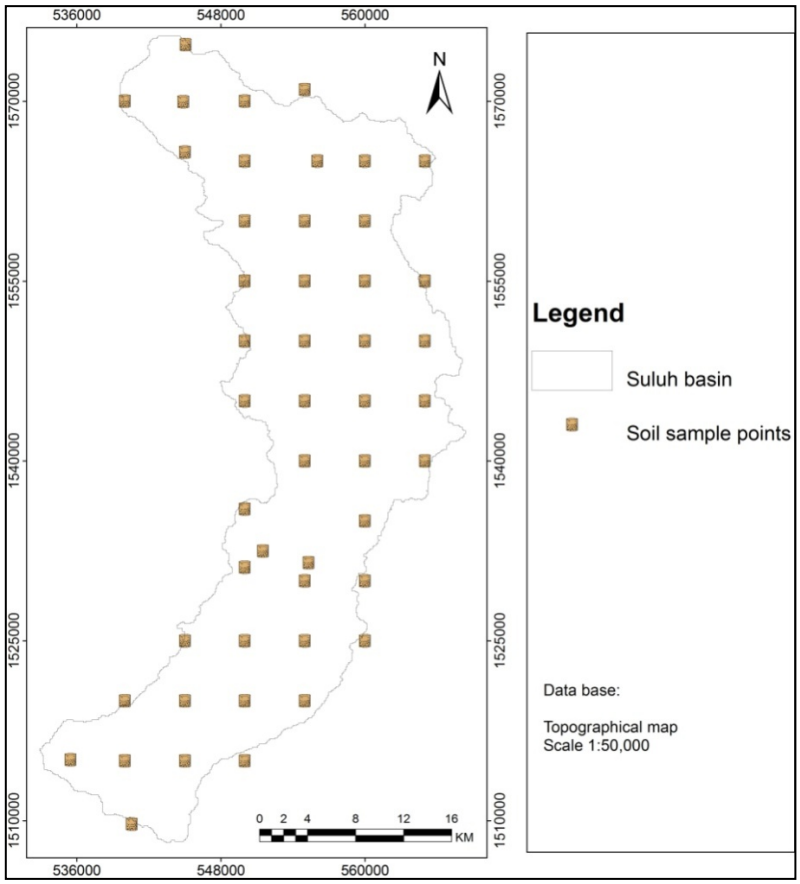

Figure 3-1: Soil sampling locations' layout in the Suluh basin.

51 disturbed surface soil samples were collected from the Suluh catchment based on a predefined grid basis (5 km x 5 km) during the 2011 field campaign (Figure 3-1; Appendix B, Table-D). The purpose of the grid based sampling was to ensure that the sampling points were well distributed across the catchment. Additionally, previous soil samples collected for the Tekeze Basin Master Plan Studies (NEDECO, 1997) and for the Suluh Valley Integrated Rural, Agriculture and Water Resources Development Study (WAPCOS, 2002) were integrated. Sampling stations were geo-positioned by using the topographical maps (scale 1:50 000) and Garmin GPS.

In the Geotechnical and Soil Laboratory of the Mekelle University of the Department of Civil Engineering, the soil samples were analyzed based on the standard laboratory procedures adopted from ASTM designation: D422–63 (ASTM, 1998). Grain-size analysis was conducted to determine the relative proportions of the different grain-sizes which make up a given soil mass. This test is performed by sieve analysis. Dry sieving was used only for soils with a negligible amount of plastic fines, such as gravels and clean sands, whereas wet sieving was applied to soil samples with high content of plastic fines. Additionally, for particles <75µm in diameter the hydrometer method was applied. Prior to particle size analysis the sample was dispersed using sodium hexametaphosphate as an agent. The grain-size distribution of mixed soils was determined by combined sieve and hydrometer analyses. Finally, using United States Department of Agriculture (USDA, 1999) soil triangle as a base, soil texture classification was done and further processed and mapped using Arc GIS 9.3 tools.

As a baseline a soil map of the Suluh basin was obtained from the Soil and Terrain database for northeast Africa developed by the Food and Agricultural Organization (FAO) of the United Nations (FAO, 1998). Missing data were filled from the Soil and Terrain Database for Eastern Africa obtained from the Data Exchange Platform for the Horn of Africa (DEPHA). Soil type classes of FAO were translated into soil texture classes, using the percentage of the topsoil textures (coarse, medium and fine) from the universal soil texture triangle and further supported by the laboratory analysis result.

3.2 Geomorphologic map

Geomorphological maps are one of the most appropriate and synthetic ways to analyze the distribution of landforms, surface and near-surface deposits including the processes that shape landforms (Huggett, 2007). Beyond this, lithology, structure, land use/land cover and artificial features can be incorporated in a geomorphological map according to their importance (Gebremariam, 2010).

Geomorphological map preparation started with field survey which was carried out in two successive field campaigns (March–April 2012 and October–November 2012). Additional provided data was: i) the collection of topographical maps, aerial photographs, thematic maps like geological maps and soil maps and other regional and local study outputs and ii) the Digital Elevation Model (DEM) 90 m x 90 m resolution. Field observation data were recorded on a topographical map and aerial photographs using the legend after Leser and Stäblein (1985).

During field data collection a detailed topographic transect from watershed divide to divide was recorded for each valley supported by GPS, steel meter to measure soil depth, meter tapes (5 and 50 meters) and digital camera. Focus was on morphological landforms and depositional elements, mainly:

- Gravitational elements: mass wasting and colluvial deposits,
- Fluvial elements: gullies, ephemeral streams, alluvial deposits and fans,
- Anthropogenic elements: land use, road, footpath, water diversion, hand dug well, soil and water conservation works.

Settlements and other important parameters were recorded and mapped with Arc GIS 9.3. DEM (90 m x 90 m) derivative parameters were included. Finally, it was attempted to see the relation between geological structure and land forms, soil type and soil depth and lithology with longitudinal and cross-sectional profiles of the test site.

3.3 Data preprocessing

3.3.1 Preprocessing mapping data

3.3.1.1 Base map of the study site

The study area is covered by seven topographic maps (Table 3-1) of 1:50 000 scale provided by the Ethiopian Mapping Authority (EMA), with Transverse Mercator Projection (grid: UTM zone 37N), Clarke 1880 as spheroid and Adindan datum.

Table 3-1: List of topography maps (data source: Ethiopian Mapping Authority (EMA)).

St. No.	Topographical sheet number	Location name	Ordering or position	
1	1439C4	Nebelet		
2	1439D3	Sinkata (Firewayni)	1439 C2 Adigrat	
3	1339A2	Hawzen		
4	1339B1	Wukro	1439 C4 Neblet	1439 D3 Sinkata
5	1339B3	Agulae		
6	1339A4	North Mekelle	1339 A2 Hawzen	1339 B1 Wukro
7	1439C2	Adigrat	1339 A4 North Mekelle	1339 B3 Agulae

Delineated maps were digitized using Arc GIS 9.3 tools. Figure 3-2 depicts the steps for the preparation of a base map. The base map was utilized as a reference to operate geometric corrections on other thematic maps and remote sensing data.

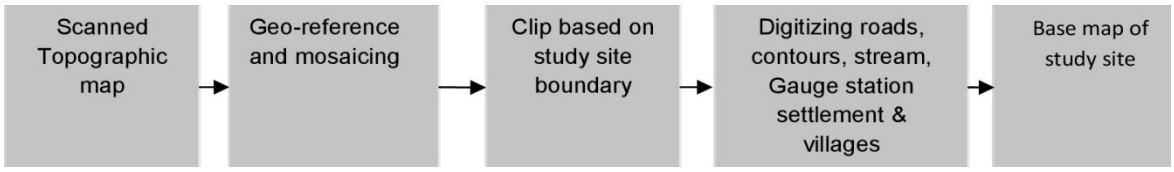

Figure 3-2: Schematic representation of base map preparation.

3.3.1.2 Watershed analysis

The analysis of morphometric characteristics of a catchment like drainage network, slopes, divides and sub-basin boundaries is the prerequisite for hydrological modeling (Johnson, 2009). Watershed analysis includes initial parameter estimation for rainfall-runoff modeling and determination of DEM derivatives for further analysis and simulation.

The Hydrologic Engineering Center Geospatial Hydrologic Modeling Extension (HEC-GeoHMS) and Arc Hydro tools coupled with Arc GIS 9.3 were used for watershed analysis and relate with the HEC-HMS model (Figure 3-3). The Arc Hydro tools are utilities based on the Arc Hydro data model for deriving hydrography data from DEMs, such as delineating watersheds, drainage networks and its derivatives for flow tracing (Johnson, 2009). The tools provide raster, vector, and time-series functionality, and many of them populate the attributes of Arc Hydro features. Further, the Arc Hydro tool provides a data base (spatial data management) that uses various applications to develop hydrologic model (Johnson, 2009).

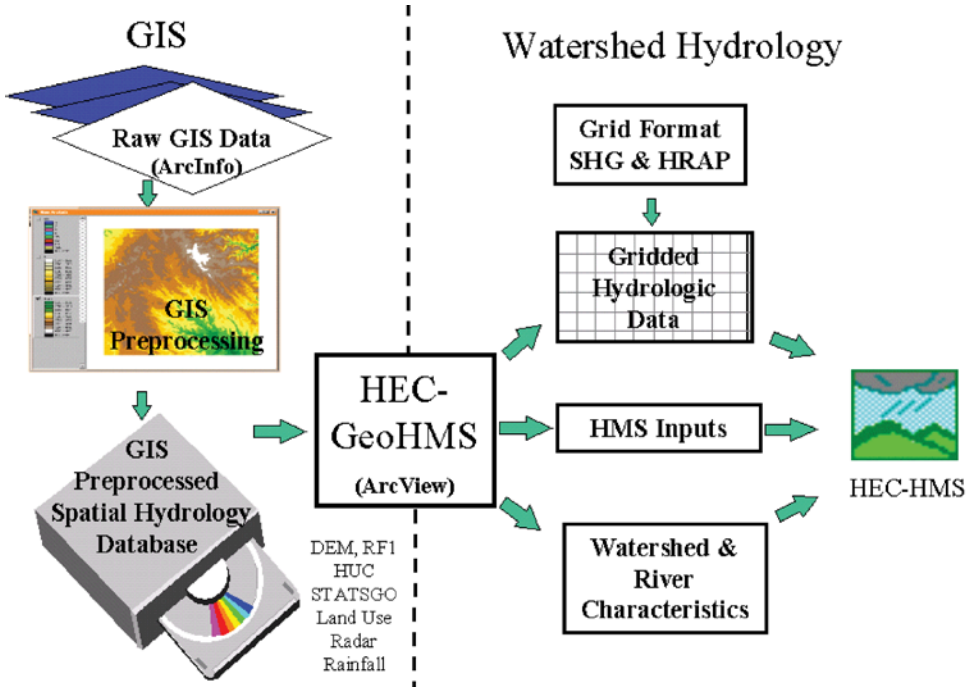

Figure 3-3: Relation between GIS, HEC-GeoHMS and HEC-HMS.

The Digital Elevation Model (DEM) with 90 m x 90 m resolution provided from the Shuttle Radar Topography Mission (SRTM) was used to derive parameters for the hydrological modeling (Figure 3-4). The program features are terrain preprocessing, basin processing, hydrologic parameter estimation and Hydrologic Engineering Center Hydrologic Modelling Systems (HEC-HMS) model support (Feldman and Doan, 2009). The first two features are accomplished through a number of procedural steps. Terrain preprocessing includes filling sinks, assigning flow direction and flow accumulation, defining stream network, sub-watershed area sizes, basin slope and some other watershed characteristics that collectively describe the drainage pattern and geometry of a basin. Additionally, parameters like river slope, river length, watershed centroid, and longest and centroidal flow path were also determined (Fleming and Doan, 2009). Finally, the automatically generated drainage network from the DEM will be compared with the topographic maps at scale 1:50 000.

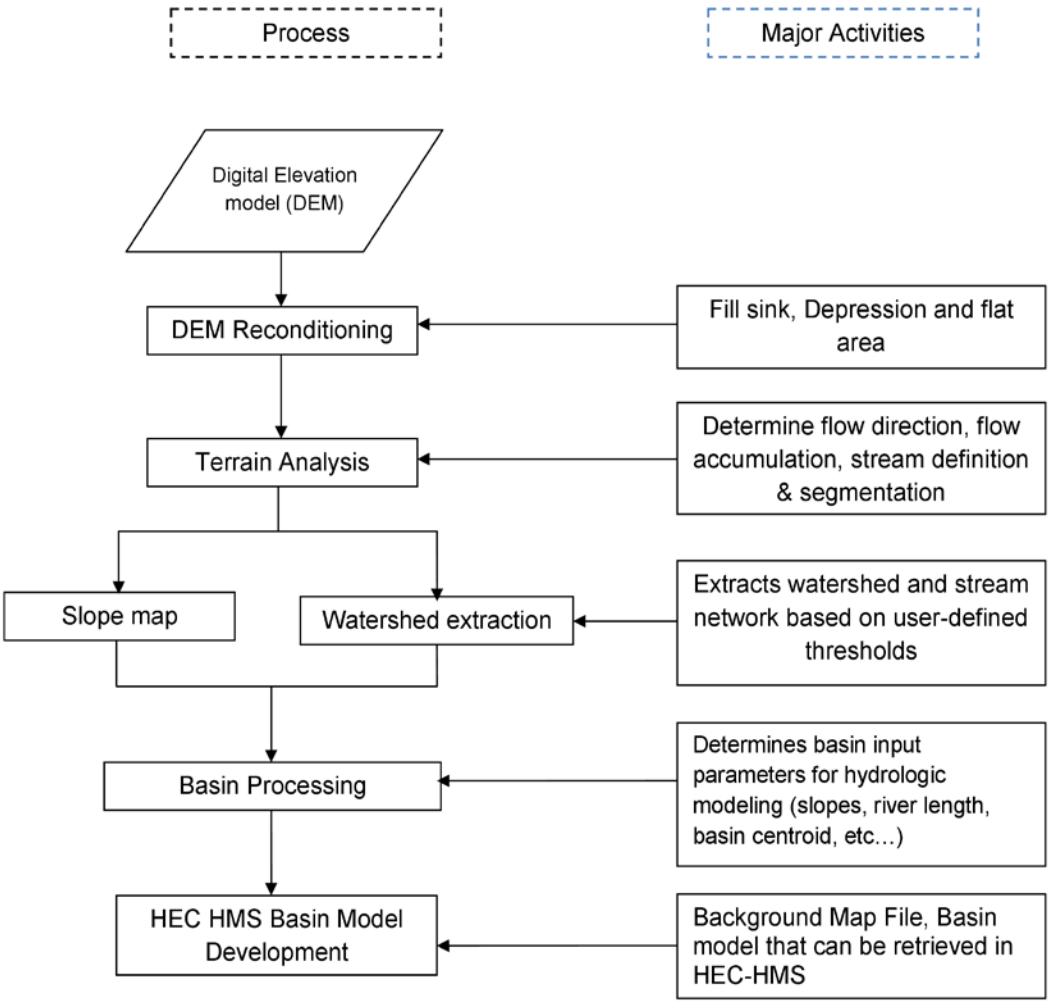

Figure 3-4: Flow chart for watershed processing in HEC-GeoHMS and Arc Hydro tools.

3.3.1.3 Land use and land cover map

During the first field survey in May to July 2011, the general land use, land cover pattern and the general land forms of the study site were mapped in detail. Agricultural fields were often found to be scattered everywhere and alternated with natural vegetation and rural settlements. It was found as a recurrent situation and in most cases it was impossible to make a separation between these fields. For this reason a mixed land cover class was introduced. The survey was supported by topographical maps (scale: 1:50 000). A Global Positioning System (GPS) was used to collect ground truth points for further analysis of satellite images. The field data supported the analysis of the aerial photographs and satellite image analysis.

3.3.1.4 Data extraction and image processing

Data sources

Landsat imagery is available since 1972 from six satellites in the Landsat series: MSS (Multi-spectral Scanner), TM (Thematic Mapper), and ETM+ (Enhanced Thematic Mapper Plus). Landsat supplies high 30mx30m invisible and infrared imagery, with thermal imagery and a panchromatic image also available from the ETM+ sensor (NASA, 2003). Landsat images of the Suluh catchment were available for the years 1972, 1986 and 2000 through Global Land Cover Facility (GLCF). Based on the location of the study site a four-band MSS for the year 1972, a six-band TM for the year 1986 and a seven-band ETM+ for the year 2000 were downloaded from GLCF data base (Table 3-2).

Table 3-2: Details of the acquired Landsat images (data source: GLCF).

Satellite	Sensor	Band	Date of production	Pixel resolution	Path / Row
L 1-4	MSS multi-spectral scanner	1,2,3,4	1972-11-02	60 meter	181/51
L 4-5	TM multi-spectral	1,2,3,4,5,7		30 meter	
L 4-5	TM thermal	6	1986-01-05	120 meter	169/50
L 7	ETM+ multi-spectral	1,2,3,4,5,7		30 meter	
L 7	ETM+ thermal	6.1, 6.2		60 meter	
Panchromatic	ETM+ thermal	8	2000-01-27	15 meter	169/50

All the images were acquired for the Ethiopian dry season (December to February) to keep seasonal consistency of the time series. Additionally the following information was collected:

- 1:50 000 topographical maps for verification and geo-referencing of the acquired imagery,
- Land use map prepared by Hunting Technical Service Limited (HTSL) (1976),
- Land use map with a scale of 1:100 0000 prepared by the Ministry of Agriculture (1985),
- Land use map prepared by Woody Biomass Inventory and Strategic Planning Project (WBISPP, 2003) with a scale of 1:250 000,
- 110 ground truth data collected for a supervised land cover classification and classification accuracy assessment, and
- Available aerial photographs (1965, 1986, 1994).

Image analysis

ERDAS Imagine (version 9.2) and Arc GIS (version 9.3) software packages were used for the classification of land use and land cover. The satellite data were imported into ERDAS IMAGINE 9.2 in an image format for geometric correction. Geometric distortions in a satellite image are introduced by the sensor system. Images were geo-referenced.

Land use and land cover classification from satellite image needs a prior knowledge of the study site including ground truth and secondary data to support the interpretation and to analyze the historical images. The steps taken as a general procedure can be summarized as (i) preprocessing of the images

including spatial, radiometric and Spectra enhancement, (ii) unsupervised classification, (iii) supervised classification, (iv) accuracy assessment and (v) land use change detection and analysis (Figure 3-5).

Landsat ETM+ images have 8 individual bands, each representing a single layer of continuous imagery. Due to their low spatial resolution (60 m) the thermal bands (bands 6.1 and 6.2) were not used (Table 3-1). The images of the non-thermal bands (30 m) were stacked into a multilayer image and clipped with the study area boundary. Image fusion (or pan-sharpening) techniques have proven to be effective tools for providing better image information (Saadat et al., 2011). Hence, the 30 m multilayer image was fused with the 15 m panchromatic band (band 8) using the Principal Component Analysis (PCA) method to increase the resolution of the image. 110 ground truth points were collected in the field for a pixel based image training supervised classification and accuracy assessment.

Supervised classification was done followed by unsupervised classification. The maximum likelihood algorithm was used for classification because the algorithm takes the distributions of the classes into account via a variance-covariance matrix (Adnan, 2010). Based on the multivariate Gaussian distribution the algorithm estimates the probability that a given pixel belongs to a specific land use class. The processes involved the generation of land use maps for the 1972, 1986 and 2000 images (Figure 5-1).

3.3.1.5 Spatial maps overlay

To generate the input parameters for ongoing modeling various spatial maps were processed using Arc GIS 9.3. Soil map, land use/land cover map and slope map were generated. Further, an overlapped map intersecting with sub-basins was generated with HEC-GeoHMS model. Based on the overlapping map homogeneous sub-basins with known attributes are available for model simulation.

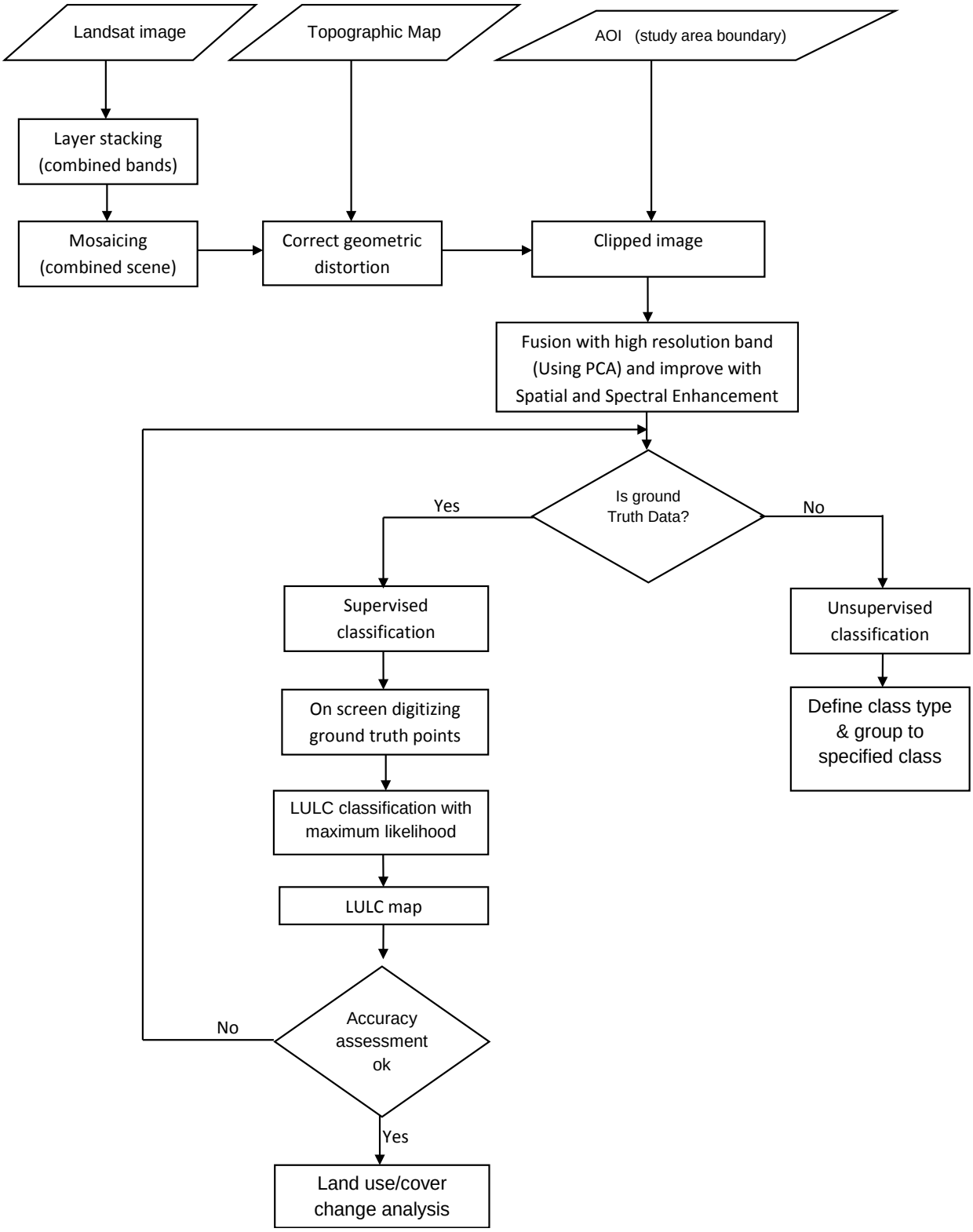

Figure 3-5: Work flow adopted for processing Landsat images.

3.3.2 Preprocessing of meteorological data

3.3.2.1 Rainfall

To establish a rainfall-runoff relationship for a catchment, historical meteorological data are required. In this study those data were required for two main purposes. First, the data were used as an input to the HEC-HMS model in the hydrological model setup and development. Second, the data were used for downscaling the Global Circulation Model (GCM) data using Statistical DownScaling Model (SDSM) for impact assessment. Meteorological data were collected from the Ethiopian National Meteorological Service Addis Ababa and Mekelle branch office. Since there are only few meteorological stations with relatively long records inside the catchment, data include neighboring stations too (Figure 4-1).

A 37 year period (1973–2010) of daily data for seven weather stations were collected for the analysis (Table 3-3, Figure 4-2).

Table 3-3: Weather stations providing meteorological data for this study (data source: Ethiopian National Meteorological Service Agency (ENMSA)).

St. No.	Station name	Location		Altitude (m a.s.l.)	Measured period	Number of missing years
		Easting	Northing			
1	Edaga-Hamus	556082	1565413	2720	1974–2010	3
2	Adigrat	548533	1575362	2506	1970–2010	5
3	Hager-Selam	533434	1505715	2608	1973–2010	11
4	Hawzein	542062	1535564	2255	1971–2010	10
5	Mekelle airport	551768	1494659	2267	1959–2010	3
6	Wukro	564710	1514559	1995	1963–2010	17
7	Senkata	556082	1544408	2437	1973–2010	18

However, the number of meteorological variables collected varies from station to station depending on the class of the stations; some of the station became inoperative during the civil war. The only station in the study area which has data for more than 37 years is Mekelle airport meteorological station. Data provided are rainfall, relative humidity, wind speed, sunshine hours, maximum temperature and minimum temperature.

Data were quality controlled to identify inconsistencies as caused for example by changes in measurement device, changes in climate, natural disasters etc. For the statistical analysis and the data filling process, Mekelle airport station was considered as the base station. For monthly data gaps long term average of the base station, regression techniques (both linear and multiple) and Maintenance of Variance-Extension, type 1 (MOVE.1) were applied (Helsel and Hirsch 1992). Finally, heterogeneity of the data was detected using double mass curve, residual mass plot and accumulated residual method (ellipse test).

The rainfall at a single station is considered as point rainfall. The required watershed precipitation depth can be inferred from the depths at gauges using an averaging scheme (Feldman, 2000). Thus, computation of average depth of rainfall over the watershed is:

$$P_{average} = \frac{\sum_i \left(w_i \sum_t p_i(t) \right)}{\sum_i w_i} \qquad \text{Equation 3-1}$$

Where:

$P_{average}$ is average depth of rainfall over the watershed,
$p_i(t)$ is precipitation depth measured at time t at gauge i and
w_i is weighting factor assigned to gauge/observation i.

HEC-HMS model has performed internally using Inverse-distance-squared Method and Thiessen polygons during basin model preparation under HEC-GeoHMS and offers the opportunity to apply user specified gauge weight.

The Thiessen polygons were constructed around rainfall stations using Arc GIS 9.3 to obtain the area-weighted average rainfall for Suluh catchment (Figure 4-2). Application of the Thiessen polygons is suitable for non-homogenous distribution of rain gauges, however, the method does not consider other than station spacing and precipitation amounts (WMO, 1994). Although the isohyetal method is suitable to consider physiographic relationships, storm tracks and types (WMO, 1994). It was not used in this study as there are not enough stations available.

To assess the relationship between rainfall and altitude rainfall, both factors were compared on a seasonal basis (considering Ethiopian traditional seasons). Additionally, the mean annual total rainfall for the 37 years of recorded data (1973 to 2010) was related to altitude information of the seven stations integrated into this study.

The inter-annual variations in seasonality of precipitation are analyzed quantitatively by using Seasonality Indices SI_i derived by Walsh and Lawler (1981). SI_i is a measure to evaluate the spread of the monthly rainfall with respect to an ideally uniform monthly distribution in all 12 months (Sumner et al., 2001; Livada and Asimakopoulos, 2005; Mwchahary and Nath, 2013):

$$SI_i = \frac{1}{R_i} \sum_{n=1}^{12} \left| X_{in} - \frac{R_i}{12} \right| \qquad \text{Equation 3-2}$$

Where:

R_i is the total annual precipitation for the particular year under study and
X_{in} is the actual monthly precipitation for month n.

Then from the accumulated SI_i, a long-term mean $\overline{SI_i}$ was calculated as (Walsh and Lawler, 1981):

$$\overline{Si_i} = \frac{1}{38} \sum_{j=1}^{38} SI_{ij} \qquad \text{Equation 3-3}$$

Another seasonality index $\overline{SI}$ was calculated in order to estimate the mean seasonality over the study period by using directly long-term average monthly rainfall data (Walsh and Lawler, 1981):

$$\overline{SI} = \frac{1}{R}\sum_{n=1}^{12}\left|\overline{X}_n - \frac{\overline{R}}{12}\right| \qquad \text{Equation 3-4}$$

Where:

$\overline{Xn}$ is the mean rainfall of month *n* and

$\overline{R}$ is the mean annual rainfall.

Seasonality index is equal to zero when all months share the same amount of rainfall and equal to 1.83 when all rainfall incidences occur in a single month (Livada and Asimakopoulos, 2005). In order to indicate whether or not the wettest period occurred over a small range of months, or whether it occurred in any month during the year a Replicablity Index (RI) was obtained by Walsh and Lawler (1981):

$$RI = \frac{\overline{SI}}{\overline{SI}_i} \qquad \text{Equation 3-5}$$

A high replicability index indicates that the wettest month of a year generally occurrs stable in the same month each year; whereas a lower replicability index indicates that the wettest month of the year tends to be more evenly spread amongst a larger time period. The seasonal variations are studied on a monthly base (Sumner et al., 2001)

Another step processing the meteorological data was the trend analysis of rainfall and temperature time series. Spearman's rank-correlation method was selected as an appropriate approach. It is simple and distribution free, i.e. it does not require the assumption of an underlying statistical distribution (Dahmen and Hall, 1990). Yet another advantage is nearly uniform power for linear and non-linear trends (Mitchell et al., 1966). The Spearman's rank-correlation coefficient, R_{sp}, is defined as:

$$R_{sp} = 1 - \frac{6*\sum_{i=1}^{n}\left(D_i * D_i\right)}{n*\left(n*n-1\right)} \qquad \text{Equation 3-6}$$

Where:

n is the total number of data,

D is difference and

i is the chronological order number.

The difference between rankings is computed with:

$$D_i = Kx_i - Ky_i \qquad \text{Equation 3-7}$$

Kx_i is the rank of the variable, x, which corresponds to the chronological order number of the observations. The series of observations, y_i, is transformed to its rank equivalent, Ky_i, by assigning the chronological order number of an observation in the original series to the corresponding order number in the ranked series, y. If there are ties, i.e. two or more ranked observations, y, with the same value, the convention is to take Kx as the average rank. One can test the null hypothesis, H_0:$R_{sp} = 0$ (there is no trend), against the alternate hypothesis, H_1:$R_{sp} < > 0$ (there is a trend), with:

$$t_t = R_{sp}\left[\frac{n-2}{1-R_{sp} * R_{sp}}\right]^{0.5} \qquad \text{Equation 3-8}$$

Where:

R_{sp} is Spearman's rank-correlation coefficient and

t_t is student's t-distribution.

Student's t-distribution is symmetrical around t = 0. At a significance level of five percent (two-tailed), the two-sided critical region, U, of t_t is bounded by:

$$\{-\infty, t\{\upsilon, 2.5\%\}\} \bigcup \{t\{\upsilon, 97.5\%\}, +\infty\} \qquad \text{Equation 3-9}$$

Where:

υ is n-2 degrees of freedom.

The null hypothesis is accepted if t_t is not contained in the critical region. In other words, the time series has no trend if:

$$t\{\upsilon, 2.5\%\} < t_t < t\{\upsilon, 97.5\%\} \qquad \text{Equation 3-10}$$

3.3.2.2 Evapotranspiration

Evapotranspiration is an integral part of HEC-HMS continuous simulation module while it is neglected for event based simulation. It is possible to analyze watershed response to longer precipitation records that include both, periods of rainfall and periods without rainfall. In periods without rainfall the state of basin moisture directly corresponds to the temperature with evaporation and transpiration as the critical components (McEnroe, 2010). The input data for the HEC HMS model were prepared based on the monthly averages of the potential evapotranspiration. The preferred method to calculate a

reference evapotranspiration is the Penman-Monteith method as presented in the United Nations Food and Agriculture Organization's report FAO-56 (Allen et al., 1998). The required meteorological inputs are solar radiation, temperature, humidity and wind speed. Long term records of the climate variables are not available for most of the weather stations of the study site. In consequence, these data have been extracted from FAO climate data base with the help of New-LocClim local climate estimator.

FAO-56 Penman-Monteith method (Allen et al., 1998):

$$ET_0 = \frac{0.408 * \Delta * (R_n - G) + \gamma * \left(\frac{900}{T_{mean} + 273}\right) * u_2 * (e_s - e_a)}{\Delta + \gamma * (1 + 0.34 * u_2)} \qquad \text{Equation 3-11}$$

Where:

ET_0	is reference evapotranspiration rat [mm/day],
R_n	is net radiation at the crop surface [MJ/m^2/day],
G	is soil heat flux density [MJ /m^2 /day],
T_{mean}	is daily air temperature at 2 m height [°C],
u_2	is wind speed at 2 m height [m/s],
e_s	is saturation vapour pressure [kPa],
e_a	is actual vapour pressure [kPa],
e_s - e_a	is saturation vapour pressure deficit [kPa],
Δ	is slope vapour pressure curve [kPa/°C] and
γ	is psychrometric constant [kPa/°C].

The conversion factor is:

$$\frac{1mm}{2.45MJ / m^2} = \frac{0.408mm * m^2}{MJ} \qquad \text{Equation 3-12}$$

Where:

MJ	is Mega Joule,
mm	is millimeter and
m	is meter.

3.3.2.3 Downscaling of climate data

The predictor variables used for the Statistical DownScaling Method (SDSM) is provided by the Canadian Institute for Climate Studies website for model output of HadCM3 (CICS, *http://www.cics.uvic.ca/scenarios/sdsm/select.cgi*). Predictor variables were supplied on a grid basis. The data provided include the following three directories:

NCEP_1961–2001: This directory contains 41 years of daily observed predictor data, derived from the National Centre for Environmental Prediction (NCEP) reanalysis, normalized (with respect to the mean

and standard deviation) over the complete 1961–1990 period. These data were interpolated to the same grid as HadCM3 (2.5° latitude x 3.75° longitude) before normalization.

H3A2a_1961–2099: This directory contains 139 years of daily GCM predictor data, derived from the HadCM3 A2 (a) experiment, normalized over the 1961–1990 period.

NCEP data are reanalysis sets from the National Centre for Environmental Prediction which was regrided to match with the grid system of the HadCM3. These data were used for model calibration. Both, the NCEP and HadCM3 data have daily predictors. And also CGCM3 (*http://loki.qc.ec.gc.ca/DAI/CGCM3_predictors-e.html*) predictor variables were supplied on a grid basis. Data provided include the following three directories:

NCEP_1961–2003: 41 years of daily predictors derived from the NCEP/NCAR reanalysis,

CGCM3A2_1961–2000: 40 years of daily GCM predictor data, derived from the CGCM3.1 A2 historical GHG and aerosol concentration experiment, and

CGCM3A2_2001–2100: 100 years of daily GCM predictor data, derived from the CGCM3.1 A2 SRES A2 scenario. All details concerning the development of the CGCM3 predictors can be found in the DAI CGCM3 Predictors (2008) documentation.

The predictands (maximum temperature, minimum temperature and precipitation) for Mekelle station can be prepared in the same format as the predictor. On this basis adjustment of the model parameters for downscaling climate data (year length, event thresholds, model transformation, variance inflation and bias correction) were set.

The selection of predictor variables is based on the empirical relationships between regridded predictors and single site predictands. The explanatory power of individual predictor variables varies spatially and temporally (Wilby and Dawson, 2007). In SDSM, the predictors are selected on the bases of their linear and partial correlation between the predictors (from GCM) and the predictands variables (local weather station) (Yimer et al., 2009). Finally, the scatter plot indicates whether this result is due to a few outliers or it is a potentially useful downscaling relationship. The calibration of the model and scenario generation was executed according to SDSM guide manual.

3.3.2.4 Statistical Downscaling of climate parameters

The Statistical DownScaling Model (SDSM) is a hybrid of a multiple linear regression model. It is used for climate change studies at local scale by creating statistical relation with GCM outputs (Wilby and Dawson, 2007). Applying these methods for the Suluh basin a multiple linear regression model is developed between a selected GCM (HadCM3 and CGCM3) predictor variables and its predictands such as temperature and precipitation (Yimer et al., 2009).

Selection of climate stations

Seven weather stations are available in the Suluh river basin (Table 3-3; Figure 4-2). However, to execute climate downscaling; Mekelle Airport weather station has the only reasonably good quality daily temperature and precipitation data for the period of 1961–2010.

Predictor variables for statistical downscaling

Two sets of large scale climate change predictor variables are used for climate studies (Table 3-4 and 3-5). Data were were provided for a grid box by grid box with 2.5^{o} * 3.75^{o} in size for the Hadley Centre Coupled Model version 3 (HadCM3) and 3.75° * 3.75^{o} for the third generation Coupled Global Climate Model (CGCM3). The drainage basin area of Suluh basin is located in 13.3^{o}–14.25^{o} latitude and 38.63^{o}–39.8^{o} longitude and is covered by a single grid box.

i. Hadley Centre Coupled Model version 3 (HadCM3) A2 and B2 scenario were obtained from the Canadian Institute for climate studies (CICS).

Table 3-4: Description of large scale atmospheric variables from the NCEP reanalysis and HadCM3 simulations output used as predictors
(data source: *www.cics.uvic.ca/scenarios/sdsm/select.cgi*).

No.	Predictor variable	Predictor description	No.	Predictor variable	Predictor description
1	mslpaf	Mean sea level pressure	14	p5_uaf	500 hpa zonal velocity
2	p_faf	Surface air flow strength	15	p5_vaf	500 hpa meridional velocity
3	p_uaf	Surface zonal velocity	16	p5_zaf	500 hpa vorticity
4	p_vaf	Surface meridional velocity	17	p500af	500 hpa geopotential height
5	p_zaf	Surface vorticity	18	p5thaf	500 hpa wind direction
6	p5zhaf	500 hpa divergence	19	p850af	850 hpa geopotential height
7	p8_faf	850 hpa airflow strength	20	p8thaf	850 hpa wind direction
8	p8_uaf	850 hpa zonal velocity	21	p8zhaf	850 hpa divergence
9	p8_vaf	850 hpa meridional velocity	22	r500af	Relative humidity at 500 hpa
10	p8_zaf	850 hpa vorticity	23	r850af	Relative humidity at 850 hpa
11	p_thaf	Surface wind direction	24	rhumaf	Near surface relative humidity
12	p_zhaf	Surface divergence	25	shumaf	Surface specific humidity
13	p5_faf	500 hpa airflow strength	26	tempaf	Mean temperature at 2 m

ii. The third generation Coupled Global Climate Model (CGCM3) were obtained through Data Access Integration Portal (*http://loki.qc.ec.gc.ca/DAI*). All details concerning the development of the CGCM3 predictors can be found in the DAI CGCM3 predictors (2008) documentation.

Table 3-5: Description large scale atmospheric variables from the NCEP reanalysis and CGCM3 simulations output used as predictors (data source: *http://loki.qc.ec.gc.ca/DAI*).

No.	CGCM3	Predictor description	No.	CGCM3	Predictor description
1	mslpgl	Mean sea level pressure	14	p5zhgl	500 hPa divergence
2	p__fgl	Surface airflow strength	15	p8_fgl	850 hPa airflow strength
3	p__ugl	Surface zonal velocity	16	p8_ugl	850 hPa zonal velocity
4	p__vgl	Surface meridional velocity	17	p8_vgl	850 hPa meridional velocity
5	p__zgl	Surface vorticity	18	p8_zgl	850 hPa vorticity
6	p_thgl	Surface wind direction	19	p850gl	850 hPa geopotential height
7	p_zhgl	Surface divergence	20	p8thgl	850 hPa wind direction
8	p5_fgl	500 hPa airflow strength	21	p8zhgl	850 hPa divergence
9	p5_ugl	500 hPa zonal velocity	22	s500gl	Specific humidity at 500 hPa
10	p5_vgl	500 hPa meridional velocity	23	s850gl	Specific humidity at 850 hPa
11	p5_zgl	500 hPa vorticity	24	shumgl	Surface specific humidity
12	p500gl	500 hPa geopotential height	25	tempgl	Mean temperature at 2m
13	p5thgl	500 hPa wind direction	–	–	–

3.3.3 Preprocessing hydrological data

The Suluh river has only one gauge station sited near Hawzen at the crossing of Hawzen to Senkata road (552902m E and 1549136m N; Figure 4-1). The gauge was operative from 1973 to 2002 under the Ministry of Water and Energy, Department of Hydrology; since 2002 it is inoperative. Additionally, the data have a number of gaps during the civil war. In general, the quality of the discharge data is poor, because most of the time rating curves were determined when the gauging station was established, but never were updated. Also cross-sections of the river have been determined only once. Hence, before using the data for further analysis a thorough scrutiny/gap filling with different techniques was applied.

3.4 Basics of hydrological models

HEC-HMS hydrologic model is used for modeling of both, individual (single) rainfall events and long, continuous sequences of precipitation data (Scharffenberg and Fleming, 2010). In the HEC-HMS model interception, infiltration, storage, evaporation, and transpiration are collectively called losses. The sub-basin element conceptually represents infiltration, surface runoff, and subsurface processes interacting. The actual infiltration calculations are performed by a loss method contained within the sub-basin. A total of twelve different loss methods are provided. Some of the methods are designed primarily for simulating events while others are intended for continuous simulation. All of the methods conserve mass implying that infiltration and precipitation left on the surface will always be equal to total incoming precipitation (Scharffenberg and Fleming, 2010).

3.4.1 Runoff volume models

The deficit constant loss method uses a single soil layer to account for continuous changes in moisture content and the Soil Moisture Accounting loss method uses three layers to represent the dynamics of water movement in the soil. It is often used in conjunction with a canopy cover and surface method. Layers within the method include soil storage, upper groundwater, and lower groundwater. The soil layer is subdivided into tension storage and gravity storage. Groundwater layers follow the principle of linear reservoir structure which is designed to simulate the interflow and base flow rather than representing the detail aquifer processes of a basin. The above mentioned methods provide output for wetting and recovery cycles and can be used for long periods of continuous simulation (Feldman, 2000). The model requires the input of daily data on rainfall, estimated potential evapotranspiration, soil moisture conditions, land use and various hydrometeorological data. Daily rainfall and stream flow data for a period of eight years (1992−1999) were used to calibrate and validate the model.

3.4.1.1 Basic concept of deficit constant loss model

HEC-HMS includes a quasi-continuous model of precipitation losses, known as the deficit constant loss model. This model is similar to the initial and constant loss model, but the initial loss can 'recover' after a prolonged period of no rainfall (Feldman, 2000).

To apply this model in HEC-HMS, the initial loss and constant rate plus the recovery rate must be specified. Each soil has a specific water holding capacity, controlled by the active rooting depth of the vegetation. It is assumed that also infiltration rate is fixed, approximated by the saturated hydraulic conductivity; due to simplified assumptions infiltration only occurs when the soil is saturated. Water is removed from the soil to simulate evapotranspiration (Ford et al., 2008).

3.4.1.2 Basic formulation of Soil Moisture Accounting model

The HEC-HMS Soil Moisture Accounting model simulates both, wet and dry weather behaviors. The HEC-HMS SMA model (Figure 3-6) is patterned after Leavesley's Precipitation-Runoff Modeling System (Leavesley et al., 1983). Soil Moisture Accounting (SMA) models consider soil moisture balances in an extended period of time. They are suited for the simulation of stream flows for all time scales (daily, monthly, or seasonal) (Roy et al., 2013). Soil Moisture Accounting (SMA) models include all runoff components. The model requires inputs of daily data on rainfall, soil moisture conditions and various hydro meteorological data. The model has five storage layers (Figure 3-6), namely canopy storage, surface depression storage, soil storage, groundwater storages 1 and 2. These model components are simulated separately in the HEC-HMS model (Roy et al., 2013) (Figure 3-6).

The Soil Moisture Accounting (SMA) model computes flow into the system, out of from the system and between the storages. The order of computations in each time step depends upon the occurrence of precipitation or evapotranspiration as follows:

The drainage basin precipitation first satisfies the canopy storage considered as initial loss before it reaches the soil surface. The precipitation which reaches the ground then fills depressions and infiltrates into the soil. During this process already water is water lost by evaporation. The water volume that exceeds the filling capacity of the depressions as well as the infiltration capacity overflow

and become surface runoff (direct runoff). Canopy interception is computed identically for the pervious and impervious parts of the sub-basin (McEnroe, 2010). Infiltration or depression-storage losses are not deducted from precipitation onto impervious surfaces. All impervious surfaces are assumed to be "directly connected"; i.e. runoff from impervious surfaces has no second chance to infiltrate. Water is removed from canopy storage by evaporation. Water is removed from depression storage by evaporation and infiltration (Feldman, 2000).

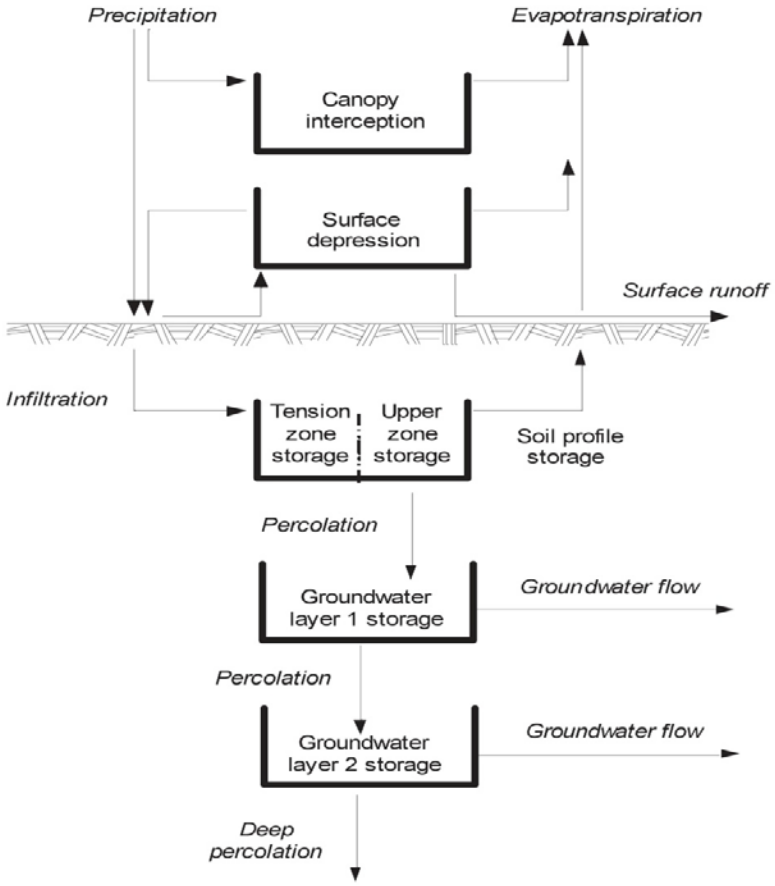

Figure 3-6: Conceptual schematic of the continuous Soil Moisture Accounting algorithm (Feldman, 2000).

Infiltrated water enters the soil storage, with the tension zone filling first. Water in the soil profile, not in the tension zone, percolates to the first groundwater layer. Groundwater flow is routed from the groundwater layer 1, and then any remaining water may percolate to the groundwater layer 2. Percolation from layer 2 is to a deep aquifer and is lost to the model (Feldman, 2000).

If precipitation incides during the analyzed time interval, evapotranspiration is not modeled. If precipitation does not occur, evapotranspiration is modeled. The water stored in the canopy storage and in depressions is removed by evapotranspiration and consequently satisfies the potential evapotranspiration (Bennett and Peters, 2000). Finally, if the saturation vapor pressure is still not satisfied, water is removed from the upper-soil profile storage. The model then continues as described above for the precipitation periods (Feldman, 2000).

3.4.2 Direct-runoff models

Translation and attenuation processes are considered during the transformation of excess rainfall to runoff by the Clark unit hydrograph model (Cunderlik and Simunovic, 2004). Translation is based on a synthetic time- area histogram and the time of concentration, the time-area histogram specifies the area contributing to flow at the outlet as a function of time. Attenuation is modeled with a linear reservoir (Feldman, 2000). The reservoir represents the aggregated impacts of all basin storage (St). The average outflow from the reservoir (Feldman, 2000) during a period (t) is:

$$O_t = C_A I_t + C_B O_{t-1} \qquad \text{Equation 3-13}$$

Where:

I_t is the average inflow to storage at time and

C_A and C_B are routing coefficients.

The routing coefficients are given by:

$$C_A = \frac{\Delta t}{St + 0.5\Delta t} \quad and \quad C_B = 1 - C_A \qquad \text{Equation 3-14}$$

Where:

Δt is the computational time step.

The required parameters of the Clark method are time of concentration (hr) and storage coefficient (hr). Both parameters can be estimated via calibration.

3.4.3 Base flow models

Base flow model simulates the storage and movement of subsurface flow as storage and movement of water through reservoirs. The reservoirs are assumed to be linear: the outflow at each time step of the simulation is a linear function of the average storage during the time step. Mathematically, this is identical to the approach of the Clark's Unit Hydrograph model (Feldman, 2000).

The outflow from groundwater layer 1 of the soil moisture accounting is inflow to one linear reservoir, and the outflow from groundwater layer 2 of the soil moisture accounting is inflow to deep aquifer. The outflow from the two linear reservoirs is combined to compute the total base flow for the watershed. The Soil Moisture Accounting method is designed to be used in conjunction with the linear reservoir base flow model (Feldman, 2000). Required parameters of the linear reservoir base flow model are: Storage coefficient (hr) and number of reservoirs.

3.4.4 Channel flow

The Lag model is the simplest of the HEC-HMS routing models. In the Lag model, the outflow hydrograph is simply the inflow hydrograph, but with all ordinates translated (lagged in time) by a specified duration. The flows are not attenuated, so the shape is not changed. This model is widely used, especially in urban drainage channels (Pilgrim and Cordery, 1993).

Mathematically, the downstream ordinates are computed by:

$$Ot = \begin{cases} I(t) & t \le \text{lag} \\ I(t - lag) & t \ge \text{lag} \end{cases} \qquad \text{Equation 3-15}$$

Where:

O_t is outflow hydrograph ordinate at time t,

I_t is inflow hydrograph ordinate at time t and

lag is time by which the inflow ordinates are to be lagged.

3.4.5 Sensitivity analysis

Sensitivity analysis determines which parameters of the model have the greatest impact on the runoff hydrograph. By using local sensitivity analysis the effects of each input parameter are calculated separately with the other parameters kept constant or at their initial values (Vaze et al., 2011). The analysis was done by adjusting the input model parameters using -20% to +20% from the initial model input parameters. Relative variation of the model output was calculated as:

$$\text{Output variation} = \left[\left(O_t - O_b \right) \Big/ O_b \right] * 100 \qquad \text{Equation 3-16}$$

Where:

O_b is a value of the output variable for a given simulation and

O_t is the value of the initial output.

Then the model was repeatedly run with different values according to the percentage values as described above and compared. Based on the derived results, the sensitivity index and rank of parameters were calculated for the basin according to its effect on the peak flow and runoff volume. From the parameter rank, model calibration was performed.

3.4.6 Calibration and validation parameters

The Soil Moisture Accounting model parameters were calculated by observed data. For this iterative process candidate parameter values are proposed and the model is trained with these parameters including precipitation and evapotranspiration inputs. The resulting computed hydrograph is compared with an observed hydrograph of the corresponding period. If it matches not satisfactory, the parameters are adjusted, and the search continues. Most parameters can be defined automatically using the optimization manager (Fleming, 2004). Observed discharge must be available for at least one element before optimization can start. HEC-HMS includes automatic calibration capabilities and offers six different objective functions (sum of squared residuals, sum of absolute residuals, percent error in peak flow, percent error in volume, the root mean square log error and time weighted functions) and one of two different search algorithms: the univariate-gradient search algorithm (Scharffenberg and Fleming, 2006) and the derivative-free minimization algorithm (Nelder and Mead, 1965). HEC-HMS supports constrained optimization for both search methods.

3.4.7 Model performance evaluation criteria

The performance of a model must be evaluated on the extent to which it satisfies its objective to simulate the real world phenomena (accuracy). A criterion is therefore necessary to evaluate the performance of the model. The criterion used should be linked directly to the objective function used. The criteria used in this study for evaluating the model performance are:

1. Nash-Sutcliffe efficiency (NSE)

The Nash-Sutcliffe efficiency (NSE) normally is used to assess the predictive ability of a models considering the relative magnitude of the residual variance (simulated value) compared to the measured (observed) data variance (Nash and Sutcliffe, 1970), mathematically given by:

$$NSE = 1 - \frac{\frac{1}{N}\sum_{i=1}^{N}\left[(Q_o)_i - (Q_s)_i\right]^2}{\frac{1}{N}\sum_{i=1}^{N}\left[(Q_o)_i - \left(\overline{Q_o}\right)_i\right]^2} \qquad \text{Equation 3-17}$$

Where:

$(Q_o)_i$ is the i^{th} observation for the constituent being evaluated,

$(Q_s)_i$ is the i^{th} simulated value for the constituent being evaluated,

$\left(\overline{Q_o}\right)i$ is the mean of observed data for the constituent being evaluated and

N is the total number of observations.

2. Index of volumetric fit

The index of volumetric fit is a measure which indicates whether or not the volume of the estimated flows of a model agrees with the observed flow volume in a test period. A value of unity for index of volumetric fit indicates a perfect volumetric match of the observed flows with the estimated flow in a certain period, i.e. it indicates that the model has achieved water balance in the period of test considered. The index is given by (Ahsan and O'Connor, 1994):

$$\text{Index of volumetric fit} = \left[\frac{\sum_{I=1}^{N}(Q_s)_i}{\sum_{I=1}^{N}(Q_o)_i}\right] * 100 \qquad \text{Equation 3-18}$$

Where:

$(Q_s)_i$ is the i^{th} simulated value for the constituent being evaluated and

$(Q_o)_i$ is the i^{th} observation for the constituent being evaluated.

3. Index of Agreement (IoA)

The index of agreement (IoA) was developed by Willmott (1981) and varies between 0 and 1. A computed value of 1 indicates that the model has the capability to replicate the measured data, while 0 indicates that the model is unable to perform well and simulated and observed values are not in agreement (Willmott, 1981).

The index of agreement, IoA, is defined as (Willmott, 1981):

$$\text{Index of agreement} = 1 - \frac{\sum_{i=1}^{N}\left[(Q_o)_i - (Q_s)_i\right]^2}{\sum_{i=1}^{N}\left(\left|(Q_o)_i - \bar{Q}_O\right| + \left|(Q_S)_i - \bar{Q}_O\right|\right)^2} \qquad \text{Equation 3-19}$$

Where:

$(Q_o)_i$ is the i^{th} observation for the constituent being evaluated,

$(Q_s)_i$ is the i^{th} simulated value for the constituent being evaluated,

$\left(\bar{Q}_o\right)$ is the mean of observed data for the constituent being evaluated,

$\left(\bar{Q}_s\right)$ is the mean of simulated data for the constituent being evaluated and

N is the total number of observations.

4. Coefficient of determination (R^2)

It describes the degree of collinearity between simulated and measured data. Similarly, R^2 describes the proportion of the variance in measured data explained by the model (Krause et al., 2005). The value ranges between 0 and 1, with higher values indicating less error variance and the ability of the model to perform the simulation. R^2 has been widely used for model evaluation (Legates and McCabe, 1999), is given by:

$$R^2 = \left[\frac{\sum_{i=1}^{N}\left[(Q_o)_i - \bar{Q}_O\right] * \left[(Q_S)_i - \bar{Q}_s\right]}{\left\{\sum_{i=1}^{N}\left[(Q_o)_i - \bar{Q}_O\right]^2\right\}^{0.5} * \left\{\sum_{i=1}^{N}\left[(Q_S)_i - \bar{Q}_s\right]^2\right\}^{0.5}}\right]^2 \qquad \text{Equation 3-20}$$

Where:

$(Q_o)_i$ is the i^{th} observation for the constituent being evaluated,

$(Q_s)_i$ is the i^{th} simulated value for the constituent being evaluated,

$\left(\bar{Q}_o\right)$ is the mean of observed data for the constituent being evaluated,

$\left(\bar{Q}_s\right)$ is the mean of simulated data for the constituent being evaluated and

N is the total number of observations.

5. Relative error of peak

The relative error of the peak is defined as (Goswami et al., 2002):

$$\text{Relative error of peak} = \frac{\left|(Q_P)_S - (Q_P)_O\right|}{(Q_P)_O} * 100 \qquad \text{Equation 3-21}$$

Where:

$(Q_p)_o$ is observed peak flows and

$(Q_p)_s$ is and simulated peak flows.

6. Percent bias

The % BIAS is defined as the mean residual expressed as percentage of mean observed discharge, and is given by (Srivastava et al., 2013):

$$\%BIAS = \frac{\sum_{i=1}^{N}\left[(Q_S)_i - (Q_O)_i\right]}{\sum_{i=1}^{N}(Q_o)_i} * 100 \qquad \text{Equation 3-22}$$

Where:

$(Q_o)_i$ is observed flows and

$(Q_s)_i$ is and simulated flows.

Chapter 4

4 Study area

The area of investigation is the Suluh river basin in northern Ethiopia, a sub-basin of the Tekeze river basin (Figure 4-1). This chapter initially outlines the overall characteristics of the watershed, followed by a detailed description of the selected test sites within the watershed. It includes the location of the study area, its topographic characteristics, the geology, the land use/land cover and the hydro-climatic features. The soils of the study area are also briefly introduced.

4.1 Suluh river basin

4.1.1 Regional settings and landscape units

Tigray regional state is located in northern Ethiopia. It is one of the drier parts of the country and belongs to the African dry lands in the Sudano-Sahelian region (Kumasi and Asenso-Okyere, 2011). The region stretches across three major river basins of the Tekeze, Mereb and Danakil depression. The Tekeze river basin covers approximately 70% of the Tigray region. The Tekeze river further joins Angereb and Gonga valley to form the Atbara River in Sudan feeding into the Nile river (NEDECO, 1997).

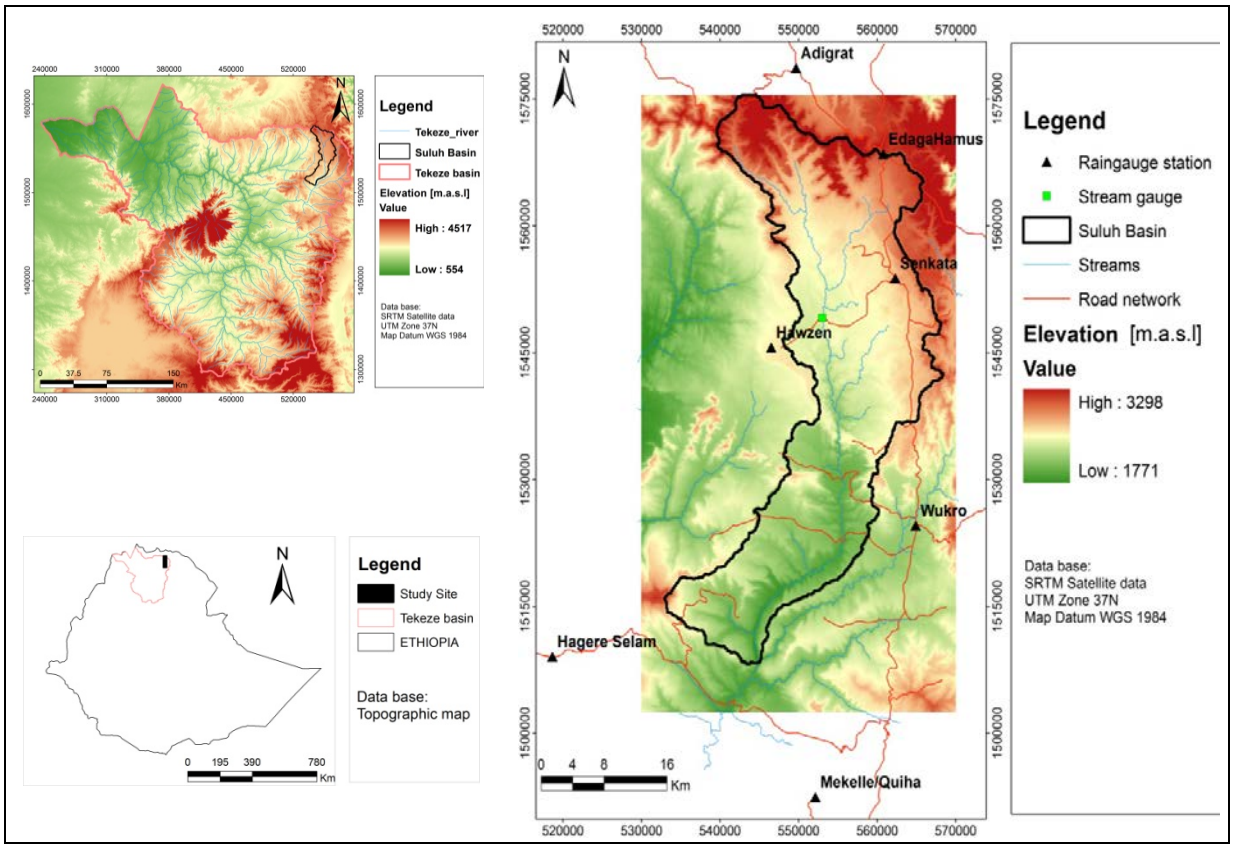

Figure 4-1: Location of the Suluh basin (data base: Jarvis et al., 2008 and EMA).

The Suluh river basin (Figure 4-1) is found in the highlands of the northeastern Tigray region. It is a tributary of the Geba River and drains from the volcanic mountains of Mugulat near Adigrat ridge to the south (Figure 4-1). The drainage basin area of the Suluh River totals 967 km^2. The basin is approximately 10–15 km wide in EW-direction and 90–95 km long in NS-direction. It ends at the confluence of the Suluh and Genfel River.

4.1.2 Climate

The geographic location and altitude characteristics of Ethiopia cause different climates (IAO, 2008). According to the National Strategy and Action Plan for the Implementation of the Great Green Wall Initiative in Ethiopia (2012) almost 90% of the Tigray region is characterized by a semi-arid climate. Rainfall occurs quantitatively and seasonally highly variable. The occurrence of rainfall periods is associated with the seasonal migration of the inter-tropical convergence zone (ITCZ) and the complex topography (HTSL, 1976; Nyssen et al., 2005; Abebe 2007). During the northern hemisphere winter, the ITCZ is located at the Equator; hot and dry winds from the Sahara reach the western highlands of Ethiopia and cause a dry season (*Bega*). From March to May, the ITCZ moves north allowing humid air masses from the Equator to reach Tigray and causing a short rainy season (*Belg*). From June to September (*Kiremt*), the ITCZ is localized in its northern position which is around 16°C (IAO, 2008). The south-east Monsoon and air masses from the Indic ocean cause the great rainy season (*Kiremt*).

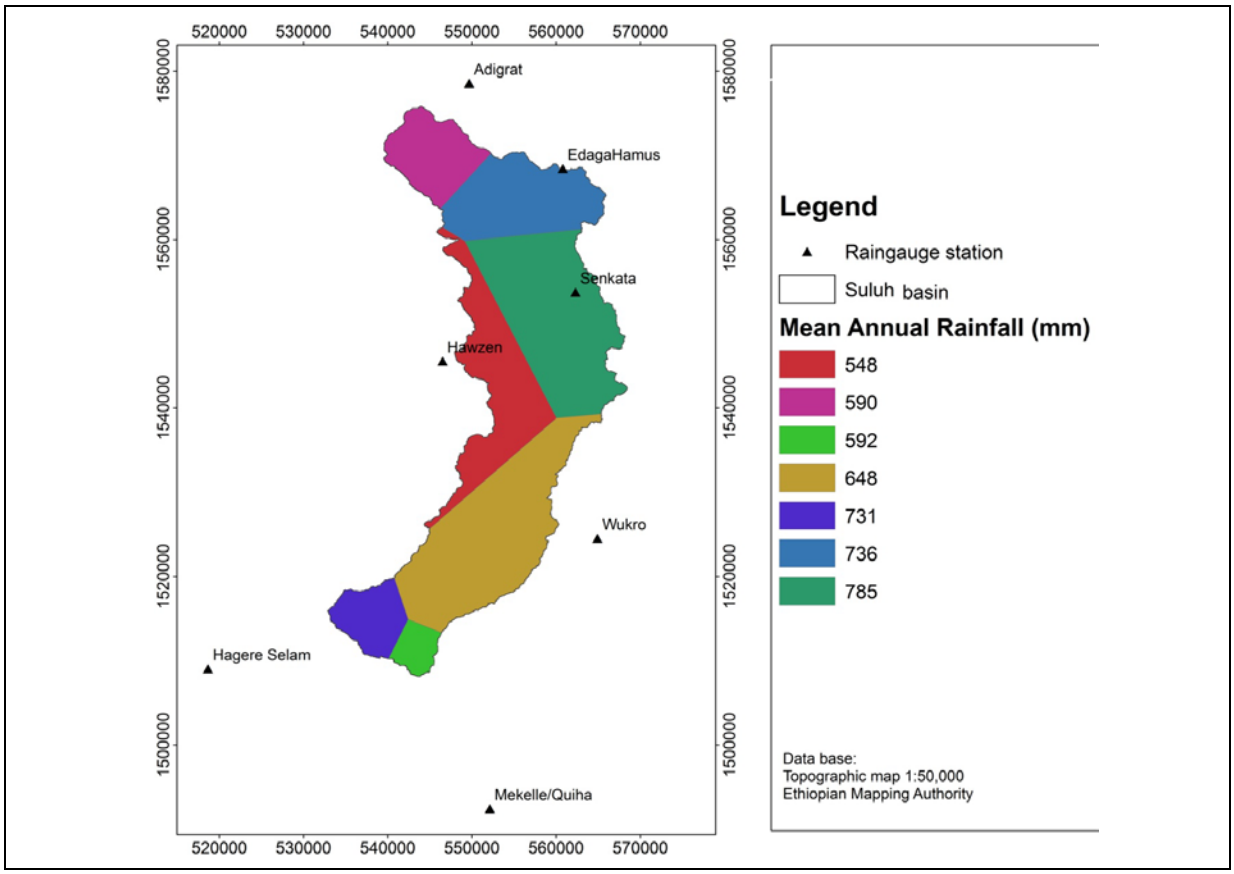

Figure 4-2: Mean annual rainfall and Thiessen polygons methods in the Suluh drainage basin (data base: ENMSA and EMA).

In the Suluh basin annual rainfall is highest in the northeast and southwest and lowest in the western part of the basin, where Hawzen meteorological station annually receives less than 550 mm rainfall. In contrast, Senkata meteorological station receives more than 750 mm annual rainfall. Annual rainfall of the basin is 678 mm in average; estimated by applying the Thiessen polygon methods (Figure 4-2). Figure 4-3 shows the average monthly precipitation over the Suluh basin; more than 75% of the total rainfall occurs during the rainy months of the *kirmet*.

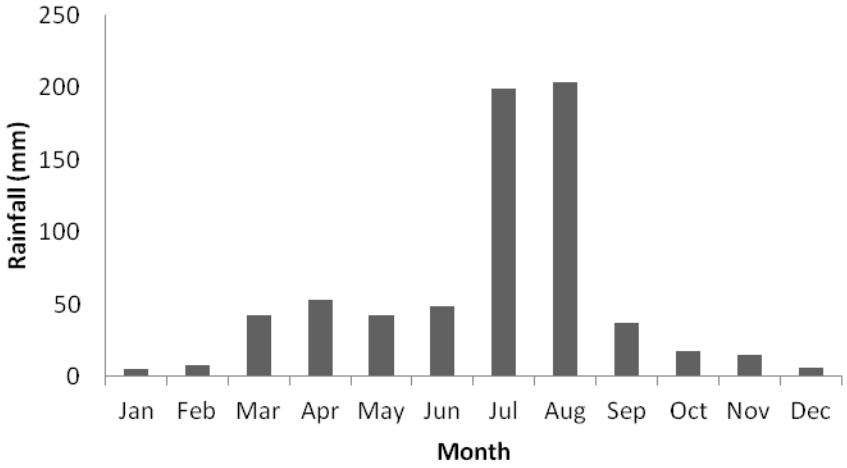

Figure 4-3: Average monthly rainfalls for the Suluh basin; data from 1973–2010 (data source: ENMSA).

For northern Ethiopia relationships between rainfall variations and change in altitude are documented by a several authors: For example Nyssen et al. (2005) correlate between precipitation and altitude in an 80 km^2 large mountainous area of the Geba catchment (2100–2800 m a.s.l.) by installing 16 rain gauges over a period of six years (1998 to 2003). Zenebe (2009) analyzes for the same area mean annual rainfall and altitude including additional eight weather stations from northern Ethiopia outside the Geba basin. In both cases significant relationship between the two variables could not be found.

In the Suluh basin rainfall and altitude were correlated on seasonal bases (considering Ethiopian traditional seasons) using the mean monthly rainfall (1973 to 2010). It gets evident that the average monthly precipitation during *Belg* season, particularly in March (n=7; R^2=0.447; α>0.05), April (n=7; R^2=0.55; α<0.05) and May (n=7; R^2=0.771; α<0.05) shows dependence on altitude. During *Bega* and *Tseday* season only in the months of January (n=7; R^2=0.628; α<0.05) and October (n=7; R^2=0.665; α<0.05) correlation with altitude can be detected. For the other months lower determination coefficients were found, ranging from R^2=0.0001 to R^2=0.373 (α>0.05). However, mean annual precipitation depends not on altitude (n=7; R^2=0.232; α>0.05). Nyssen et al. (2005) notice, that the relation between altitude and mean annual rainfall in mountainous regions is covered by additional factors such as slope, aspect and characteristics of air masses. All weather stations considered (Figure 4-2) show considerable degrees of precipitation seasonality. Traditionally four seasons are considered in the region (Table 4-1).

Table 4-1: Traditional seasons of Ethiopia (data source: HTSL, 1976).

Season	Duration	Description
Bega	December to February	Dry and hot period
Beleg	March to May	Small rainy season
Kiremt	June to August	Big rainy season and cold
Tseday	September to November	Very few rainfall and raising of temperature

Figure 4-4 shows mean rainfall (mm) for the Suluh basin for the four Ethiopian seasons. During the *Bega* (January–February) and *Tseday* (September–December) all parts of the basin receive very low rainfall amounts. With the exception of area around Senkata and Edagahamus the rainfall in the study area has high peak rainfall in *Kiremt*.

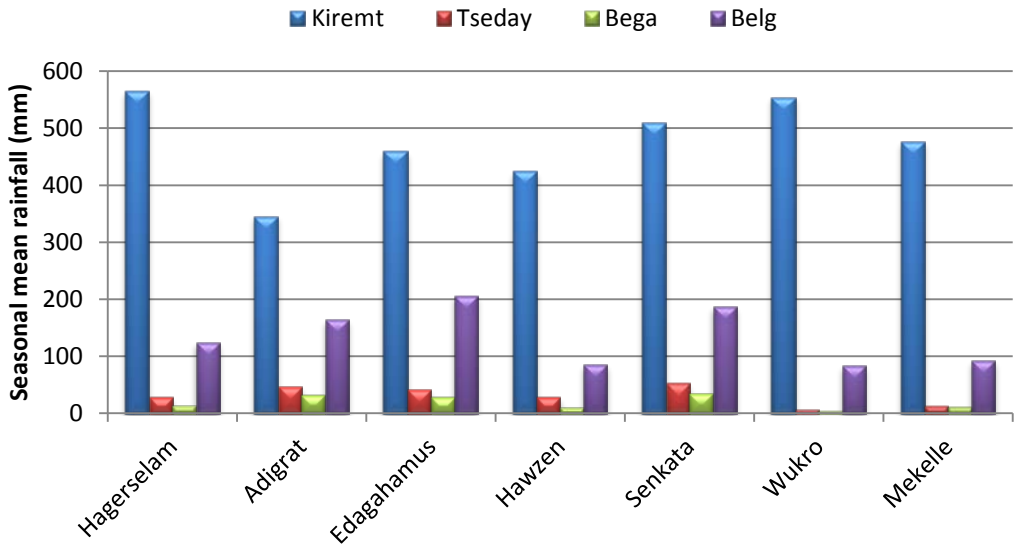

Figure 4-4: Seasonal mean rainfall in the Suluh basin (data source: ENMSA, 1973–2010).

Table 4-2: Seasonal precipitation regimes as classified by Seasonality Index (after Walsh and Lawler, 1981).

SI	Precipitation regime
<0.19	Precipitation spread throughout the year
0.20–0.39	Precipitation spread throughout the year, but with a definite wet season
0.40–0.89	Rather seasonal with a short dry season
0.60–0.79	Seasonal
0.80–0.99	Markedly seasonal with a long dry season
1.00–1.19	Most precipitation in less than 3 months
>1.20	Extreme seasonality, with almost all precipitation in 1 to 2 months

The variability of monthly rainfall during a year is experessed by the relative seasonality index (Walsh and Lawler, 1981; Livada and Asimakopoulos, 2005). Hence, the changing pattern of rainfall seasonality in applying Seasonality Index based on equation 3.2 can be confirmed. The analysis of seasonality indices using the data period 1973–2010 includes SI_a, the long-term mean, SI_{mean}, Replicability Index (RI), minimum and maximum SI value with the corresponding year (Table 4-3).

Table 4-3: SI_i mean values and years with extreme SI_i for each rain gauge station.

Station	SI_a	SI_{mean}	$SI_{minimum}$	Year	$SI_{maximum}$	Year	RI
Hagereselam	0.88	1	0.68	1990	1.29	1988	0.88
Adigrat	0.76	0.93	0.55	1990	1.19	1973	0.82
Edagahamus	0.79	0.99	0.68	1990	1.44	1999	0.99
Hawzen	0.95	1.05	0.71	1992	1.5	2009	1.05
Senkata	0.72	0.97	0.54	1979	1.34	1974	0.75
Wukro	1.12	1.24	0.91	1992	1.67	1973	0.91
Mekelle	1.04	1.24	0.83	1993	1.46	1981	0.92

Generally, higher index values indicate a greater overall divergence from an equal distribution of precipitation throughout the year, while values near zero indicate that there is little or no seasonal variation in precipitation (Sumner et al., 2001). The maximum value of seasonality index is detected for Wukro and Mekelle weather stations (southeastern part of the basin). Mean SI > 1.2 indicates that most of the rain occurred in one to two months (Table 4-3). Relatively low values of the seasonality index are identified for Senkata, Edagahamus and Adigrat weather stations (northeastern part of the basin), ranging between 0.8 and 0.99. This indicates that the precipitation appears relatively concentrated in two periods separated by a marked dry season. The seasonality index of Hawzen and Hagerselam weather station (western part of the basin) lies in the range of 1.00 and 1.19 indicating that most of the rain occurred in less than three months.

Replicability Index (RI) values vary between 0.75 and 0.92, with overall higher values found for Mekelle, Wukro and Hawzen weather stations. The smallest value is observed at the Senkata weather station and reflects that each month (with the exception of *Bega* season) has been at least once the wettest month of the year. The highest RI value detected for the Mekelle weather station indicates that months with the maximum rainfall amount occur reliably in certain months (*Kiremt*).

Temperatures are highly modified by altitude (Abebe, 2007). Consequently, primarily based on altitude, temperature and rainfall traditionally, the country is subdivided into four climatic altitudinal zones (HTSL, 1976). According to this classification the Suluh basin is located in the moderately hot humid climate (Weine Dega region*;* Table 4-4).

Table 4-4: Climatic altitudinal zones of Ethiopia (data source: HTSL, 1976).

Name of climatic zone	Altitude (m a.s.l.)	Mean annual temperature (°C)	Mean annual rainfall (mm/year)
Hot regions (*Kolla*)	< 1500	> 20	200–800
Moderately hot and humid (*Weyna Dega*)	1500–2300	16–20	800–1200
Moderately cold (*Dega*)	2300–3200	10–16	1200–2200
Cold (*Wurch*)	>3200	<10	>2200

In general, temperature of the Suluh basin is moderate and varies with altitude. The maximum mean monthly temperature varies between 20 to 30°C and the minimum mean monthly temperature varies between 3 to 12°C depending on the altitude of the weather station. Warmest months are May and June and coldest months are December and January.

Time series analysis was conducted by using non-parametric Spearman's rank correlation methods of rainfall and temperature time series (1973–2010). The results for the seven weather stations illustrate that rainfall data show no trend since 1973 ($\alpha>0.05$). The results agree with Goitom (2012) analyses of time series for weather stations in and around Geba basin using Mann-Kendall test.

Table 4-5: Time series analysis of annual rainfall (1973–2010) applying Spearman's rank correlation trend test (data source: ENMSA).

Weather station	Number of years used (n)	Critical values of t		t_t calculated	Result
		(40, 2.5%)	(40, 0.975)		
Hagerselam	37	-2.02	2.02	-1.41	no trend
Adigrat	37	-2.02	2.02	-0.26	no trend
Edagahamus	37	-2.02	2.02	-1.76	no trend
Hawzen	37	-2.02	2.02	-0.94	no trend
Senkata	37	-2.02	2.02	-1.59	no trend
Wukro	37	-2.02	2.02	-0.29	no trend
Mekelle airport	37	-2.02	2.02	-0.19	no trend

Time series of temperature data are analyzed with the Spearman's rank correlation test only for Mekelle weather station due to absence of the long term data series for the other stations. All months show an increasing temperature trend ($\alpha>0.05$) except September ($\alpha<0.05$) (Table 4-6).

Table 4-6: Spearman's rank correlation trend test result for the mean monthly temperature for Mekelle weather station (1973–2010) (data source: ENMSA).

Month	Number of years used (n)	Critical values of t		t_t calculated	Result
		(40, 2.5%)	(40, 0.975)		
January	37	-2.02	2.02	3.47	Increasing trend
February	37	-2.02	2.02	3.33	Increasing trend
March	37	-2.02	2.02	3.19	Increasing trend
April	37	-2.02	2.02	3.57	Increasing trend
May	37	-2.02	2.02	3.53	Increasing trend
June	37	-2.02	2.02	2.23	Increasing trend
July	37	-2.02	2.02	4.61	Increasing trend
August	37	-2.02	2.02	5.30	Increasing trend
September	37	-2.02	2.02	1.84	No trend
October	37	-2.02	2.02	2.40	Increasing trend
November	37	-2.02	2.02	5.21	Increasing trend
December	37	-2.02	2.02	5.95	Increasing trend

4.1.3 Geology

Bed rock of the study area corresponds to strongly folded and foliated Precambrian rocks (Mohr, 1962). The main rock types are greenstones of basic volcanic origin, but slates, phyllites, granites are also common. The intensively folded and faulted rocks of the Upper Precambrian, mostly metasediments and metavolcanics, are unconformably overlain by Palaeozoic and Mesozoic sub-horizontal sandstones, limestones, shales and tillites constituting the outcropping bedrock in the Central Plateau of Tigray around Mekele (Gebreyohannes et al., 2010). Tertiary lavas, 200–600 m thick (trap basalts), unconformably overlie these sedimentary formations, representing the youngest rocks in the area apart from the Quaternary terrestrial sediments, which are found along the major river valleys, as well as in softly undulating areas and tectonic depressions (Berakhi et al., 1998).

The Suluh basin is mainly characterized by Precambrian basement rocks, Paleozoic, Mesozoic rocks and Younger tertiary and Quaternary deposits (HTSL, 1976; WAPCOS, 2002). The stratigraphy of the study area encompasses lithological units at the Precambrian basement, Enticho sandstone, Tillite, Adigrat sandstone, Transition, Mesozoic limestone, and Quaternary alluvial sediments (Table 4-7, Figure 4-5).

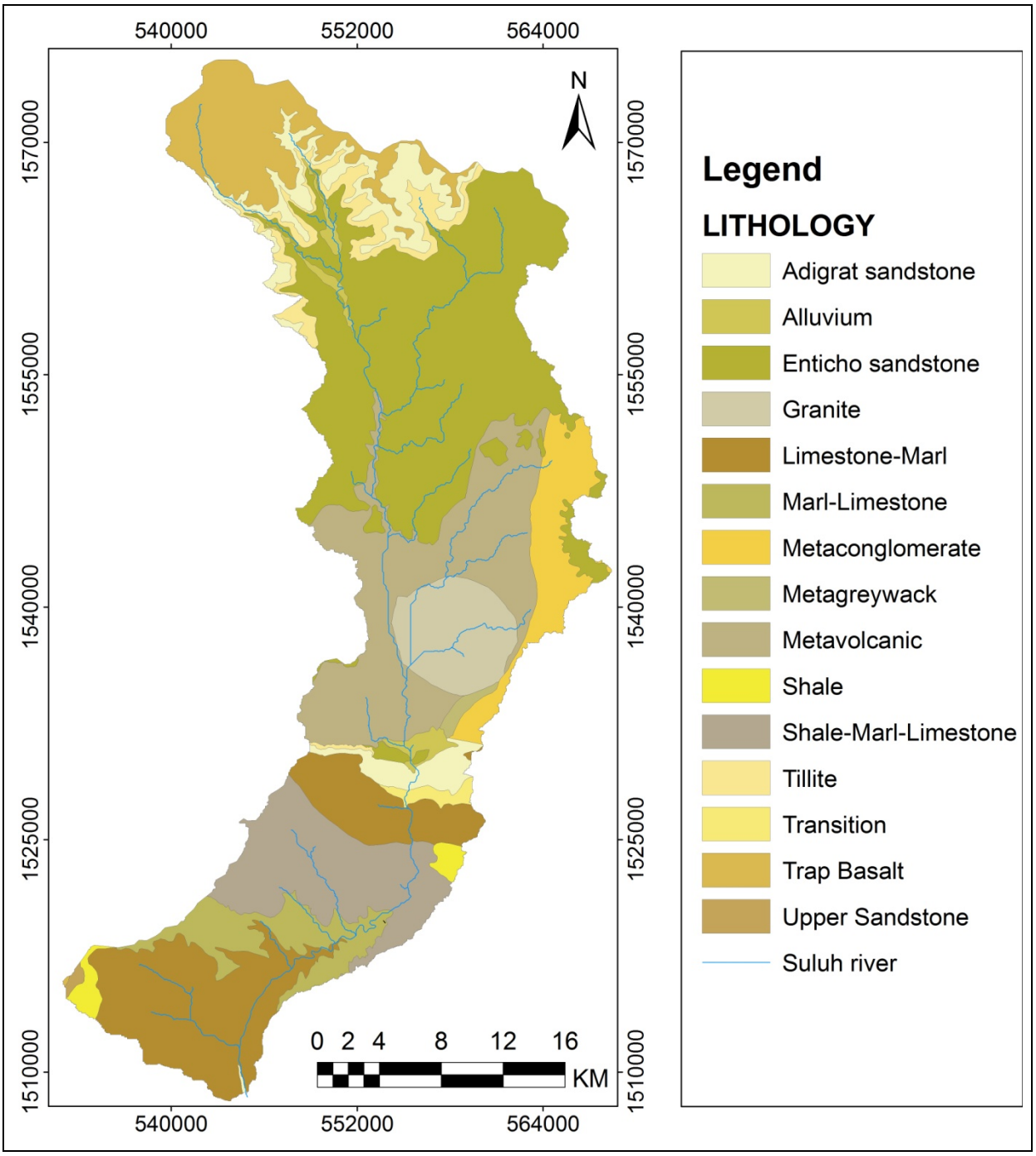

Figure 4-5: Geology of the Suluh basin (data base: Gebreyohannes et al., 2010).

The basement rocks are dominantly found in the middle of the Suluh basin circling Negash village. The area is dominated by three lithological units: the metavolcanic unit of the Tsaliet group, metagrawacky and metaconglomerates (Gebreyohannes et al., 2010). Besides, granites occur, forming a ring type exposure (Figure 4-5).

Table 4-7: Areal coverage of dominant geology (lithology) in the Suluh basin (data source: Gebreyohannes et al., 2010).

Lithology	Area (km^2)	Areal coverage in %
Entichosandstone	280.71	29.06
Adigratsandstone	55.31	5.73
Limestone-Marl	135.21	14.00
Metavolcanic	143.40	14.84
Granite	47.44	4.91
Shale-Marl-Limestone	86.20	8.92
Marl-Limestone	41.48	4.29
Metaconglomerate	46.21	4.78
Trap Basalt	72.53	7.51
Tillite	31.59	3.27
Shale	8.99	0.93
Alluvium	10.51	1.09
Transition	5.11	0.53
Upper Sandstone	1.32	0.14

These basement rocks are usually highly weathered saprolites with relatively high silt contents (HTSL, 1976). The weathering product of the metavolcanic/volcanoclastic rocks are also rich in acidic components, dark grey to brownish in color, and show a fine to medium-grained texture (Gebreyohannes et al., 2010).

Figure 4-6: Metavolcanic outcrops along the Suluh river.

Areas with outcropping Enticho sandstone are characterized by an undulating topography. The Enticho sandstone is whitish, fine to medium grained and with calcareous (locally siliceous) cement which is leached at the surface (HTSL, 1976).

Figure 4-7: Enticho sandstone outcrop along the Suluh river.

The Adigrat sandstone is found near Adigrat in the northern part of the study area, forming steep cliff topography. Weathering products of the Adigrat sandstones are non-calcareous, reddish colored with a high fine sand content (HTSL, 1976; Gebreyohannes et al., 2010).

According to Bosellini et al. (1997), shale-marl-limestone formations are named as transition beds. They are located in the southern part of the study area. The unit consists of sandstone, shale, marl and limestone. It crops out along the road from Aberha Atsebha to Wukro and around Batiakor villege. Quaternary alluvial deposits are mainly found in the flood plains of the Suluh river and its tributaries.

Figure 4-8: Shale-marl-limestone outcrop along Batiakor stream.

4.1.4 Relief and hydrology

Morphometric and geomorphologic properties of the Suluh basin can be grouped in four categories: topographic, areal, relief and network properties (Koshak and Dawod, 2011; Table 4-8). Among others, drainage density indicates the closeness of spacing between channels and is a measure of the total length of the stream segment of all orders per unit area (Koshak and Dawod, 2011). It reflects a balance between erosive forces and the resistance of the ground surface, and is therefore related closely to climate, lithology, and vegetation.

The drainage pattern of the Suluh basin is dendritic and its drainage shape is elongated. Water runs from north to south and turns to southwestern direction just downstream Abreha-we-Atsebha village. The northern and northeastern part of the Suluh basin is steeply dissected and mountains are formed in the trap basalts, which occur west of Adigrat. Altitude varies between 2,500 to 3,000 m a.s.l., locally rising to over 3,300 m a.s.l. The basalts directly overlie the Adigrat sandstones and the landforms are strongly controlled by the erosion of the sandstone, resulting in a linear ridge systems branching out from a central massif (HTSL, 1976). The land has generally very steep slopes, is highly degraded and has initial soils only. The area is unsuitable for agricultural activities.

Table 4-8: Morphometric characteristics of the Suluh basin (data source: Jarvis et al., 2008).

Properties	Value	Reference
Area (A, km^2)	967	
Effective area (EA, km^2)	957	
Basin perimeter (BP, km)	304	
Minimum elevation (Hmin, m)	1769	
Maximum elevation (Hmax, m)	3301	
Mean elevation (Hmean, m)	2350	
Height difference (HD, m)	1521	
Total drainage length (TDL, km)	8203	
Longest flow path length (LFPL, km)	94.77	
Horizontal length (HL, km)	66.60	
Sinuosity (SIN)	1.42	SIN = LFPL/HL (Schumm 1956 in Selby, 1985)
Drainage density (DD, km/ km^2)	8.48	DD = TDL/A
Average basin slope (ABS, %)	14.85	
Slope along drainage line (SADL, %)	1.61	
Hypsometric integral (HI)	0.382	H = (Hmean-Hmin)/(Hmax-Hmin)
Relief length ratio (RLR)	0.023	RLR = HD/HL
Form factor (FF)	0.11	FF = A/$LFPL^2$ (Horton 1932 in Selby, 1985)
Compactness coefficient or shape complex index (CC/SCI)	2.76	$CC = BP/2\sqrt{A\pi}$
Basin elongation (BE)	0.37	BE = [2√(A/π)]/LFPL (Schumm 1956 in Selby, 1985)

The gently undulating plains formed in the Enticho sandstones extend from Negash northwards to Edagahanmus and Hawzen (Figure 4-1). The soil texture is of sandy clay loam to clay loam and soil depth is moderately deep. Shallow soil depth exists where the Enticho sandstone or inliers of basement rocks occur near the surface (Nedaw and Walraevens, 2009).

The lower parts of Suluh basin are characterized by river valleys flanked by steep slopes or cliffs and deeply incised into undulating to rolling tablelands. The dominant bedrock is limestone with locally outcropping shales and marls (Gebreyohannes et al., 2010). The soils, which are formed on calcareous shales and marls, are shallow to moderately deep (HTSL, 1976).

The elevation map (Figure 4-9) shows the high altitudinal difference between the headwater area and the mouth of the river which totals within 95 km 1521 m: Average altitude is 2,350 m a.s.l. Figure 4-10 shows a slightly right skewed distribution of altitude of the Suluh basin. Most of the area of the basin lies in an altitudinal range of 176 to 2,500 m a.s.l. The slope gradient map (Figure 4-11) provides information on the steepness of the slopes; distribution of slope classes show a right skewed distribution (Figure 4-12). The areas with slopes of less than 10° cover 73% of the basin surface. About 25% of the area has moderate slopes with inclinations between 10° and 35°. Approximately 2% of the area show slopes with an inclination steeper than 35°.

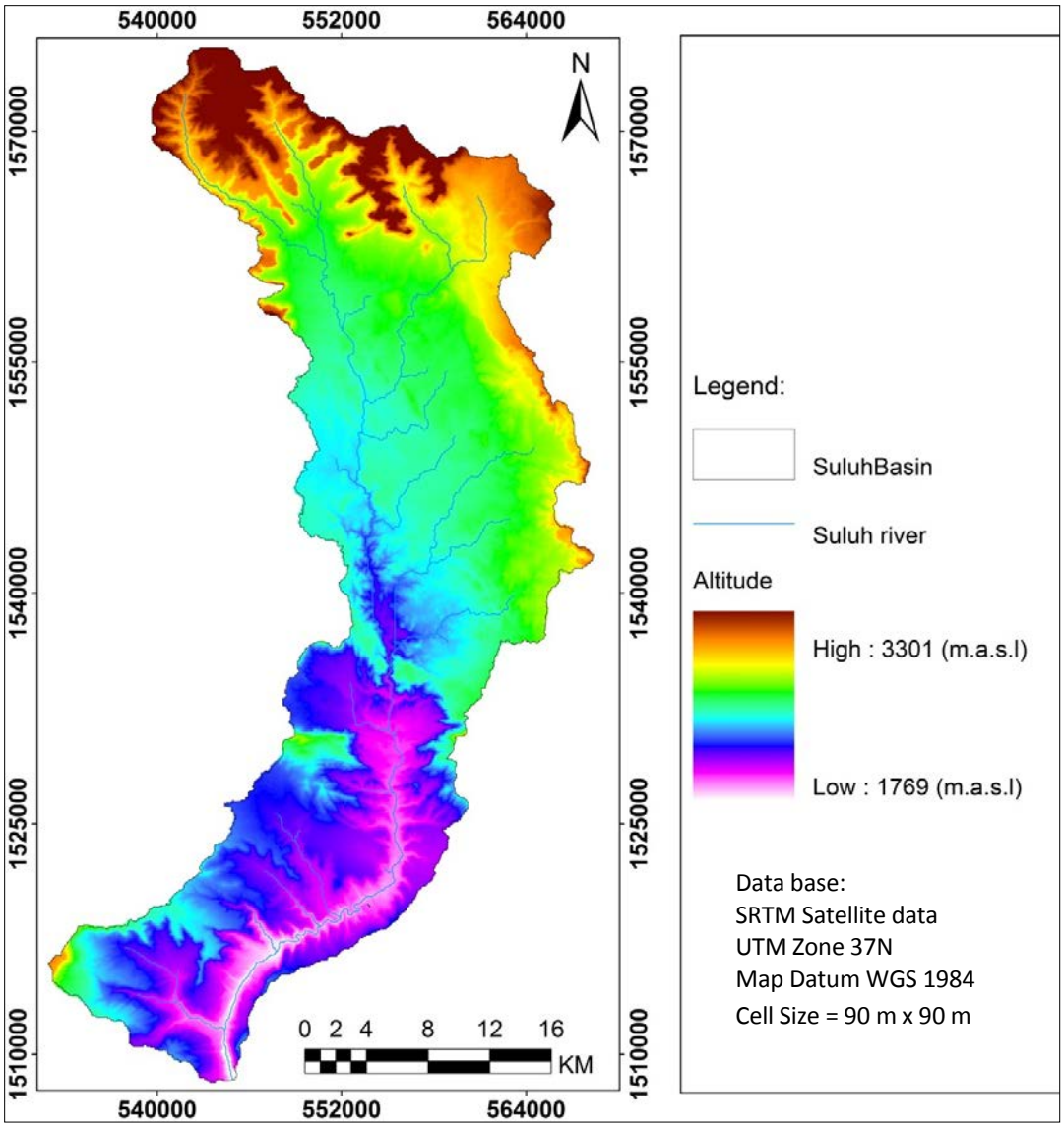

Figure 4-9: Elevation map of the Suluh basin (data base: Jarvis et al., 2008).

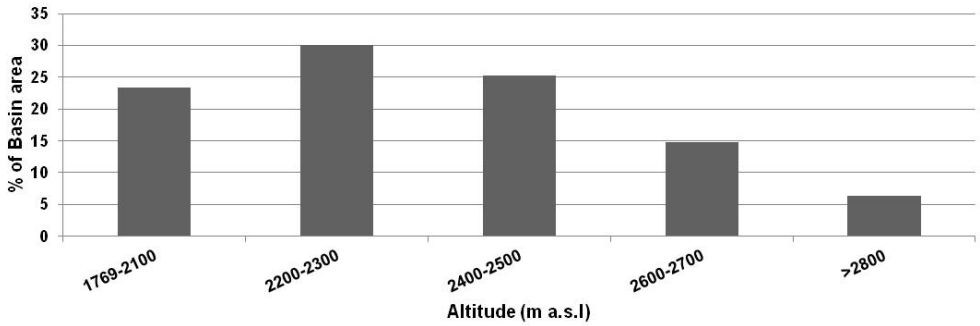

Figure 4-10: Distribution of elevation classes of the Suluh river basin (data source: Jarvis et al., 2008).

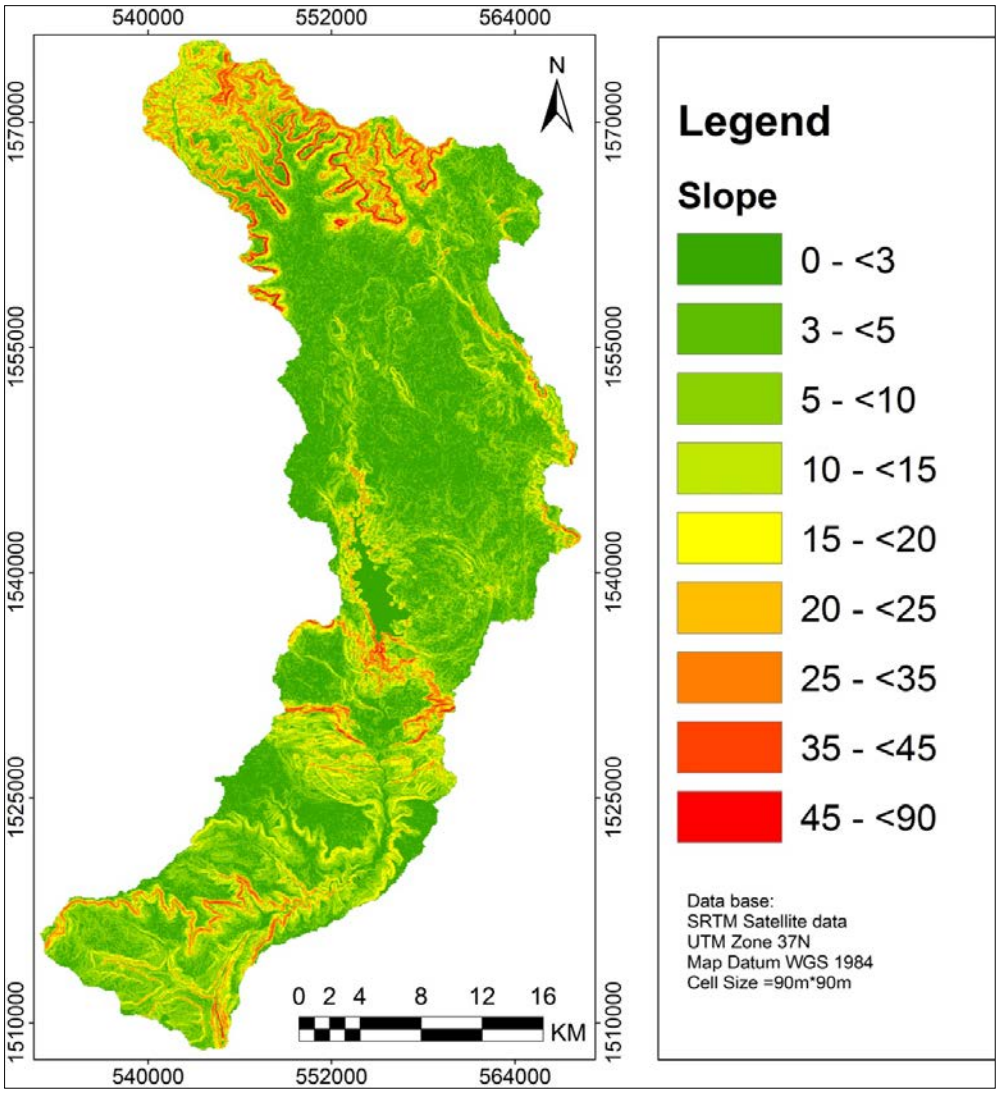

Figure 4-11: Slope gradient map of the Suluh basin (data base: Jarvis et al., 2008).

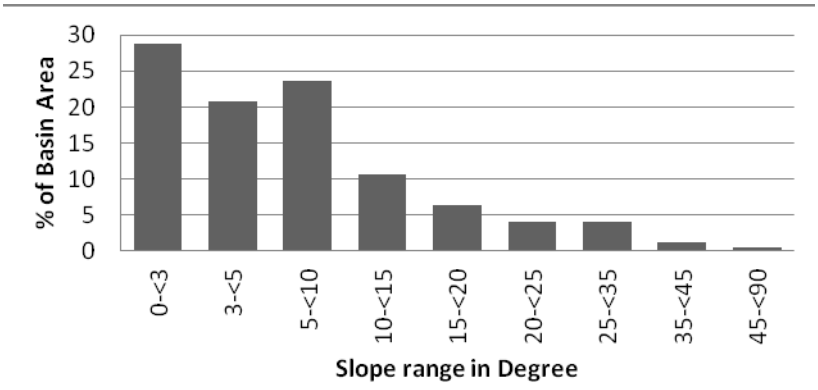

Figure 4-12: Distribution of slope classes of the Suluh river basin (data soure: Jarvis et al., 2008).

The longitudinal profile of the Suluh basin's main stream has a length of 94.77 km starting from an elevation of 2,866 m a.s.l. in the volcanic mountains of Mugulat and ending at the embouchure into Genfel River on an elevation of 1770 m a.s.l. The slope of the stream averages 1.61%. The longitudinal profile of the river (Figure 4-13) indicates a sudden slope break around 40 km upstream, the mouth indicating the transition from metavolcanic series to the Adigrat sandstone; as consequence deep alluvial deposits can be found downstream.

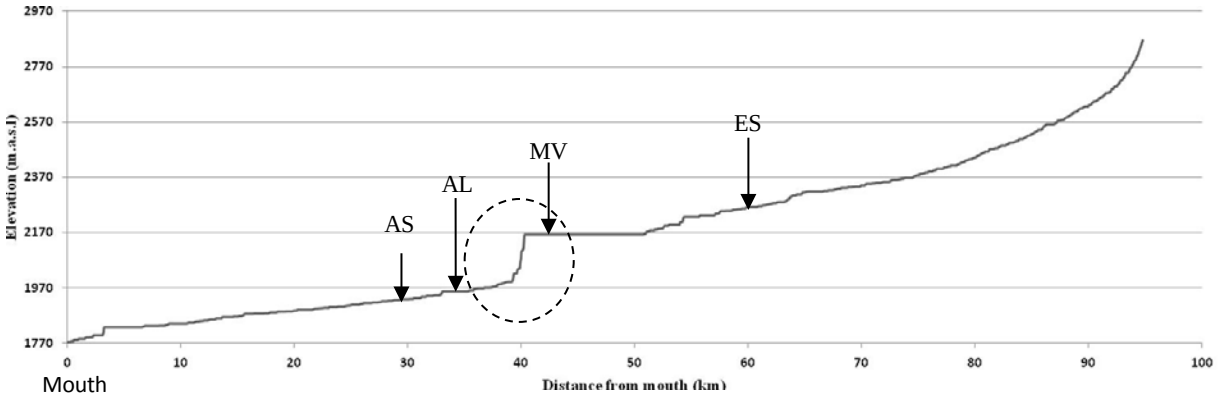

Figure 4-13: Longitudinal profile of the Suluh river: AS=Adigrat sandstone, AL=Alluvium, MV=Metavolcanic and ES-Enticho sandstone (data source: Jarvis et al., 2008 and Gebreyohannes et al., 2010).

Figure 4-14 shows the basin area versus the longitudinal distance of the Suluh river. The breaks in the graph indicate the mouthing of tributaries.

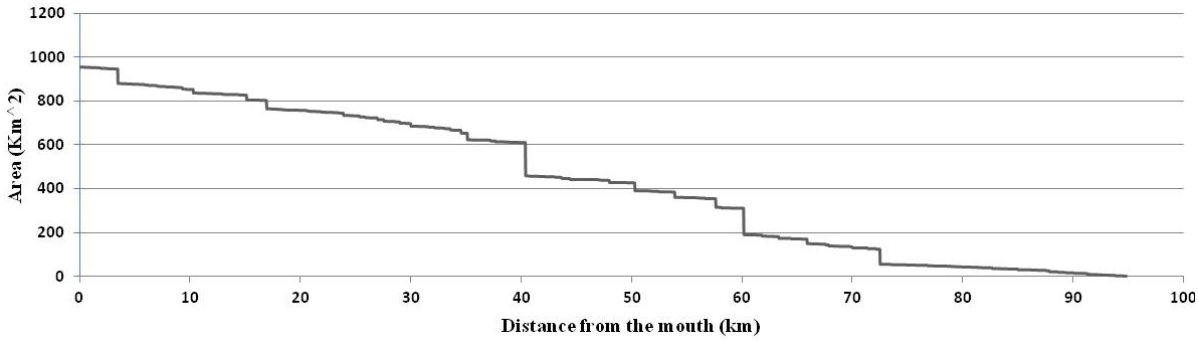

Figure 4-14: Drainage area evolving along the channel course of the Suluh river (data source: Jarvis et al., 2008).

4.1.5 Soils

According to FAO (1998) five major soils types are identified for the study area (Figure 4-15). Lithic Leptosols (silty clay loam) are found in the mountainous part of the study area. Haplic Lixisols (clay loam) can be found at hill foots and in flat undulating areas. Eutric Leptosols (loam) occur in the middle part of the basin while Vertic Cambisols (clay) can be found in the downstream parts of the basin

Lithic Leptosols (silty clay loam) are very shallow soils, limited in depth by bedrock or a continuous cemented layer of 10–25 cm depth. These soils are found dominantly in the mountainous parts of the

Suluh basin, mainly in the headwater area of the Suluh river, and are not suitable for crop production, but farmers use it nevertheless for cultivation due to shortage of arable land (Zenebe, 2009).

Haplic Lixisols (clay loam) are widely spreaded in the Suluh river basin and are predominantly. These soils are found west of the Senkata-Edagahamus road and northeast of Hawzen. Haplic Lixisols occur extensively in freely draining sites especially on the sandy parent materials. They are soils which lack the characteristics of salinity, alkalinity, cracking clay and water logging (HTSL, 1976). The areas are flat to moderately undulating and intensively cultivated. Soil depths range between 25 and 50 cm.

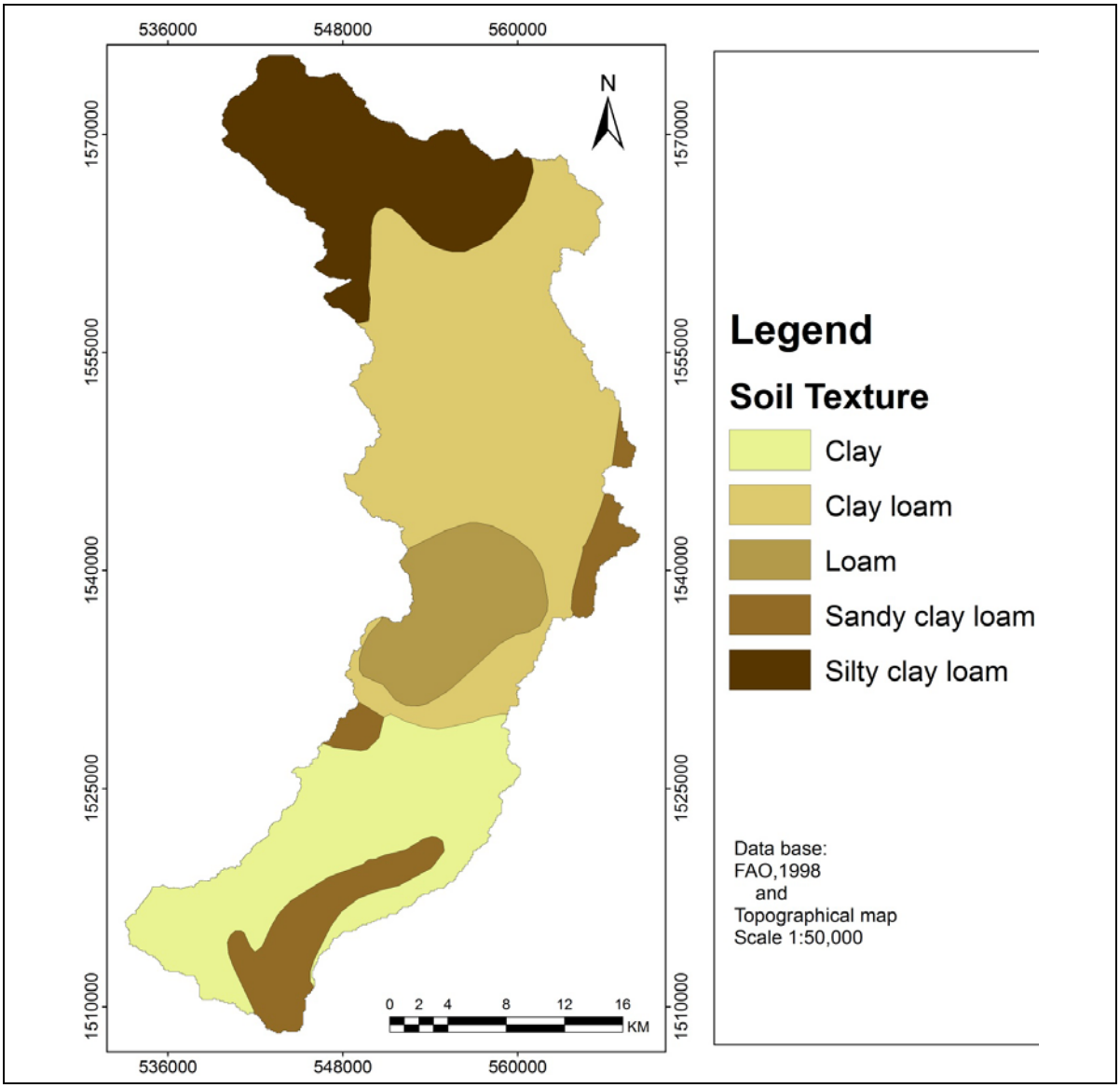

Figure 4-15: Distribution of soil texture in the Suluh river basin (data base: FAO, 1998).

Vertic Cambisols (clay) are found south of the Abreha-we-Atsebha-Hawzen road in the moderately to shallow inclining areas. The soils are shallow with less than 10 cm in depth in the southwest of the basin while in the rest of the area soil depth varies between 25 and 50 cm (FAO, 1998).

According to Nyssen et al. (2007) the major controlling factors for the formation and spatial distribution of soils in the region are the bedrock and the position of the slope. However, soils developed on siliceous parent materials (gneiss, quartzite, ferruginous sandstone, metamorphic and other granitic rocks) degrade very rapidly, especially when they are used for arable production (Wright, 1984).

- Soil data and analysis

The samples were taken from the upper 50 cm of soil since it is the useful root depth for most agricultural crops, and so it is useful for the evaluation of hydrologic parameters (Rabia et al., 2013). Soil texture is an inherent attribute of the soil and the most often used to characterize its physical composition.

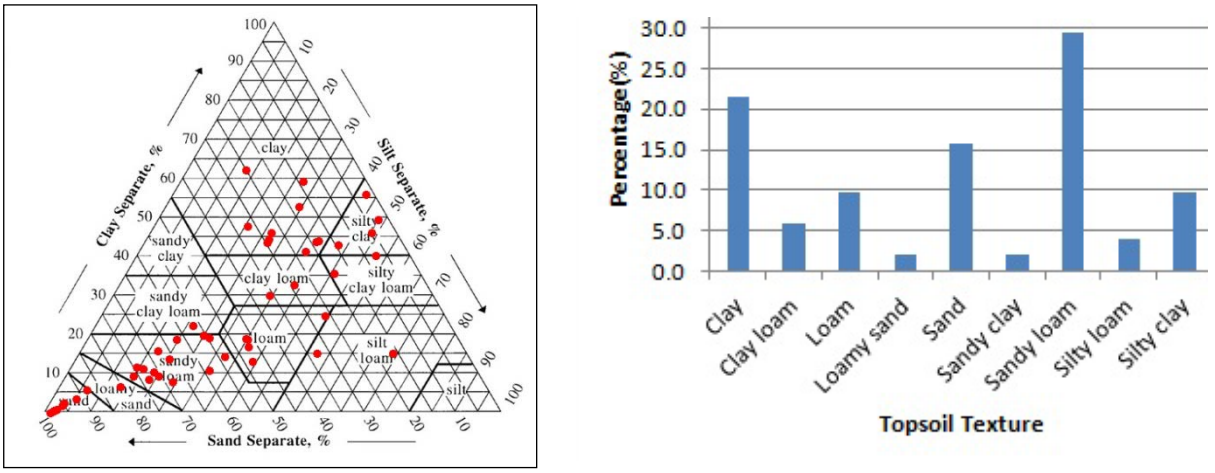

Figure 4-16: Soil texture distribution of the Suluh basin (data source: USDA, 1999).

The dominate soil textures are sandy loam, clay and sand (Figure 4-16). Analyzing the spatial distribution of the different texture classes spatial differences get obvious (Figure 4-17). High contents of sand are observed in the soils in the northern part of the basin. According to HTSL (1976) the area is dominated by the Enticho plateau; the lithology of the area is entirely dominated by Enticho sandstone. The clayey soils concentrate in the southern part of the basin, dominated by the Mekelle and Geba plateaus. Lithology of the area is dominated by Agula marls and shales with locally some limestone occurring. Silty soils predominate around the headwater area around Mugulat and Negash village and in the southern part of the basin. The headwater area is characterized by the Adigrat ridge and is dominated by Tertiary trap basalts and trachytes (HTSL, 1976), while the Negash area is dominated by basement metavolcanics, metasediments and dolomites (Gebreyohannes et al., 2010).

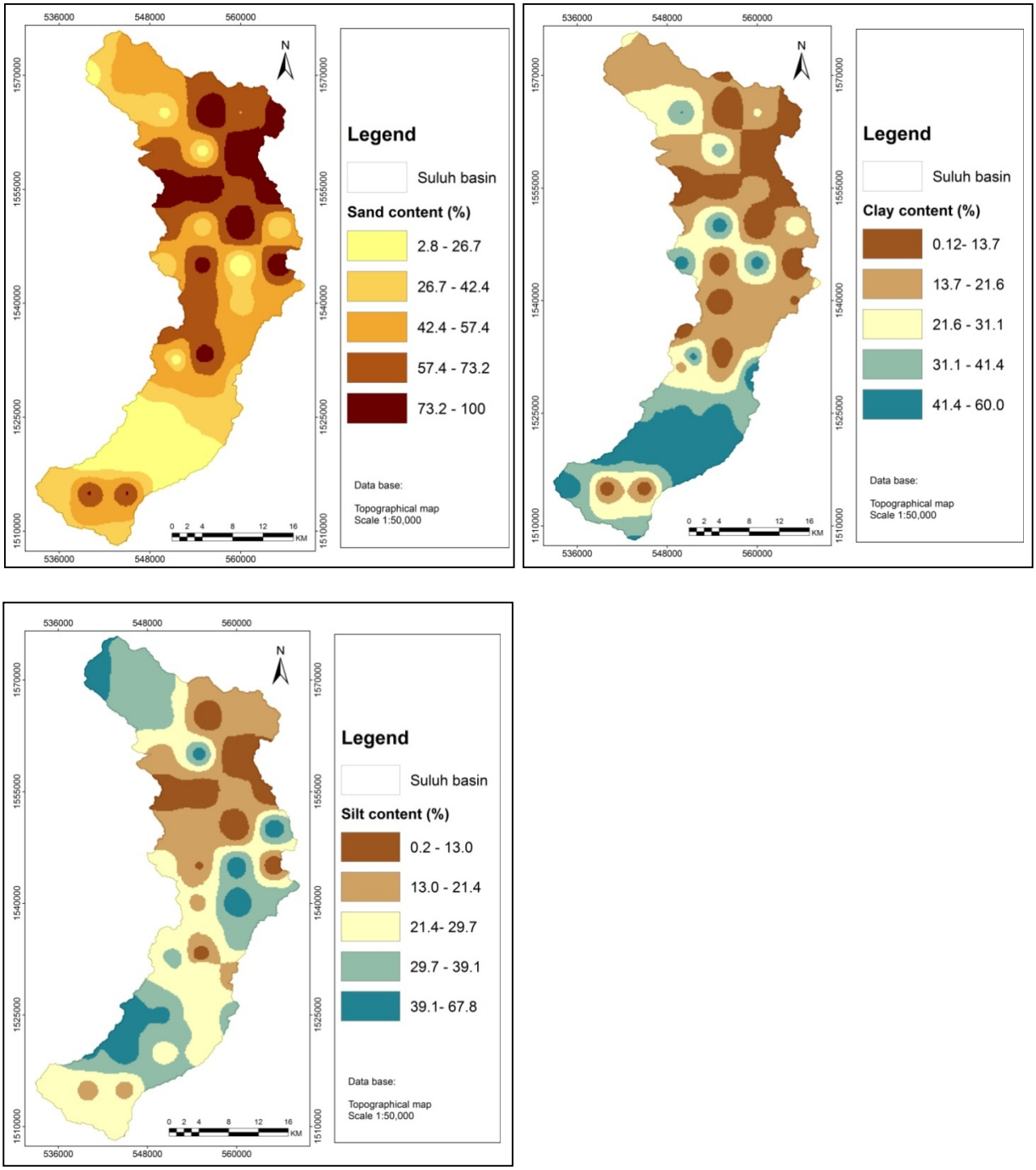

Figure 4-17: Spatial distribution maps of textural fractions: (a) sand content (%), (b) clay content (%), and (c) silt content (%) (data base: EMA).

In general, the spatial distribution of soil texture shows a strong correlation to the lithology of the basin. For example the sand concentrated on Entichio sandstone and Adigrate sandstone whereas the silt content lies at trap basaltic and metasediments and dolomites area. The clay content is concentrated in Agula marls and shales lithology.

4.1.6 Vegetation and land use

Little of the natural vegetation of the highlands remains today. The influence of human and his domestic animals has profoundly altered both, the vegetation and the landscape. Ecological degradation, including deforestation and soil erosion, is widespread particularly in the northern and central highlands of Ethiopia (FAO, 1986). The Suluh basin is highly degraded and the natural woodlands have been largely destroyed (HTSL, 1976). The original Olea Juniperus-Acacia woodland in the headwater of the basin survives only in remote areas on the main mountain ranges locally rise to 3300 m.a.s.l. The lower parts of the Suluh basin are covered by the low thorny Acacia bush and scrub is interspersed in cultivated areas. Edaphic grasslands occur on non-cultivated depression of the Central Plateau (HTSL, 1976).

Severe land degradation in the Highlands of Tigray is induced by dense population, coupled with unchanged agricultural technology causing high stress on the natural resources, including soil and water (Kumasi and Asenso-Okyere, 2011). The process of degradation of the natural vegetation occurs due to overgrazing, as well as the progressive increase in demand for fuel wood and for cultivation (Nyssen et al., 2004). The main effect of the destruction of the natural vegetation has been an acceleration of erosion and a consequent depletion of soil depth and soil moisture (Descheemaeker et al., 2006). Figure 4-18 shows spares bush cover of in the lower part of Suluh basin.

Figure 4-18: Typical major land cover types in the lower part of the Suluh basin.

According to the WAPCOS report (2002), except for the very steep slopes most of the Suluh basin is used for cereal cropping (Figure 4-19). The major cereals cultivated in the area are teff, wheat, maize, barley and millet. However, over large areas of the highlands of Tigray, particularly the Suluh basin, soil erosion and deforestation are the main causes of land degradation.

The land use system can be further separated into subsistence farming based on dispersed individual homestead settlements and nucleated village settlements. Since the country's development is totally dependent on its land resources, the loss of productivity due to degradation has serious implications on social and economic development endeavors (Taha, 2002).

Figure 4-19: Typical cereal cultivation on steep slope at the headwater of Suluh basin.

The Woody Biomass Inventory and Strategic Planning Project (WBISPP, 2003) prepared land use and land cover maps for the whole Ethiopia at a scale of 1:250 000 derived from Landsat ETM+ imagery. They also provide a comprehensive woody biomass stock inventory covering all land cover types. Additionally WBISPP (2003) provides an eight year long annual tree yield study of all major species in the main agro-ecological zones (Figure 4-20).

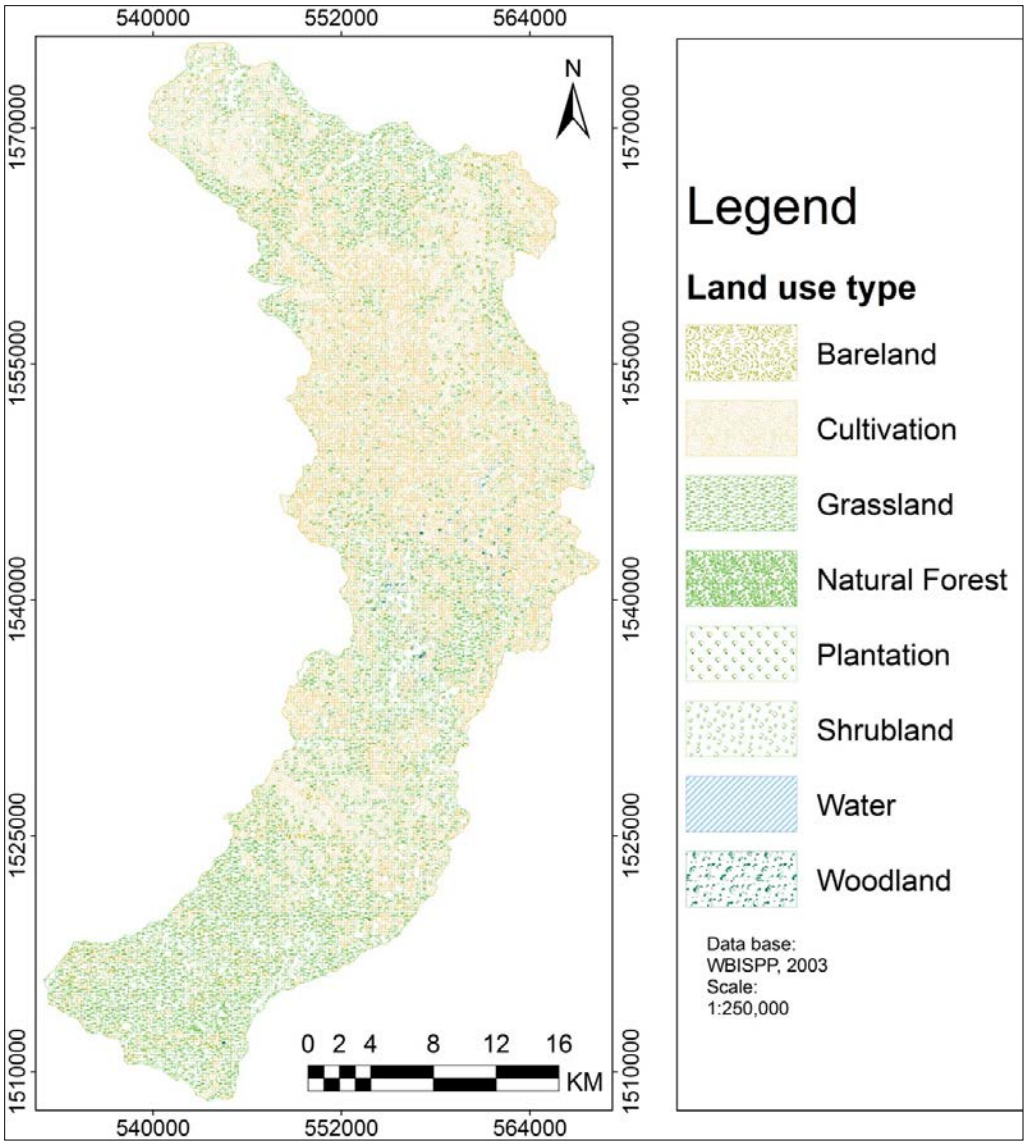

Figure 4-20: Land use and land cover of the Suluh basin (data base: WBISPP, 2003).

According to the woody biomass land use and land cover map, eight major land use and land cover units of the Suluh basin were identified: cultivated land (51.2%), grass land (25.8%), shrub land (20.3%), bare land (2%), woodland (0.6%), natural forest land (0.074%), plantation (0.05%) and water body (0.004%). Based on the above classification the cultivated land takes the dominant share in the Suluh basin.

4.1.7 Soil and water conservation activity

Many areas in the Tigray region are subject to severe soil erosion due to prevalence of steep slopes, erosive rains and overgrazing, all due to population pressure. Hence, the regional government and the people at large exert captured many efforts to restore and conserve the degraded landscapes (Feoli et al., 2002). The major strategies for environmental rehabilitation in the Tigray highlands are the construction of stone terraces, soil bunds, trenches, micro dams including gully treatment, establishment and development of area enclosures and community woodlots, enforcement of used rules, regulations for grazing lands and reduced burning activities (Kumasi and Asenso-Okyere, 2011). Figure 4-21 shows some of the typical soil and water conservation activities carried out in the Suluh basin.

Figure 4-21: Above left: Stone faced soil trench bund, Above right: Trench, Below left: Hill side stone terrace and below right: Area enclosures.

4.2 Test sites

Three sub-catchments of the Suluh basin were selected as test sites (Figure 4-22): Tsenkanet watershed in the Enticho Plateau is characterized by undulating plains, the Abreha-we-Atsbeha watershed in the Atsaf Hills is characterized by steep hills and undulating pediments and the Bat'kor watershed in the Mekelle Plateau shows a undulating to rolling relief.

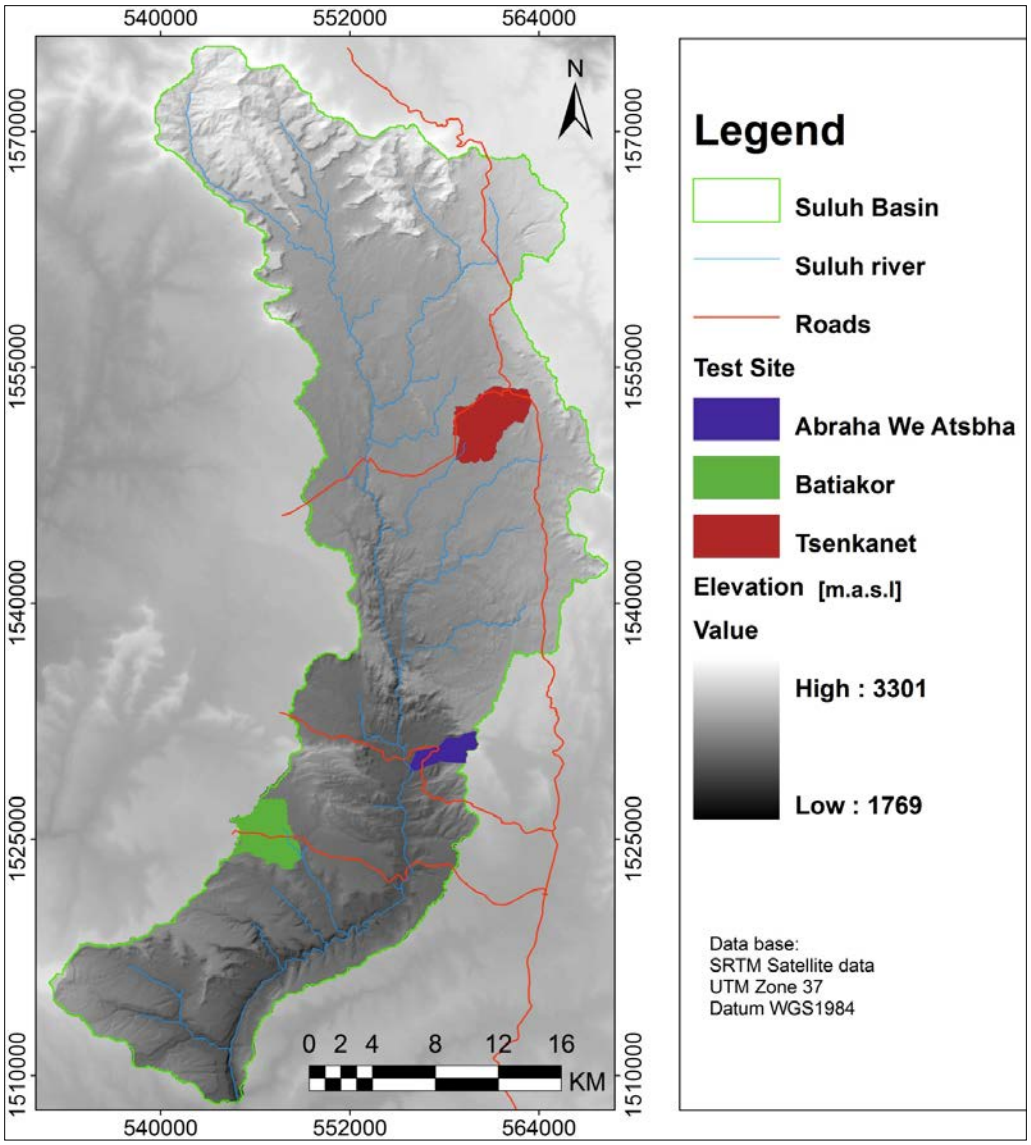

Figure 4-22: Study sites within the Suluh basin (data base: Jarvis et al., 2008 and EMA).

4.2.1 Tsenkanet

The Tsenkanet watershed covers an area of 15.4 km² and its perimeter is 19 km considering Tsenkanet pond as an outlet. Geographically, it is located between 14° 0' 46"-14° 03' 11" North and 39°32' 40"- 39° 35' 11" East in the northeastern part of Suluh basin near Senkata town (Figure 4-23). The stream is a direct tributary of Suluh river and drains the flat undulating agricultural land.

Along the watershed, various settlements are located mostly on the top of smaller hills or in the foot zone of the higher ridges. At the foot of the mountains colluvial sediments occur, whereas alluvial sediments are mainly deposited along the main stream. The Tsenkanet pond is located in the center of the alluvial basin bounded by outcropping rocks.

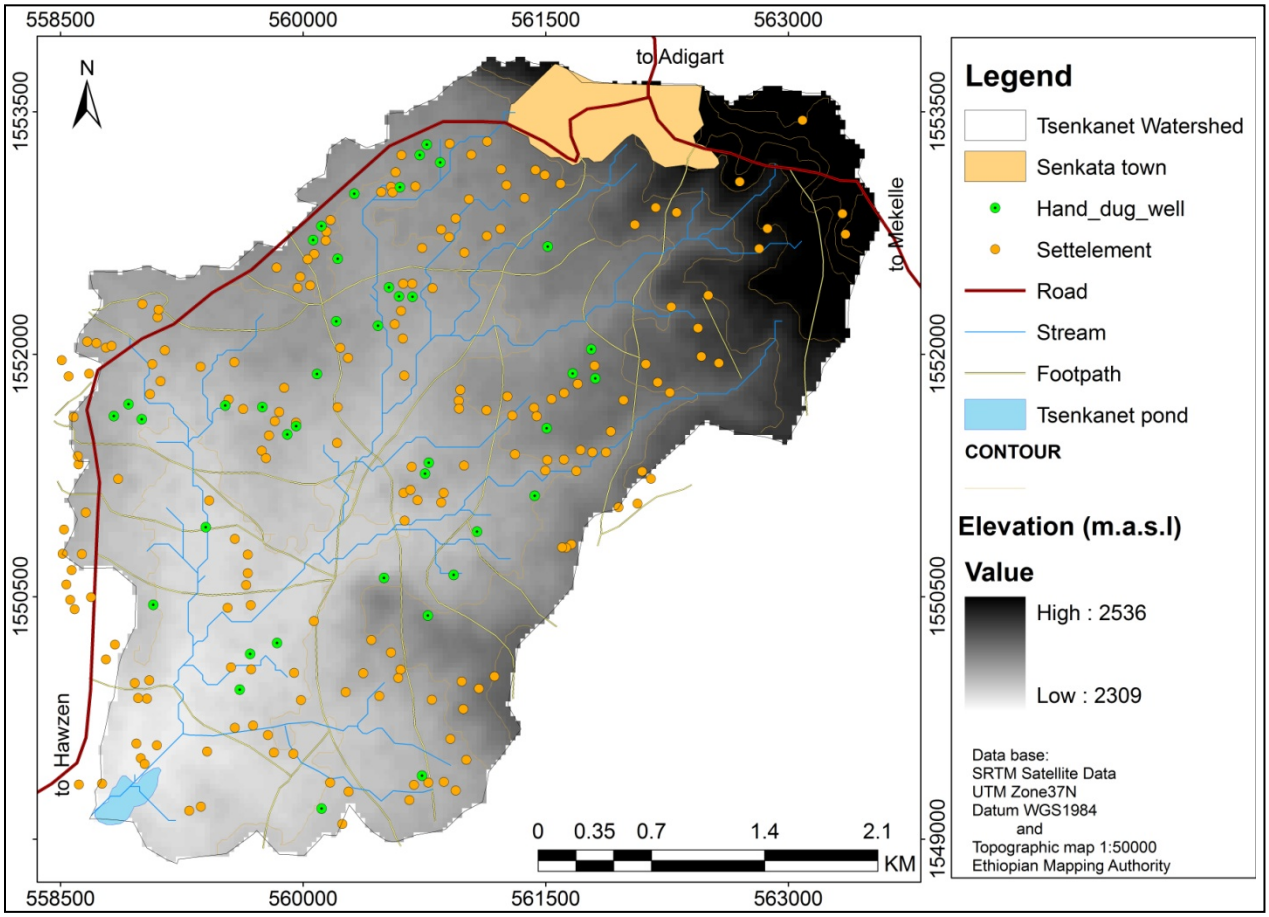

Figure 4-23: Tsenkanet study site: relief and settlement (data base: Jarvis et al., 2008 and EMA).

The landscape is characterized by flat to moderately steep slopes, which alternate with almost flat areas of the alluvium and steep slopes of the headwater area. More than 90% of the area has slopes of less than 15°. The maximum elevation is 2,534 m a. s. l. on the ridge and the minimum 2,325 m a. s. l. at the pond. Relative relief ratio is 3%. The drainage density of the catchment is 2 km/km². The basin length along the principal flow path is 7.23 km.

The climatic condition of the catchment can be characterized as moderately hot and humid (*Weyna Dega*). At Senkata meteorological station the annual temperature averages 18°C and its average annual rainfall is 785 mm (1973–2010). The rainfall regime shows a bimodal rainfall distribution with a lesser maximum spring (*belg*) from March to May and a larger maximum summer (*kiremt*) from June to September.

Two lithological units are found in the study area: Precambrian metavolcanic bedrock and Enticho sandstone (Figure 4-24). The Precambrian metavolcanics corresponds to the metamorphic basement, overlaying by the Paleozoic Enticho sandstone (Nedaw, 2010; Figure 4-25). Due to the cementation of the sandstone and the crystalline character of the metamorphic rocks the groundwater flow of the area is mainly controlled by fractures, only in the new surface saprolithic weathering zones pore water occurs (Nedaw, 2010). During site survey it was identified that more than 40 shallow hand dug wells of 3–4.5 m depth exist in the study area, most of them drying out during dry months.

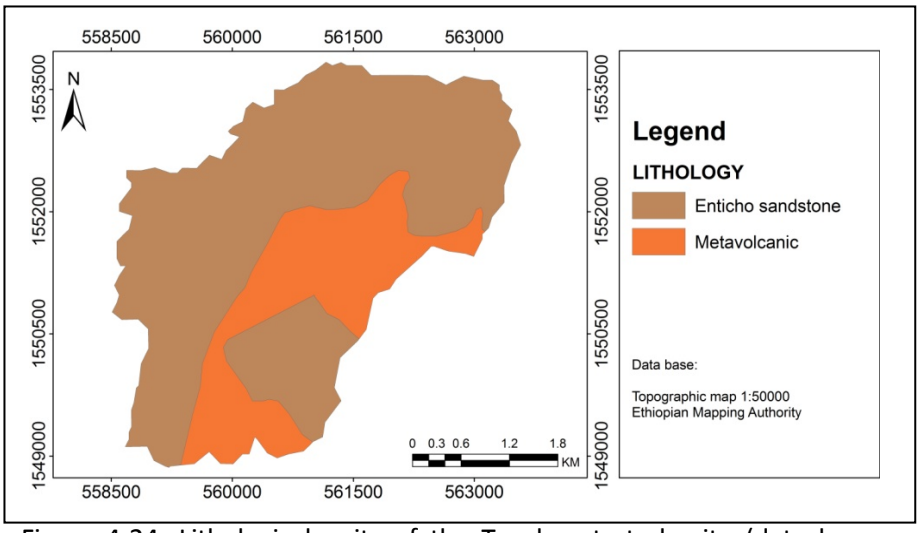

Figure 4-24: Lithological units of the Tsenkanet study site (data base: Gebreyohannes et al., 2010).

Figure 4-25: Rocks outcrops on previously cultivated land in the Tsenkanet study site.

Field survey shows that more than 75% of the study area is covered by clay loam corresponding to the saprolithic weathered Paleozoic sandstone and Precambrian basement rocks, mostly occurring on the moderately undulating slopes and plains (Figure 4-26). Soil depth varies between 50 cm to 100 cm. The clay soils occur predominantly in the alluvium plains. They vary in depth from 100 cm to 200 cm (Figure 4-27). Sandy clay and sandy clay loam soils can be mostly found in the upland and hillside part of the catchment. Generally, these soils have a limited areal coverage and are characterized by a shallow depth and repeated rock outcrops that document their strong degradation.

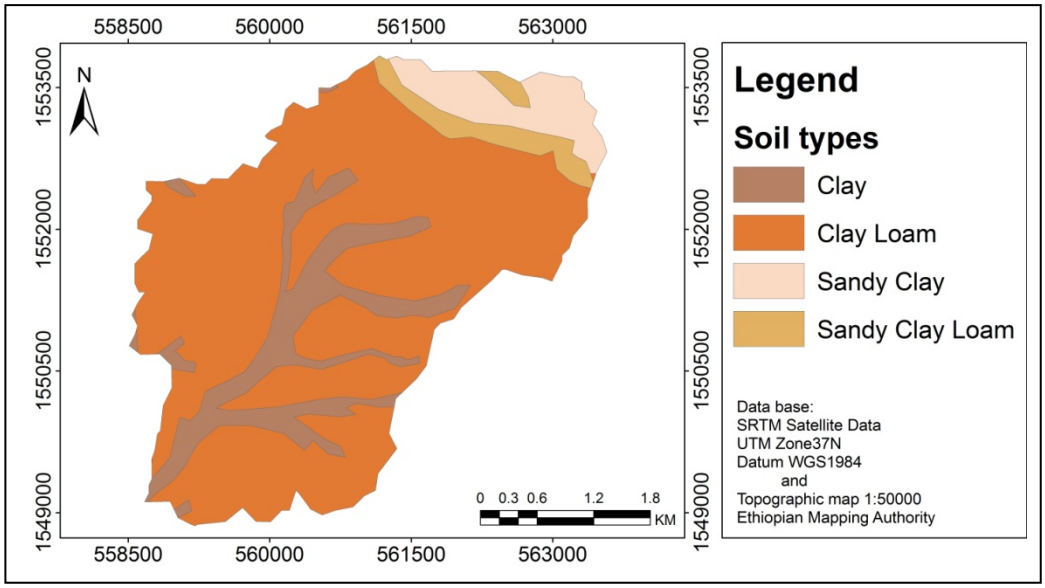

Figure 4-26: Soil map of the Tsenkanet study site (data base: Jarvis et al., 2008 and EMA).

Figure 4-27: Major soil types in the Tsenkanet study site: Left: Eutric Vertisols, Right: Eutric Cambisols.

Around Tsenkanet most of the vegetation is very sparse. The hillside is generally bare, with very thin soil patches systematically lacking organic horizons as a consequence of soil erosion processes. Sparsely distributed, some native big and old trees with some religious function remain as well as small forests around churches. Tree like eucalyptus has been planted in wetter areas. The original native olive trees have largely disappeared, however recently efforts have been made for their revival. Cultivated land dominates the catchment; only the alluvial plain is used as grazing land (Figure 4-28).

Figure 4-28: Different land use types in the Tsenkanet study site: Above left: Terraced hillside, Above right: Grazing land and below left: Cultivated land.

Figure 4-29 shows the transects that have been conducted to provide a general overview on the study area's geomorphological units and their soil and land use characters.

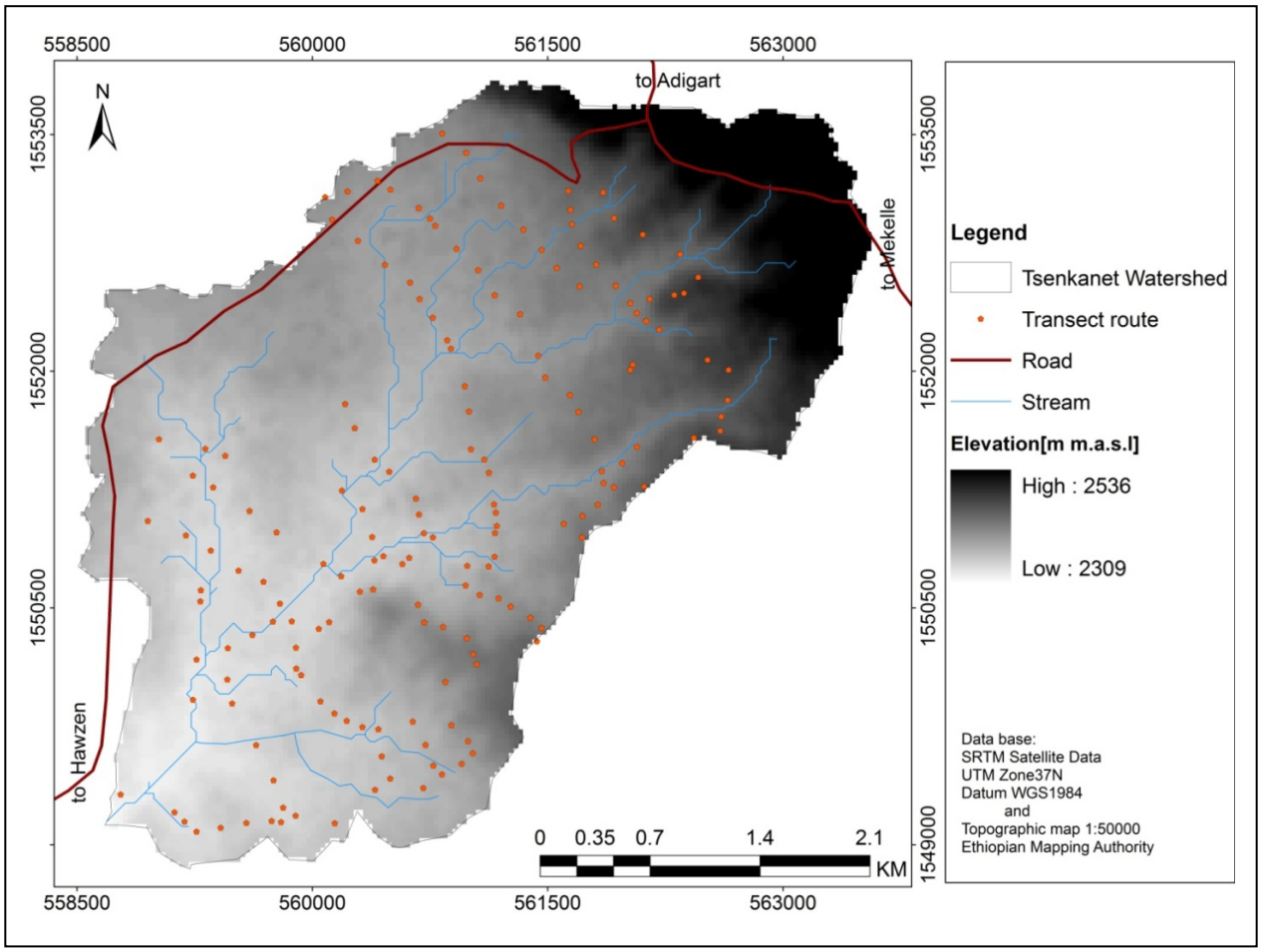

Figure 4-29: Transect route during field survey (data base: Jarvis et al., 2008 and EMA).

Field survey shows that a gully system occurs along the colluvial zone following footpaths; in the alluvial plain their incision is less measured (Figure 4-30). Most settlements are scattered all over the catchment, being usually located on the most favorable topographic locations, such as flat interfluves surfaces and foot slopes or colluvial deposits. Generally, relief forming processes are mainly controlled by human intervention and water erosion (Coltorti et al., 2009). In the colluvial deposits at the foot slopes most subsistence farming activities are practiced; the resulting soil erosion causes shallow soil and frequently outcropping bedrock.

The main geomorphological processes in the region are gravity-driven mass movements and slope erosion due to running water (Coltorti et al., 2009). They affect human activities, especially in terms of agriculture and infrastructure management. The geomorphological units of Tsenkanet watershed are controlled by weathering and soil erosion processes (Figure 4-31). The headwater area corresponds to an upland plateau formed in the Enticho sandstone. The Mekelle-Adigrat road crosses this area, along with it multiple settlements occur.

Figure 4-30: Gully formation on the colluvial zone in the Tsenkanet study site.

Since the road is constructed across the natural drainage system, multiple gullies developed immediately down slope of the road segment. In steep slopes, weathering products (regolith), are transported and deposited down slope to form colluvia. In the Tsenkanet watershed colluvial deposits consist of massive sands, clay and silts with scattered debris fragments. Alluvial deposits are occurring in the lower landscape position, mainly deposited alongside shallow, low grade stream areas.

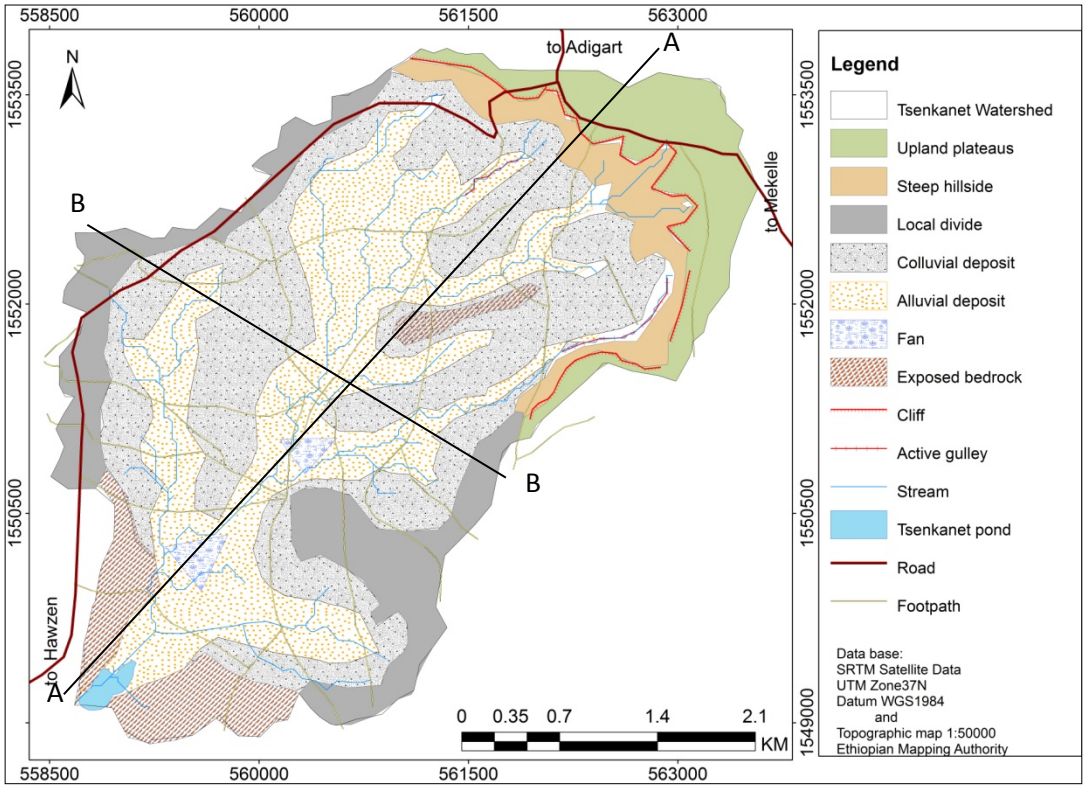

Figure 4-31: Geomorphological unit of the Tsenkanet watershed (data base: Jarvis et al., 2008 and EMA).

Longitudinal and cross-sectional profiles (Figure 4-32 and 4-33) indicate the general form of the landscape units. The profiles indicate the convex, concave, straight and irregular slope forms of the watershed. In general profile curvature indicates two basic processes: convex (cx): predominance of mass movement, and concave (cv): predominance of processes controlled by running water.

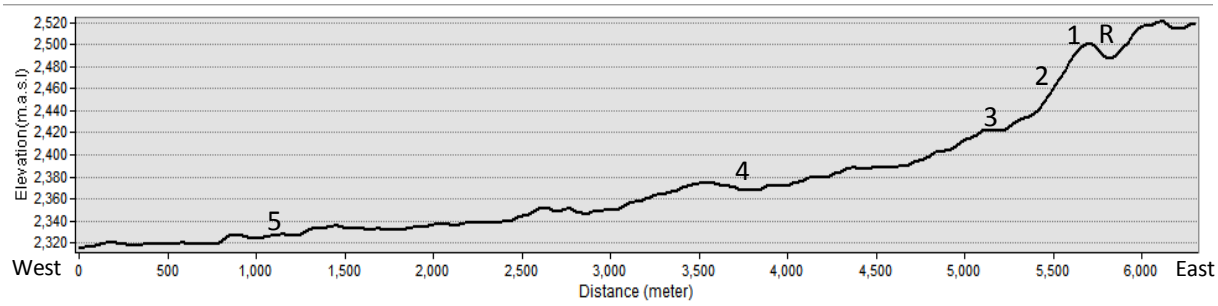

Number	1	2	3	4	5
Slope form (curvature)	Convex (cx)	Straight (str)	Concave (cv)	Concave (cv)	Straight (str)
Soil type	Sandy clayclay	Sandy clay loam	Sandy clay loam	Clay loam	clay
Lithology	Enticho sandstone[1-4]			Metavolcanic[4-5]	

Figure 4-32: Longitudinal profile for section AA (location see figure 4-31), R = Road Mekelle to Adigrat (data source: Jarvis et al., 2008).

The cross-sectional profile across the natural watershed indicates the number of streams, interfluves and slope processes among stream sides.

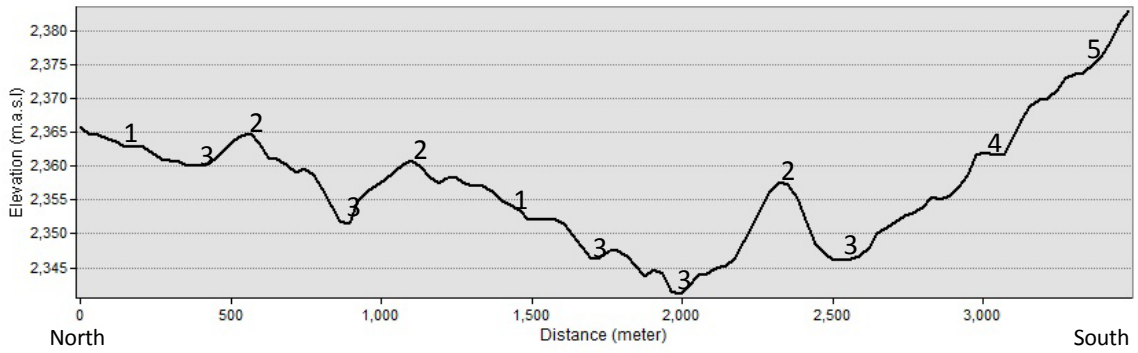

Number	1	2	3	4	5
Slope form (curvature)	Straight (pstr)	Convex (cx)	Concave (cv)	Straight (pstr)	Convex (pcx)
Soil type	Sandy clay	Sandy clay loam	Sandy clay loam	Clay loam	clay
Lithology	Enticho sandstone[1-4]			Metavolcanic[4-5]	

Figure 4-33: Cross-sectional profile section BB (location see figure 4-31) (data source: Jarvis et al., 2008).

4.2.2 Abraha-we-Atsbeha

The Abraha-we-Atsbeha area is located in the central Suluh basin. It is bounded between 13° 50' 01" - 13° 51' 25" North and 39°31' 05"- 39° 33' 20" East. It covers a total area of 5.4 km^2 and its perimeter is 12.8 km (Figure 4-34). The stream is a direct tributary of Suluh river. The landscape is characterized by flat to undulating slopes in the downstream part of the catchment, which is dedicated for intensive cultivation. The headwater area is generally mountainous with steep slopes. 51.4% of the area has slopes with less than 15^o inclination, 31.5% of the area has an inclination in between 15^o to 30^o and 14% of the area has an inclination of more than 30^o. The maximum elevation is 2539 m a.s.l. on the ridge and the minimum 1948 m a.s.l. at the embouchure in to the Suluh river; relief ratio is 12%. The drainage density of the catchment is 3 km/km² and its basin length along the principal flow path is 4.88 km.

Abraha-we-Atsbeha belongs to the historical areas of Ethiopia, particularly characterized by rock churches. Human settlements in the area have a long lasting history. Human settlements are scattered around on the colluvial and alluvial deposits and are forming nucleated villages along the divide.

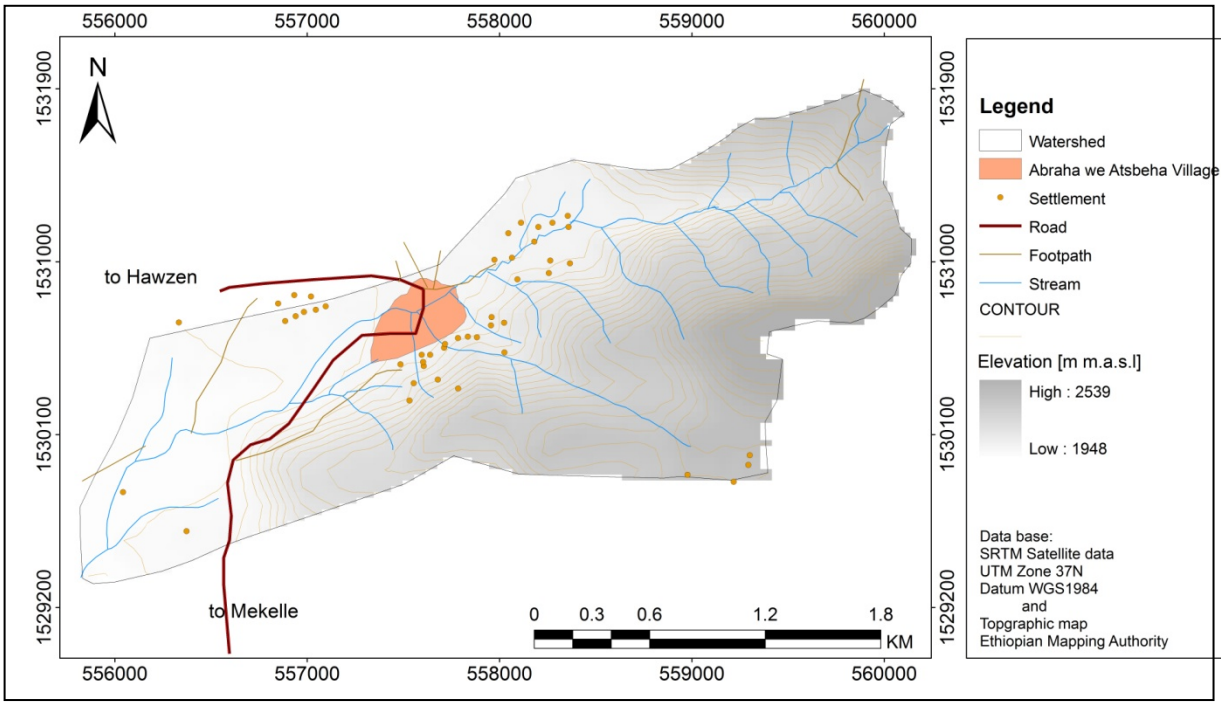

Figure 4-34: Abraha-we-Atsbeha study site: relief and settlement (data base: Jarvis et al., 2008 and EMA).

Data from the meteorological stations of Wukro and Hawzen show, that the rainfall regime is unimodal with a main rainy season in summer (*kiremt*) from June to September while the rest of the months are dry. The annual temperature average is 19^{o}C and its average annual rainfall is 585 mm (1973–2010).

Lithological units found in the area are Metaconglomerates, Enticho sandstone, Limestone-Marl, Adigrat sandstone and Alluvium (Gebreyohannes et al., 2010). Adigrat sandstone dominates the

eastern part of the area and forms a steep to very steep cliff topography and covered with scattered trees and bushes. Besides, the area is subjected to the east-west striking Wukro fault that affects the Precambrian basement, as well as the Phanerozoic and Mesozoic units and passes through the central part of the catchment (WAPCOS, 2002).

Soil texture distribution shows that most of the area is dominated by sandy clay loam and loamy sand (Figure 4-35). Sandy clay loam occurs in the hill sides and headwater areas with Adigrat sandstone as parent material and is covered by sparse bush land. Loamy sand is found along the stream beds in the alluvial deposits, and is highly suitable for agriculture.

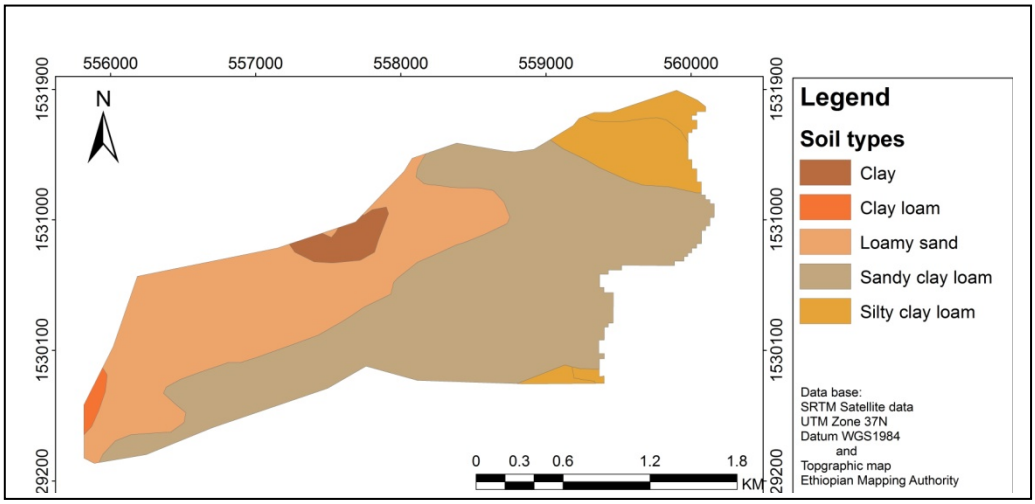

Figure 4-35: Soil map of the Abraha-we-Atsbeha study site (data base: Jarvis et al., 2008 and EMA).

The human impact on the geomorphological processes of the Abraha-we-Atsbeha is very high. Sand quarrying is one of the major activities of the population and results in the disturbance of the river morphological system and aggravating soil erosion (Figure 4-36). Abraha-we-Atsbeha is also exemplary in terms of the occurrence of soil and water conservation measures as well as water harvesting activities. It is known that intensive soil conservation activities result in the regeneration of natural vegetation and improve the microclimate of the watershed (Flint et al., 2010). However, most of the soil conservation measures were traditionally built in the alluvial zone and are at present severely damaged, cause severe downstream scour and a migrating channel due to the unstable behavior of river banks.

Deforestation and land degradation also severely affect the catchment. Recently planted trees follow the soil and water conservation activities. Areal enclosure systems and irrigation areas for fruits and vegetation cropping at household level have significantly revived the vegetation cover of the area. The vegetation is dominated by thorn bushes and cactus; grow in drier, slopy areas. Big trees with broader leaves such as Fig and Eucalyptus grow around water points and along the main stream in the flood plain area. Generally, the land use pattern in the catchment can be grouped into intensively cultivated land with scattered trees, woodland with scattered shrubs, grazing land, scattered settlement of rural communities (village) and rock outcrops.

Figure 4-36: Above left: Sand quarry on stream bed, Above right: Stream bank instability and Below left: Gabion work across stream.

The steep hillsides of Abraha-we-Atsbeha watershed are dissected by a number of gullies which are surrounded by sharp cliffs and sparsely covered with shrubs. The cliff is highly exposed to mass wasting and mass movements. The main stream is incised and forms a v-shape valley in the headwater area and a wide u-shaped valley in the downstream area with a distinct alluvial zone and a meandering channel.

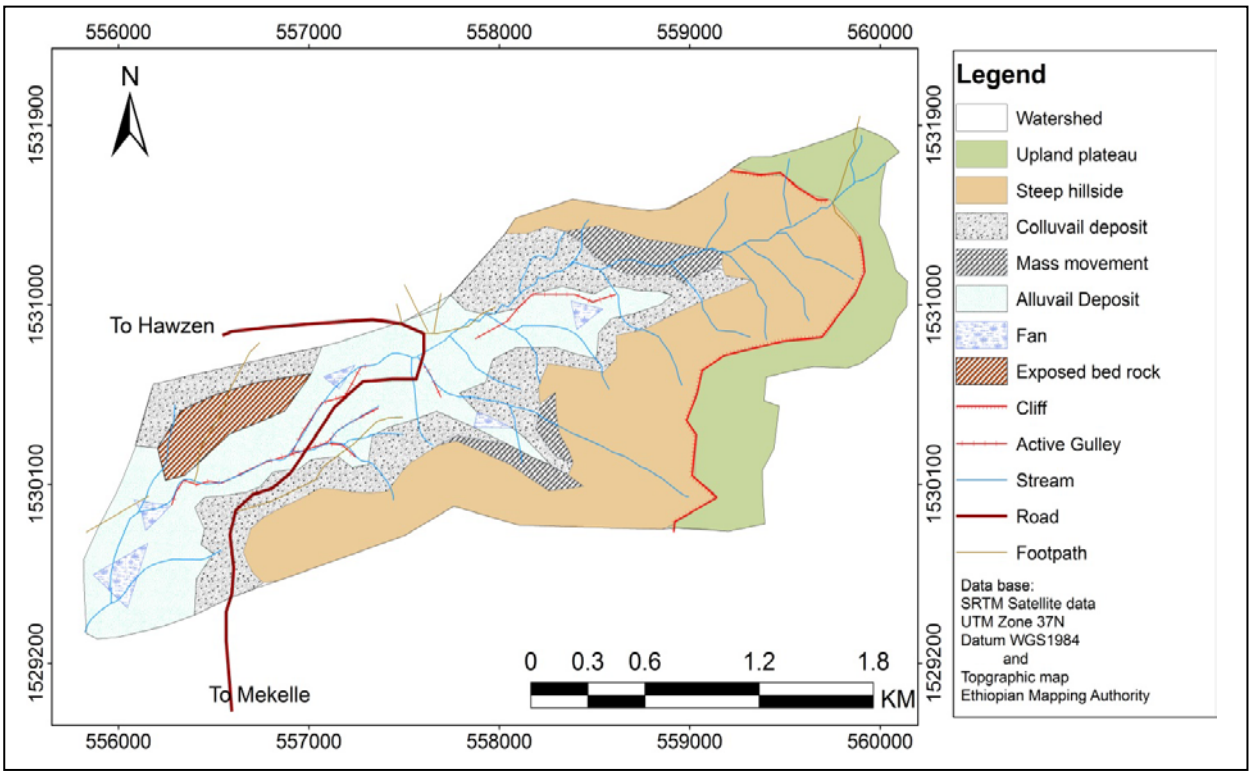

Figure 4-37: Geomorphological units of the Abraha-we-Atsbeha study site (data base: Jarvis et al., 2008 and EMA).

4.2.3 Bat'akor

The Batiakor watershed is located in the southwestern part of the Suluh basin. It is bounded between 13° 46' 40"-13° 49' 06" North and 39°26' 49"- 39° 25' 48" East. It has a total area of 12.2 km^2 and its perimeter is 23.46 km (Figure 4-38). It is accessible by the all-weather road from Wukro to Tsegareda village.

The landscape is characterized by flat to undulating slopes in the headwater area, which are dedicated to intensive cultivation. The lower course of the main stream is deeply insected, forming steep slopes with mountainous relief. 89.3% of the Batiakor area has slopes of less than 10^o inclination, 10.5% of the area has slopes in between 10^o to 25^o inclination and only 0.2% of the area has slopes with more than 25^o inclination. The maximum elevation is 2,195 m a. s. l. in the headwater area and the minimum 2,036 m a. s. l. at the embouchure into the Batiakor stream. The relief ratio of the watershed is 3.3% and its basin length totals 4.75 km. The drainage density of the watershed is 2.4 km/km^2.

Settlements are scattered in the colluvial zone and upland plateau and are concentrated in the peripheral parts of the relatively deep incised valley (Figure 4-38).

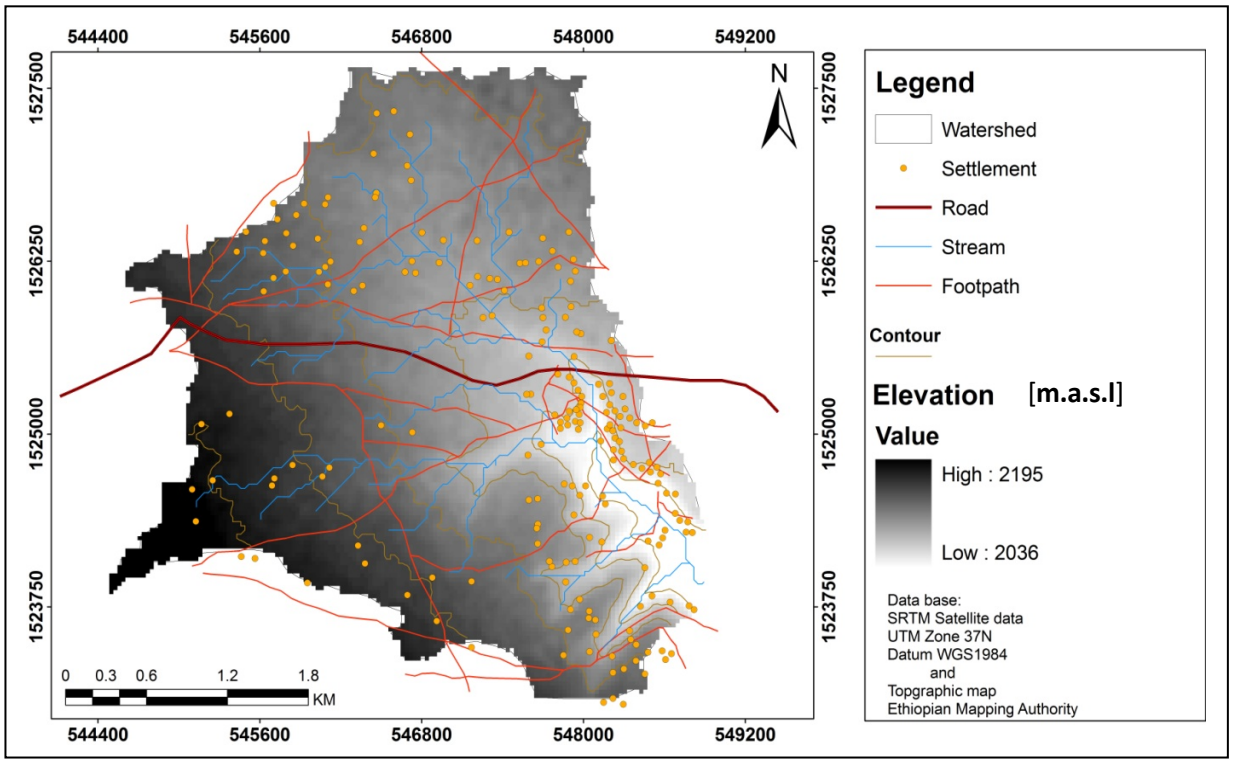

Figure 4-38: Bat'akor study site: relief and settlement (data base: Jarvis et al., 2008 and EMA).

Since there is no meteorological station in the study site, the climatic conditions of the Batiakor watershed are estimated with the help of New_LocClim, which was used to present the local climatic conditions from FAO data base. New_LocClim is a software program with an extensive database that provides estimates of average climatic conditions at locations where weather observations are not available (FAO, 2010). The rainfall pattern in the area is unimodal with an average annual rainfall of 620 mm. The main rainy season is from June to Mid-September, also known as *Kiremt* with a mean annual temperature of 18°C.

Shale-Marl-Limestone is the dominant lithological unit in the area, which outcrops along the main channel. Typical soils that develop on the limestone are Calcic Luvisols in the slope positions and Eutric Cambisols in the flatter areas. The depth of the soils varies from shallower in the upland plateau to deep in the alluvium zone.

The dominant land use in the watershed is rainfed agriculture. The main crops cultivated are wheat, teff and barley. However, there are also small patches of bush land with limited areal extent in the southwest of the watershed around the churches. Small patches of communal grazing land occur in the valley bottom. Small scale irrigation is practiced in the valley bottom.

Most of the drainage basin has a plateau like relief which is totally dedicated for intensively cultivated land use (Figure 4-39). The stream network is well developed and starts along the rolling hills of the catchment. Footpaths contribute to the formation of discontinuous gullies in the watershed. The steep hillsides of the eastern Bati'kor watershed are highly controlled by soil conservation measures mainly by old stone band and newly constructed hillside stone terraces. The cliff is highly exposed to mass wasting and mass movements.

The main stream is incised and forms a v-shaped valley in the headwater area; in the downstream part of the watershed a wide u-shape valley is formed with unstable stream banks and a meandering channel in the alluvial zone.

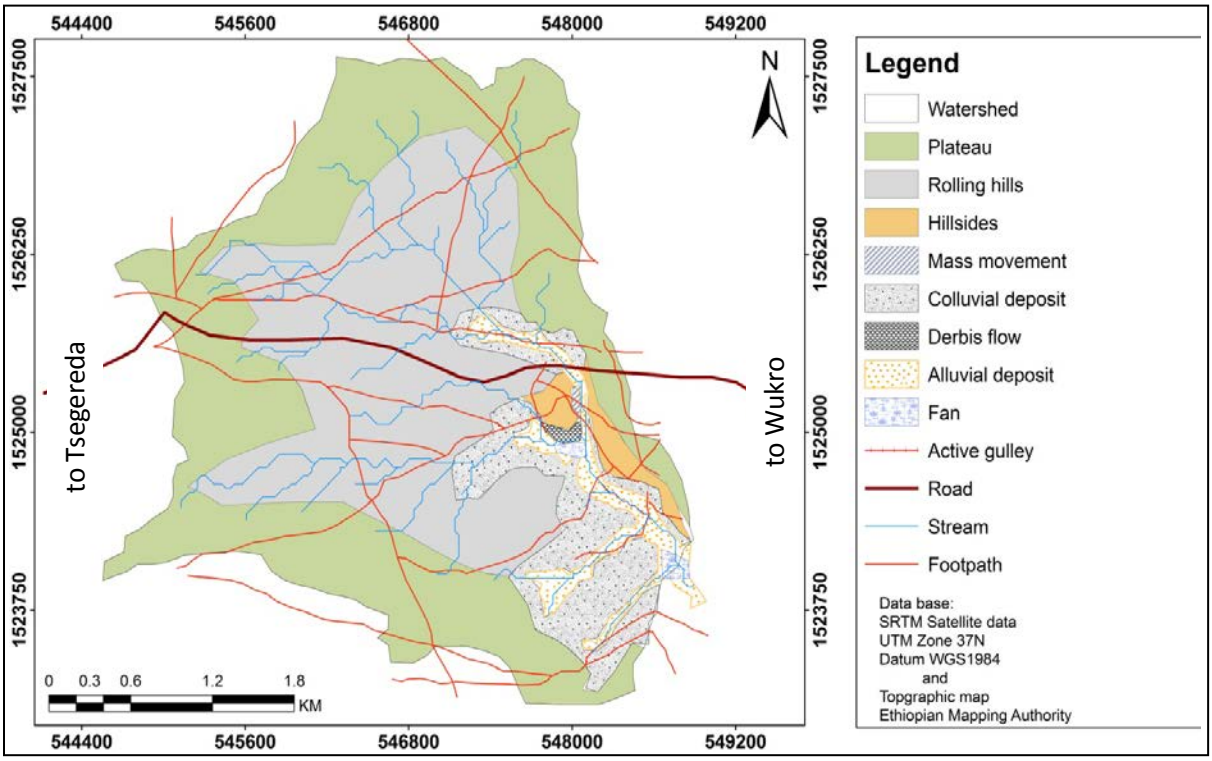

Figure 4-39: Geomorphological units of the Bat'akor study site (data base: Jarvis et al., 2008 and EMA).

Chapter 5

5 Land use and land cover and climate change scenario

5.1 Land use and land cover change

The spatial distribution of land cover change within of the Suluh basin from 1972 to 2003 considers the woody biomass project land use and land cover map from 2003 (WBISPP, 2003) (Figure 5-2). Table 5-2 shows the basin-wide cover change between 1972 and 2003. From 1972 to 1986 the greatest land cover changes occurred with rapid loss in natural forest and bush land, which were converted into cultivated land. Additionally, significant bare land also transformed into cultivated and grazing land. Similarly, between 1986 and 2003 all of the natural forest was converted into cultivated land. Exceptionally, shrub land increased in the period from 1986 to 2003 with an average rate of 1.57% per year (Table 5-2). The probable reason is due to the regional government policy of environmental rehabilitations program including the implementation of area enclosures and the protection of degraded land resources from grazing or cultivation (Reda, 2007; Nyssen et al., 2008). Especially since 1991 the regional government and the local population have put special effort in the rehabilitation and development of the region's natural resources (Tafere, 2002).

Table 5-1: Classification accuracy report.

Accuaracy totals						Kappa statistics
Class name	Reference totals	Classified totals	Number correct	Producers accuracy	Users accuracy	Conditional Kappa by category
Forest land	2	1	1	50,00%	100,00%	1,000
Grazing land	5	6	5	100,00%	83,33%	0,8182
Mixed landuse	7	6	5	71,43%	83,33%	0,8113
Bareland	10	15	9	90,00%	64,29%	0,5714
Bushland	9	10	8	88,89%	80,00%	0,7647
Cultivated land	25	22	21	84,00%	95,45%	0,9221
Totals	59	60	50			
Overall	83,33%					0,7814

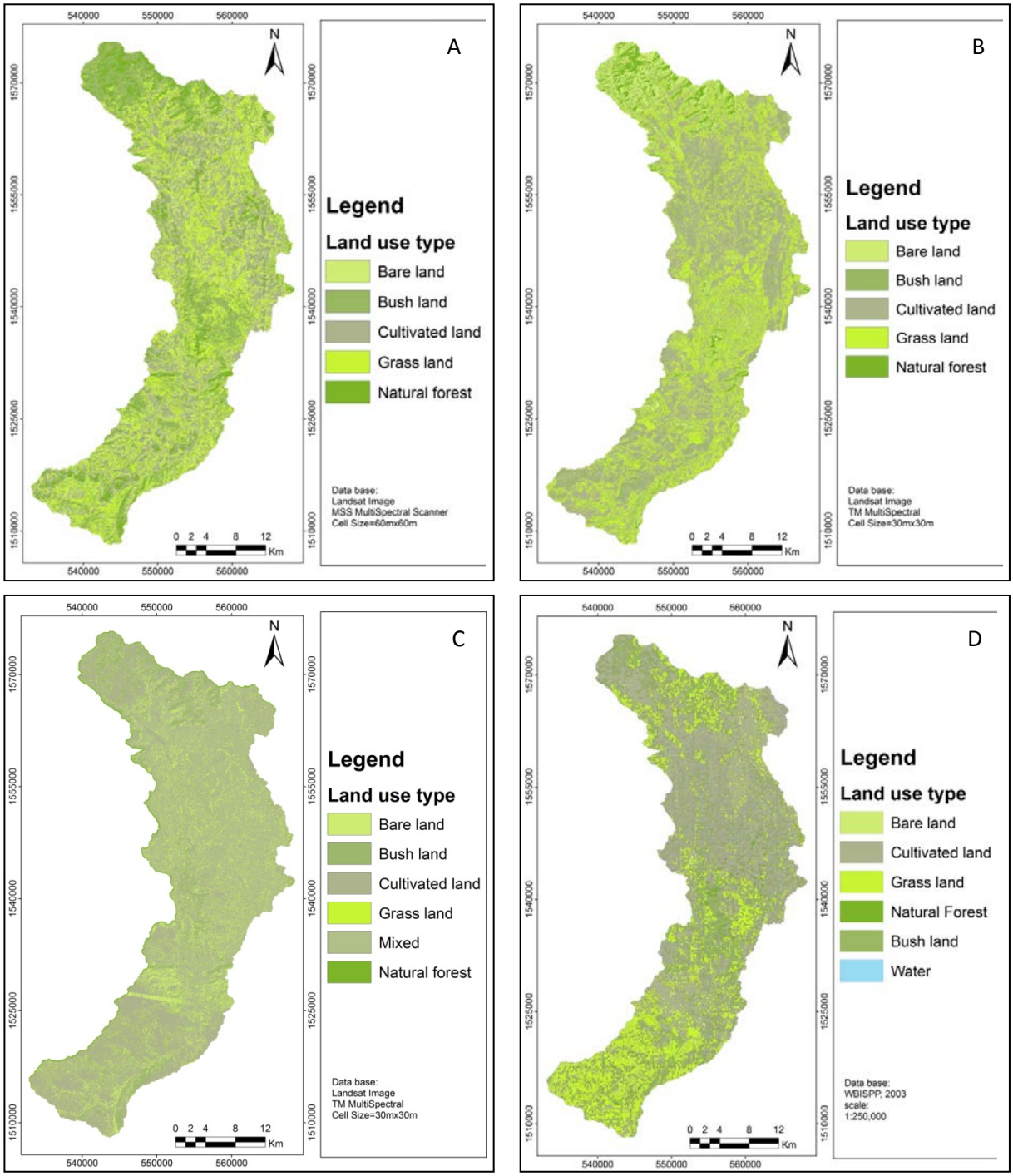

Figure 5-1: Land cover map of the Suluh basin: (A) 1972, (B) 1986, (C) 2000 and (D) WBISPP, 2003 (data base: *http://www.landcover.org* and WBISPP, 2003).

The accuracy assessment was carried out based on spilt sampling technique procedure. Accuracy assessment revealed that the accuracy of classification for the Landsat image was 83.33% with a Kappa coefficient of 0.78 (Table 5-1). Meanwhile, for the year 1972, the accuracy was 76.9% with a Kappa coefficient of 0.71.

Table 5-2: Summary land use and land cover types and changes from 1972–2003 of the Suluh basin (data source: *http://www.landcover.org* and WBISPP, 2003).

Land use and land cover type	Land use and land covers						Land use/land cover change		
	1972		1986		2003		1972–1986	1986–2003	1972–2003
	Area		Area		Area				
	Km²	%	Km²	%	Km²	%	%	%	%
Forest area	102.0	11	45.4	5	7.1	1	-55.5	-84.5	-93.1
Shrub land	237.0	25	154.3	16	195.5	20	-34.9	26.7	-17.5
Grass land	232.3	24	278.7	29	249.3	26	20.1	-10.7	7.3
Cultivated land	273.3	28	387.3	40	493.3	51	41.7	27.4	80.5
Bare land	119.4	12	98.2	10	19.0	2	-17.8	-80.6	-84.1
Total	964	100	964	100	964	100	-	-	-

In general, significant land use and land cover changes can be observed between 1972 and 2003: bare land and natural forest show almost a similar trend with dramatic decrease almost to zero (Figure 5-2). A distinct increase of cultivated land and minor increment of grass land also observed for this period.

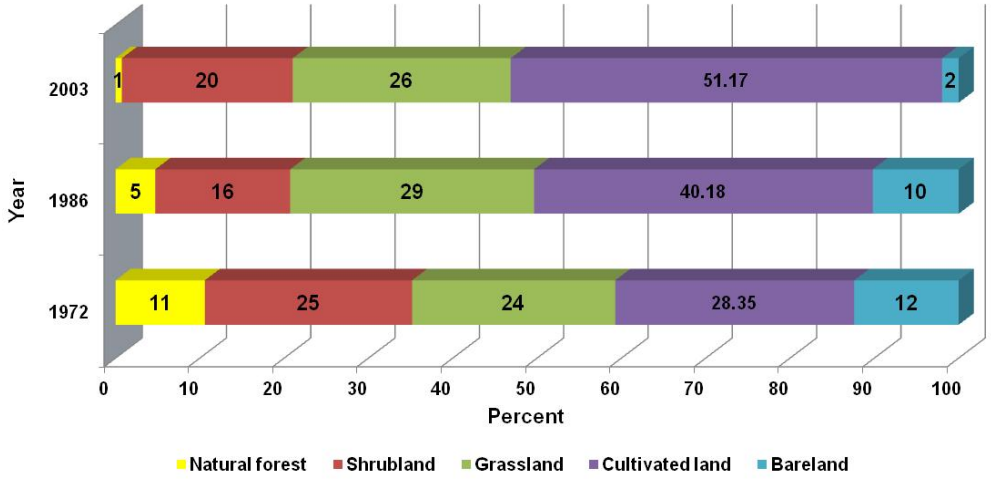

Figure 5-2: Percentage changes of land use and land cover classes of the Suluh basin (data source*: http://www.landcover.org* and WBISPP, 2003).

Land use/land cover change for gauged basin

To quantify the effect of land use and land cover change on the water resources, preparation of land use data for the gauged watershed is required. For this purpose land use change analysis was carried out using the land use maps of the years 1972 and 2003. Figure 5-3 depicts the land use maps for the gauged area of the Suluh basin. Land use was represented by five classes: natural forest, shrub land, grass land, bare land and cultivated land. Land use change analysis was undertaken for thirteen sub-basins, which correspond to the stream gauge stations of Suluh river (Table 5-3).

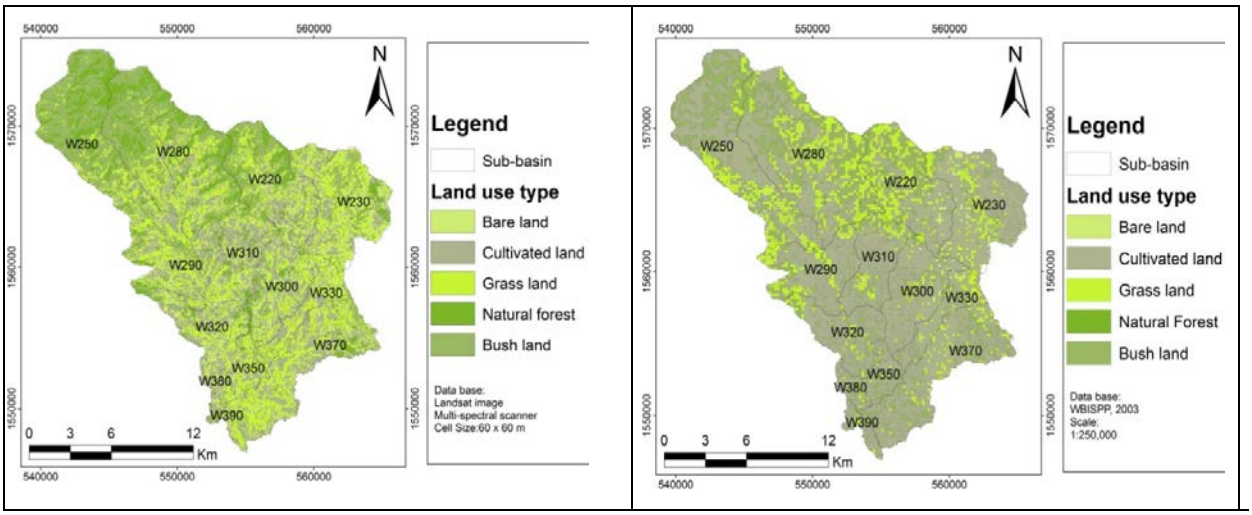

Figure 5-3**:** Land cover map of 1972 (A) and 2003 (B) at gauged part of the Suluh basin (data base: *http://www.landcover.org* and WBISPP, 2003).

Table 5-3: Land use/land cover classes distribution in the sub-basin (data source: *http://www.landcover.org* and WBISPP, 2003).

	Area	Land use type 1972					Land use type 2003				
Sub-basin	(km^2)	Bareland	Cultivated land	Grassland	Shrub land	Forest land	Bareland	Cultivated land	Grassland	Shrub land	Forestland
W390	4.21	0.82	1.61	0.99	0.44	0.36	0.00	3.55	0.31	0.33	0.00
W380	4.40	1.02	2.36	0.70	0.26	0.05	0.00	3.55	0.35	0.50	0.00
W370	39.03	5.65	14.85	12.86	3.77	1.90	0.66	30.40	3.20	4.76	0.00
W350	7.53	1.43	2.37	2.58	0.98	0.17	0.00	6.20	0.30	1.02	0.00
W330	12.68	2.11	3.98	4.77	1.69	0.14	0.38	9.44	2.09	0.77	0.00
W320	20.60	4.22	8.94	4.24	1.56	1.63	0.00	16.00	1.79	2.80	0.00
W310	20.78	3.04	10.55	4.23	1.11	1.85	0.40	15.50	2.54	2.34	0.00
W300	25.66	4.37	11.50	6.03	1.61	2.15	0.50	21.67	1.72	1.77	0.00
W290	25.26	2.76	9.79	6.65	3.99	2.08	0.20	17.41	4.85	2.80	0.00
W280	68.69	2.96	8.80	12.91	28.89	15.13	0.62	21.11	21.69	25.14	0.12
W250	54.90	1.60	4.24	7.01	29.80	12.26	0.93	29.83	9.09	15.06	0.03
W230	39.45	8.56	8.91	11.34	8.12	2.52	2.38	29.22	5.56	2.29	0.00
W220	35.36	4.01	7.79	6.57	11.59	5.40	0.70	10.55	12.33	11.73	0.04
Total areal coverage (Km^2)		**42.55**	**95.69**	**80.85**	**93.80**	**45.66**	**6.77**	**214.45**	**65.83**	**71.31**	**0.19**
percentage share (%)		**11.87**	**26.69**	**22.55**	**26.16**	**12.73**	**1.89**	**59.81**	**18.36**	**19.89**	**0.05**

The relative increase in cultivated land has almost occurred in all sub-basins (Figure 5-4). In sub-basins W280, W250 and W220 there was a decrease of natural forest due to expansion of cultivated land. There was a small increase of grassland and shrub land observed in some of the sub-basins. This may be due to area enclosure and zero grazing policy of the regional government (Reda, 2007).

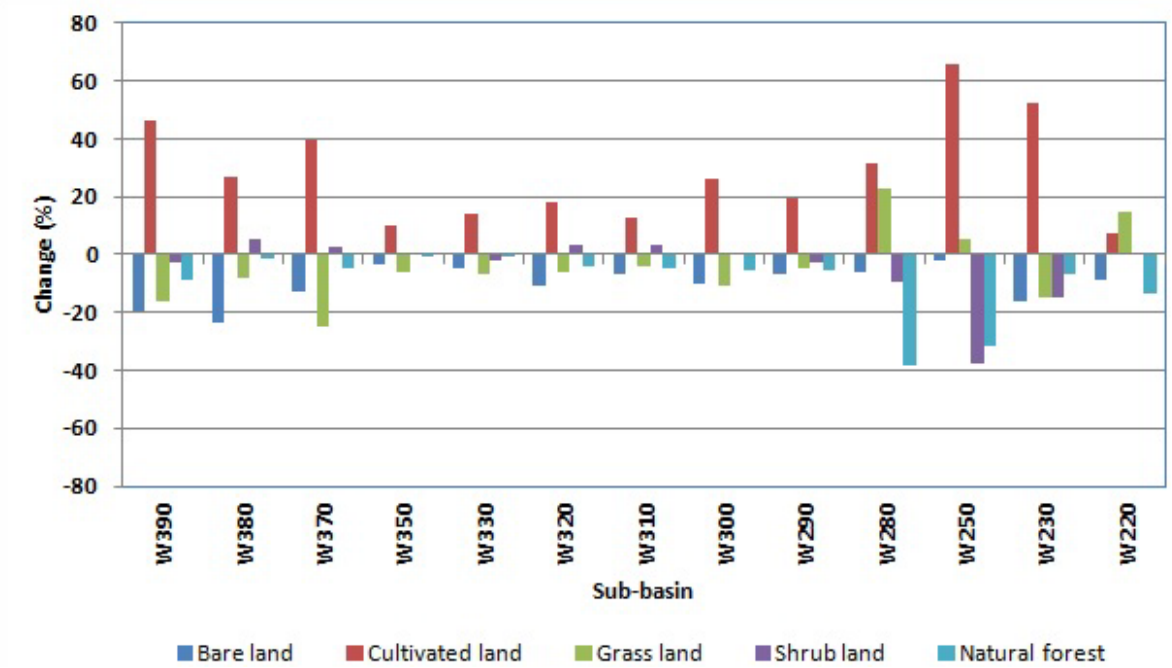

Figure 5-4: Percentage change of land use and land cover in each sub-basin period of 1972–2003 (data source: *http://www.landcover.org* and WBISPP, 2003).

It is noticed that the changes in land use mainly resulted from a transformation of natural forest and bare land into cultivated land (Figure 5-5). These classes are the dominant land use classes in the land use dynamic process of the study area and have a significant impact on the hydrological response. Analysis of the sub-basin shows that the area of cultivated land has more than doubled from 1972 to 2003, while shrub land and grass land show reduction (Figure 5-5).

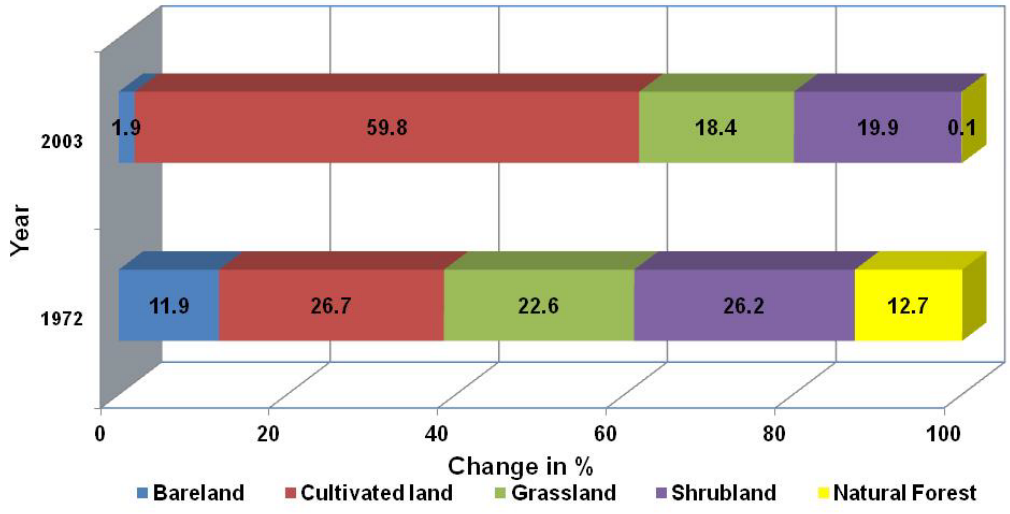

Figure 5-5: Percentage changes of land use and land cover from 1972–2003 (data source: *http://www.landcover.org* and WBISPP, 2003).

This documents the severe effects of the growing population pressure on the natural resources in the northern Ethiopian highlands. According to WAPCOS (2002) the Suluh river basin experiences human impact due to agricultural expansion, and increasing urban demand for charcoal, fuel wood and timber.

Different research results in the region confirm the detected land use changes of the Suluh basin. For example Alemayehu et al. (2009) conducted a research on the Geba basin (Agula watershed); documenting land use and land cover change over the last four decades (1965–2005). Hadgu (2008) did undertake a research in the same region on land use and land cover change over the past 41 years (1964–2005) and pointed out that agricultural land areas increased significantly from 10% to 40% while the woodlands decline from 28% to 3% during the same period. Gebresamuel et al. (2010) tested land use change in two small catchments between 1964 and 2006. Results show that, for all periods, cultivated land increases up to 1.7 ha/year while parallel forest and woodland were nearly completely destroyed (Gebresamuel et al., 2010).

5.2 Statistical downscaling of climate parameters

5.2.1 Selection of predictor variables

Selection of predictor variable(s) is one of the critical stages in the processes of statistical downscaling model (Yimer et al., 2009). This recognized as entirely on the character of the downscaled scenario. A fourth root transformation and conditional process were set for daily precipitation data while linear and non conditional process were used for both maximum and minimum temperature data. The spatial and temporal variation of each predictor variables has significant impact on decision process during the selection of predictor variables (Wilby and Dawson, 2007).

In statistical downscaling model, scatter plots, linear and partial correlation analysis were used to evaluate the significance of the predictor-predictand relationships. The daily minimum and maximum temperatures and daily rainfall data from Mekelle airport weather station and the reanalysis data sets of the National Centre for Environmental Prediction (NCEP) representing the current situation were used to look into the percentage of variance explained by each predictand-predictor pairs (Yimer et al., 2009). Table 5-6 shows the description of the most significant ($\alpha<0.05$) NCEP predictor variables selected for prediction of maximum temperature, minimum temperature and precipitation at Mekelle Airport weather station with the corresponding predictor.

During model calibration and validation the variance inflation, event threshold and bias correction should be set properly to obtain a good statistical performance of the model. The model calibrated based on the selected predictor variables (Table 5-6) from NCEP data set and observed data to estimate coefficients the multiple linear regression equation. The data period of 1961–2000 was chosen to represent the current climate condition. A split year approach was followed to calibrate the model for the period 1961–1980 and validate it independently for the period 1981–2000.

Table 5-4: Selected predictor variables.

Predictor	Predictand	Predictor variables	Symbol
HadCM3	Maximum temperature	Mean sea level pressure	mslpaf
		850 hpa divergence	p8zhaf
		Relative humidity at 500 hpa	r500af
		Mean temperature at 2 m	tempaf
	Minimum temperature	surface zonal velocity	p_uaf
		Relative humidity at 500 hpa	r500af
		Near surface relative humidity	rhumaf
		Mean temperature at 2 m	tempaf
	Precipitation	Surface divergence	p_zhaf
		850 hpa meridional velocity	p8_vaf
		Relative humidity at 500 hpa	r500af
CGCM3	Maximum temperature	Mean sea level pressure	Mslpgl
		Surface zonal velocity	p__ugl
		850 hPa airflow strength	p8_fgl
		850 hPa zonal velocity	p8_ugl
		Specific humidity at 500 hPa	s500gl
		Mean temperature at 2m	tempgl
	Minimum temperature	Mean sea level pressure	mslpgl
		Surface airflow strength	p__fgl
		Surface zonal velocity	p__ugl
		500 hPa airflow strength	p5_fgl
		850 hPa vorticity	p8_zgl
		Surface specific humidity	shumgl
		Mean temperature at 2m	tempgl
	Precipitation	Surface airflow strength	p__fgl
		850 hPa zonal velocity	p8_ugl
		Specific humidity at 500 hPa	s500gl
		Surface specific humidity	shumgl

Figures 5-6 and 5-7 show the performance of the model during validation period. The graph shows a good agreement between the observed and simulated mean daily precipitation and simulated mean daily maximum and minimum temperature showed good agreement for all months of the year.

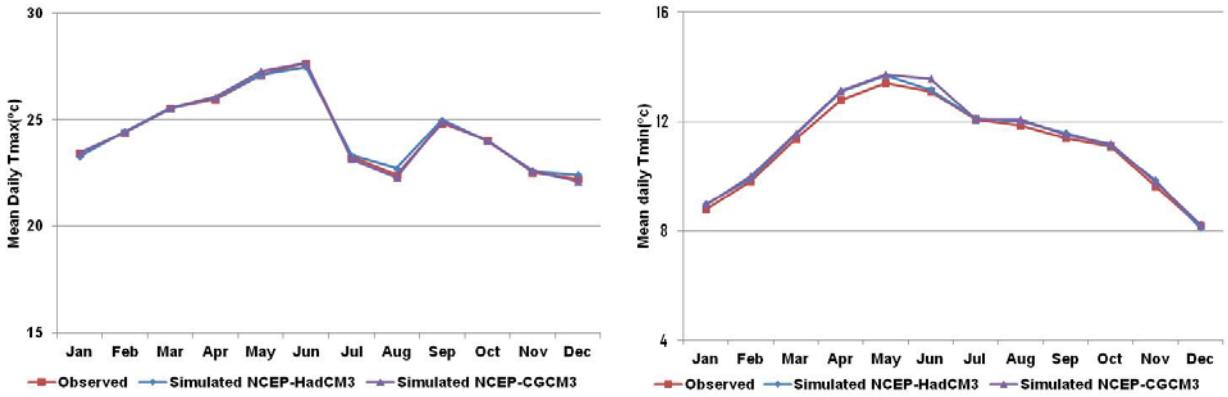

Figure 5-6: Comparison plots of observed and NCEP simulated (using SDSM) average daily (a, left) maximum and (b, right) minimum temperatures during the validation period (1981–2000) at Mekelle airport (data source: CICS: HadCM3 A2 and B2 emission scenario (*http://www.cics.uvic.ca/scenarios/sdsm/select.cgi*), data access integration: CGCM3 A2 emission scenario; *http://loki.qc.ec.gc.ca/DAI/CGCM3_predictors-e.html* and ENMSA).

Precipitation is subjected for local process i.e. the occurrence of humidity, cloud cover, local topographic and wet-days. Hence a conditional process and fourth root transformation were applied during calibration and validation of statistical downscaling model. As a result precipitation downscaling is more problematic parameters than temperature downscaling (Yimer et al., 2009).

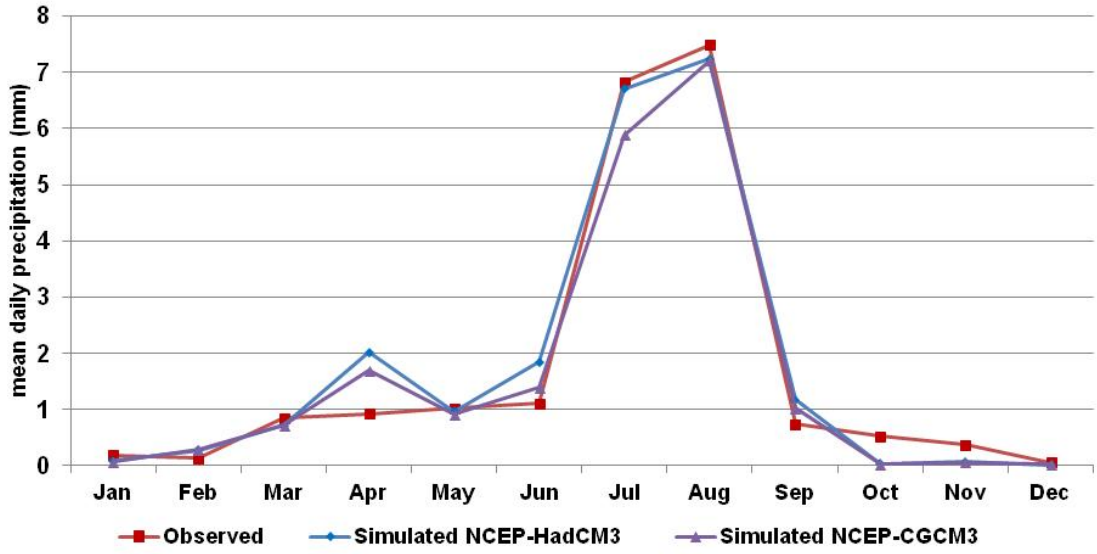

Figure 5-7: Comparison plots of observed and NCEP simulated (using SDSM) average daily precipitation during the validation period (1981–2000) at Mekelle airport (data source: CICS: HadCM3 A2 and B2 emission scenario: *http://www.cics.uvic.ca/scenarios/sdsm/select.cgi*), data access integration: CGCM3 A2 emission scenario*; http://loki.qc.ec.gc.ca/DAI/CGCM3_predictors-e.html* and ENMSA).

5.2.2 Downscaling the Global Circulation Model (GCM) output with SDSM

Following calibration and validation of the SDSM model the scenario generation operation was performed. Hence, the same empirical relationship with predictors, were used to downscale the future climate change scenario data simulated by HadCM3 and CGCM3. A20 ensembles of synthetic daily time series were generated for HadCM3 A2a and B2a SERS emission scenarios for the period of 139 years (1961–2099) and similarly for CGCM3 predictors covering the future period 100 years (2001–2100) for the SRES A2 scenario (Yimer et al. 2009). For further analysis the ensemble mean of the 20 ensemble members were considered to keep the inter-variable relationships for the period (2011–2040), (2041–2070) and (2071–2099), were used as input climatic data to HEC-HMS semi distributed hydrological model for impact assessment (Yimer et al., 2009). Thus, the mean of 20 ensemble members downscaled for the baseline period from HadCM3 A2 and B2 and CGCM3 A2 emission scenarios were aggregated to monthly totals to compare statistically by correlation coefficient(R^2), mean and variance with observed data (Ayalew et al., 2012). Parry et al. (2007) recommend 1961–2000 as climatological baseline period for impact assessment. Therefore this period was also used as baseline period for this study. The downscaling experiment was conducted for minimum temperature, maximum temperature and precipitation based on the data from Mekelle airport weather station.

Downscaling the Global Circulation Model (GCM) for the baseline period

Figures 5-8, 5-9 and 5-10 show the general trend in the mean daily precipitation and the mean daily maximum and minimum temperature at Mekelle weather station corresponding to the baseline period downscaled with SDSM.

- *Minimum temperature*

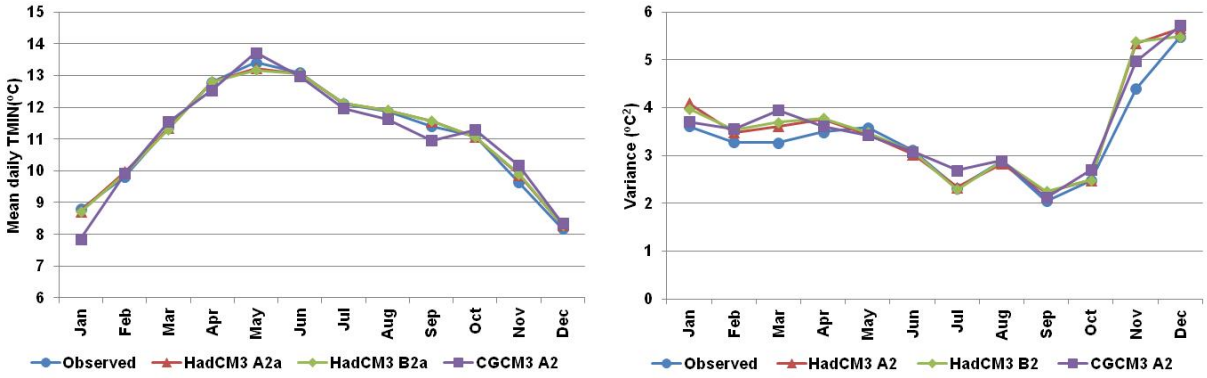

Figure 5-8: Observed and downscaled monthly mean minimum temperature for the baseline period (1961–2000) at Mekelle airport (data source: CICS: HadCM3 A2 and B2 emission Scenario: *http://www.cics.uvic.ca/scenarios/sdsm/select.cgi*), data access integration: CGCM3 A2 emission scenario; *http://loki.qc.ec.gc.ca/DAI/CGCM3_predictors-e.html* and ENMSA).

- *Maximum temperature*

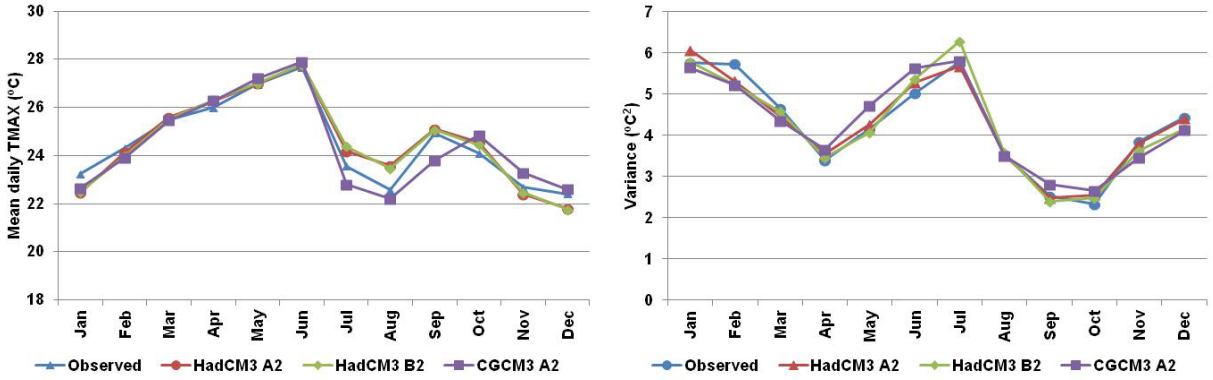

Figure 5-9: Observed and downscaled monthly mean maximum temperature for the baseline period (1961–2000) at Mekelle airport (data source: CICS: HadCM3 A2 and B2 emission Scenario: *http://www.cics.uvic.ca/scenarios/sdsm/select.cgi*), data access integration: CGCM3 A2 emission scenario; *http://loki.qc.ec.gc.ca/DAI/CGCM3_predictors-e.html* and ENMSA).

- *Precipitation*

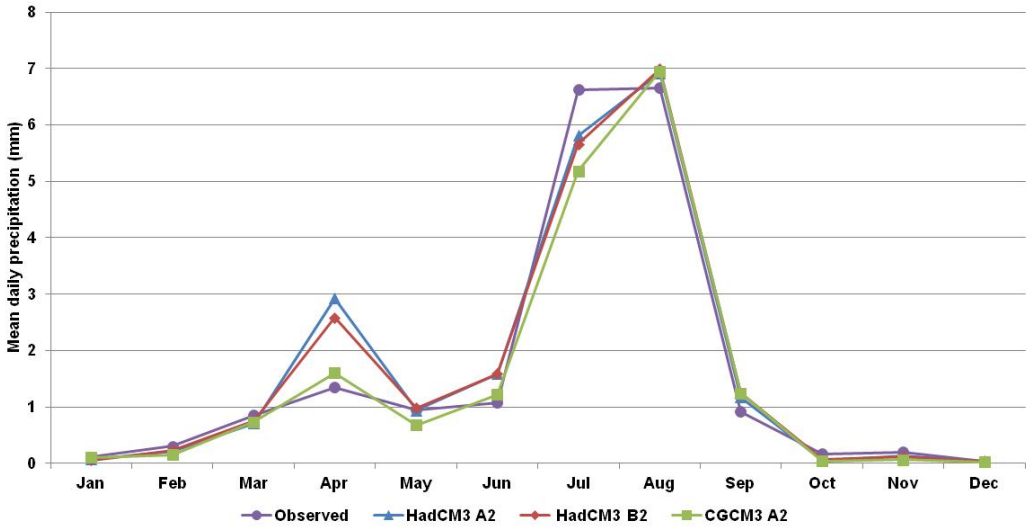

Figure 5-10: Mean daily observed and downscaled precipitation for the baseline period (1961–2000) at Mekelle airport (data source: CICS: HadCM3 A2 and B2 emission Scenario: *http://www.cics.uvic.ca/scenarios/sdsm/select.cgi*), data access integration: CGCM3 A2 emission scenario*; http://loki.qc.ec.gc.ca/DAI/CGCM3_predictors-e.html* and ENMSA).

Downscaling the GCM for future scenarios

- *Minimum temperature*

The downscaled minimum temperature shows an increasing trend in all future time horizons for HadCM3 A2 and B2 and CGCM3 A2a scenarios (Figure 5-9). The average annual minimum temperature will increase by 0.2°C and 0.14°C respectively in 2011–2040. In 2041–2070 the increment will be 0.5°C, 0.4°C and 0.4°C for HadCM3 A2, B2 and CGCM3 A2a scenario respectively. For the 2071–2099 the average annual minimum temperature will be increased by 0.8°C, 0.54°C and 0.7°C for HadCM3 A2, B2 and CGCM3 A2 scenario respectively.

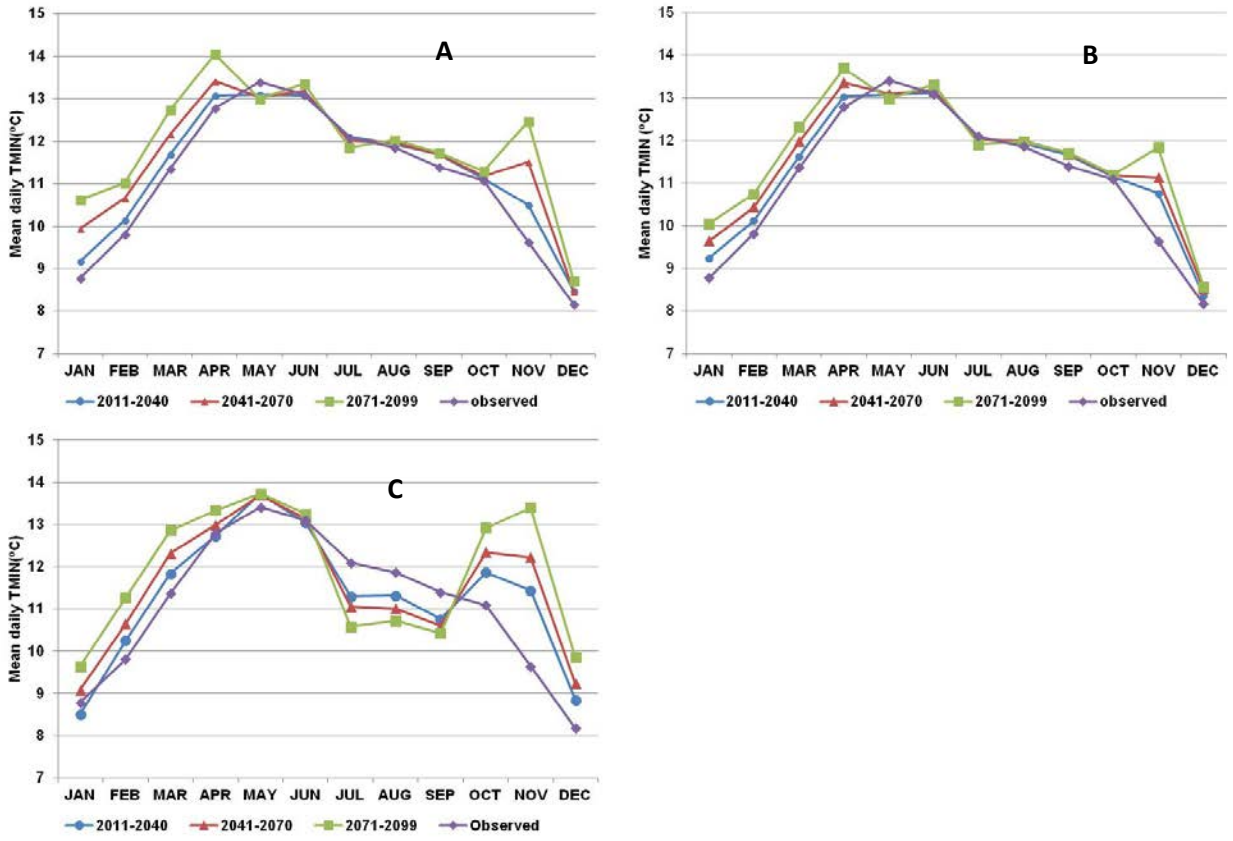

Figure 5-11: Predicted in daily minimum air temperature: (A) for the HadCM3 A2 climate scenario, (B) for the HadCM3 B2 climate scenario and (C) for the CGCM3 A2 climate scenario at Mekelle airport weather station
(data source: CICS: HadCM3 A2 and B2 emission scenario: *http://www.cics.uvic.ca/scenarios/sdsm/select.cgi*), data access integration: CGCM3 A2 emission scenario; *http://loki.qc.ec.gc.ca/DAI/CGCM3_predictors-e.html* and ENMSA).

The annual mean minimum temperature in the long run shows an increasing trend as compared to the baseline period for all scenarios (Figure 7-1). In 2011–2040 the net annual mean minimum temperature change may be minor resulting from all scenarios since the increase from the baseline period is small in all months. In 2041–2070 and 2071–2099 all the months except May and July show a possible increase

in mean minimum temperature for HadCM3 A2 and B2 scenarios. During same period CGCM3 A2a scenarios show a decrease in month July, August and September (main rainy season). In general the net effect shows an increase in mean minimum temperature in the whole seasons except for the summer for CGCM3 A2a scenario.

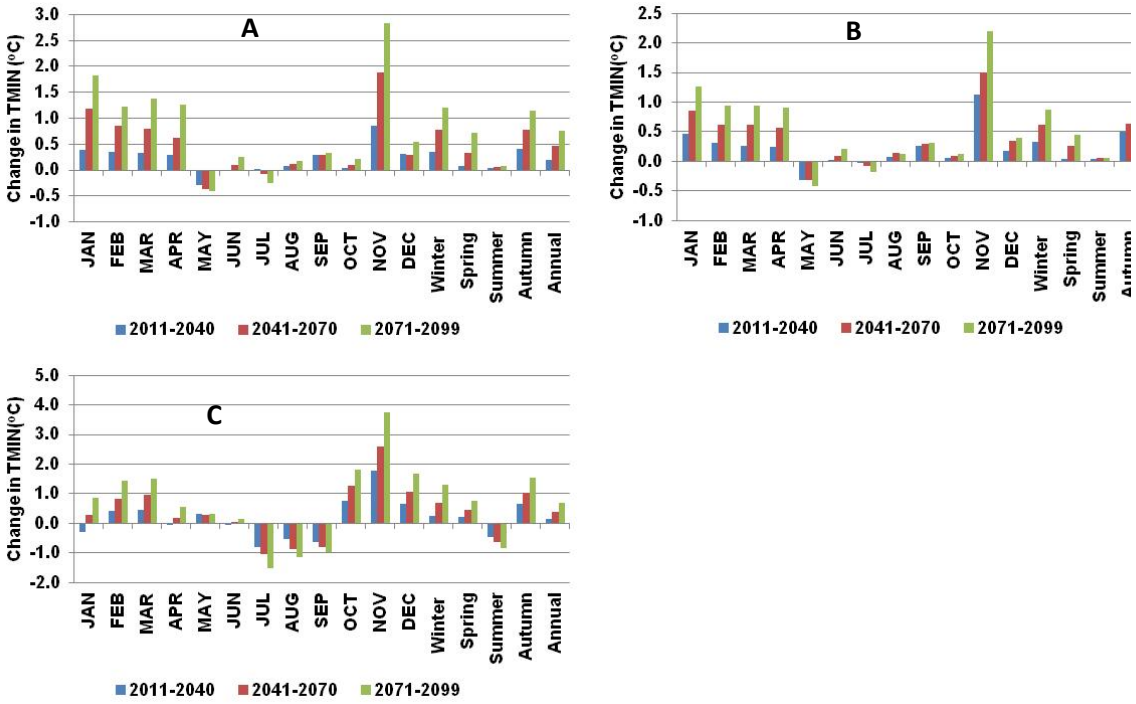

Figure 5-12: Change in the mean minimum temperature (2011–2099) from the baseline period mean minimum temperature: (A) HadCM3 A2a; (B) HadCM3 B2a and (C) CGCM3 A2a climate scenario at Mekelle airport weather station (data source: CICS: HadCM3 A2 and B2 emission scenario: *www.cics.uvic.ca/scenarios/sdsm/select.cgi*), data access integration: CGCM3 A2 emission scenario; *http://loki.qc.ec.gc.ca/DAI/CGCM3_predictors-e.html* and ENMSA).

- *Maximum temperature*

The downscaled maximum temperature scenario data also indicates that there will be an increasing trend for HadCM3 A2 and B2 and CGCM3 A2a scenario (Figure 5-10). The average annual maximum temperature will increase by 0.3°C and 0.25°C respectively in 2011–2040. In 2041–2070 the increment will be 0.6°C, 0.54°C and 0.4°C for HadCM3 A2, B2 and CGCM3 A2a scenario respectively. For the 2071–2099 the average annual maximum temperature will increase by 1.0°C, 0.82°C and 0.7°C for the HadCM3 A2, B2 and CGCM3 A2 scenario respectively.

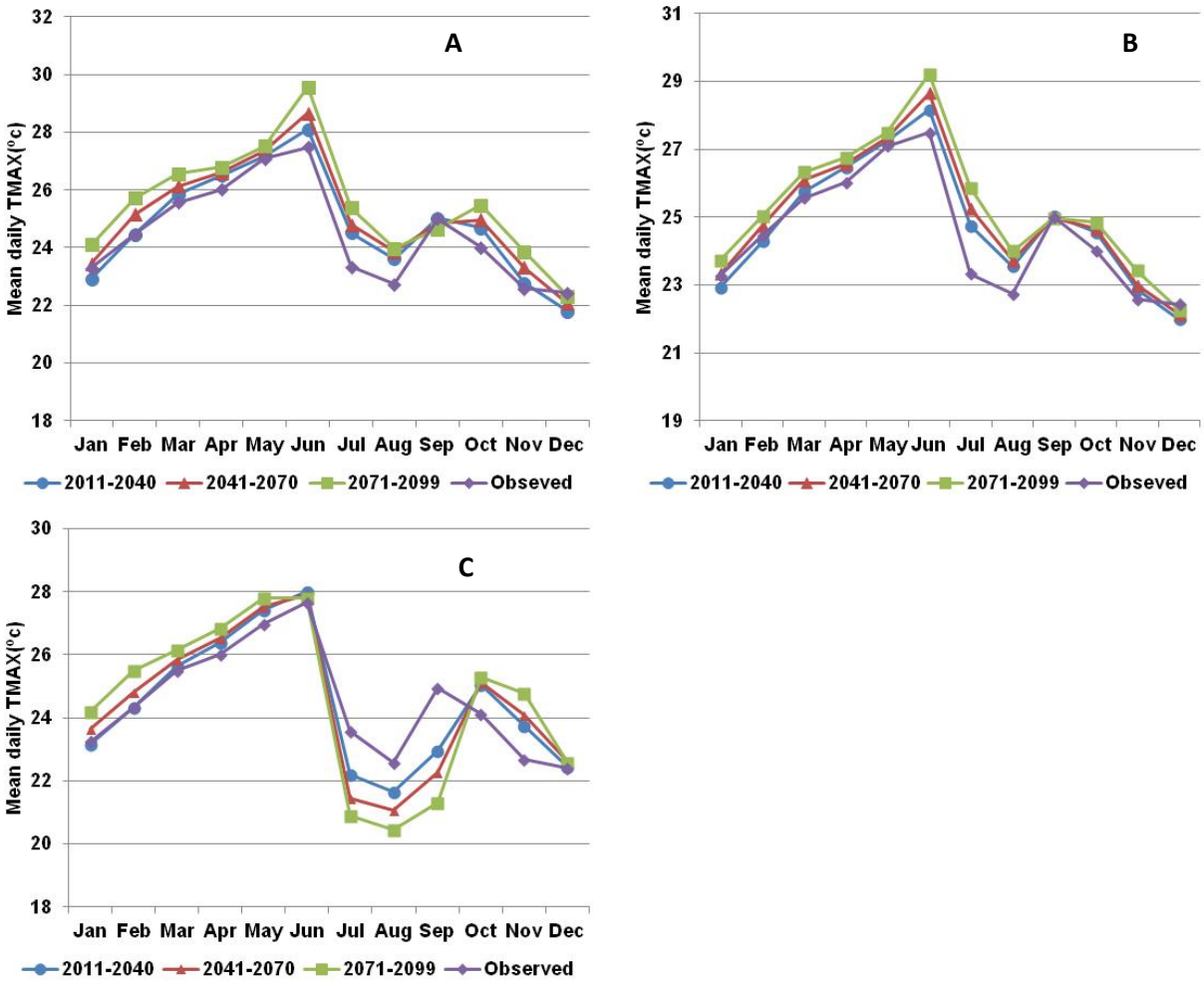

Figure 5-13: Predicted in the daily maximum air temperature: A) for the HadCM3 A2 climate scenario, (B) for the HadCM3 B2 climate scenario and (C) for the CGCM3 A2 climate scenario at Mekelle airport weather station (data source: CICS: HadCM3 A2 and B2 emission scenario: *http://www.cics.uvic.ca/scenarios/sdsm/select.cgi*), data access integration: CGCM3 A2 emission scenario: *http://loki.qc.ec.gc.ca/DAI/CGCM3_predictors-e.html* and ENMSA).

The downscaled monthly maximum temperature shows an increasing trend in all months except for January, February and December for the period 2011–2040 and for September and December for the period 2041–2070 for the HadCM3 A2 and B2 scenario. In 2071–2099 there may be an increase in temperature in all the months except September and December for the HadCM3 A2 and for December for the B2 Scenario (Figure 7-2). In the case of the CGCM3 A2a scenario the monthly maximum temperature show decreases for July, August and September (summer season) in all future time horizons and has similar trends like the mean minimum temperature (Figure 7-1). Seasonally, a pronounced increase in mean maximum temperature is observed in the summer (main rainy season) and spring (small rainy season) in the case of HadCM3 A2 and B2. In general, the annual mean maximum temperature shows an increasing trend in all scenarios (Figure 7-2). The findings of this study well agree to the previous studies in the region regardless of the magnitude of changes.

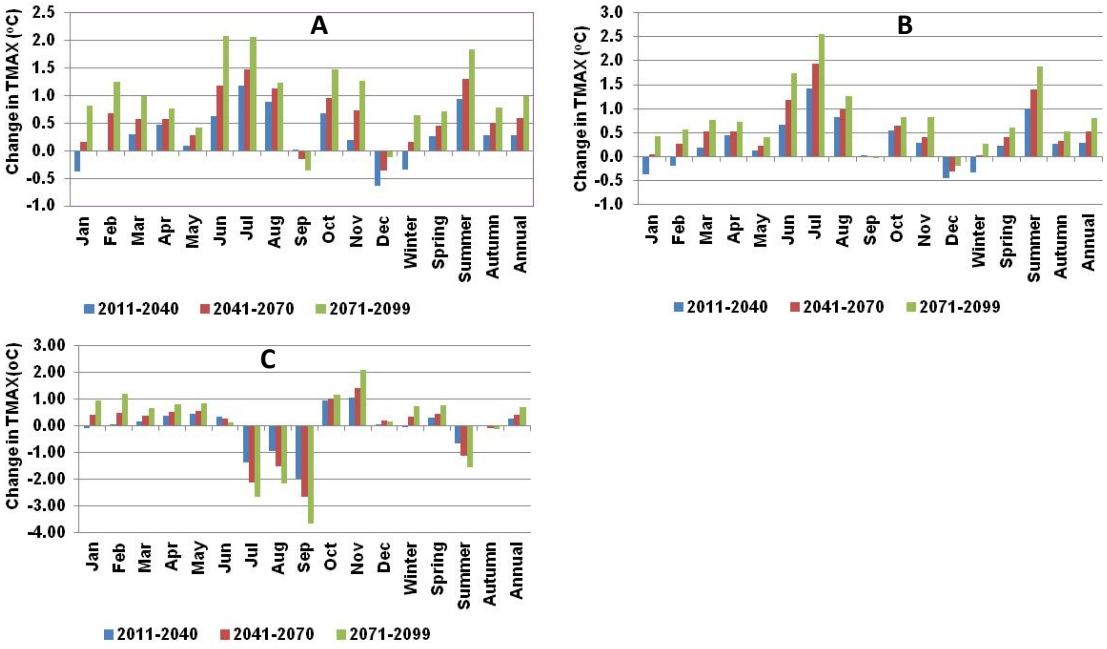

Figure 5-14: Change in the mean minimum temperature (2011–2099) from the baseline period mean minimum temperature: (A) HadCM3 A2a; (B) HadCM3 B2a and (C) CGCM3 A2a at Mekelle airport weather station (data source: CICS: HadCM3 A2 and B2 emission scenario: (*http://www.cics.uvic.ca/scenarios/sdsm/select.cgi*), data access integration: CGCM3 A2 emission scenario; *http://loki.qc.ec.gc.ca/DAI/ CGCM3_predictors-e.html* and ENMSA).

- *Precipitation*

Future projections of rainfall did not document a systematic increase or decrease. The rainfall amounts generally show a decrease trend in the spring rainy season especially in the month of March and May and a dramatic increase for the month of April for all scenarios in all future time horizons (Figure 5-11). Also the rainfall in the beginning of main rainy season (June) will increase while it will decrease in the month of July. Towards the end of the main rainy reason (August and September) the rainfall increases for all future scenarios.

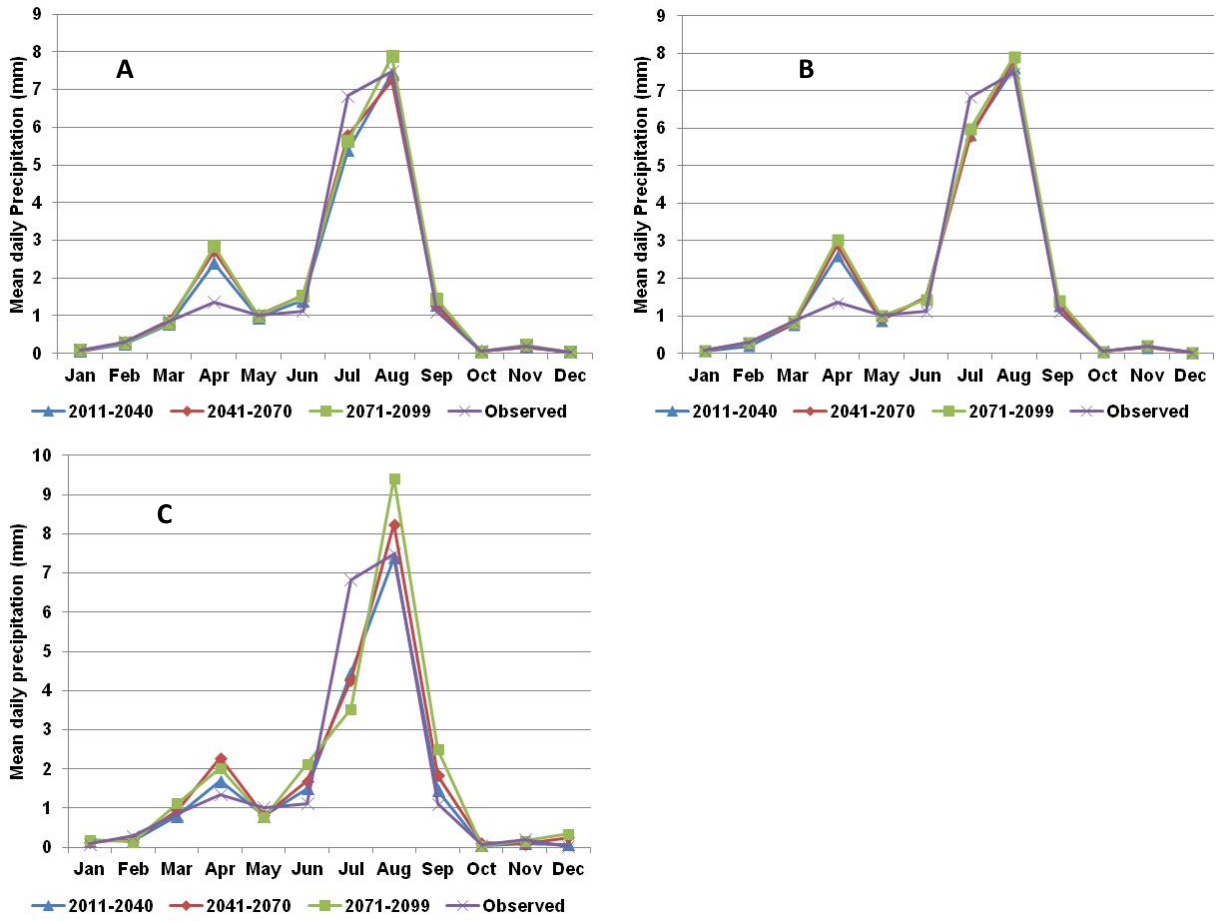

Figure 5-15: Predicted in daily precipitation: A) for the HadCM3 A2 climate scenario, (B) for the HadCM3 B2 climate scenario and (C) for the CGCM3 A2 climate scenario at Mekelle airport weather station (data source: CICS: HadCM3 A2 and B2 emission Scenario: *http://www.cics.uvic.ca/scenarios/sdsm/select.cgi*), data access integration: CGCM3 A2 emission scenario; *http://loki.qc.ec.gc.ca/DAI/CGCM3_predictors-e.html* and ENMSA).

The precipitation projection points to a decrease in mean annual precipitation by 1% for the HadCM3 A2a scenario and by 9.2% for the CGCM3 A2a scenario, contrary it shows an increase by 2.8% for HadCM3 B2a scenario for the period 2011–2040. In the 2041–2070 periods the mean annual precipitation is expected to increase by 2.9, 4.5 and 3.0% and for the 2071–2099 periods by 6.6, 8.1 and 12.5% for HadCM3 A2a, B2a and CGCM3 A2a scenarios respectively (Figure 7-2). Rainfall in Suluh basin is concentrated in the main rainy season *Kiremt* (June to September) and the minor rainy season *Belg* (March to May). Relatively high changes in of rainfall in the other months therefore are negligible due to the small magnitude of the base line precipitation (<0.05 mm).

Looking to the relative precipitation changes considering two rainy seasons for the future, the HadCM3 A2a scenarios indicate a monthly mean precipitation decrease in July and an increase in April, June and September for all time periods examined. Integration of HadCM3 B2a scenario shows a decrease of precipitation in May and July and an increase in April, June and September during the 2041–2070 and 2071–2099 periods. Integration of the CGCM3 A2a scenario shows a monthly mean precipitation decrease for May and July and an increase for April, June and September for all examined time periods. It is observed that the change of precipitation during the two rainy seasons shows similar trend regardless of the magnitude for all climate change scenarios. However, the downscaling of precipitation is highly uncertain due to the influence of the seasonal cycle of temperature and precipitation (Hulme et al., 2001).

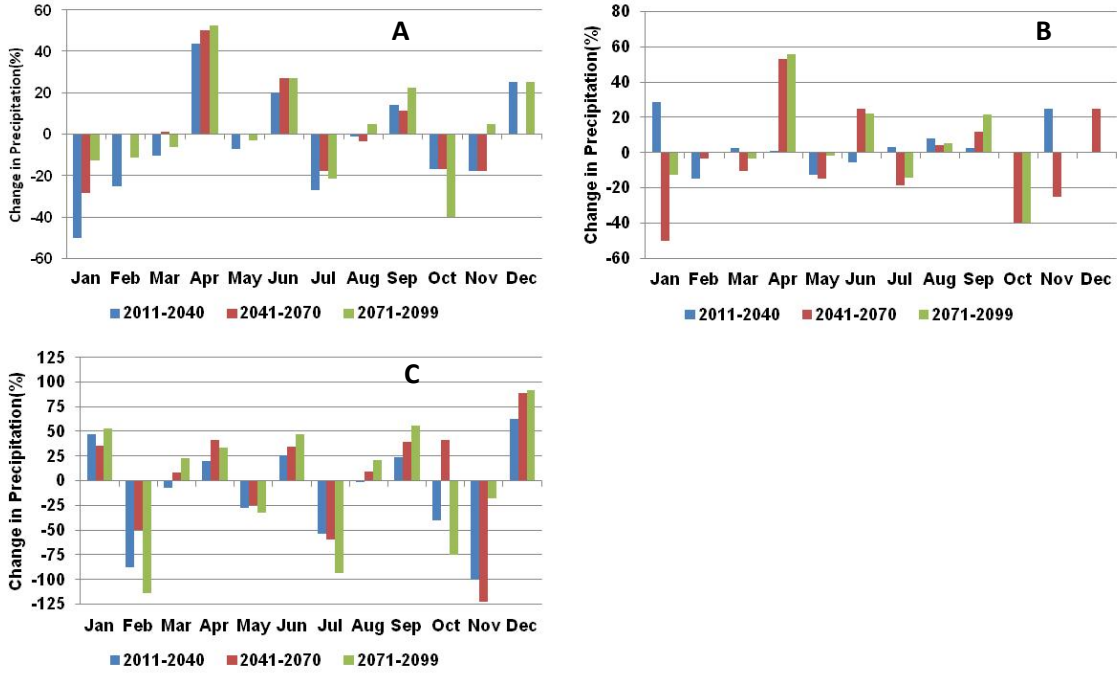

Figure 5-16: Percentage change in monthly precipitation in the future from the baseline period average precipitation: (A) HadCM3 A2a; (B) HadCM3 B2a and (C) CGCM3 A2a at Mekelle airport weather station (data source: CICS: HadCM3 A2 and B2 emission Scenario: *http://www.cics.uvic.ca/scenarios/sdsm/select.cgi*), data access integration: CGCM3 A2 emission scenario; *http://loki.qc.ec.gc.ca/DAI /CGCM3_predictors-e.html* and ENMSA).

Chapter 6

6 Effects of climate and land use change on water resources

6.1 Hydrologic Engineering Center's Hydrologic Modeling System (HEC-HMS)

The rainfall-runoff model was performed to quantify the effect of climate and land use/land cover change factors on the hydrological response (Legesse et al., 2010; Pechlivanidis et al., 2011). The HEC-HMS model is capable to simulate a continuous based runoff process (Figure 6-1). A continuous simulation model was deemed suitable to analyze changes in water resource, due to the effects of climate and land use change on hydrological response (Haberlandt, 2010; Meenu et al., 2012).

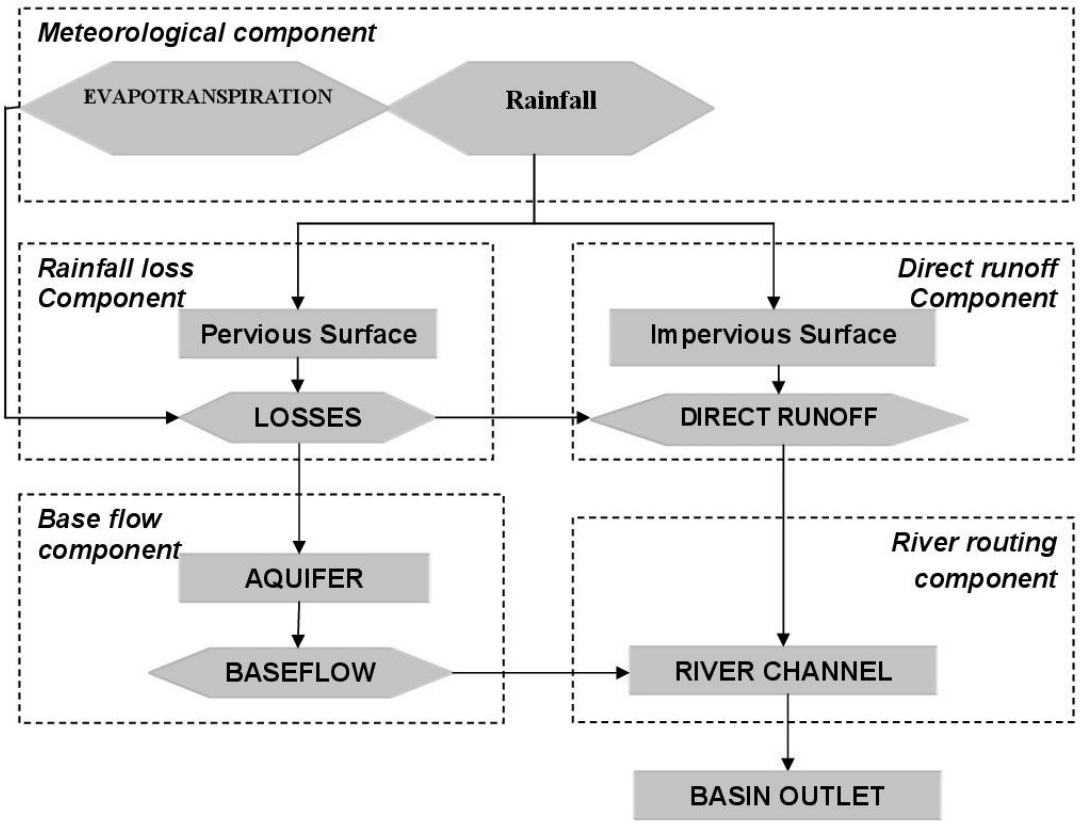

Figure 6-1: Runoff generation process with continuous model structure in HEC-HMS.

6.1.1 Terrain preprocessing

Terrain preprocessing requires a series of steps including the computing of flow direction, flow accumulation, stream definition, stream delineation, watershed delineation. Watershed aggregation was performed step by step to derive the drainage networks (Figure 6-2).

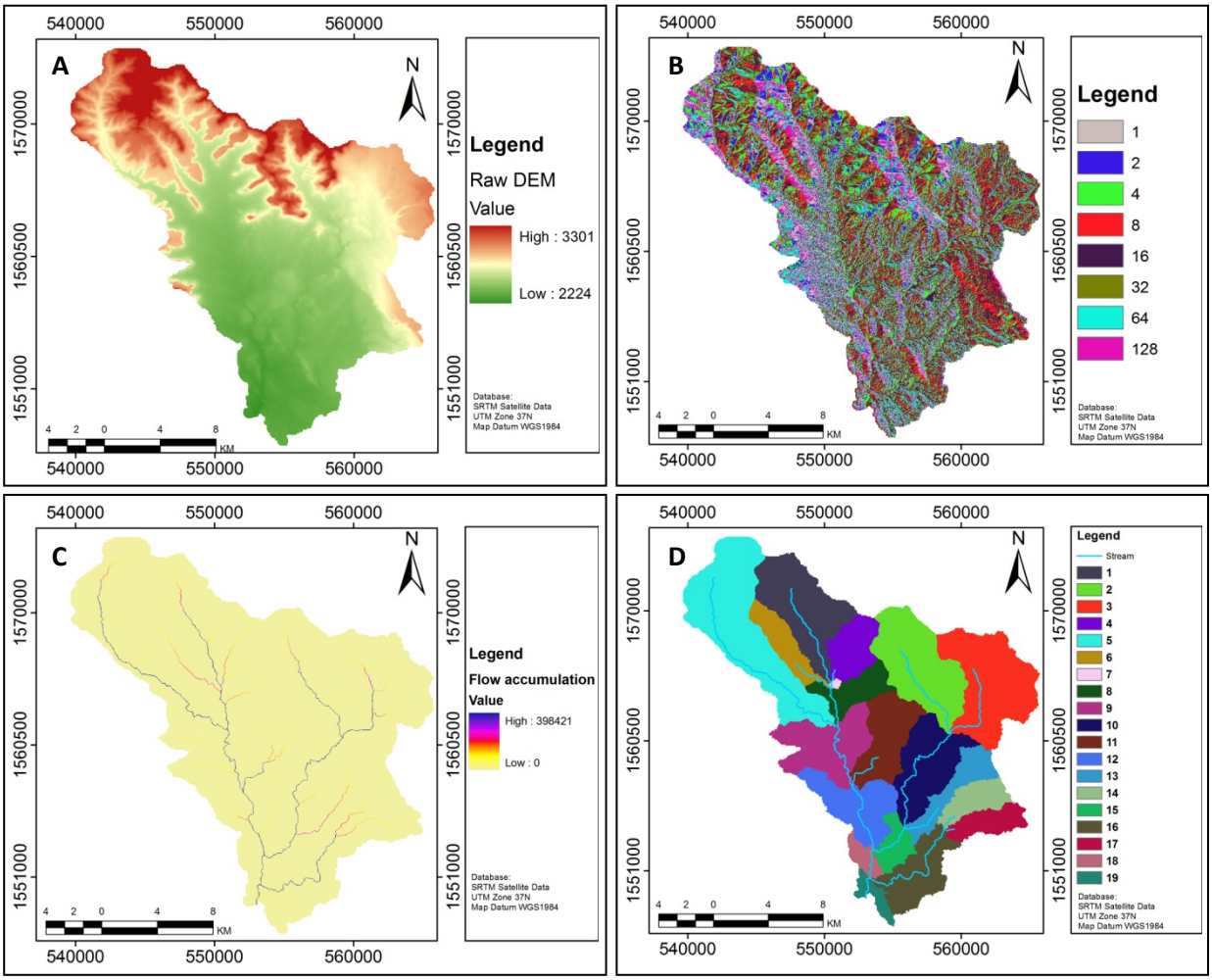

Figure 6-2: Terrain pre-processing: A) Raw DEM, B) Flow direction grid, C) Flow accumulation grid and D) Catchment polygon of the gauged part of the Suluh basin (data source: Jarvis et al., 2008).

6.1.2 Basin processing

To revise the catchment delineation, including basin merge, basin subdivision, river merge, river profile, split basin at confluences and batch sub-basin delineation basin processing was conducted after preprocessing of the terrain model. The sub-basins were further merged with land use, soil map and slope map. Figure 6-3 shows the final thirteen sub-basin polygons derived for the gauged part of Suluh basins for the hydrological model setup. In addition, several topographic characteristics of streams and sub-basins like river length, river slope, basin slope, longest flow path, basin centroid, centroid elevation and centroidal flow path are the main morphometric information derived from Digital Elevation Model (Fleming and Doan, 2009) that can be used for estimating initial hydrologic parameters.

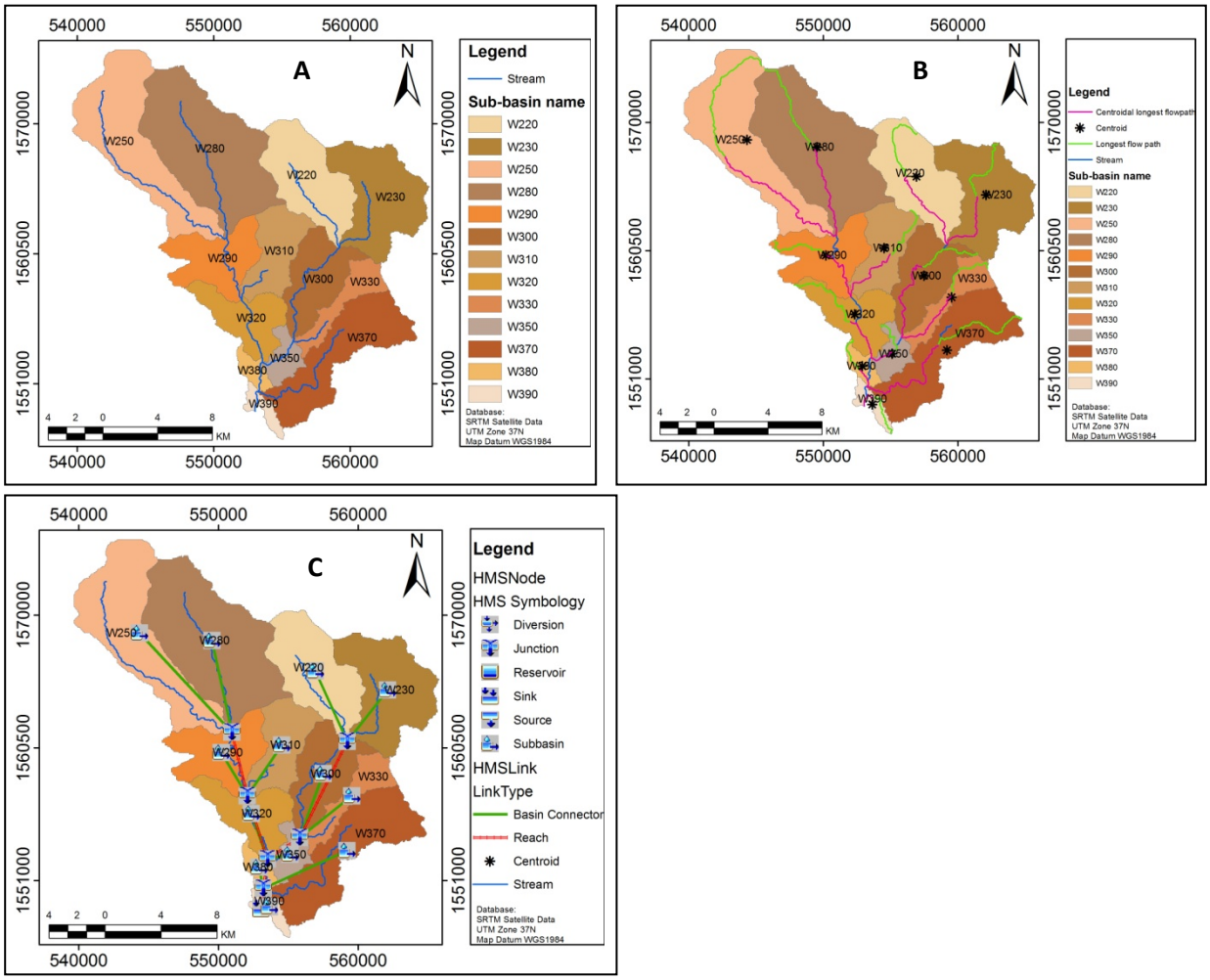

Figure 6-3: Basin processing: A) Sub-basin processing, B) Centroidal and longest flow path and C) HEC-HMS schematic map of the gauged part of the Suluh basin (data source: Jarvis et al., 2008).

6.1.3 Initial parameter estimation

The HEC-HMS hydrologic model includes several possibilities to represent the different components of the rainfall-runoff modeling process (Figure 6-1). These are the selected options to execute the HEC-HMS Continuous model simulation:

Table 6-1: Selected model algorithm.

Model operation	Selected algorithm
Loss model	Soil Moisture Accounting (SMA) and deficit and constant loss method
Runoff transform	Clark Unit Hydrograph method
Flow routing	Lag method
Base flow routing	Linear reservoir

The model parameters included in the four algorithms (Table 6-1) are measurable and non-measurable parameters by indirect/direct means. Measured parameters may be obtained for example through observation of catchment characteristics in the field or through GIS measurement (SKM, 2009; Adnan, 2010). These measured parameters may include sub-basin area (km^2), slope (%), flow length (km) and percentage of impervious surface. Seven of the twelve parameters are needed for the Soil Moisture Accounting algorithm (Table 6-2): canopy storage, surface depression storage, maximum infiltration rate, maximum soil storage, tension zone storage, soil zone percolation rate, and groundwater-1 percolation rate. Since most of the model parameters were entirely depend on the inherent properties of soil, land use and topography further processing is mandatory to estimate the initial model value (Neary et al., 2004). To estimate the initial model parameter map overlay and derivation of attribute were carried out corresponding to each sub-basin. Groundwater-1 and 2 storage depths and storage coefficients parameters were entirely dependent on basin lithological units (SKM, 2009). These estimated parameters are subjected to sensitivity analysis and calibration processes. However, the groundwater-2 percolation rate is depending on the complex aquifer system and the parameter value entirely depends on the local lithology, the value of the parameter is difficult to estimate by physical means and conceptually it was determined based on model calibration (Neary et al., 2004). The rainfall-runoff process was modeled at the sub-basin level within HEC-HMS. Hence, in all sub-basins the initial values of model parameters were obtained through clustering the sub-basin based on soil texture, land use and slope. Silt clay loam and clay loam are the two major soil textures found in the basin. Fortunately, these soil textures have nearly the same character and both are under hydrologic soil group D (USDA, 1999). Although, in each sub-basin there are five land use class, namely shrub land, grass land, bare land, forest and cultivated land (Section 5-1-3). For the estimation of the initial model parameters a) shrub land, grassland and minor forests, and b) cultivated and bare land for each of the sub-basins were grouped. From the knowledge on soil texture, slope and land use and land cover, the thirteen sub-basins were grouped into three homogeneous sub-basins. Finally, the initial model parameters were set based on different empirical formulas and extracted from scientific literatures for example Fleming and Neary (2004); Neary et al. (2004); Bashar and Zaki (2005); Ayka (2008); García et al. (2008); SKM (2009) and Meenu et al. (2012) (Table 6-3).

Group1 includes sub-basins W390, W380, W370, W350, W330, W320, W310, W290 and W230 which have slopes with an inclination of 5–15%, cultivated land as the dominant land use (>75%) and a clay loam soil texture. Group2 includes only sub-basin W250 and has slope inclination of 15–30% and is dominated by both bush grassland (44%) with cultivated land (56%) with silt clay loam soil textures dominating. Group3 includes sub-basins W220 and W280 and has slope inclination of >30%, the dominant land use is bush and grassland and silt clay loam soil textures dominate.

Table 6-2: Description of Soil Moisture Accounting model parameters (data source: SKM, 2009).

Parameter	Units	Description of parameter
Canopy storage capacity	mm	Depth of water potentially held by the canopy storage zone.
Surface storage capacity	mm	Depth of water potentially held by the surface storage zone. This is essentially the initial loss, and becomes less influential with increasing flood magnitude.
Maximum infiltration	mm/hr	Upper limit to the soil infiltration rate. Actual infiltration capacity is scaled based on the soil moisture deficit.
Impervious area	%	Impervious proportion of the catchment connected to drainage channels.
Soil storage capacity	mm	Depth of water potentially held in the soil moisture storage zone. Equal to tension zone storage plus upper zone storage.
Tension zone capacity	mm	Depth of water potentially held in the tension zone compartment of soil moisture storage. Must be less than or equal to the soil storage capacity.
Maximum soil percolation rate	mm/hr	Upper limit of the rate of percolation to GW1. Actual percolation is limited based on the GW1 storage deficit and the amount of soil moisture storage.
GW1 storage capacity	mm	Depth of water potentially held in GW1.
GW1 percolation rate	mm/hr	Upper limit of the rate of percolation from GW1 into GW2. Actual GW1 percolation is limited based on the storage values of GW1 and GW2.
GW1 coefficient	hr	Determines the proportion of storage in GW1 that is routed to stream flow in each time step.
GW2 storage capacity	mm	Depth of water potentially held in GW2.
GW2 percolation rate	mm/hr	Upper limit of the rate of percolation from GW2 out of the system (i.e. deep percolation). Actual GW2 percolation is limited based on the storage value of GW2.
GW2 coefficient	hr	Determines the proportion of storage in GW2 that is routed to stream flow in each time step.

Since the surface area of the study site is less than 450 km² the initial value of ground layer 1 was taken with 25 mm storage depth and of ground layer 2 storage with 35 mm storage depth. Simultaneously, for initial model setup the storage coefficient of ground layer 1 was taken with 300 hrs and of ground layer 2 with 1000 hrs (García et al., 2008).

Table 6-3: Initial model parameters of the sub-basins of the gauged Suluh watershed.

Homogeneous group	Canopy storage capacity (mm)	Surface storage capacity (mm)	Maximum soil infiltration (mm/hr)	Soil storage capacity (mm)	Tension storage capacity (mm)	Soil percolation (mm/hr)
Group1	1	6	5.85	24	21	3.9
Group2	2	1	4.85	20	18	2.8
Group3	2.5	1	4.67	14	10	2.8

6.2 Hydrologic modeling using HEC-HMS

6.2.1 Basin Model

The basin model represents the spatial configuration of the watershed (Figure 6-4). The basin model contains the physical attributes and the topology of stream network (Scharffenberg and Fleming, 2010). The watershed elements can be modified, added or removed. In the basin model, river reach, reservoir, diversion and sink/source can be connected in a network imitating basin hydrologic structure (Cunderlink and Simunovic, 2004). HEC-HMS allows seven different watershed elements for the construction of the basin model: sub-basins, reach, junction, source, sink, reservoir and diversion.

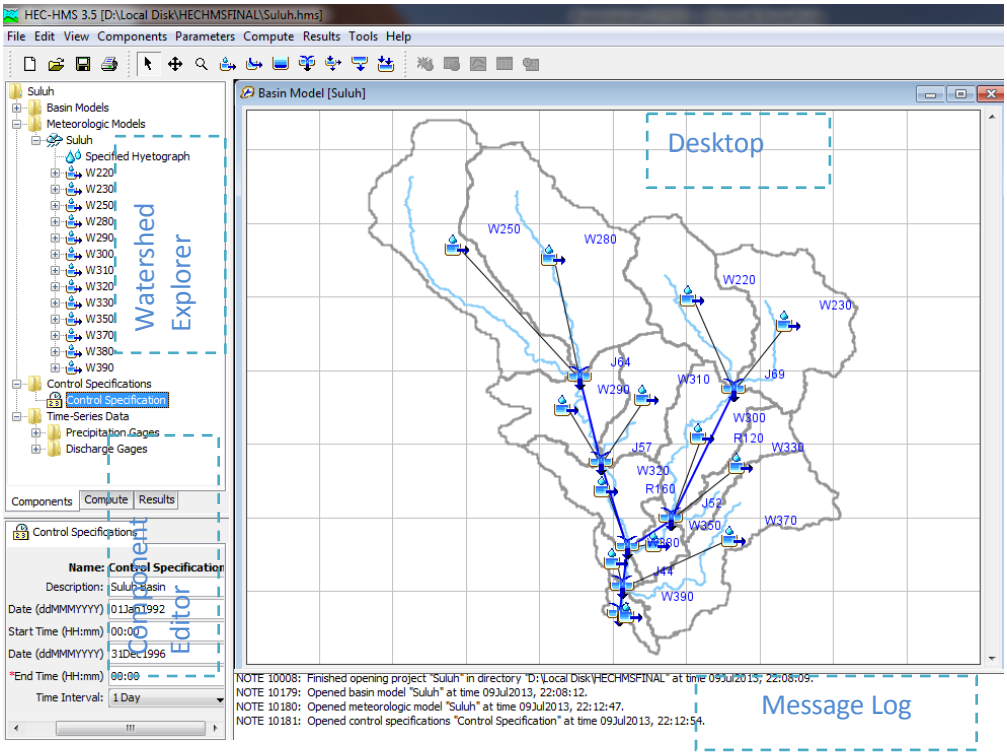

Figure 6-4: Basin model spatial configuration of the area of the gauged Suluh basin.

6.2.2 Meteorological model

The meteorological model in HEC-HMS includes precipitation and evapotranspiration for continuous runoff modeling (Feldman, 2000). Precipitation is the driving factor for the watershed responses in the case of HEC-HMS model; in turn a major effort was to compute the meteorological model to receive spatially and temporally distributed precipitation input data (Yimer et al., 2009). The Thiessen polygon technique was selected to determine the gauge weights. Edagahamus, Adigrat and Hawzen weather stations are used for the estimation of daily areal rainfall. The monthly potential evapotranspiration data was used as input to the meteorological model. The HEC-HMS model has capable to compute potential evapotranspiration from net radiation and temperature data by Priestly-Taylor method. However the methods are not suitable for arid and semi-arid climates (Scharffenberg et al., 2010). The FAO Penman-Monteith method was applied used for the computation of monthly potential evapotranspiration externally by applying CROPWAT model (Allen et al., 1998).

6.2.3 Control specification model

The control specification model provides time related information for the model simulation such as the start and end of the computation period and the computation time interval (Scharffenberg and Fleming, 2010). Since the available data are daily the computation time interval was one day. However, since some small sub basins in the study area have a concentration time shorter than 24 hours, the model computation time step was changed to 6 hours. As a result, values of the daily input data were divided into four 6-hour intervals.

6.3 Hydrologic model results

The rainfall runoff modeling was carried out using two combinations:

1) Soil Moisture Accounting loss model, the Clark unit hydrograph transformation, linear reservoir base flow model and lag model channel routing.
2) Deficit and constant loss model, the Clark unit hydrograph transformation, linear reservoir base flow model and lag model channel routing.

6.3.1 Model sensitivity analysis

The sensitivity analysis was implemented prior to calibration to be able to assess the impact of the model input parameters on the modeling results (Vaze et al., 2011). During the analysis the Morris screening method consisting of a random one-factor-at-a-time was adopted (Morris, 1991), which is a powerful approach widely used for sensitivity studies of individual models (Feyen and Zambrano, 2010). Hence, one input parameter of the model is typically varied at a time and the model re-run to test the change in the output produced by the change in the single input parameter. The value of each of the input parameters was modified up to +20% to -20% to check the percentage change in the mean annual runoff volume and peak flow from the baseline.

Applying the Soil Moisture Accounting component five layers were included (12 loss parameters with 5 parameters defining initial conditions, 2 transform parameters and 4 baseflow parameters), in total accounting 23 parameters for the continuous model. The Soil Moisture Accounting initial parameters

were not included in the sensitivity analysis due to their minor impact (Cunderlik and Simonovic, 2004); the subsequent seasons have initial conditions automatically set to the conditions at the end of the previous season. Due to the large number of model parameters and model uncertainty in the semi distributed hydrological model it is difficult to achieve a valid relationship between simulated and observed data. Therefore, sensitivity analysis is carried out aiming to reduce the number of parameters. This also helps to minimize over-parameterization risk of individual model parameters, especially in distributed models (Feyen and Zambrano, 2010). Figure 6-5 shows the effect of input parameters on the total runoff volume in the Suluh basin. The maximum soil infiltration, soil percolation, GW1 percolation, GW1 storage coefficient, GW1 and 2 storage capacity and soil storage capacity have significant influence on the simulated runoff volume. The most sensitive parameters are modified by model calibration through the comparison of observed and simulated data intending to minimize the targeted objective function (White and Chaubey, 2005).

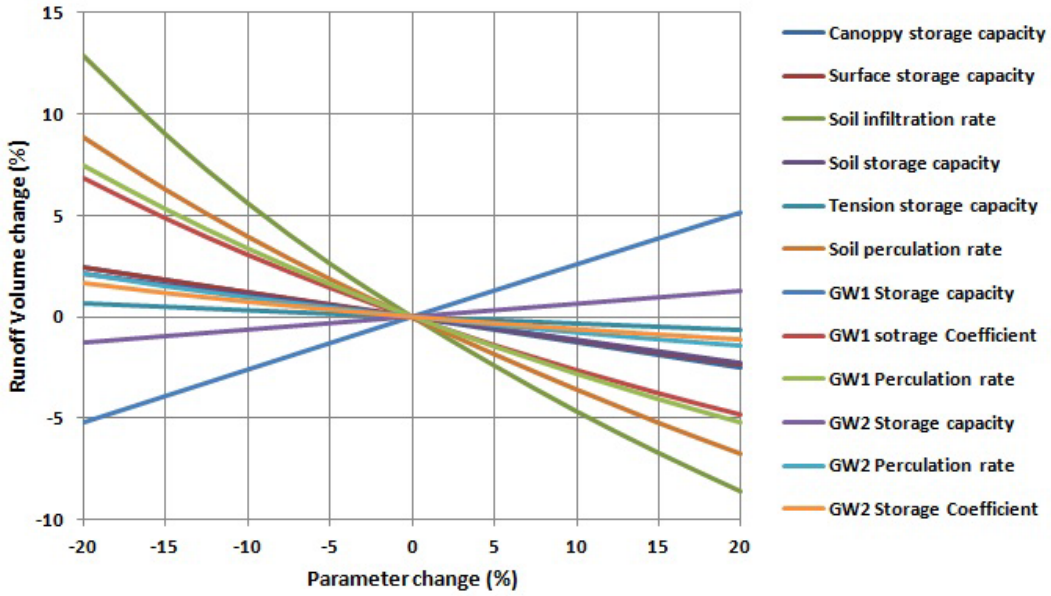

Figure 6-5: Model results (total runoff volume (%)) generated from the sensitivity scenarios of the change in the Soil Moisture Accounting model parameters in the Suluh basin.

Similarly, Figure 6-6 shows the effect of input parameters on the peak runoff responses of the Suluh basin. The soil percolation, soil infiltration and GW1 percolation are the most sensitive parameters for peak flow. Additionally, the deficit and constant loss model was processed integrating a total 13 parameters 4 loss parameter, 5 initial condition parameters, 2 transform parameters and 2 base flow parameters. The 5 initial condition parameters of the deficit and constant loss module were not included during sensitivity analysis due to its effect in the model at the beginning only. Hence the total number of parameters is reduced to 8 (Figure 6-7 and 6-8). Figure 6-7 shows the effect of input parameters on the runoff volume total responses of the basin in the case of deficit and constant loss module. The maximum soil storage capacity is the most sensitive parameter and had significant influence on the simulated runoff volume.

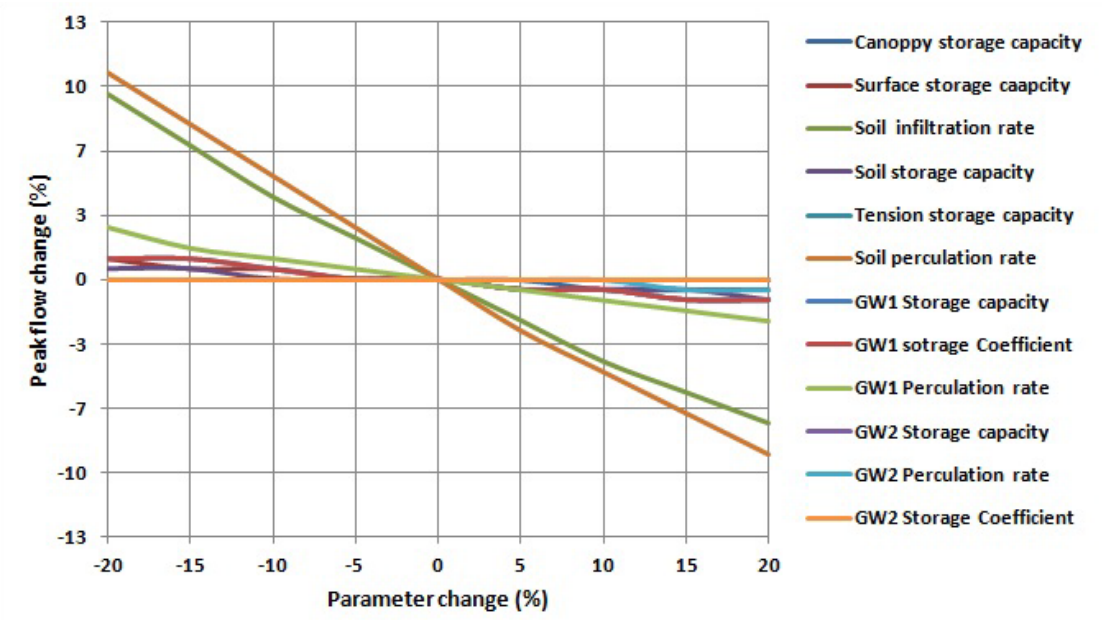

Figure 6-6: Model results (peak runoff (%)) generated from the sensitivity scenarios of the change in the Soil Moisture Accounting model parameters of the Suluh basin.

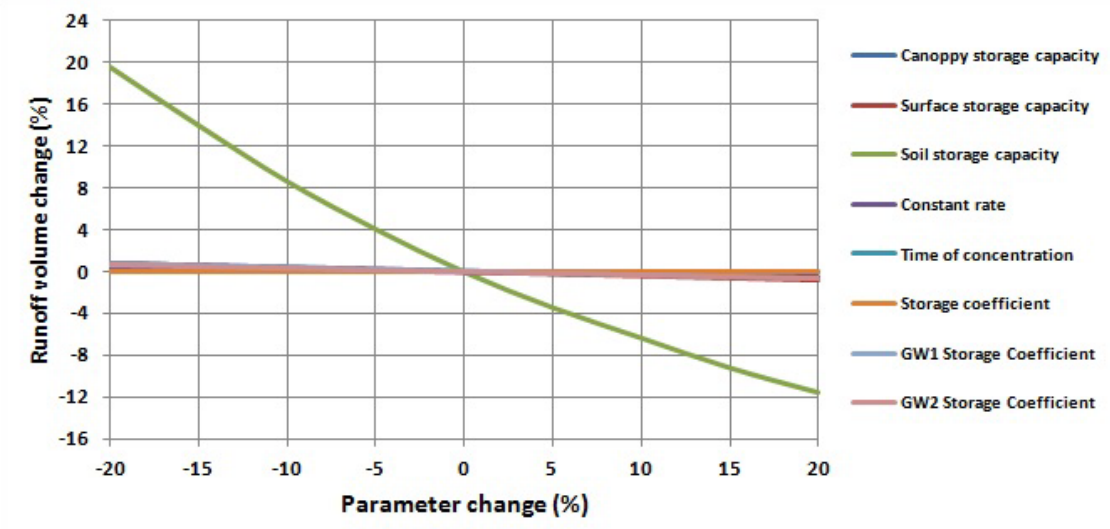

Figure 6-7: Model results (total runoff volume (%)) generated from the sensitivity scenarios of the change in the deficit and constant loss model parameters of the Suluh basin.

Figure 6-8 shows the effect of input parameters on the peak runoff responses of the Suluh basin. The storage coefficient and constant rate are the most sensitive parameters. They have significant influence on the simulated peak runoff response.

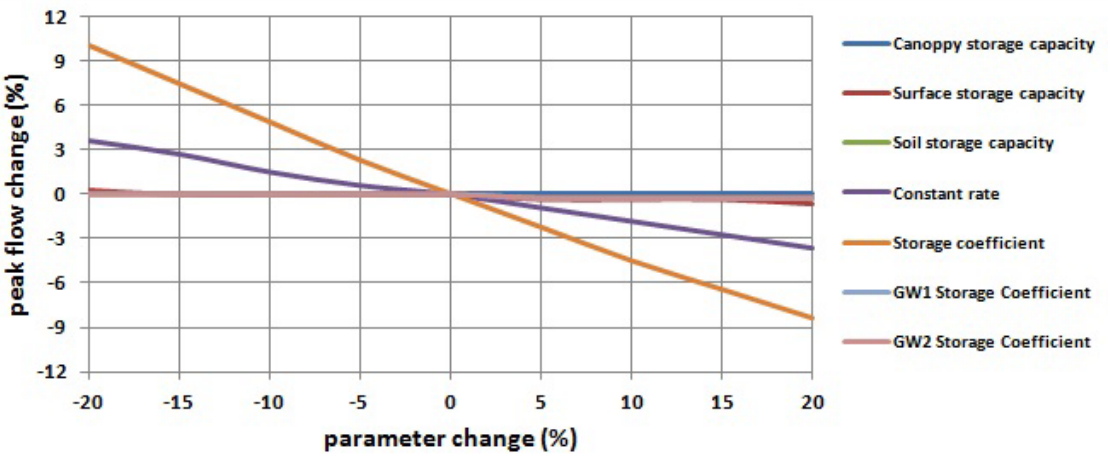

Figure 6-8: Model results (peak runoff (%)) generated from the sensitivity scenarios of the change in the deficit and constant loss model parameters of the Suluh basin.

6.3.2 Calibration and validation

Calibration considered the least sensitive model parameter first and subsequently followed the more sensitive parameters by systematic adjustment of the initial value to optimize the candidate parameter which provides the best fit of the observed stream flow and simulated flow (Vaze et al., 2011). HEC-HMS has internally embedded an optimization manager and has the capabilities to process automated calibration that can be used to estimate model parameter values. The objective function such as sum of the absolute error, sum of the squared error, percent error in peak, percent error in volume and peak-weighted root mean square error were implemented during optimization process to estimate the goodness-of-fit between simulated and observed value (Feldman, 2000). Manual calibration helps to adjust the soft constraints keeping the HEC-HMS hard constraints in preserving the hydrograph shape and minimum error in volume (Yimer et al., 2009). In this study the Nelder and Mead search algorithm of the HEC-HMS optimization manager was applied in the automated model calibration to optimize the set of initial model parameters within the limits obtained by manual calibration.

Model validation is one of the most important steps in rainfall-runoff modeling (Vaze et al., 2011). Validation has often been achieved using a split sample process and is common in the model testing (Meenu et al., 2012). During the validation process the model that was calibrated using the calibration data set for the validation period without changing the model parameters and the goodness of fit statistics are computed for the validation period. 5 years (1992–1996) of observed rainfall and stream flow data are used for calibrating the hydrological model and the remaining 3 years data (1997–1999) for validation. To minimize the model error during initial model set up, the start and finish dates of the simulation were locked to represent inactive hydro-meteorological conditions (Bashar and Zaki, 2005). Graphical and different statistical measures were used to assess the performance of the hydrologic model, including error in peak flow, error in volume, Nash and Sutcliffe (1970) efficiency criterion, %Bias, coefficient of determination and Index of Agreement.

A. Performance of continuous Soil Moisture Accounting loss model

The canopy storage capacity and the surface depression storage parameter were assumed to stay constant during calibration and validation due to their minimum impact on model result. In contrast, the highly sensitive parameters values as maximum infiltration rate, maximum soil storage, tension zone storage, groundwater 2 percolation rate, groundwater 1 and 2 storage depths and groundwater 1 and 2 storage coefficients were modified during the calibration process (Roy et al., 2013). The first three parameters were used to adjust the hydrograph shape during medium and high water periods, while the last four parameters were used to fit the recession curve and the base flow (García et al., 2008). The groundwater 2 percolation rate was adjusted to match with the total runoff volume. For each sub-basin, the modification of the values for the indicated parameters was carried out following homogeneous criteria. Figure 6-9, 6-10 and Table 6-4 show the graphical and different statistical performance measures of Soil Moisture Accounting continuous model for both calibration and validation period with daily and monthly time steps.

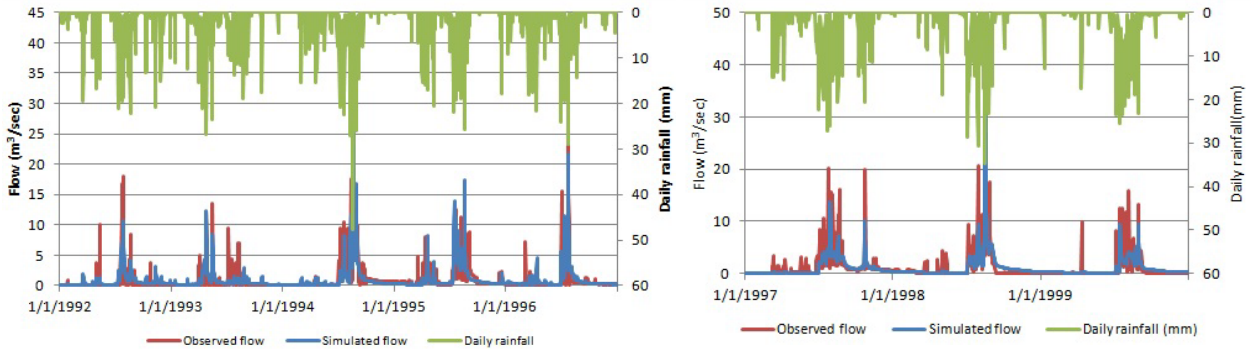

Figure 6-9: Daily calibration (1992–1996) and daily verification (1997–1999) of the Soil Moisture Accounting continuous models for the Suluh basin.

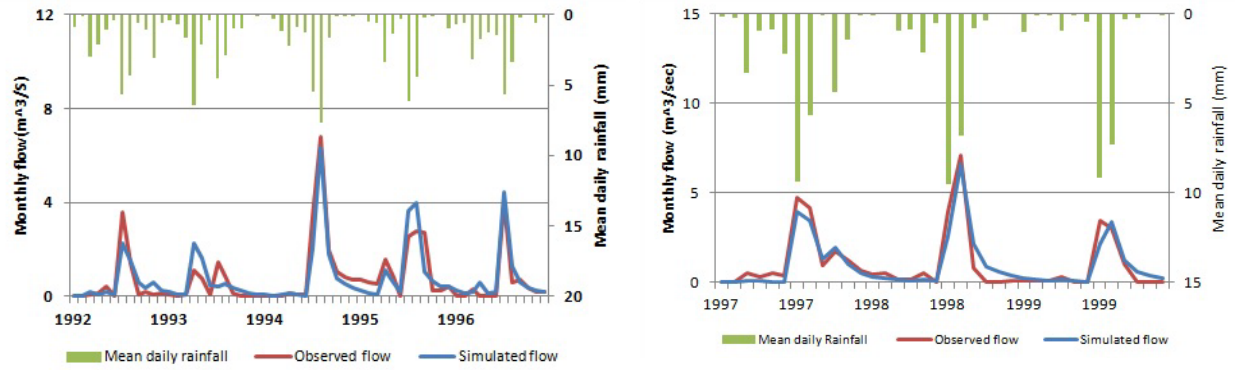

Figure 6-10: Monthly calibration (1992–1996) and monthly verification (1997–1999) of the Soil Moisture Accounting continuous models for the Suluh basin.

Table 6-4: HEC-HMS performance during the calibration and validation periods.

No.	Model efficiency criteria	Daily time step		Monthly time step	
		Calibration	Validation	Calibration	Validation
1	Nash Sutcliffe Efficiency, NSE	0.56	0.52	0.83	0.90
2	Index of Agreement, IoA	0.86	0.83	0.95	0.97
3	Coefficient of determination, R^2	0.57	0.52	0.83	0.91
4	The Index of Columetric Fit, IVF	1.17	4.84	1.01	4.83
5	The relative error of the peak	-22.75	15.13	-6.63	-7.20
6	%Bias	17.31	-4.84	1.19	-4.83

B. Deficit and constant rate loss model

The second approach considers the deficit and constant loss model and is used to compute the losses from the watershed. The deficit and constant loss model uses a single soil layer to account for continuous changes in moisture content (Scharffenberg and Fleming, 2008). It is a quasi-continuous model; as a result computation of actual evapotranspiration in each sub-basin is an integral part of the model simulation based on the monthly input potential evapotranspiration (Meenu et al., 2012). The parameters for the deficit and constant rate loss model include initial deficit, maximum deficit, constant rate, and impervious percentage. Above, based on the Clark unit hydrograph transformation it is assumed that linear reservoir base flow model and lag model channel routing parameters are the same with Soil Moisture Accounting model. Figure 6-11, 6-12 and Table 6-5 document the graphical and statistical performance of deficit and constant loss model for both calibration and validation period with daily and monthly time steps.

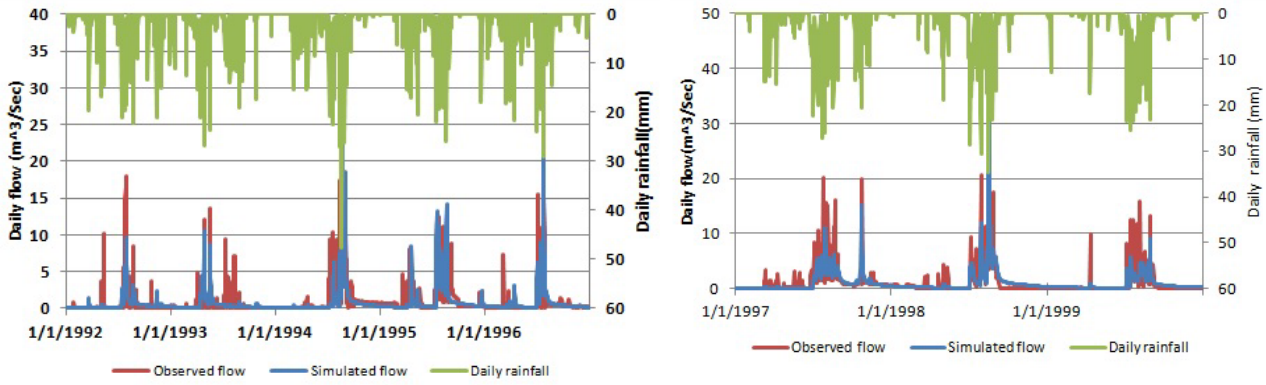

Figure 6-11: Daily calibration (1992–1996) and daily verification (1997–1999) of the deficit and constant loss model for the Suluh basin.

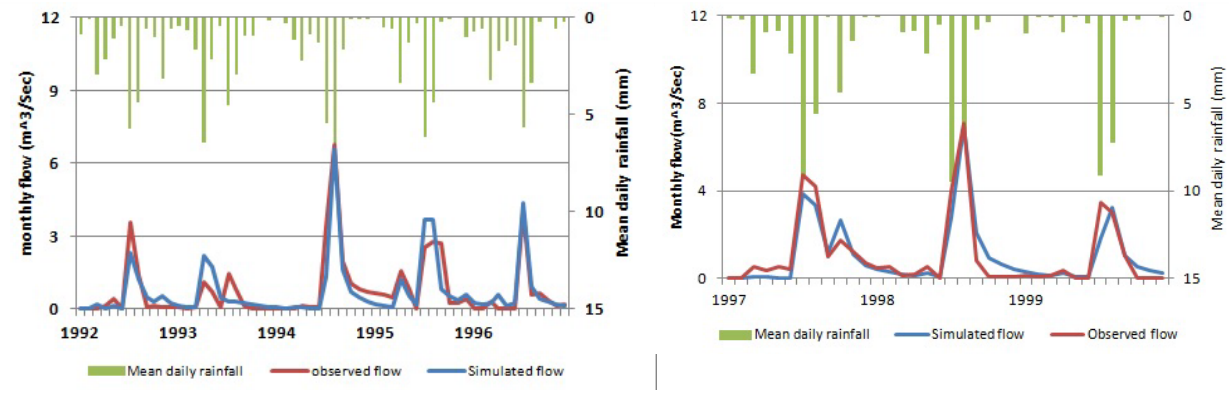

Figure 6-12: Monthly calibration (1992–1996) and monthly verification (1997–1999) of the deficit and constant loss model for the Suluh basin.

Table 6-5: HEC-HMS performance during the calibration and validation periods for the Suluh basin.

St. No.	Model efficiency Criteria	Daily time step		Monthly time step	
		Calibration	Validation	Calibration	Validation
1	Nash Sutcliffe Efficiency, NSE	0.55	0.46	0.80	0.89
2	Index of Agreement, IoA	0.85	0.85	0.95	0.98
3	Coefficient of determination, R^2	0.56	0.49	0.81	0.89
4	The Index of Volumetric Fit, IVF	0.96	2.93	0.96	2.83
5	The relative error of the peak	-9.83	29.61	-2.50	-1.55
6	%Bias	-4.19	-2.93	-4.11	-2.83

6.3.2.1 Time series output for sub-basins

The HEC-HMS model provides complete time series output for various hydrologic process and storage unites for each sub-basin (Table 6-6). All-time series output data are accessed through HEC-DSSVue, HEC Data Storage System (US Army Corps of Engineers Institute for Water Resources - Hydrological Engineering Center, 2009).

Among the simulated model results evapotranspiration, surface runoff, base flow and deep percolation are the most important components in long-term annual water balance calculation. The simulated areal mean annual surface runoff totals 68.3 mm and ranges from a minimum value of 57.3 mm to a maximum value of 93 mm across the sub-basins. Mean annual base flow ranges between from 26 mm and 61.4 mm and deep percolation values ranges between 13.9 mm to 51.5 mm. Figure 6-13 shows the simulated spatial distribution of the annual surface runoff, base flow and deep percolation in each sub-basin.

Table 6-6: Time series output of HEC HMS Model.

1	Outflow (total stream flow) m^3/sec	12	Soil saturation fraction (mm)
2	Potential evapotranspiration (mm)	13	Groundwater layer 1 storage (mm)
3	Canopy overflow (mm)	14	Groundwater layer 1 lateral flow (mm)
4	Canopy evapotranspiration (mm)	15	Groundwater layer 1 percolation (mm)
5	Canopy storage (mm)	16	Groundwater layer 2 storage (mm)
6	Surface evapotranspiration (mm)	17	Groundwater layer 2 lateral flow (mm)
7	Surface storage (mm)	18	Groundwater layer 2 percolation (mm)
8	Incremental precipitation (mm)	19	Excess precipitation (mm)
9	Soil storage (mm)	20	Precipitation loss (mm)
10	Soil percolation (mm)	21	Direct runoff (m^3/sec)
11	Soil evapotranspiration (mm)	22	Base flow (m^3/sec)

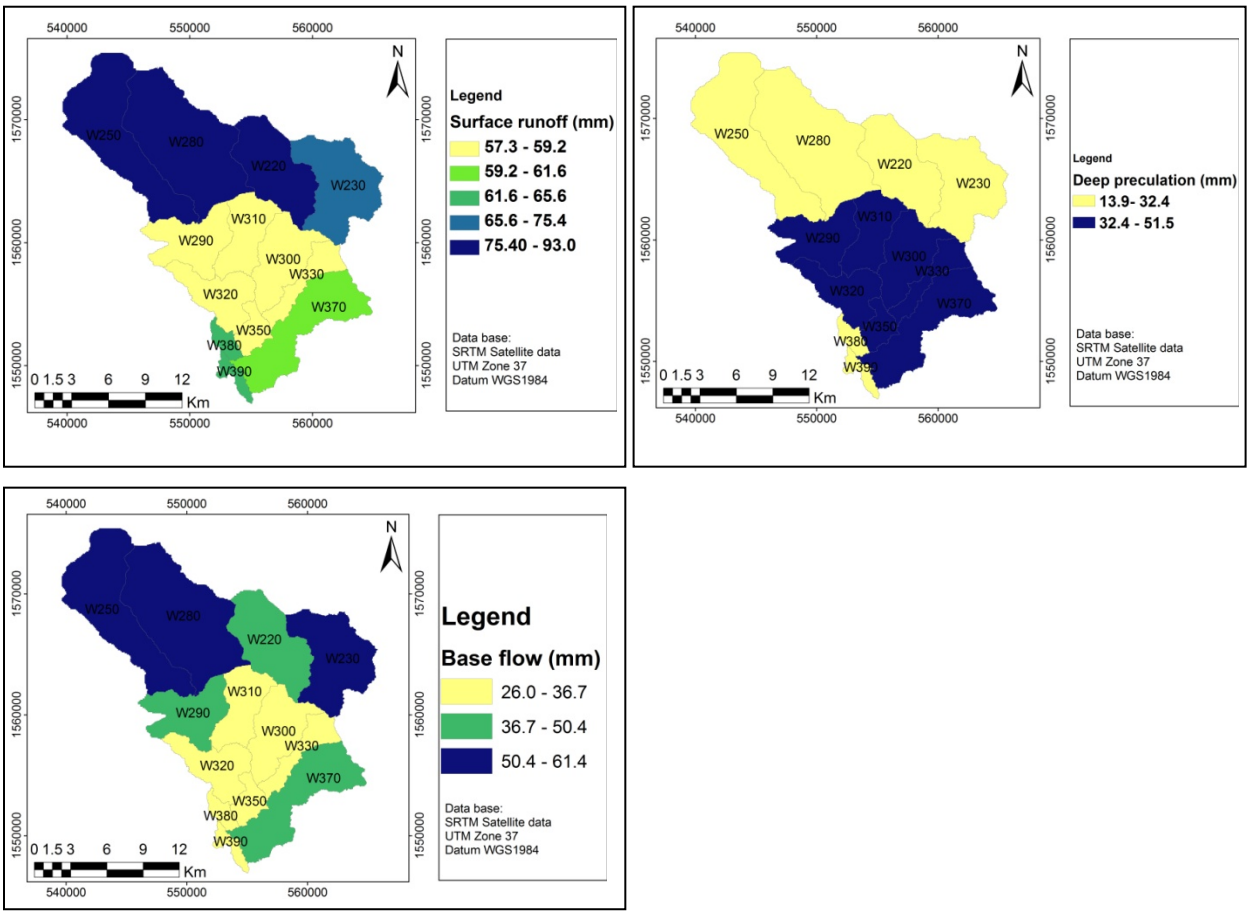

Figure 6-13: Spatial distribution of the annual surface runoff, base flow and deep percolation in each sub-basin of the Suluh basin (data base: Jarvis et al., 2008).

6.4 Runoff simulation using scenario data

6.4.1 Land use change effects

Two land use maps were used to assess the effect of land use change on water resource. The Ethiopian woody biomass land use database (WBISPP, 2003) is used for as a base line to calibrate and validate the HEC-HMS 3.5 hydrologic model.

The 1972 land use map was used for the impact assessment; data were derived by classifying Landsat MSS images. Overall, natural forests, shrubland and grassland covered in 1972 61.5% of the area, cultivated land and bare soil covered a total of 38.5%. In 2003 natural forests diminished to 0.1% and shrubland and grassland cover an area of 38.3%. In 2003 cultivated land dominants and covers 59.8% of the total area. A summary of the annual water balance in the Suluh basin for the baseline simulation (2003 land use map) and 1972 land use map conditions is provided in Table 6-7.

Table 6-7: Summary of long term mean annual water balance based on land use change scenario in the Suluh basin.

Hydrologic process	1972 land use map	2003 land use map
Evapotranspiration (mm)	468.26	472.20
Surface runoff (mm)	65.30	68.28
Base flow (mm)	46.32	41.65
Deep percolation (mm)	43.29	40.09
Total annual yield (mm/year)	111.61	109.94

6.4.2 Climate change effects

The ultimate goal of the meteorological downscaling is to estimate meteorological variables corresponding to a given scenario of future climate and to make them available for hydrological impact assessments. Even though the calibrated and validated hydrological model was found to be competent in replicating the observed stream flow reasonably, its ability to predict the watershed response under future climate conditions completely depends on the model performance under the current scenarios (Dibike and Coulibaly, 2005). Hence, the downscaled daily rainfall data and the monthly potential evapotranspiration data were used to simulate the baseline stream flows. Finally, the mean observed monthly stream flows, the simulated stream flows using observed rainfall, and the baseline stream flows for the period 1992–1999 were compared to validate to validate the model (Dibike and Coulibaly, 2005). After calibration and validation of the hydrological model with the historical data they were tested with downscaled baseline data. The next step was to simulate flows corresponding to future climate conditions by using the downscaled precipitation and temperature data for the emission scenario used in the downscaling experiment HadCM3 A2a, B2a and CGCM3 A2a scenario. Stable soil and land use/ land cover patterns are assumed for the future scenarios.

The future simulation (2011–2040, 2041–2070 and 2071–2099) were carried out with the downscaled precipitation and temperature data. Figure 6-14, 6-15 and 6-16 show the change in simulated daily mean flows of Suluh river corresponding to the downscaled precipitation and temperature data of the

future climate (2011–2040, 2041–2070 and 2071–2099) as compared with observed data. The simulation results show a mean river flow increase in April (minor rainy season) and in the end of the main rainy season (August). However, reduced mean river flow can be expected in the mid of the main rainy season (July) for all future scenarios.

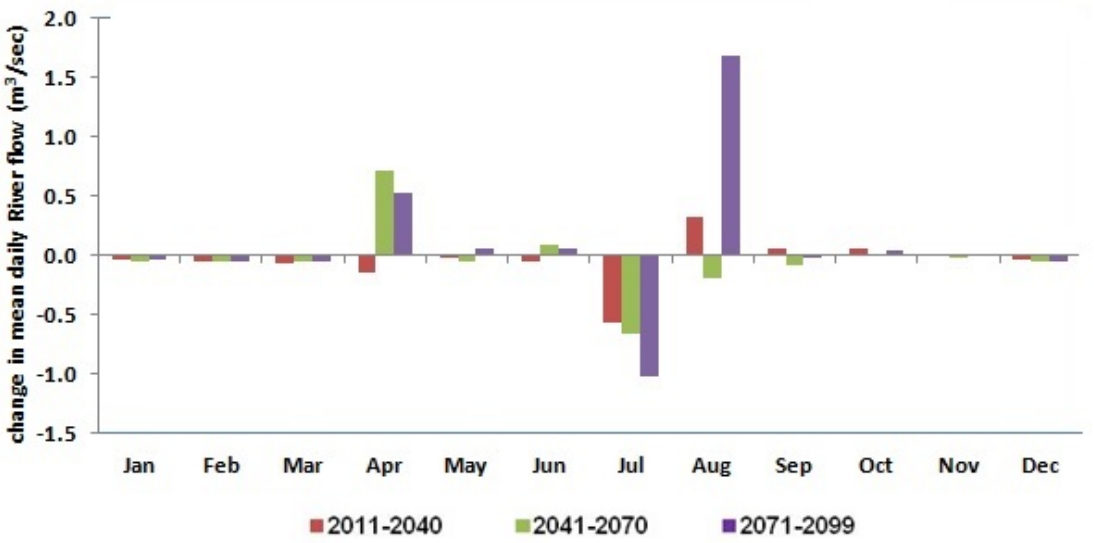

Figure 6-14: Predicted change in mean daily river flow of the Suluh river: HadCM3 A2a climate scenario.

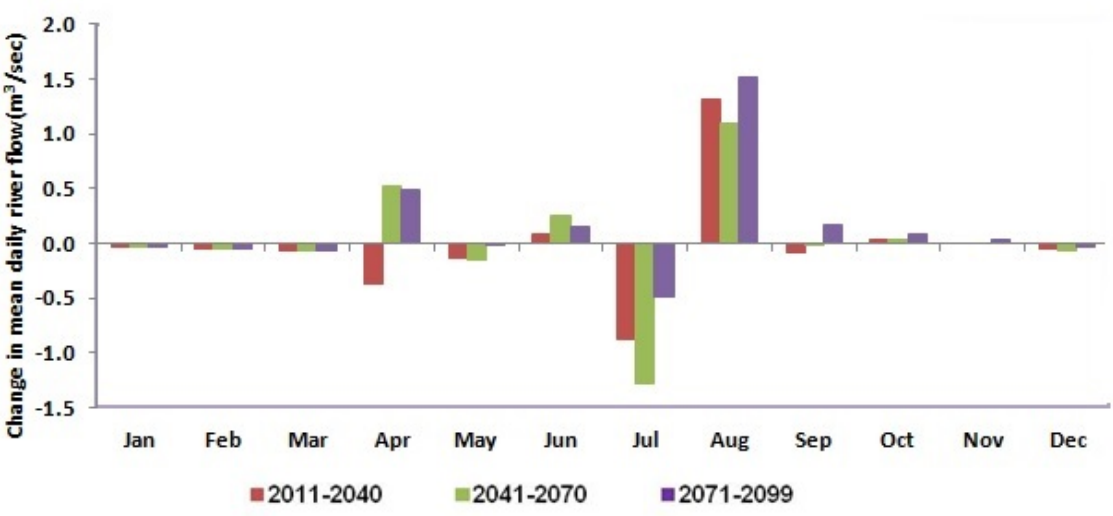

Figure 6-15: Predicted change in mean daily river flow of the Suluh river: HadCM3 B2a climate scenario.

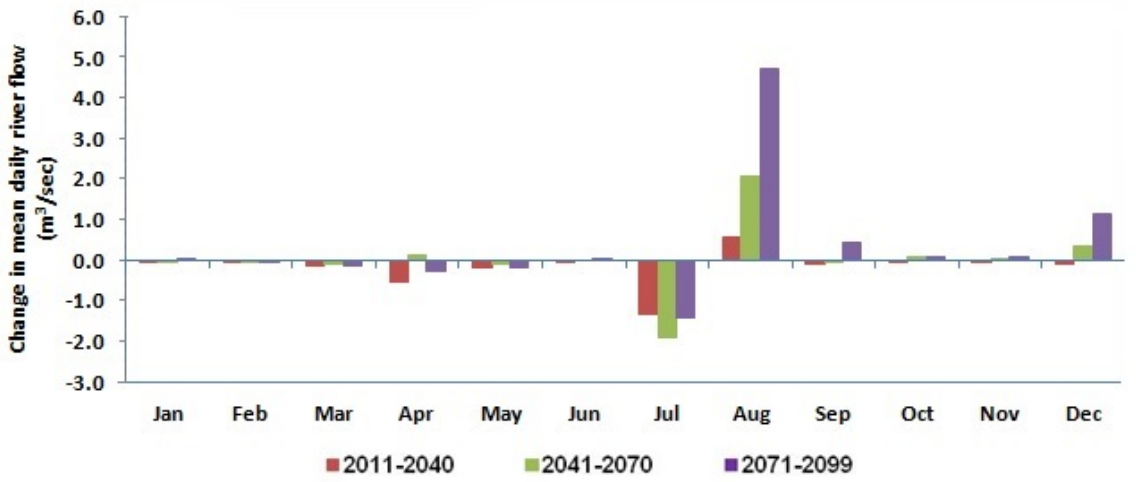

Figure 6-16: Predicted change in mean daily river flow of the Suluh river: CGCM3 A2a climate scenario.

Further comparison of the long term mean annual water balance, i.e. evapotranspiration, stream flow (surface flow and base flow) and deep percolation under present and expected future conditions is performed in order to quantify the changes in hydrology of the watershed due to future climate change in 2011–2040, 2041–2070 and 2071–2099 (Table 6-8, 6-9 and 6-10).

Table 6-8: Summary of long term mean annual water balance of the Suluh river basin 2011–2040.

Hydrologic process	Base line	2011–2040 climate change scenario		
		HadCM3 A2a	HadCM3 A2a	CGCM3 A2a
Evapotranspiration (mm)	472.2	476.5	493.5	451.0
Surface runoff (mm)	68.3	54.0	63.0	47.7
Base flow (mm)	41.7	44.3	42.3	36.7
Deep percolation (mm)	40.1	41.1	41.2	34.6
Total annual yield (mm/year)	109.9	98.4	105.4	84.4

Among the hydrological process the surface runoff will highly susceptible to climate change effect. For example Figure 6-17 shows the sub-basin response to the observed and the projected precipitation of 2020s time horizon with mean annual total rainfall decrease by 1%, 9.2% HadCM3 and CGCM3 A2a scenario respectively and an increase 2.8% HadCM3 B2a during the same period.

The impact of climate change on the hydrology of the Suluh basin shows mixed results. For the HadCM3 A2a scenario, the mean annual water yield decreases 11.7% in 2011–2040, decreases 6.5% in 2041–2070 and increases 4.6% in 2071–2099. Similarly, the mean annual water yield decreases 4.3% in 2011–2040, decreases 1.5% in 2041–2070 and increases 14.7% in 2071–2099 in case of HadCM3 B2a scenario. The CGCM3 A2a climate change projection shows a critically decreases of mean annual water yield in 2011–2040 by 30.2% and increases by 2.4% in 2041–2070 and 25.6% in 2071–2099. Future projection of total water yield in the Suluh basin generally shows a decrease in 2011–2040 and an increase in 2071–2099 (Table 6-10).

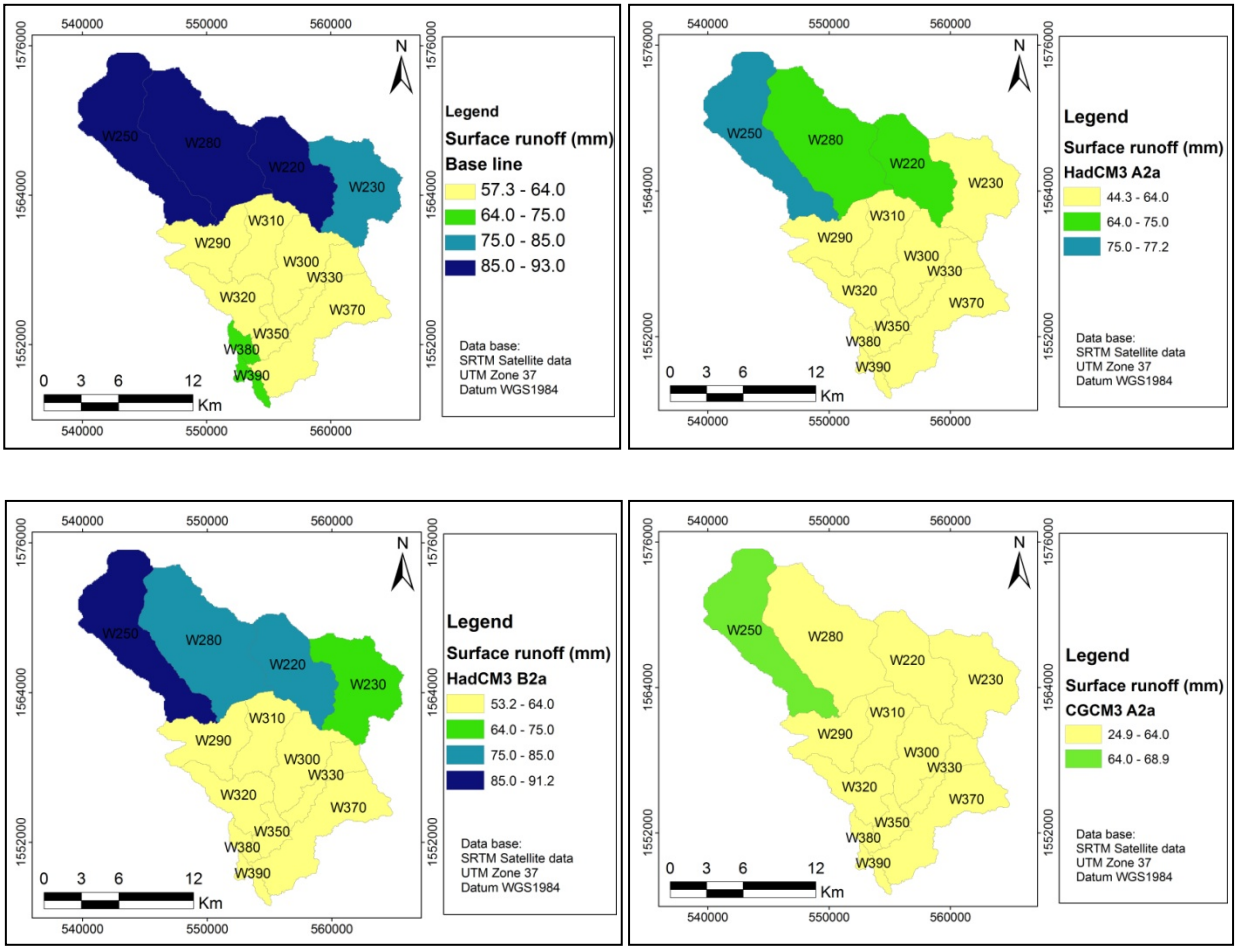

Figure 6-17: Climate change effects on surface runoff of the Suluh river basin for the 2011–2040 climate change scenario (data base: Jarvis et al., 2008).

Table 6-9: Summary of long term mean annual water balance in the Suluh river basin 2041–2070.

Hydrologic process	Base line	2041–2070s climate change scenario		
		HadCM3 A2a	HadCM3 A2a	CGCM3 A2a
Evapotranspiration (mm)	472.2	495.6	501.24	489.5
Surface runoff (mm)	68.3	60.9	66.6	70.7
Base flow (mm)	41.7	42.3	41.7	41.9
Deep percolation (mm)	40.1	41.2	40.5	38.9
Total annual yield (mm/year)	109.9	103.2	108.3	112.6

Table 6-10: Summary of long term mean annual water balance in the Suluh river basin 2071–2099.

Hydrologic process	Base line	2071–2099 climate change scenario		
		HadCM3 A2a	HadCM3 A2a	CGCM3 A2a
Evapotranspiration (mm)	472.2	506.6	498.17	511.3
Surface runoff (mm)	68.3	69.8	79.3	103.0
Base flow (mm)	41.7	45.5	49.6	44.7
Deep percolation (mm)	40.1	41.2	45.7	41.0
Total annual yield (mm/year)	109.9	115.2	128.8	147.7

The climate change impact on actual evapotranspiration is also observed during impact assessment. The predicted minimum and maximum temperature series are used to calculate the potential evapotranspiration (PET) with the FAO Penman-Monteith method (Allen et al., 1998) keeping other climatic factors constant. The canopy, soil and surface evapotranspiration are time series outputs of HEC-HMS model and are together called 'actual evapotranspiration'. It shows an increasing value for all future scenarios except HadCM3 B2a scenario for 2071–2099 (Table 6-7, 6-8 and 6-9).

Chapter 7

7 Discussion

7.1 Land use/land cover change

Changes in land use/land cover at the Suluh basin were analyzed over a period of 31 years (1973–2003). The result reveals significant modification and conversion of land use and land cover of the Suluh basin over the last three decades. A significant part of the Suluh basin was increasingly cultivated. Within the last 31 years, the natural forest cover declined by 93.08%, findings which are confirmed by Hadgu (2008), Tefera and Sterk (2008), Gebresamuel et al. (2010), Fisseha et al. (2011) and Bewket and Abebe (2013). Tekle and Hedlund (2000) and Bewket and Sterk (2005) document a decrease in shrub land that agrees well with the findings of this study which shows a decline of 17.52% for the Suluh basin. Cultivated land includes various types of land use; since it is difficult to differentiate the rural settlement, agricultural land and homestead plantation independently and they are integrated in this category (Tefera and Sterk, 2008; IAO, 2008). Driving forces like population pressure, income growth and declining productivity of existing cultivated land, trigger a sharp increase of cultivated land on the expense of other types of land use which in the case of the Suluh basin causes that more than 80% of the drainage basin area is cultivated (NEDECO, 1997; Donkor and Yilma, 1999; Hadgu, 2008; Alemayehu et al., 2009; Emiru et al., 2012; Hamza and Iyela, 2012; Bewket and Abebe, 2013). An increase in grassland areas is a result of implementation of integrated watershed management measures and environmental rehabilitation programs since 1991 (Taffere, 2003) and zero grazing as well as area enclosure policy of the regional government (Reda, 2007). The land use change rates from 1972 to 1986 and 1986 to 2003 have to be analyzed differentiated. For example, the shrubland decline by 34.9% during the first period and it increases by 26.7% during the second period, meaning a net decrease of 17.5 % between 1972 and 2003. While the decrease in the first period was due to land grabbing, the increase in the second period was mainly due to area protection by the government as well as by government interventions for improved and integrated land use and natural resource management (Taffere, 2003; Bewket and Sterk, 2005; Alemayehu et al., 2009; Emiru et al., 2012). According to Tegene (2002) the expansion of cultivated land is reduced since 1986 as most of the land suitable for cultivation was already in use and the limit for expansion had almost been reached in the highlands. Similarly, for the Suluh valley integrated rural, agriculture and water resources development studies (WAPCOS, 2002) document that the expansion of cultivated land in the basin stagnated as all possible land was already converted including hill slopes.

Individual sub-basins (Figure 5-3; Table 5-3) in the beginning of the 21st century lacked forest cover (sub-basin W250 and W230), a finding confirmed by Gebresamuel et al. (2010) This complete forest degradation was caused by communities who massively expanded the agricultural lands (Hadgu, 2008), cultivated hill slopes (WAPCOS, 2002) and had increased energy demand (Feoli et al., 2002).

7.2 Climate change

7.2.1 Minimum temperature

According to Abebe (2007), based on IPCC mid-range (A1B) emission scenario the projected mean annual temperature will increase in the range of 0.9–1.1^{o}C by 2030, 1.7–2.1^{o}C by 2041–2070 and 2.7–3.4^{o}C by 2071–2099 in Ethiopia as compared to the baseline (1961–1990). However, the result varies according to GCM outputs used, the type of downscaling techniques applied and the geographical location as well.

Among other studies on the region for example Goitom et al. (2012) point out that the mean minimum temperature generally shows a decreasing trend for A2 and B2 scenario of HadCM3 experiment for Geba basin which is in contrary of this study. Similar studies in Baro-Akobo basin (Kebede et al., 2013) based on data downscaled from REMO and CGCM3.1 A1B and B1 scenarios document that the minimum temperature of future scenario does not show uniform trends across the basin, with both a decreasing and an increasing trend observed. For the lake Tana basin Yihun (2009) states as the mean minimum temperature increase by 0.43^{o}C per decade based on the A2a scenario and 0.27^{o}C per decade based on the B2a scenario, both based on the HadCM3 experiment.

7.2.2 Maximum temperature

Previous studies in Ethiopia and the Tekeze basin in particular using HadCM3 A2a and B2a scenario show similar patterns to the findings of this study. Goitom et al. (2012) pointed out that the annual mean maximum temperature shows an increasing trend in the range of 0.86 to 3.10^{o}C and 0.28 to 0.72^{o}C for HadCM3 A2 and B2 emission scenario. In the upper Blue Nile basin, around lake Tana basin, Yihun (2009) reports that the mean maximum temperature will increase by 0.52^{o}C per decade and 0.34^{o}C per decade for the HadCM3 A2a and B2a scenarios. According to Kebede et al. (2013), future scenarios on maximum temperature show mixed results across the Baro-Akobo basin. There is an incremental trend in the range of +0.1^{o}C to +1.23^{o}C for the period of 2011–2030 and of +0.1^{o}C to +1.3^{o}C for the period of 2031–2050 based on REMO A1B and B1. Other studies in the Blue Nile basin confirm an increase trend of maximum temperatures. For example the mean annual temperature over the country is expected to increase by 0.8^{o}C in 2011−2040 and 1.2^{o}C in 2041–2070 based on the CGCM1 B1 emission Scenario (Hulme et al., 2001). Ayalew et al. (2012) report based on the application of HadCM3 A2a scenario, that both, maximum and minimum temperatures will show in the northwestern Ethiopia increasing values in the ranges of 1.55^{o}C to 6.07^{o}C and from 0.11^{o}C to 2.81^{o}C, respectively in 2071–2099.

7.2.3 Precipitation

Previous studies on Ethiopia pointed out that there is a considerable uncertainly and disparity in spatial and temporal predictions of change in precipitation in both magnitude and spatio-temporal distribution (Beyene et al., 2007). It shows great variation related to the GCM outputs and the method of downscaling techniques applied. For example Kebede et al. (2013) identified a change of -2% to +21% from the base period for both A1B and B1 scenarios applying REMO, in contrast: the A1B scenario of

CGCM3.1 predicts -25% to +22% changes of annual rainfall in the study area. In the upper Blue Nile basin (Girma, 2012) tested both CCLM and REMO with ECHAM5 A1B scenario. The result indicates a decrease of precipitation of 6.4 to 6.6% for CCLM and an increase of 9.2 to 22.3% in case of REMO during the same period (Girma, 2012). However, other studies in the same basin (Zelalem, 2013) confirm that spring and summer precipitation will decrease between -36% to 1% and the autumn and winter it will increase up to 126% in future, regardless of the SRES scenario used. The downscaled precipitation in the Geba basin (Goitom et al., 2012) indicates a decrease of rainfall for the forthcoming decades which contradicts to the present study. This 'unpredictable' behavior of precipitation makes the analysis of implications of these changes for streamflow more complicated and uncertain. Hence, there is a need of investigation in both the use of GCM outputs and the downscaling technique.

7.3 Hydrological model

HEC-HMS simulates the hydrologic processes, such as vertical soil moisture flow, evapotranspiration (ET), infiltration, overland flow, channel flow, and ground-water flow within a river basin (Bashar and Zaki, 2005). HEC-HMS includes Soil Moisture Accounting method and deficit and constant loss module which counts on rainfall depths and evapotranspiration rate, as inputs to define the rainfall, runoff, storage and losses relationships. The HEC-HMS simulations were tested by applying two loss model algorithms (Soil Moisture Accounting and deficit and constant loss module). The Soil Moisture Accounting module performs well in both daily and monthly time steps. The accuracy of model calibration and validation were evaluated by qualitatively (graphical) and quantitatively (statistical) approach (Figure 6-9, 6-10, 6-11, 6-12 and Table 6-4, 6-5).

The model performance for the calibration and validation period between the observed and simulated hydrographs in monthly time steps for both model algorithms indicates a good performance, documented by Nash-Sutcliffe efficiency of (0.8) for calibration and (0.9) for validation. The deficit and constant loss model shows weak performance for daily time step especially for validation, documented by a Nash-Sutcliffe efficiency of (0.55) for calibration and (0.46) for validation. The coefficient of determination (R^2) of deficit and constant loss model is lower than the acceptable value for validation (0.49). The model is also unable to capture the peak flow, overestimating it by 29.61% for the validation period. The Soil Moisture Accounting algorithm shows satisfactory performance simulating daily time steps (Table 6-4). The model is unable to capture the peak flow, underestimating it by 22.75% and 17.3% Bias simulating runoff volume during calibration.

It is also noticed that the appearance of peak flow of the observed and simulated flow has an offset between 0 to 1 days. Ayka (2008) explains this due to improper observed rainfall and the poor quality of the collected hydro-meteorological data. Additionally, the model is weak simulating the runoff during the rainy season. This is due to lack of proper data on areal rainfall distribution in the sub-basins as a consequence of inadequate distribution of weather stations inside the Suluh basin. As shown in chapter 4.1.2 March, April and May rainfall correlates with elevation. According to Gebreyohannes (2009) the spring rainfall concentrates north east of the basin and cannot be recorded by the available weather station. In contrast during the main rainy season in summer rainfall the distribution is more or less uniform over the basin and independent from elevation, in consequence areal rainfall can be estimated from the available weather station.

On the other side climatic and hydrological characteristics of the study area have great impact on the model efficiency. According to Goitom (2012) the relative weak performance of WetSPa hydrologic model in the Geba basin is due to the arid climate conditions which greatly depends on topography and results in erratic rainfall events causing flash floods. Similarly the Nash-Sutcliffe efficiency of the HEC-HMS applied to generate in daily time steps is low due to localized precipitation and poor quality rainfall and stream flow data. However, it can be concluded that the HEC-HMS model can simulate the daily stream flow and the water balance of the hydrological processes adequately in case of the Soil Moisture Accounting module.

The HEC-HMS model results provide several hydrologic outputs in time series. Most important for the present study are actual evapotranspiration, annual surface runoff, base flow and deep percolation. The results are provided in the form of time series graphs. The simulated annual water balance represents a summary of the overall basin hydrological components. The long term water balance is the relationship between precipitation as input to the system and evapotranspiration, stream flow (surface and subsurface flow) and deep percolation/groundwater recharge are output from the system. The water balance of a basin usually is affected by the temporal and spatial variation of the input parameters, the local condition and anthropogenic impacts. Keeping the factors constant on annual bases water balance calculations show that long term there is no net change in soil moisture storage due to averaging and neglecting the hydraulic connectivity of neighboring basins (Nedaw, 2010).

The mean annual precipitation falling in the basin is estimated at 624 mm as calculated by Thiessen polygon method. Correspondingly water balance output totals 64.20 mm/year (10.3%) canopy evapotranspiration, 409.80 mm/year (66%) soil and surface evapotranspiration, 68.30 mm/year (11%) surface runoff, 41.65 mm/year (6.3%) base flow and 40.09 mm/year (6.4%) deep percolation or recharge to the deep aquifer.

- *Evapotranspiration*

The annual evapotranspiration is calculated by HEC-HMS model as a sum of evaporation from surface, soil and canopy transpiration of the vegetated cover. Evapotranspiration is the most important component of the hydrological cycle in the Suluh basin with 76.3% of the total precipitation. The high volume of evapotranspiration is related to the semi-arid climatic condition of the area (Aridity Index=0.43). According to Gebreyohannes (2009), the highest potential evapotranspiration in the Suluh basin can be recorded in the northeastern of the basin around Edagahamus-Senkata area. Similarly, the fast increase of vegetation in the rainy season (Goitom, 2012) has great contribution to the high potential evapotranspiration in the basin. Previous studies in the basin reveal that the annual evapotranspiration accounts for 462 mm/year (76%) (Gebreyohannes, 2009), 546.6 mm/year (87.3%) (Goitom, 2012), 440 mm/year (81%) (Arefaine et al., 2012) and 405.6 mm/year (71.7%) (Negusse et al., 2013) of the mean annual precipitation. The model result in this study is in line with these results.

- *Surface runoff*

Annual surface runoff in the gauged Suluh basin ranges between 57.3 mm/year and 93 mm/year with a mean value of 68.3 mm/year (n=13), which is equivalent to an annual total flow of 24.5 million m^3 (Figure 6-11). This amounts 11% of the annual precipitation in the Suluh basin which is in line with the findings of other previous studies in the basin (Table 7-1). In general, according to Zenebe et al. (2011, 2013), the basin runoff coefficient varies between 9 to 47% and decreases with catchment area.

Table 7-1: Summary of surface runoff estimates by different studies.

Author	Annual surface runoff (mm/year)	% of annual rainfall	Methods	Studied basin
Goitom (2012)	74.6	11	WetSpa model	Geba
Arefaine et al. (2012)	40	7	WetSpa model	Ilala
Gebreyohannes (2009)	108	18	WetSpa model	Geba
Nedaw (2010)	73.3	13	Water balance	Koraro

Sub-basins W250, W280 and W220 have relatively high surface runoff response compared to the other sub-basins (Figure 6-13). These three sub-basins are characterized by very steep slopes (>30%), silty clay loam soil texture, shallow soil depth (FAO, 1998) and more than 68% the land use/land cover dominated by shrub land. It is observed that in the Suluh basin soil texture and slope have a strong influence on the generation of surface runoff. Previous studies in the Geba basin (Gebreyohannes, 2009) found that soil texture has stronger impact than land use on surface water modeling applying WetSpa model. The rest of the sub-basins have gentle slopes, sand dominated clay loam soil textures, medium soil depth and are fully dominated by cultivated land. In consequence, surface runoff generated for these sub-basins is relatively low (Figure 6-13).

- *Base flow*

Baseflow is the portion of stream flow that is sustained between precipitation events and fed delayed to the stream channel by subsurface pathways (Price, 2011). The base flow is simulated with the linear reservoir method provided by the HEC-HMS model. During simulation of the rainfall-runoff process the soil moisture accounting algorithm shows a linear relationship between the potential infiltration rate and the water content of the soil. Hence, this linear structure may be a source of error which is actually a non-linear process (Bashar and Zaki, 2005). The base flow is the main component of annual water balance (Figure 6-13). The base flow response of the sub-basin ranges between 26 mm/year to 61.4 mm/year and an averages at the gauge station 41.65 mm/year (6.3%), while Gebreyohannes (2009) estimated as 72 mm/year (11.5%) for Suluh basin.

The sub-basin W250, W280 and W230 contribute relatively high amounts of base flow. These sub-basins are characterized by high elevation as well as a highly dissected topography and have only a low soil and surface evaporation (Gebreyohannes, 2009; Tafere, 2002; Goitom, 2012). Besides, those sub-basins are hydraulically remote from the basin outlet. In contrast, the rest of the sub-basins are characterized by gentle slopes, sand dominated clay loam soil textures and cultivated land resulting in low base flow contribution. The contribution of base flow to stream flow is influenced by basin geology, topography and soil characteristics (SKM, 2009 and Price, 2011).

- *Deep Percolation*

Deep percolation contributes to recharge the aquifer system. In general groundwater recharge in the sub-basin is promoted by low evapotranspiration and low surface runoff, i.e. flat topography and permeable soils. Figure 6-13 shows the annual deep percolation map resulting from the application of the HEC-HMS soil moisture model. Deep percolation in the gauged Suluh basin ranges between 13.85 to 51.46 mm/year, with a mean value of 41.09 mm/year (which is equivalent to 14.4 million m^3/year). This makes up 6.4% of the total annual precipitation in the basin. This result is consistent with the previous studies in the basin (Table 7-2).

Table 7-2: Summary of deep percolation/recharge estimates by different studies.

Author	Deep percolation/ recharge (mm/year)	% of annual rainfall	Methods	Studied basin
Tesfagiorgis et al. (2011)	21.3	4	WetSpa model	Geba
Teferi (2009)	32	5	WATBAL model	Aynalem
Arefaine et al. (2012)	66	12	WetSpa model	Ilala
Gebreyohannes (2009)	37	6	WetSpa model	Geba
Kahsay (2008)	30–40	4.5–6	Chloride mass balance method	Aynalem
Nedaw (2010)	56.7	10.3	Water balance	Koraro

The sub-basins (Figure 6-13) W380, W370, W350, W320, W310, W300, W290 are identified and mapped by Gebreyohannes (2009) as high recharging site of the Geba basin. This corresponds to the results of this study. Main factors controlling deep percolation are soils with a sandy texture and the predominance of gentle slopes.

7.4 Effect of land use change on water resources

According to Donkor and Yilma (1999) deforestation considerably affects quantity and quality of water resources. The land use and land cover change on the water resources of the Suluh basin is assessed based on the comparison of the Woody Biomass Inventory and Strategic Planning Project (WBISPP, 2003) and the 1972 land use map. The results from the application of the HEC-HMS soil moisture model show that the average annual stream flows remained stable between 1972 with 111.3 mm and 2003 with 109.9 mm. Besides, also the actual evapotranspiration remained stable (1972: 468.3 mm, 2003: 472.2 mm). Also changes in surface runoff are only slight (1972: 65.3 mm, 2003: 68.28 mm) as well as changes in base flow (1972: 46.32 mm, 2003: 41.65 mm) and deep percolation (1972: 43.29 mm, 2003: 40.1 mm). The slight increase of surface runoff and the slight decrease of base flow are associated with the land use and land cover change but remain small in magnitude. Haberlandt (2010) compared hydrological models fed with three different land use change scenario. In the 'deforestation scenario' the agricultural area has been increased by 15% at the expense of forested area. For the 'urbanization scenario' the urban area has been increased by 26% at the expense of agricultural land. In the 'afforestation scenario' the forested areas have been increased by 30% at the expense of agricultural land. Result of HEC-HMS model application show only very small differences between the results of these scenarios while at the same time WaSIM-ETH shows considerable reactions for the afforestation

and deforestation scenario. Applying SWAT Girma (2012) found only weak responses for upper Blue Nile basin integrating land use/ land cover change scenarios. These differences in the result of different model application might be due to the model set up: WaSIM-ETH is a fully distributed hydrological model considering the change in cell by cell bases while HEC-HMS and SWAT hydrologic models are sub-basin configurated and have lumped parameter values.

The model output parameters that strongly relate to land use/land cover (SKM, 2009) are the following: maximum soil infiltration rate, canopy storage capacity and soil and tension zone thicknesses. The parameter controlled by land use change with the strongest impact on flood generation is the maximum soil infiltration rate (SKM, 2009). However, this parameter is more dependent on soil texture rather land use/land cover type. Several other studies on the effects of land use change in Ethiopia (Legesse et al., 2003; Bewket and Sterk, 2005; Gebresamuel et al., 2010) documented a decreasing of stream flow with increasing area of arable land.

Generally, the observed changes on mean annual surface runoff, base flow, and deep percolation from the sub-basin are linked to the changes in land use/land cover associated with expanding cultivated land and degradation of catchment resources (expansion of degraded grazing lands and reduction of vegetative cover, particularly shrubs and natural forest). However, the increment of evapotranspiration is partly linked to climate change due to the increment of temperature.

7.5 Effects of future climate change on water resource

The effect of climate change on water resources concentrates on the two Ethiopian rainy seasons: the lesser rainy season (*Belg*) from March to May and the main rainy season (*Kiremit*) from June to September. *Kiremit* and *Belg* are the cropping seasons in Ethiopia, particularly in Suluh basin.

Different climate change scenarios were used as input data for HEC-HMS for impact assessment on water balance. In the coming 90 years the future projections of mean monthly flow indicate mixed results for the two rainy seasons *Belg* and *Kiremit* (Table 7-3).

The projected stream flow shows a decline in the months December to March in all the three future periods under the A2 and B2 scenarios of the HadCM3 and CGCM3 experiments. There is an increase in the flows of April in 2041–2070 and 2071–2099 under all scenarios except for the CGCM3 A2a scenario in 2071–2099. Stream flows in May and July also decrease in all three periods under both scenarios with exception of the HadCM3 A2 scenario in 2071–2099 for the month May. The mean monthly stream flow in June increases in all future time periods except for 2011–2040 under the HadCM3 and CGCM3 A2a scenarios. In August stream flow will increase with exception of the HadCM3 A2a scenario in 2041–2070.

Table 7-3: Projected relative (%) change of mean monthly stream flows at the outlet of the Suluh basin under different climate change scenarios.

Month	HadCM3 A2a			HadCM3 B2a			CGCM3 A2a			Ethiopian season
	2011–2040	2041–2070	2071–2099	2011–2040	2041–2070	2071–2099	2011–2040	2041–2070	2071–2099	
Dec	-17.4	-28.6	-22.7	-22.7	-28.6	-12.5	-35.0	57.8	81.1	*Bega*
Jan	-28.6	-38.5	-28.6	-28.6	-28.6	-20.0	-50.0	-5.9	25.0	
Feb	-50.0	-50.0	-50.0	-50.0	-50.0	-50.0	-66.7	-36.4	-7.1	
Mar	-41.2	-26.3	-33.3	-41.2	-33.3	-33.3	-118.2	-41.2	-84.6	
Apr	-10.1	30.5	24.1	-29.1	24.4	23.0	-45.1	8.4	-18.8	
May	-2.6	-18.2	11.4	-50.0	-69.6	-2.6	-77.3	-30.0	-69.6	*Belg*
Jun	-50.0	33.3	25.0	30.8	59.1	45.5	-38.5	0.0	14.3	
Jul	-21.0	-25.7	-45.1	-36.1	-64.0	-17.6	-67.3	-139.4	-75.4	
Aug	6.5	-4.6	26.8	22.4	19.2	24.9	11.6	31.3	50.9	
Sep	5.0	-10.3	-1.1	-9.1	-1.1	15.0	-10.3	-3.2	30.9	*Kiremt*
Oct	9.6	2.1	7.8	6.0	6.0	14.5	-2.2	17.5	19.0	
Nov	2.9	-3.1	2.9	0.0	0.0	8.3	-10.0	2.9	19.5	*Tseday*

Applying the HadCM3 A2a scenario climate change will impact the hydrology of the Suluh basin in the way that the mean annual water yield decreases in 2011–2040 by 11.7%, in 2041–2070 by 6.5% and increases in 2071–2099 by 4.6%.

Similarly, the mean annual water yield will decrease by 4.3% in 2011–2040, by 1.5% in 2041–2070 and increase by 14.7% in 2071–2099 applying the HadCM3 B2a scenario. The CGCM3 A2a climate change projection causes a critically decrease on mean annual water yield in 2011–2040 by 30.2% and an increase by 2.4% in 2041–2070 and 25.6% in 2071–2099. The mean annual surface runoff is more sensitive to climate change compared to other hydrological process. The sub-basin response (Figure 6-17) indicates the effect of future climate change on mean annual surface runoff. Future projection of total water yield in the Suluh basin generally shows a decrease in 2011–2040 and an increase in 2071–2099 for all climate change scenarios. Previous studies in the basin indicate that stream flow of the Geba basin will be reduced and predict an increasing water stress under future climate change (Goitom et al., 2012). Other studies show inconsistent results. For example Girma (2012) reports there will be an increase in the future runoff using the regional climate change projections of ECHAM5-A1B downscaled by the REMO and CCLM whereas Zelalem (2013) points out a decrease of stream flow for the Blue Nile basin by 10 to 60% for downscaled predictors from three GCMs (ECHAM5, GFDL21 and CSIRO-MK3) under the SRES scenarios A1B and A2. Similarly, Yihun (2009) reports an increase of seasonal flow volume up to 136% during *Belg* and 36% during *Kiremt*. In contrast Abdo (2008) and Yimer et al. (2009) state a runoff decrease during the main rainy season (June–September) by 12% in 2071–2099 around Tana lake basin. These results indicate that there is a need for further studies to better understand the reasons for contrasting results on impact assessment of future climate change. The uncertainty of GCM outputs, downscaling techniques and the type of hydrological model applied have a significant impact on the result.

Chapter 8

8 Conclusions and Recommendations

8.1 Conclusions

In order to assess the potential effects of land use and land cover change and climate change on the water resources of the Suluh basin the hydro-climatology, geomorphology, geology, land use and land cover and soils of the basin has been investigated. Emphasis was made to create a database on all information relevant for water resource impact assessment of the basin. To attain the overall objective several activities were undertaken: (1) statistical analyses of historic climate trends and seasonality patterns, (2) field and laboratory based soil mapping, (3) geomorphological mapping of the test sites (4) analysis of land use/land cover change in the basin since 1972, (5) downscaling of GCM's output climate data using the Statistical DownScaling model (5) calibration and validation of the HEC-HMS semi distributed model and simulation of hydrological processes with scenario data for impact assessment on water resources of the basin. Based on the results the following main conclusions can be drawn:

- **Statistical analysis of climate data**

Statistical methods have been applied to characterize the seasonality and temporal variability of the past climatic records of 37 years observed at seven weather stations in and around Suluh basin. Seasonality index technique was used to analyze the degree of variability in monthly rainfall patterns, while Spearman's rank correlation non parametric statistical trend test was used to detected temporal changes.

The calculated Relative Seasonality Index for the area revealed that rainfall regime is markedly seasonal with a long dry season. The analysis of the seasonality index shows for Wukro and Mekelle weather stations that most of the rain occurs in one to two months of the year, concentrated on the main rainy season. At Senkata, Edagahamus and Adigrat weather stations rainfall is relatively concentrated on the two rainy seasons separated by a marked dry season. At Hawzen and Hagerselam weather stations most rain occurs in less than three months of the year.

Based on 37 years of data records and seven weather stations, time series analysis shows that the annual precipitation lacks a trend. In contrast, the mean monthly temperature at Mekelle weather station shows increases.

- **Geomorphological mapping**

A direct interrelationship between natural processes and human impact is observed for the Tsenkanet, Abraha-we-Atsebeha and Bat'akor test sites. The high population pressure on landscape stability causes humans degradation processes. Geomorphological survey clearly indicated soil erosion due to running water, mass movements and human induced landscape modification as the dominant relief shaping processes. Erosion forms and badlands develop consequentially to clearance of natural vegetation and overgrazing as well as to a lack of maintenance of existing soil conservation measures. The development of gully systems also indicates the alarming impact of channeled runoff along footpaths and cattle treads.

- **Land use change dynamics**

This research tried to examine the long-term dynamics in land use/land cover change and the driving forces for changes in the Suluh basin. It revealed that there were substantial land use changes in the area during the past 31 years (1972–2003). The most important changes were destruction of the natural vegetation, an increase of area with cultivated land, a slight expansion of grazing land and a decline of shrub land and bare land. The basic driving force is the rapidly growing population with a rate of 2.6% per annum (CSA, 2008), in turn leading to an increased demand for food, water and energy.

- **Climate change**

Already in previous studies it was tried to predict the impact of climate change on the water resource in the Suluh basin, mostly based on a single GCM output. Since each GCM and downscaling tool has its own strength and weakness, it may be not acceptable to rely on the outputs of one GCM. These shortcomings of the previous climate impact studies in the Suluh basin are addressed to some extent in this study.

Downscaling was attempted based on the HadCM3 and CGCM3 GCMs outputs under two SRES emission scenarios (A2a and B2a) using Statistical DownScaling Methods (SDSM) on a local watershed scale for the 2011–2040, 2041–2070 and 2071–2099 time interval.

The results reveal that an increase of the mean annual maximum and minimum temperature in the time intervals 2041–2070 and 2071–2099 has to be expected. The mean annual precipitation also indicates a decrease for 2011–2040 and an increase for 2071–2099 for all emission scenarios.

- **HEC-HMS model application**

The HEC-HMS semi-distributed hydrological model was tested for the Soil Moisture Accounting algorithm and the deficit and constant loss model. The deficit and constant loss model performs well in both daily and monthly time steps. The calibrated and validated Soil Moisture Accounting module has been used for prediction of its hydrologic response to land use/land cover and climate change effect in the Suluh river basin.

The local sensitivity analysis shows that soil infiltration rate, soil storage, tension zone storage and groundwater 1 storage coefficient are the most sensitive parameters for the simulation of stream flow. The Nash-Sutcliffe model efficiency, the Index of Agreement (IoA), the percentage error in volume and the percentage error in peak were used for performance evaluation, for calibration and validation; all indicating a good performance of the model for the simulation of hydrological processes.

- **Impact of land use on water resource**

The impact assessment of land use/ land cover change on water resources is based on the 1972 land use map derived from LandSat MSS image and the 2003 woody biomass land use map. Land use change between 1972 and 2003 resulted in deforestation and expansion of cultivated land. In turn the surface runoff increased by 4.6% and base flow and deep percolation were reduced by 10.08% and 7.4% respectively. Also evaporation rate shows a slight increment. The annual water yield reduced by 1.5%.

- **Impact of climate change on water resource**

The impact assessment of climate change is carried out for the time intervals 2011–2040, 2041–2070 and 2071–2099. On the annual bases the climate change will cause a decrease of mean annual water yield by 11.7% in 2011–2040, by 6.5% 2041–2070 and an increase by 4.6% in 2071–2099 applying the HadCM3 A2a scenario. Similarly, the application of HadCM3 B2a scenario shows that the mean annual water yield decreases by 4.3% in 2011–2040, by 1.5% in 2041–2070 and an increase by 14.7% in 2071–2099. The CGCM3 A2a climate change projection shows a critically decrease of the mean annual water yield of 30.2% in 2011–2040 and an increase of 2.4% in 2041–2070 and of 25.6% in 2071–2099. Among the hydrological processes surface runoff is identified the most sensitive one reacting on climate changes.

8.2 Recommendations

During this study it was tried to identify and come across various problems, which not all could be answered in this study, but need to be addressed in future research. The following list shows the most important issues:

Field sampling and laboratory based soil mapping is bulky, time intense and expensive on river basin scale. Due to the case, soil properties investigations undertaken for these studies have a coarse spatial resolution and are only for soil texture classification. For further field investigation it is recommended to include in-situ soil infiltration tests, hydraulic conductivity test and soil compactness.

It is known that different soil and water conservation measures have certain impact on rainfall-runoff relationships. The research presented not fully considers the soil conservation measures. It should be addressed for future research.

River discharge data in the Suluh basin are limited and the accuracy of the data is poor. The installation of more river gauging stations in the basin and updating of the rating curve will improve data availability and quality. As all currently available weather stations are found only in the vicinity of the Suluh basin, it is mandatory to install at least one additional weather station inside the basin for better estimation of areal rainfall distribution. This will help to improve the water resources assessment in the future.

In the climate change impact assessment, this study did not cover uncertainties due to the selection of GCMs outputs or selection of different emission scenarios, nor did this study quantify the possible bias. This will address in the future.

Downscaling of large scale climate variables was done only for Mekelle airport weather station. This is due to the lack of long term climate data in other stations in the basin or its surroundings. It is recommended to include downscaling of other station data to improve the climate change impact assessment across the basin.

The present day land-use data were used for simulating future hydrological processes. It is more accurate that considering future land-use change scenarios along with fully distributed hydrological model. It is therefore recommended to follow a careful study of the combined effects of climate and land-use change on the hydrological processes and water resources in the study area.

Finally, this study involved a number of models and model outputs each including a certain level of uncertainty. However, it is believed that the results of this study give an indication and increase awareness on the changes of land use/land cover and future risks of climate change. Hence, such studies should continue on different basins considering the wide range of uncertainties associated with models and try to reduce the uncertainties by the use of different GCM outputs, downscaling techniques, and emission scenarios as well as different hydrological models.

9 References

Abdo, K. S. (2008). Assessment of Climate Change Impacts on the Hydrology of Gilgel Abbay Catchment in Lake Tana Basin, Ethiopia. Master's thesis, Institute for Geo-information Science and Earth Observation, Enschede, The Netherlands.

Abdurahman, M. A. (2009). Assessment of Micro-Dam Irrigation Projects and Runoff Predictions for Ungauged Catchments in Northern Ethiopia. PhD thesis, Westfälische Wilhelms-Universität Münster, Germany.

Abebe, S. (2010). Mitigating Drought: Policy Impact Evaluation A Case of Tigray Region, Ethiopia. Unpublished Master's thesis, International Institute for Geo-information Science and Earth Observation (ITC), Enschede, The Netherlands.

Abebe, T. (ed.) (2007). Climate Change National Adaptation Programme of Action (NAPA) of Ethiopia. Addis Ababa, Ethiopia.

Adnan, N. A. (2010). Quantifying the Impacts of Climate and Land Use Changes on the Hydrological Response of a Monsoonal Catchment. PhD thesis, University of Southampton, United Kingdom.

Ahsan, M. and O'Connor, K. M. (1994). A simple Non-Linear Rainfall-Runoff Model with a Variable Gain Factor. *Journal of Hydrology* **155**(1–2): pp. 151–183.

Alemayehu, F., Nurhussen, T., Nyssen, J., Girma, A., Zenebe, A., Behailu, M., Deckers, S. and Poesen, J. (2009). The Impacts of Watershed Management on Land Use and Land Cover Dynamics in Eastern Tigray (Ethiopia). *Resources, Conservation and Recycling* **53**(4): pp. 192–198.

Allen, R. G., Pereira, L. S., Raes, D. and Smith, M. (1998). Crop Evapotranspiration - Guidelines for Computing Crop Water Requirements. Irrigation and Drainage Paper 56. Food and Agriculture Organization of the United Nations (FAO). Rome, Italy.

American Society for Testing and Materials (ASTM) (1998). Designation: D 422 – 63 (Reapproved 1998). Standard Test Method for Particle-Size Analysis of Soils. ASTM, West Conshohocken, PA, USA.

Amsalu, A., Stroosnijder, L. and De Graaff, J. (2007). Long-term Dynamics in Land Resource Use and the Driving Forces in the Beressa Watershed, Highlands of Ethiopia. *Journal of Environmental Management* **83**(4): pp. 448–459.

Anderson, S., Gundel, S. and Vanni, M. (2010). The Impacts of Climate Change on Food Security in Africa: A Synthesis of Policy Issues for Europe. International Institute for Environment and Development (IIED). London, United Kingdom.

Araya, H. and Edwards, S. (2006). The Tigray Experience: A Success Story in Sustainable Agriculture. Environment & development series 4. Third World Network. Penang, Malaysia.

Arefaine, T., Nedaw, D. and Gebreyohannes, T. (2012). Groundwater Recharge, Evapotranspiration and Surface Runoff Estimation Using WetSpass Modeling Method in Illala Catchment, Northern Ethiopia. *Momona Ethiopian Journal of Science* (MEJS) **4**(2): pp. 96–110.

Asmamaw, L. B., Mohammed, A. A. and Lulseged, T. D. (2011). Land Use/Cover Dynamics and their Effects in the Gerado Catchment, Northeastern Ethiopia. *International Journal of Environmental Studies* **68**(6): pp. 883–900.

Ayalew, D., Tesfaye, K., Mamo, G., Yitaferu, B. and Bayu, W. (2012). Outlook of Future Climate in Northwestern Ethiopia. *Agricultural Sciences* **3**(04): pp. 608–624.

Ayka, A. (2008). Hydrological Models Comparison for Estimation of Floods in the Abaya-Chamo Sub-Basin. Thesis, Addis Ababa University, Ethiopia.

Bashar, K. E. and Zaki, A. F. (2005). SMA Based Continuous Hydrologic Simulation of the Blue Nile. A paper published in the International Conference of UNESCO Flanders FUST FRIEND/NILE Project "Towards a Better Cooperation". Sharm El-Sheikh, Egypt.

Behailu, M. (2002). Assessment and Optimization of Traditional Irrigation of Vertisols in Northern Ethiopia: A Case Study at Gumselasa Microdam using Maize as an Indicator Crop. PhD thesis, Universiteit Gent, Belgium.

Behailu, M. and Haile, M. (2003). Water Harvesting in Northern Ethiopia: Environmental, Health and Socio-economic Impacts. In: McCornick, P. G., Kamara, A. B. and Girma Tadesse (eds.) (2003). Integrated water and land management research and capacity building priorities for Ethiopia. Proceedings of a MoWR/EARO/IWMI/ILRI international workshop held at ILRI, Addis Ababa, Ethiopia, 2–4 December 2002. IWMI (International Water Management Institute), Colombo, Sri Lanka, and ILRI (International Livestock Research Institute). Nairobi, Kenya: pp.185–191.

Bekele, S. (2003). Challenges and opportunities in capacity building for water resources development and research in Ethiopia: The AWTI experience. In: McCornick, P. G., Kamara, A. B. and Girma Tadesse (eds.) 2003. Integrated water and land management research and capacity building priorities for Ethiopia. Proceedings of a MoWR/EARO/IWMI/ILRI international workshop held at ILRI, Addis Ababa, Ethiopia, 2–4 December 2002. IWMI (International Water Management Institute), Colombo, Sri Lanka, and ILRI (International Livestock Research Institute). Nairobi, Kenya: pp.141–148.

Bennett, T. and Peters, J. (2000). Continuous Soil Moisture Accounting in the Hydrologic Engineering Center Hydrologic Modeling System (HEC-HMS). In: Hotchkiss, R. H. and Glade, M. (eds.). Building Partnerships. Proceedings of the 2000 Joint Conference on Water Resources Engineering and Water Resources Planning and Management, held in Minneapolis, Minnesota, July 30-August 2, 2000. MN, USA: pp. 1–10.

Berakhi, O., Brancaccio, L., Calderoni, G., Coltorti, M., Dramis, F. and Umer, M. M. (1998). The Mai Maikden Sedimentary Sequence: a Reference Point for the Environmental Evolution of the Highlands of Northern Ethiopia. *Geomorphology* **23**(2–4): pp.127–138.

Bewket, W. and Abebe, S. (2013). Land-Use and Land-Cover Change and its Environmental Implications in a Tropical Highland Watershed, Ethiopia. *International Journal of Environmental Studies* **70**(1): pp. 126–139.

Bewket, W. and Sterk, G. (2003). Assessment of Soil Erosion in Cultivated Fields Using a Survey Methodology for Rills in the Chemoga Watershed, Ethiopia. *Agriculture, Ecosystems & Environment* **97**(1–3): pp. 81–93.

Bewket, W. and Sterk, G. (2005). Dynamics in Land Cover and its Effect on Stream Flow in the Chemoga Watershed, Blue Nile Basin, Ethiopia. *Hydrological Processes* **19**(2): pp. 445–458.

Beyene, T., Lettenmaier, D. P. and Kabat, P. (2007). Hydrologic Impacts of Climate Change on the Nile River Basin: Implications of the 2007 IPCC Climate Scenarios. *Climatic Change* **100**: pp. 433–461.

Bosellini, A., Russo, A., Fantozzi, P. L., Assefa, G. and Solomon, T. (1997). The Mesozoic succession of the Mekelle Outlier Tigre Province, Ethiopia. *Memorie di Scienze Geologiche* **49**: pp. 95–116.

Canadian Institute for Climate Studies (CICS): Canadian Climate and Impacts Scenarios. HadCM3 A2 and B2 Emission Scenario [online].
URL: http://www.cics.uvic.ca/scenarios/sdsm/select.cgi) [Date of access: 12/02/2011].

Central Statistic Agency of Ethiopia (CSA) (2008). Summary and Statistical Report of the 2007 Population and Housing Census of Ethiopia: Population size by age and sex. Addis Ababa, Ethiopia.

Chow, V. T, Maidment, D. R. and Mays, L. W. (1988). Applied hydrology. NY, USA.

Coltorti, M., Pieruccini, P., Berakhi, O., Dramis, F. and Asrat, A. (2009). The Geomorphological Map of Mt. Amba Aradam Southern Slope (Tigray, Ethiopia), *Journal of Maps* **5**(1): pp. 56–65.

Comenetz, J. and Caviedes, C. (2002). Climate Variability, Political Crises, and Historical Population Displacements in Ethiopia. *Global Environmental Change Part B: Environmental Hazards* **4**(4): pp. 113–127.

Coulibaly, P. and Dibike, Y. B. (2004). Downscaling of Global Climate Model Outputs for Flood Frequency Analysis in the Saguenay River System. Final Report. McMaster University, Hamilton, ON, Canada.

Cunderlik, J. M. (2003). Hydrologic Model Selection for the CFCAS Project: Assessment of Water Resources Risk and Vulnerability to Changing Climatic Conditions. Project Report I. London, United Kingdom; Canada et al.

Cunderlik, J. M. and Simonovic, S. P. (2004). Selection of Calibration and Verification Data for HEC-HMS Hydrological Model. CFCAS Project: Assessment of Water Resources Risk and Vulnerability to Changing Climate Conditions. Project Report II. London, United Kingdom; Canada et al.

Dahmen, E. R. and Hall, M. J. (1990). Screening of Hydrological Data: Tests for Stationarity and Relative Consistency. International Institute for Land Reclamation and Improvement (ILRI). Wageningen, The Netherlands.

DAI CGCM3 Predictors, (2008). Sets of Predictor Variables Derived from CGCM3 T47 and NCEP/NCAR Reanalysis, version 1.1, April 2008. Montreal, QC, Canada.

Data Access Integration (DAI): CGCM3 A2 emission scenario [online].
URL: http://loki.qc.ec.gc.ca/DAI/CGCM3_predictors-e.html [Date of access: 05/03/2013].

Demelash, M. and Stahr, K. (2010). Assessment of Integrated Soil and Water Conservation Measures on Key Soil Properties in South Gonder, North-Western Highlands of Ethiopia. *Journal of Soil Science and Environmental Management* **1**(7): pp. 164–176.

Descheemaeker, K., Nyssen, J., Poesen, J., Mitiku, H., Muys, B., Raes, D., Moeyersons, J. and Deckers, J. (2006). Soil and Water Conservation through Forest Restoration in Exclosures of the Tigray Highlands. *Journal of the Drylands* **1**(2): pp. 118–133.

DeVries, J. J. and Hromadka, T. V. (1993). Computer Models For Surface Water. In: Maidment, D. R. (ed.). Handbook of hydrology. NY, USA: pp. 21.1–21.39.

Dibike, Y. B. and Coulibaly, P. (2005). Hydrologic Impact of Climate Change in the Saguenay Watershed: Comparison of Downscaling Methods and Hydrologic Models. *Journal of Hydrology* **307**(1–4): pp. 145–163.

Donkor, S. M. K. and Yilma, E. (1999). Integrated Water Resource Management: Issues and Options in Selected African Countries. United Nations Economic Commission for Africa (UNECA). n.p.

Dubale, P. (2003). Present and future trends in natural resources management in agriculture: An overview. In: McCornick, P. G., Kamara, A. B. and Girma Tadesse (eds.) 2003. Integrated water and land management research and capacity building priorities for Ethiopia. Proceedings of a MoWR/EARO/IWMI/ILRI international workshop held at ILRI, Addis Ababa, Ethiopia, 2–4 December 2002. IWMI (International Water Management Institute), Colombo, Sri Lanka, and ILRI (International Livestock Research Institute). Nairobi, Kenya: pp: 29–37.

Emiru, N., Gebrekidan, H. and Tibebe, D. (2012). Analysis of Land Use / Land Cover Changes in Western Ethiopian Mixed Crop-Livestock Systems: the Case of Senbat Watershed. *Journal of Biodiversity and Environmental Sciences* (JBES) **2**(3): pp. 8–17.

Feldman, A. D. (ed.) (2000). Hydrologic Modeling System HEC-HMS. Technical Reference Manual. US Army Corps of Engineers (USACE), Hydrologic Engineering Center, HEC. Davis, CA, USA.

Feoli E., Vuerich, L. G. and Zerihun, W. (2002). Evaluation of Environmental Degradation in Northern Ethiopia using GIS to integrate Vegetation, Geomorphological, Erosion and Socio-Economic Factors. *Agriculture, Ecosystems & Environment* **91**(1–3): pp. 313–325.

Feyen, J. and Zambrano, R. F. V. (2010). Modeling Hydrological Consequences of Climate and Land Use Change - Progress and Challenges. Cuenca, Ecuador: pp. 1–18.

Fisseha, G., Gebrekidan, H., Kibret, K., Yitaferu, B. and Bedadi, B. (2011). Analysis of Land Use / Land Cover Changes in the Debre-Mewi Watershed at the Upper Catchment of the Blue Nile Basin, Northwest Ethiopia. *Journal of Biodiversity and Environmental Sciences* (JBES) **1**(6): pp. 184–198.

Fleming, M. (2004). Description of the Hydrologic Engineering Center's Hydrologic Modeling System (HEC-HMS) and Application to Watershed Studies. Smart Technical Notes Collection, ERDC/TN SMART-04-3, U.S. Army Engineer Research and Development Center, Vicksburg, MS, USA.

Fleming, M. and Neary, V. (2004). Continuous Hydrologic Modeling Study with the Hydrologic Modeling System. *J. of Hydrol. Eng*. **9**(3): pp. 175–183.

Fleming, M. J. and Doan, J. H. (2009). HEC-GeoHMS. Geospatial Hydrologic Modeling Extension. User's Manual, Version 4.2. US Army Corps of Engineers (USACE), Hydrologic Engineering Center, HEC. Davis, CA, USA.

Flint, L., Zenebe, A. and Girmay, G. (2010). Improving Decision Making Capacity of Small Holder Farmers in response to Climate Risk Adaptation in three Drought Prone Districts of Tigray, Northern Ethiopia. Vol. 3: Farm – Level Climate Change Perception and Adaption in Drought Prone Areas of Tigray, Northern Ethiopia. Advancing Capacity to Support Climate Change Adaptation (ACCCA), Project No. 093. Mekelle, Ethiopia.

Food and Agriculture Organization of the United Nations (FAO) (1986). Ethiopian Highlands Reclamation Study. Final Report Vol. I & II. Rome, Italy.

Food and Agriculture Organization of the United Nations (FAO) (1998). The Soil and Terrain Database for northeastern Africa. Land and Water Digital Media Series No. 2 (CD-ROM). Rome, Italy.

Food and Agriculture Organization of the United Nations (FAO) (2010). New_LocClim: Local Climate Estimator [online].
URL: http://www.fao.org/nr/climpag/pub/en3_051002_en.asp [Date of access: 08/04/2013].

Ford, D., Pingel, N. and DeVries, J. J. (2008). Hydrologic Modeling System HEC-HMS: Applications Guide. US Army Corps of Engineers (USACE), Hydrologic Engineering Center, HEC. Davis, CA, USA.

García, A., Sainz, A., Revilla, J. A., Álvarez, C., Juanes, J. and Puente, A. (2008). Surface Water Resources Assessment in Scarcely Gauged Basins in the North of Spain. *Journal of Hydrology* **356**(3–4): pp. 312–326.

Gebeyehu, A. (2003): Research and Development in Land and Water Resources. In: McCornick, P. G., Kamara, A. B. and Girma Tadesse (eds.) 2003. Integrated water and land management research and capacity building priorities for Ethiopia. Proceedings of a MoWR/EARO/IWMI/ILRI international workshop held at ILRI, Addis Ababa, Ethiopia, 2–4 December 2002. IWMI (International Water Management Institute), Colombo, Sri Lanka, and ILRI (International Livestock Research Institute). Nairobi, Kenya: pp. 3–10.

Gebremariam, Y. B. (2010). Geomorphological Mapping in the Upstreams of Muger River, Using Geospatial Tools. Unpublished Master's thesis, Addis Ababa University, Ethiopia.

Gebresamuel, G., Singh, B. R. and Dick, Ø. (2010). Land-use Changes and their Impacts on Soil Degradation and Surface Runoff of Two Catchments of Northern Ethiopia. *Acta Agriculturae Scandinavica, Section B - Soil & Plant Science* **60**(3): pp. 211–226.

Gebreyohannes, T. (2009). Regional Groundwater Flow Modeling of the Geba Basin, Northern Ethiopia. PhD thesis, Vrije Universiteit Brussel, Belgium.

Gebreyohannes, T., De Smedt, F., Hagos, M., Gebresilassie, S., Amare, K., Kabeto, K., Hussein, A., Nyssen, J., Bauer, H., Moeyersons, J., Deckers, J., Haile, M. and Taha, N. (2010). Large Scale Geological Mapping of the Geba Basin, Northern Ethiopia. Tigray Livelihood Papers No. 9. Mekelle, Ethiopia.

Girma, M. M. (2012). Potential Impact of Climate and Land Use Changes on the Water Resources of the Upper Blue Nile Basin. PhD thesis, Freie Universität Berlin, Germany.

Global Land Cover Facility (GLCF): Global Land Cover Facility; Landsat imagery [online].
URL: http://www.landcover.org [Date of access: 03/16/2013];
URL: http://glcf.umd.edu/data/landsat/ [Date of access: 07/03/2013].

Goitom, H. (2012). Modeling of Hydrological Processes in the Geba River Basin, Northern Ethiopia. PhD thesis, Vrije Universiteit Brussel, Belgium.

Goitom, H., De Smedt, F., Yohannes, T. G., Walraevens, K., Gebrehiwot, K., Bauer, H. and Deckers, J. (2012). Modeling Climate Change Impact in the Geba Basin, Ethiopia. IPCBEE 41: pp. 240–244.

Goswami, M., O'Connor, K. M. and Shamseldin, A. Y. (2002). Rainfall-Runoff Modelling of two Irish catchments (one Karstic and one Non-Karstic). Proceedings of the Third Inter-Celtic Colloquium on Hydrology and Management of Water Resources, 'Celtic Water in an European Framework'. Galway, Ireland: pp 151−164.

Haberlandt, U. (2010). From Hydrological Modelling to Decision Support. *Adv. Geosci*. **27**: pp. 11–19.

Habte, A., Cullmann, J. and Horlacher, H.-B. (2007). Application of Wasim distributed Water Balance Simulation Model to the Abbay River Basin. In: FWU Water Resources Publications 06/2007, LARS 2007 proceedings. Siegen, Germany: pp. 42–49.

Hadgu, K. M. (2008). Temporal and Spatial Changes in Land Use Patterns and Biodiversity in Relation to Farm Productivity at Multiple Scales in Tigray, Ethiopia. PhD thesis, Wageningen Universiteit, The Netherlands.

Hailu, B. (2003). Present and future trends of natural resources (land and water) management in Ethiopian agriculture. In: McCornick, P. G., Kamara, A. B. and Girma Tadesse (eds.) 2003. Integrated water and land management research and capacity building priorities for Ethiopia. Proceedings of a MoWR/EARO/IWMI/ILRI international workshop held at ILRI, Addis Ababa, Ethiopia, 2–4 December 2002. IWMI (International Water Management Institute), Colombo, Sri Lanka, and ILRI (International Livestock Research Institute). Nairobi, Kenya: pp. 22–28.

Hamza, I. A. and Iyela, A. (2012). Land Use Pattern, Climate Change, and its Implication for Food Security in Ethiopia: A Review. *Ethiopian Journal of Environmental Studies and Management* **5**(1): pp. 26–31.

Haregeweyn, N., Poesen, J., Nyssen, J., Verstraeten, G., De Vente, J., Govers, G., Deckers, S. and Moeyersons, J. (2005). Specific Sediment Yield in Tigray-Northern Ethiopia: Assessment and Semi-Quantitative Modelling. *Geomorphology* **69**(1–4): pp. 315–331.

Haregeweyn, N., Poesen, J., Nyssen, J., De Wit, J., Haile, M., Govers, G. and Deckers, S. (2006). Reservoirs in Tigray (Northern Ethiopia): Characteristics and Sediment Deposition Problems. *Land Degrad. Dev.* **17**(2): pp. 211–230.

Haregeweyn, N., Poesen, J., Deckers, J., Nyssen, J., Haile, M., Govers, G., Verstraeten, G. and Moeyersons, J. (2008). Sediment-Bound Nutrient Export from Micro-Dam Catchments in Northern Ethiopia. *Land Degrad. Dev.* **19**(2): pp. 136–152.

Helsel, D. R. and Hirsch, R. M. (1992). Statistical Methods in Water Resources. Studies in Environmental Science 49. Amsterdam, The Netherlands.

Houghton, J. T., Meira Filho, L. G., Callander, B. A., Harris, N., Kattenberg, A. and Maskell, K. (eds.) (1996). Climate Change 1995: The Science of Climate Change. Contribution of Working Group I to the Second Assessment Report of the Intergovernmental Panel on Climate Change (IPCC). Cambridge, United Kingdom.

Huggett, R. J. (2007). Fundamentals of Geomorphology. Second Edition. NY, USA.

Hulme, M., Doherty, R., Ngara, T., New, M. and Lister, D. (2001). African Climate Change: 1900-2100. *Climate Research* **17**(2): pp. 145–168.

Hunting Technical Services Limited (HTSL) (1976). Tigrai Rural Development Study. Annex 1 (Land and Vegetation Resources). Hunting Technical Services Ltd. Hemel Hampstead, United Kingdom.

Hurni, H., Kebede, T. and Zeleke, G. (2005). The Implications of Changes in Population, Land Use, and Land Management for Surface Runoff in the Upper Nile Basin Area of Ethiopia. *Mountain Research and Development* **25**(2): pp. 147–154.

Instituto Agronomico per l'Oltremare (IAO) (2008). Land Evaluation in Enderta District – Tigray Region, Ethiopia. 28th Course Professional Master “Geomatics and Natural Resources Evaluation”. Florence, Italia.

International Federation of Red Cross and Red Crescent Societies (IFRC) (2012). Long Term Planning Framework Ethiopia 2012-2015 [online].
URL: http://www.ifrc.org/docs/Appeals/annual12/SP164ET_LTPF12.pdf [Date of access: 04/18/2013]

Jarvis, A., Reuter, H. I., Nelson, A. and Guevara, E. (2008). Hole-filled SRTM for the globe Version 4, available from the CGIAR-CSI SRTM 90m Database [online].
URL: http://srtm.csi.cgiar.org [Date of access: 11/22/2010].

Johnson, L. E. (2009). Geographic Information Systems in Water Resources Engineering. Boca Raton, FL, USA.

Kahsay, G. H. (2008). Groundwater Resource Assessment through distributed Steady-State Flow Modeling, Aynalem wellfield (Mekele, Ethiopia). Unpublished Master's thesis, Institute for Geo-information Science and Earth Observation (ITC), Enschede, The Netherlands.

Karl, T. R., Melillo, J. M. and Peterson, T. C. (2009). Global Climate Change Impacts in the United States. New York, NY, USA.

Kebede, A., Diekkrüger, B. and Moges, S. A. (2013). An Assessment of Temperature and Precipitation Change Projections using a Regional and a Global Climate Model for the Baro-Akobo Basin, Nile Basin, Ethiopia. *J Earth Sci Climate Change* **4**(1): pp. 133–144.

Koshak, N. and Dawod, G. (2011). A GIS Morphometric Analysis of Hydrological Catchments within Makkah Metropolitan Area, Saudi Arabia. *International Journal of Geomatics and Geosciences* **2**(2): pp. 544–554.

Krause, P., Boyle, D. P. and Bäse, F. (2005). Comparison of different Efficiency Criteria for Hydrological Model Assessment. *Advances in Geosciences* **5**: pp. 89–97.

Kumasi, T. C. and Asenso-Okyere, K. (2011). Responding to Land Degradation in the Highlands of Tigray, Northern Ethiopia. International Food Policy Research Institute (IFPRI). IFPRI Discussion Paper 01142. Washington, D.C., USA, and Addis Ababa, Ethiopia.

Lastoria, B. (2008). Hydrological Processes on the Land Surface: A Survey of Modelling Approaches. FORALPS Technical Report 9. Trento, Italy.

Leavesley, G. H., Lichty, R. W., Troutman, B. M. and Saindon, L. G. (1983). Precipitation-Runoff Modeling System: User's manual. Water Resource Investigation Report 83-4238. Denver, CO, USA.

Legates, D. R. and McCabe Jr., G. J. (1999). Evaluating the Use of "Goodness-of-Fit" Measures in Hydrologic and Hydroclimatic Model Validation. *Water Resour. Res.* **35**(1): pp. 233–241.

Legesse, D., Vallet-Coulomb, C. and Gasse, F. (2003). Hydrological Response of a Catchment to Climate and Land Use Changes in Tropical Africa: Case Study South Central Ethiopia. *Journal of Hydrology* **275**(1–2): pp. 67–85.

Legesse, D., Abiye, T. A. and Vallet-Coulomb, C. (2010). Modeling Impacts of Climate and Land Use Changes on Catchment Hydrology: Meki River, Ethiopia. *Hydrology and Earth System Sciences Discussions* **7**(4): pp. 4535–4565.

Leser, H. and Stäblein, G. (1985): Legend of the Geomorphological Map 1:25000 (GMK 25) – Fith Version in the GMK Priority Program of the Deutsche Forschungsgemeinschaft. In: Stäblein, G. and Wöhlke, W. (Geomorphological Mapping in the Federal Republic of Germany. Contributions to the GMK-priorityprogram IV. Berliner Geographische Abhandlungen, Heft 39: pp. 61–89.

Livada, I. and Asimakopoulos, D. N. (2005). Individual Seasonality Index of Rainfall Regimes in Greece. *Clim Res* **28**: pp. 155–161.

Ludi, E. (2009). Climate Change, Water and Food Security. Overseas Development Institute (ODI) Background Note. London, United Kingdom.

Lund, J. R., Scheierling, S. M. and Milne, G. (2010). Modeling for Watershed Management: A Practitioner's Guide. Water Working Notes, Note No. 27. Washington, D.C., USA.

McCartney, M. and Smakhtin, V. (2010). Water Storage in an Era of Climate Change: Addressing the Challenge of Increasing Rainfall Variability. International Water Management Institute (IWMI) Blue Paper. Colombo, Sri Lanka.

McEnroe, B. M. (2010). Guidelines for Continuous Simulation of Streamflow in Johnson County, Kansas, with HEC-HMS. Report to Johnson County Public Works and Infrastructure, Stormwater Management Program. University of Kansas, USA.

Meenu, R., Rehana, S. and Mujumdar, P. P. (2012). Assessment of Hydrologic Impacts of Climate Change in Tunga-Bhadra River Basin, India with HEC-HMS and SDSM. *Hydrol. Process.* **27**: pp. 1572–1589.

Ministry of Water Resources (MoWR) (2002). Water Sector Development Program (WSDP). Addis Ababa, Ethiopia.

Miranda, J. D., Armas, C., Padilla, F. M. and Pugnaire, F. I. (2011). Climatic Change and Rainfall Patterns: Effects on Semi-Arid Plant Communities of the Iberian Southeast. *Journal of Arid Environments* **75**(12): pp. 1302–1309.

Mitchell Jr. J. M., Dzerdzeevskii, B. and Flohn H. (eds.) (1966). Climatic Change. Report of a Working Group to the Commission for Climatology. Technical Note No. 79, World Meteorologial Organization (WMO), No. 195. Geneva, Switzerland.

Mohr, P. A. (1962). The Geology of Ethiopia. Addis Ababa, Ethiopia.

Montoya, J. M. and Raffaelli, D. (2010). Climate Change, Biotic Interactions and Ecosystem Services. *Phil. Trans. R. Soc. B.* **365**(1549): pp. 2013–2018.

Morris, M. D. (1991). Factorial Sampling Plans for Preliminary Computational Experiments. *Technometrics* **33**(2): pp. 161–174.

Mwchahary, D. D. and Nath, D. C. (2013). A Study on Rainfall Trends in Kokrajhar District of Assam, India. *Int. J. Res. Chem. Environ.* **3**(1): pp. 74–88.

NASA Landsat Program (2003). Landsat ETM+, TM Scene (Path 169 and Row 50) and MSS (Path 181 and Row 51), Orthorectified, USGS, Sioux Falls, 10/26/2003.

Nash, J. E. and Sutcliffe, J. V. (1970). River Flow Forecasting through Conceptual Models Part I – A Discussion of Principles. *Journal of Hydrology* **10**(3): pp: 282–290.

National Strategy and Action Plan for the Implementation of the Great Green Wall Initiative in Ethiopia (2012). Addis Ababa, Ethiopia.

Ndaruzaniye, V. (2011). Water Security in Ethiopia: Risks and Vulnerabilities' Assessment. n.p.

Neary, V., Habib, E. and Fleming, M. (2004). Hydrologic Modeling with NEXRAD Precipitation in Middle Tennessee. *Journal of Hydrologic Engineering* **9**(5): pp. 339–349.

Nedaw, D. (2010). Water Balance and Groundwater Quality of Koraro Area, Tigray, Northern Ethiopia. *Momona Ethiopia Journal of Science* **2**(2): pp. 110–127.

Nedaw, D. and Walraevens, K. (2009). The Positive Effect of Micro-Dams for Groundwater Enhancement: a Case Study around Tsinkanet and Rubafeleg Area, Tigray, Northern Ethiopia. *Momona Ethiopian Journal of Science* **1**(1): pp. 59–73.

Negusse, T., Yazew, E. and Tadesse, N. (2013). Quantification of the Impact of Integrated Soil and Water Conservation Measures on Groundwater Availability in Mendae Catchment, Abraha We-Atsebaha, Eastern Tigray. *Momona Ethiopian Journal of Science* **5**(2): pp. 117–136.

Nelder, J. A. and Mead, R. (1965). A Simplex Method for Function Minimization. *Computer Journal* **7**(4): pp. 308–313.

Netherlands Engineering Consultants (NEDECO) (1997). Tekeze River Basin Integrated Development Master Plan Project. Second Phase Report Volume NR 2 - Soils and Terrain. Federal Democratic Republic of Ethiopia, Ministry of Water Resources and Energy. Addis Ababa, Ethiopia.

Nirmalakhandan, N. (2002). Modeling Tools for Environmental Engineers and Scientists. Boca Raton, FL, USA.

Nyssen, J., Poesen, J., Moeyersons, J., Deckers, J., Haile, M. and Lang, A. (2004). Human Impact on the Environment in the Ethiopian and Eritrean Highlands–a State of the Art. *Earth-Science Reviews* **64**(3–4): pp. 273–320.

Nyssen, J., Vandenreyken, H., Poesen, J., Moeyersons, J., Deckers, J., Mitiku, H., Salles, C. and Govers, G. (2005). Rainfall Erosivity and Variability in the Northern Ethiopian Highlands. *Journal of Hydrology* **311**(1–4): pp. 172–187.

Nyssen, J., Descheemaeker, K., Haregeweyn, N., Haile, M., Deckers, J. and Poesen, J. (eds.), (2007). Lessons Learnt from 10 Years Research on Soil Erosion and Soil and Water Conservation in Tigray. Tigray Livelihood Papers No. 7, Mekelle: Zala-Daget Project, Mekelle University, K. U. Leuven, Relief Society of Tigray, Africamuseum and Tigray Bureau of Agriculture and Rural Development. Mekelle, Ethiopia.

Nyssen, J., Naudts, J., De Geyndt, K., Haile, M., Poesen, J., Moeyersons, J. and Deckers, J. (2008). Soils and Land Use in the Tigray Highlands (Northern Ethiopia). Land Degrad. Dev. 19(3): pp. 257–274.

Nyssen, J., Haile, M., Naudts, J., Munro, N., Poesen, J., Moeyersons, J., Frankl, A., Deckers, J. and Pankhurst, R. (2009). Desertification? Northern Ethiopia Re-Photographed after 140 Years. *Science of the Total Environment* **407**(8): pp. 2749–2755.

Orellana B., Pechlivanidis, I. G., McIntyre, N., Wheater, H. S. and Wagener T. (2008). A Toolbox for the Identification of Parsimonious Semi-Distributed Rainfall-Runoff Models: Application to the Upper Lee Catchment. In: Proc. of the 4th Meeting iEMSs, Barcelona Jul 7–10, 2008. Spain: pp. 670–677.

Parry, M. L., Canziani, O. F., Palutikof, J. P., van der Linden, P. J. and Hanson, C. E. (eds.) (2007). Climate Change 2007: Impacts, Adaptation and Vulnerability. Contribution of Working Group II to the Fourth Assessment Report of the Intergovernmental Panel on Climate Change (IPCC). Cambridge, United Kingdom.

Pechlivanidis, I. G., Jackson, B. M., Mcintyre, N. R. and Wheater, H. S. (2011). Catchment Scale Hydrological Modelling: a Review of Model Types, Calibration Approaches and Uncertainty Analysis Methods in the Context of Recent Developments in Technology and Applications. *Global NEST Journal* **13**(3): pp. 193–214.

Pilgrim, D. H. and Cordery, I. (1993). Flood Runoff. In: Maidment, D. R. (ed.). Handbook of Hydrology. NY, USA: pp. 9.1–9.42.

Price, K. (2011). Effects of Watershed Topography, Soils, Land Use, and Climate on Baseflow Hydrology in Humid Regions: A Review. *Progress in Physical Geography* **35**(4): pp. 465–492.

Rabia, A. H., Afifi, R. R., Gelaw, A. M., Bianchi, S., Figueredo, H., Huong, T. L., Lopez, A. A., Mandala, S. D., Matta, E., Ronchi, M., Solomon, H. W., Tine, A. K., Youssef, M. S., Gutierrez, M. G., Yusuf, M. M. and Alessandro, V. (2013). Soil Mapping and Classification: a Case Study in the Tigray Region, Ethiopia. *Journal of Agriculture and Environment for International Development* (JAEID) **107**(1): pp. 73–99.

Reda, A. A. (2007): Combating Desertification in Tigray, Ethiopia. Field Study on the Implementation of the UNCCD in the Rural Region of Tigray. Unpublished Master's thesis, Linköpings Universitet, Noorköping, Sweden.

Reubens, B. (2010). Woody Vegetation for Gully Rehabilitation in Northern Ethiopia: Species Suitability, Root Structure, and Seedling Establishment, Growth and Management. PhD thesis, Katholieke Universiteit Leuven, The Netherlands.

Roy, D., Begam, S., Ghosh, S. and Jana, S. (2013). Calibration and Validation of HEC-HMS Model for a River Basin in Eastern India. *Journal of Engineering and Applied Sciences* **8**(1): pp. 40–56.

Roy, P. K. and Mazumdar, A. (2013). Water Resources in India under Changed Climate Scenario. *International Journal of Engineering Research and Applications* (IJERA) **3**(1): pp. 954–961.

Saadat, H., Adamowski, J., Bonnell, R., Sharifi, F., Namdar, M. and Ale-Ebrahim, S. (2011). Land Use and Land Cover Classification over a Large Area in Iran based on Single Date Analysis of Satellite Imagery. *ISPRS Journal of Photogrammetry and Remote Sensing* **66**(5): pp. 608–619.

Scharffenberg, W. A. (2001). Hydrologic Modeling System HEC-HMS. User's Manual, Version 2.1. US Army Corps of Engineers (USACE), Hydrologic Engineering Center, HEC. Davis, CA, USA.

Scharffenberg, W. A. and Fleming, M. J. (2006). Hydrologic Modeling System HEC-HMS. User's Manual, Version 3.0.1. US Army Corps of Engineers (USACE), Hydrologic Engineering Center, HEC. Davis, CA, USA.

Scharffenberg, W. A. and Fleming, M. J. (2008). Hydrologic Modeling System HEC-HMS. User's Manual, Version 3.2. US Army Corps of Engineers (USACE), Hydrologic Engineering Center, HEC. Davis, CA, USA.

Scharffenberg, W. A. and Fleming, M. J. (2010). Hydrologic Modeling System HEC-HMS. User's Manual, Version 3.5. US Army Corps of Engineers (USACE), Hydrologic Engineering Center, HEC. Davis, CA, USA.

Scharffenberg, W., Ely, P., Daly, S., Fleming, M. and Pak, J. (2010). Hydrologic Modeling System (HEC-HMS): Physically-Based Simulation Components. 2nd Joint Federal Interagency Conference, Las Vegas, NV, June 27 - July 1, 2010. USA.

Schütt, B. and Thiemann, S. (2001). Assessment and Monitoring of Erosion and Sedimentation in Ethiopia. Geomorphological Investigation of Erosion Processes in Eight Selected Watershed. Trier, Germany.

Selby, M. J. (1985). Earth's changing surface: An Introduction to Geomorphology. New York, NY, USA.

Sinclair Knight Merz Pty. Ltd. (SKM) (2009). Impact of Land Use Change on Floods in the Upper Waikato. PHASE 2: Model Calibration and Flood Hydrograph Generation. Auckland, New Zealand.

Srivastava, P. K., Han, D., Ramirez, M. R. and Islam, T. (2013). Machine Learning Techniques for Downscaling SMOS Satellite Soil Moisture Using MODIS Land Surface Temperature for Hydrological Application. *Water Resour Manage* **27**(8): pp. 3127–3144.

Sumner, G., Homar, V. and Ramis, C. (2001). Precipitation Seasonality in Eastern and Southern Coastal Spain. *Int. J. Climatol.* **21**(2): pp. 219–247.

Taffere, B. (2003). Efforts For Sustainable Land Management in Tigray: The Role of Extension. In: Gebremedhin, B., Pender, J., Ehui, S. and Haile, M. (eds.). Policies for Sustainable Land Management in the Highlands of Tigray. EPTD Workshop Summary Paper No.14. Summary of Papers and Proceedings of a Workshop March 28–29, 2002. Mekelle, Ethiopia: pp. 3–5.

Taha, N. (2002). Challenges and Strategies towards Sustainable Land Use in "North Wollo" Zone of the Amhara National Regional State. Proceedings of 12th International Soil Conservation Organization Conference (ISCO), May 26–31, Beijing. Vol. I Soil and Water Conservation: Regional Policies and Action. China: pp. 18–22.

Tamene, L. (2005). Reservoir Siltation in Ethiopia: Causes, Source Areas, and Management Options. PhD thesis, Rheinische Friedrich-Wilhelms-Universität Bonn, Germany.

Tamene, L., Park, S. J., Dikau, R. and Vlek, P. L. G. (2006). Analysis of Factors Determining Sediment Yield Variability in the Highlands of Northern Ethiopia. *Geomorphology* **76**(1–2): pp. 76–91.

Tefera, B. and Sterk, G. (2008). Hydropower-Induced Land Use Change in Fincha'a Watershed, Western Ethiopia: Analysis and Impacts. *Mountain Research and Development* **28**(1): pp. 72–80.

Teferi, G. G. (2009). Groundwater Resource Assessment of the Aynalem Wellfield through Transient flow Modelling (Mekele, Ethiopia). Unpublished Master's thesis, International Institute for Geo-information Science and Earth Observation (ITC), Enschede, The Netherlands.

Tegene, B. (2002). Land-Cover/Land-Use Changes in the Derekolli Catchment of the South Welo Zone of Amhara Region, Ethiopia. *Eastern Africa Social Science Research Review* **18**(1): pp. 1–20.

Tekle, K. and Hedlund, L. (2000). Land Cover Changes between 1958 and 1986 in Kalu District, Southern Wello, Ethiopia. *Mountain Research and Development* **20**(1): pp. 42–51.

Tesfagiorgis, K., Gebreyohannes, T., De Smedt, F., Moeyersons, J., Hagos, M., Nyssen, J. and Deckers, J. (2011). Evaluation of Groundwater Resources in the Geba Basin, Ethiopia. *Bull Eng Geol Environ* **70**(3): pp. 461–466.

Tesfay, G. (2011). On-farm Water Harvesting for Rainfed Agriculture Development and Food Security in Tigray, Northern Ethiopia. Investigation of Technical and Socioeconomic Issues. Drylands Coordination Group Report No. 61, 07, 2011. Oslo, Norway.

Tulu, M. D. (2010) Event Based Rainfall-Runoff Modelling in Semi-Arid Regions. PhD thesis, BOKU University Vienna, Austria.

United Nations Educational, Scientific, and Cultural Organization; World Water Assessment Program (UNESCO-WWAP, 2004). National Water Development Report for Ethiopia. Addis Ababa, Ethiopia.

United Nations Framework Convention on Climate Change (UNFCC) (2007). Climate Change: Impacts, Vulnerabilities and Adaptation in Developing Countries. Bonn, Germany.

United States Department of Agriculture (USDA) (1999). Soil Taxonomy: a Basic System of Soil Classification for Making and Interpreting Soil Surveys. Agricultural Handbook No. 436. Washington, D.C., USA.

US Army Corps of Engineers Institute for Water Resources - Hydrological Engineering Center (CEIWR-HEC) (2009). HEC-DSSVue, HEC Data Storage System, Visual Utility Engine. User's Manual, Version 2.0. US Army Corps of Engineers (USACE), Hydrologic Engineering Center, HEC. Davis, CA, USA.

Vaze, J., Jordan, P., Beecham, R., Frost, A. and Summerell, G. (eWater Cooperative Research Centre) (2011). Guidelines for Rainfall-Runoff Modelling: Towards Best Practice Model Application. Bruce, Australia.

Walsh, R. P. D. and Lawler, D. M. (1981). Rainfall Seasonality: Description, Spatial Patterns, and Change through Time. *Weather* **36**(7): pp. 201–208.

White, K. L. and Chaubey, I. (2005). Sensitivity Analysis, Calibration, and Validation for a Multisite and Multivariable SWAT Model. *Journal of the American Water Resources Association* **41**(5): pp. 1077–1089.

Wilby, R. L. and Dawson, C. W. (2007). SDSM 4.2 — A Decision Support Tool for the Assessment of Regional Climate Change Impacts. User Manual. n.p.

Willmott, C. J. (1981). On the Validation of Models. *Physical Geography* **2**(2): pp. 184–194.

Willmott, C. J., Robeson, S. M. and Matsuura, K. (2012). A Refined Index of Model Performance. *Int. J. Climatol.* **32**(13): pp. 2088–2094.

Woldearegay, K. (2002). Surface Water Harvesting and Groundwater Recharge with Implications to Conjunctive Water Resource Management in Arid to Semi-Arid Environments (with a Model Site of the Mekelle Area, Northern Ethiopia). Proceedings of the International Conference on Public Management, Policy and Development. Addis Ababa, Ethiopia.

Woody Biomass Inventory and Strategic Planning Project in Ethiopia (WBISPP) (2003). Land use and land cover database. Addis Ababa, Ethiopia.

World Bank (2010). The Little Green Data Book 2010. Washington, D.C., USA.

World Meteorological Organization (WMO) (1994). Guide to hydrological practices. WMO-No. 168. Geneva, Switzerland.

Wright, C. (1984). An Assessment of the Causes, Severity, Extent and Probable Consequences Of Degradation in the Ethiopian Highlands. Food and Agriculture Organization of the United Nations (FAO) / Ministry of Agriculture (MOA). Addis Ababa, Ethiopia.

Xu, C.-Y. (2009). Textbook of Hydrologic Models. Uppsala Universitet, Sweden.

Xu, C.-Y. and Singh, V. P. (2004). Review on Regional Water Resources Assessment Models under Stationary and Changing Climate. *Water Resources Management* **18**(6): pp. 591–612.

Yang, H., Faramarzi, M. and Abbaspour, K. C. (2013): Assessing Freshwater Availability in Africa under the Current and Future Climate with Focus on Drought and Water Scarcity. 20th International Congress on Modelling and Simulation, Adelaide, Australia, 1–6 December 2013 [online]. URL: http://www.mssanz.org.au/modsim2013 [Date of access: 06/12/2013].

Yazew, E. (2005). Development and Management of Irrigated Lands in Tigray, Ethiopia. PhD thesis, Wageningen Universiteit, The Netherlands.

Yihun, D. (2009). Hydrological Modeling to Assess Climate Change Impact at Gilgel Abay River, Lake Tana Basin, Ethiopia. Unpublished Master's thesis, Lunds Universitet, Sweden.

Yimer, G., Jonoski, A. and Van Griensven, A. (2009). Hydrological Response of a Catchment to Climate Change in the Upper Beles River Basin, Upper Blue Nile, Ethiopia. *Nile Basin Water Engineering Scientific Magazine* **2**: pp. 49–59.

Zelalem, N. (2013). Downscaling and Modeling the Effects of Climate Change on Hydrology and Water Resources in the Upper Blue Nile River Basin, Ethiopia. PhD thesis, Universität Kassel, Germany.

Zenebe, A. (2009). Assessment of Spatial and Temporal Variability of River Discharge, Sediment Yield and Sediment-fixed Nutrient Export in Geba River Catchment, Northern Ethiopia. PhD thesis, Katholieke Universiteit Leuven, The Netherlands.

Zenebe, A., Vanmaercke, M., Poesen, J., Verstraeten, G., Nyssen, J., Girmay, G., Mitiku, H., Bauer, H. and Deckers, J. (2011). Sediment Transport in the Geba River System. In: Excursion Guide: Post-Conference Excursion: Geomorphological Hazards, Land Degradation and Resilience in the North Ethiopian Highlands. Addis Ababa, Ethiopia: pp. 65–71.

Zenebe, A., Venmaercke, M., Poesen, J., Verstraeten, G., Haregeweyn, N., Mituku, H., Amare, K., Deckers J. and Nyssen, J. (2013). Spatial and Temporal Variability of River Flows in the Degraded Semi-Arid Tropical Mountains of Northern Ethiopia. *Zeitschrift für Geomorphologie* **57**(2): pp. 143–169.

Additional data sources

Ethiopian Mapping Authority (EMA). Topographical maps (scale 1:50 000).

Ethiopian Ministry of Agriculture. Land Use Map (scale 1:100 000; 1985).

Ethiopian National Meteorological Service Agency (ENMSA). Digital daily data on precipitation, temperature, wind speed, sunshine and humidity.

Water and Power Consultancy Services Ltd, India (WAPCOS) (2002). Suluh Valley Integrated Rural, Agriculture and Water Resources Development Study Identification and Reconnaissance Report (phase-1 stage-1) water resource studies volume-4, Final Report.

Appendix

Appendix A: Meteorological data analysis related

A. Data consistence check

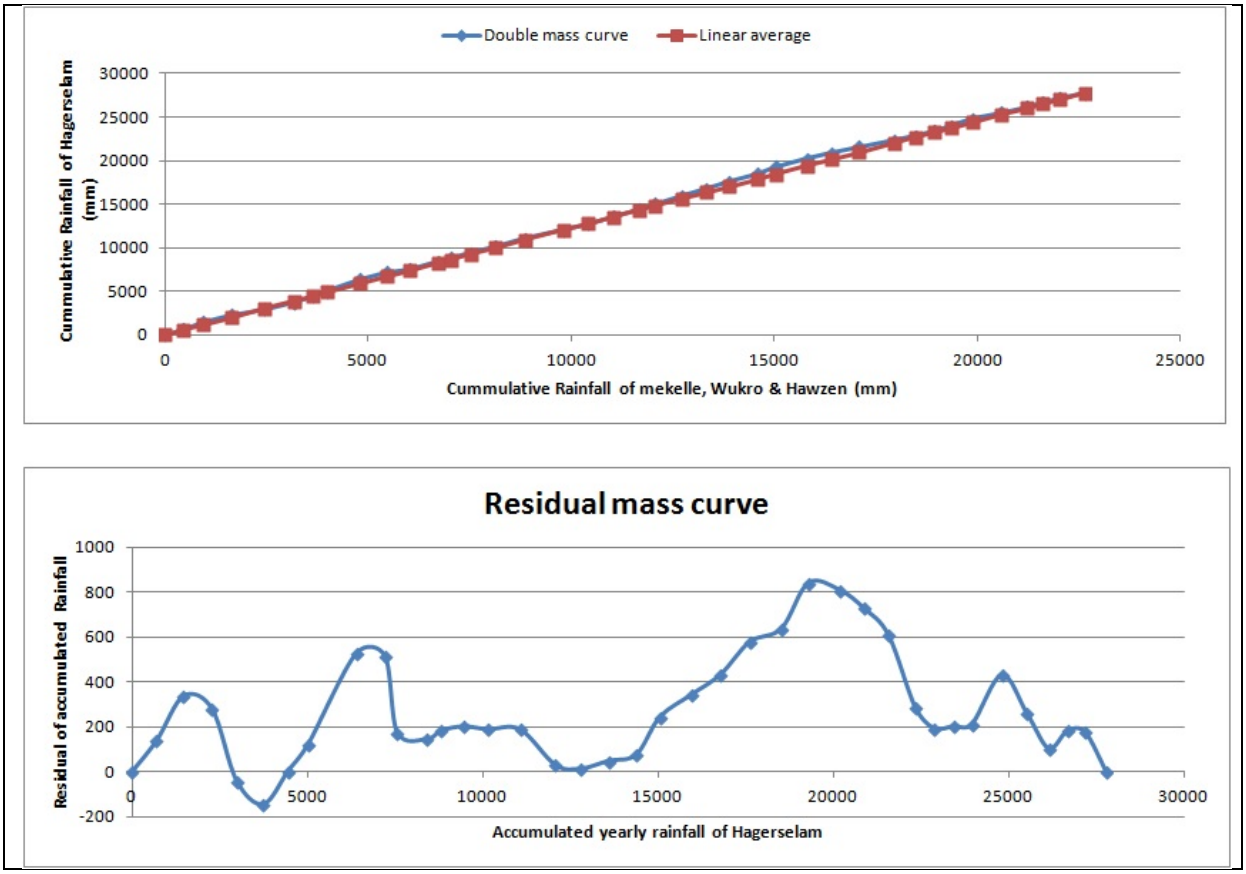

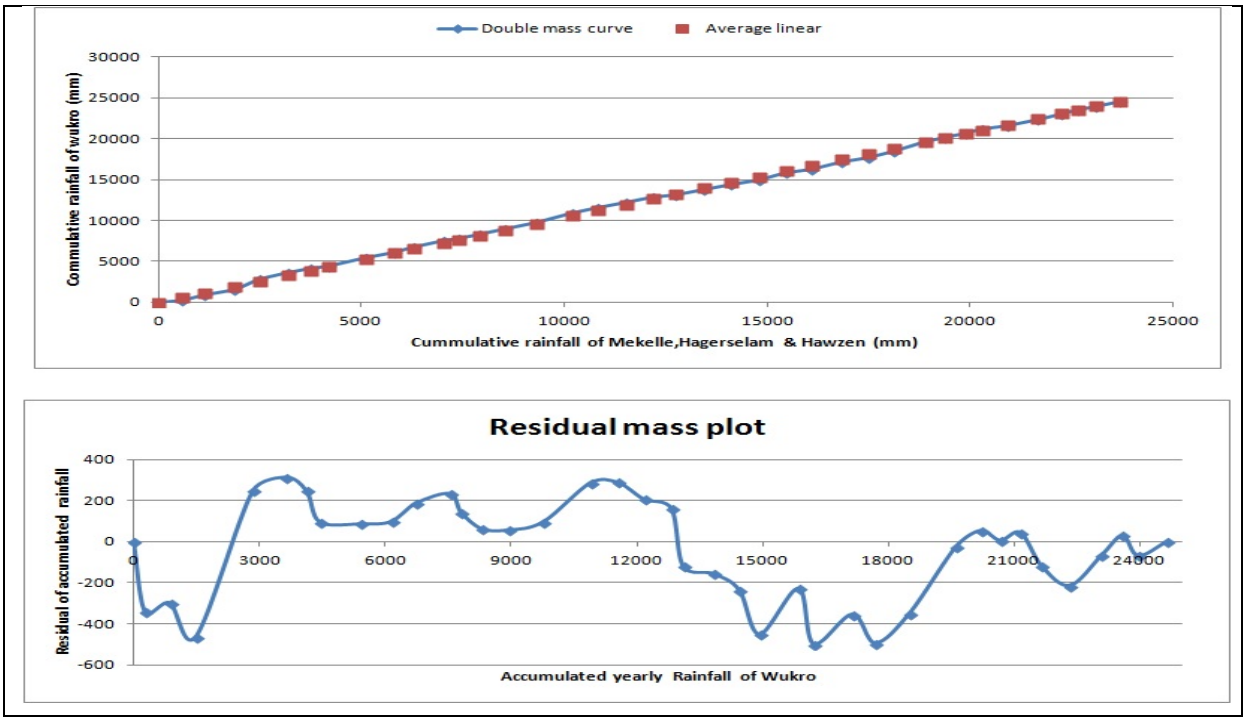
Double mass curve
Average linear
Commulative rainfall of wukro (mm)
Cummulative rainfall of Mekelle,Hagerselam & Hawzen (mm)
Residual mass plot
Residual of accumulated rainfall
Accumulated yearly Rainfall of Wukro

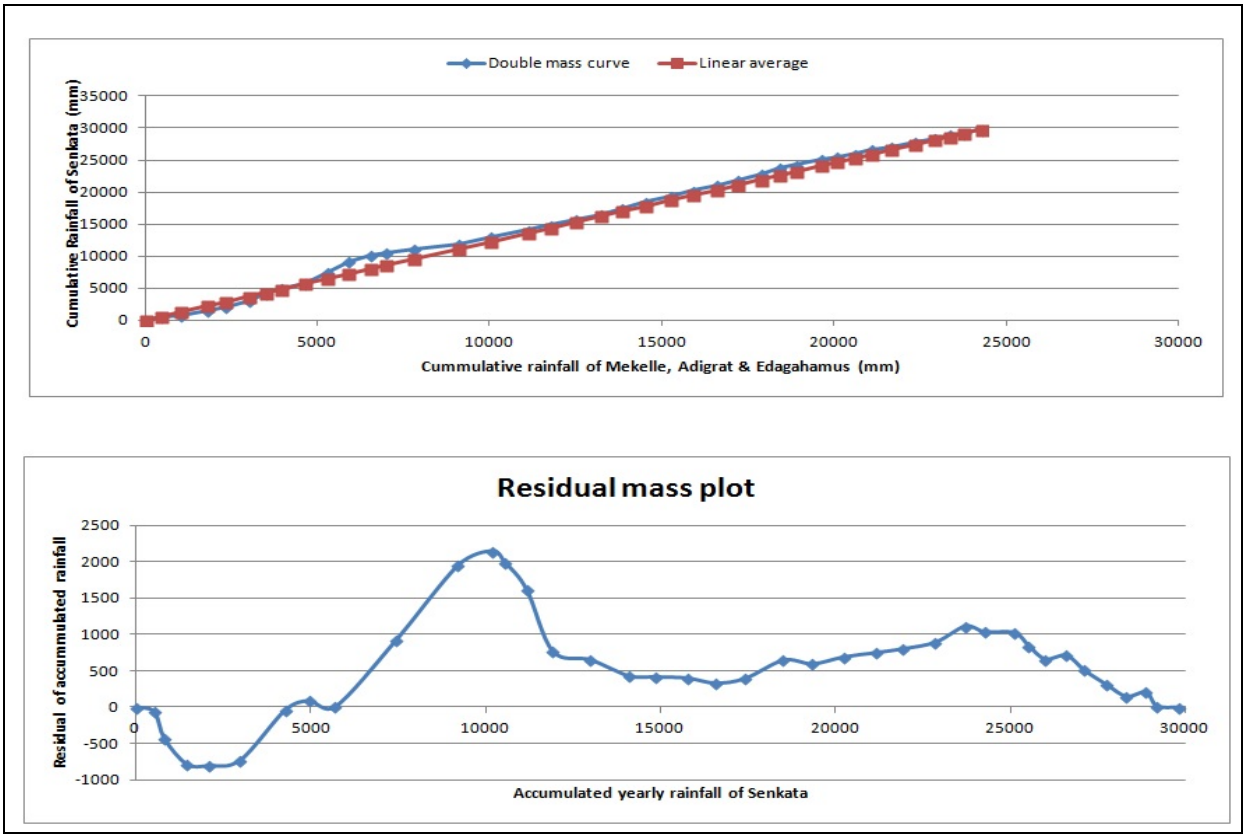
Double mass curve
Linear average
Cumulative Rainfall of Senkata (mm)
Cummulative rainfall of Mekelle, Adigrat & Edagahamus (mm)
Residual mass plot
Residual of accummulated rainfall
Accumulated yearly rainfall of Senkata

B. Spearman correlation trend test

Year	Hagreselam - observed annual rainfall data	**Kxi** - rank of the data as observed	Observed data ascending order	**Kyi** - rank of the same data in ascending order	Di = Kxi - Kyi	Di^2	
1973	689	1	359	10	-9	81	
1974	772	2	400	12	-10	100	
1975	802	3	495	37	-34	1156	
1976	706	4	517	32	-28	784	
1977	760	5	529	30	-25	625	
1978	713	6	541	36	-30	900	
1979	571	7	571	7	0	0	
1980	1372	8	579	31	-23	529	
1981	816	9	599	38	-29	841	
1982	359	10	621	35	-25	625	
1983	852	11	628	13	-2	4	
1984	400	12	673	27	-15	225	
1985	628	13	675	20	-7	49	
1986	704	14	689	1	13	169	
1987	913	15	704	14	1	1	
1988	1006	16	706	4	12	144	
1989	722	17	709	28	-11	121	
1990	792	18	713	6	12	144	
1991	797	19	720	34	-15	225	
1992	675	20	722	17	3	9	
1993	912	21	754	29	-8	64	
1994	821	22	760	5	17	289	
1995	833	23	772	2	21	441	
1996	900	24	776	25	-1	1	
1997	776	25	792	18	7	49	
1998	900	26	797	19	7	49	
1999	673	27	802	3	24	576	
2000	709	28	816	9	19	361	
2001	754	29	821	22	7	49	
2002	529	30	833	23	7	49	
2003	579	31	851	33	-2	4	
2004	517	32	852	11	21	441	
2005	851	33	900	24	9	81	
2006	720	34	900	26	8	64	

2007	621	35	912	21	14	196	
2008	541	36	913	15	21	441	
2009	495	37	1006	16	21	441	
2010	599	38	1372	8	30	900	
Mean	731				Sum Di^2	11228	
					Rsp	-0.22858	
					t	-1.40878	
					tcr	-2.02	2.02

Year	Senkata - observed annual rainfall data	**Kxi** - rank of the data as observed	Observed data ascending order	**Kyi** - rank of the same data in ascending order	Di = Kxi - Kyi	Di^2	
1973	525.2	1	290.5	2	-1	1	
1974	290.5	2	306.7	37	-35	1225	
1975	634.2	3	378.8	12	-9	81	
1976	629.7	4	405.2	30	-26	676	
1977	903.7	5	466.9	31	-26	676	
1978	1286.9	6	509.9	33	-27	729	
1979	678.7	7	525.2	1	6	36	
1980	742.4	8	552.8	28	-20	400	
1981	1736.2	9	563.3	36	-27	729	
1982	1786.3	10	564.0	35	-25	625	
1983	965.6	11	604.6	32	-21	441	
1984	378.8	12	611.9	13	-1	1	
1985	611.9	13	629.7	4	9	81	
1986	747.5	14	634.2	3	11	121	
1987	1070.6	15	642.0	34	-19	361	
1988	1101.2	16	651.6	38	-22	484	
1989	772.2	17	678.7	7	10	100	
1990	902.3	18	742.4	8	10	100	
1991	795.2	19	747.5	14	5	25	
1992	842.7	20	766.2	25	-5	25	
1993	1105.3	21	772.2	17	4	16	
1994	831.0	22	795.2	19	3	9	
1995	891.2	23	831.0	22	1	1	
1996	917.5	24	842.7	20	4	16	
1997	766.2	25	852.3	27	-2	4	

1998	941.0	26	857.3	29	-3	9	
1999	852.3	27	891.2	23	4	16	
2000	552.8	28	902.3	18	10	100	
2001	857.3	29	903.7	5	24	576	
2002	405.2	30	917.5	24	6	36	
2003	466.9	31	941.0	26	5	25	
2004	604.6	32	965.6	11	21	441	
2005	509.9	33	1070.6	15	18	324	
2006	642.0	34	1101.2	16	18	324	
2007	564.0	35	1105.3	21	14	196	
2008	563.3	36	1286.9	6	30	900	
2009	306.7	37	1736.2	9	28	784	
2010	651.6	38	1786.3	10	28	784	
Mean	785.0				Sum Di^2	11478	
					Rsp	-0.25594	
					t	-1.58852	
					tcr	-2.02	2.02

Year	Adigrat - observed annual rainfall data	**Kxi** - rank of the data as observed	Observed data ascending order	**Kyi** - rank of the same data in ascending order	Di = Kxi - Kyi	Di^2	
1973	452	1	245	15	-14	196	
1974	598	2	315	27	-25	625	
1975	862	3	372	37	-34	1156	
1976	512	4	386	16	-12	144	
1977	625	5	428	12	-7	49	
1978	482	6	436	32	-26	676	
1979	530	7	452	1	6	36	
1980	666	8	468	28	-20	400	
1981	787	9	482	6	3	9	
1982	561	10	488	36	-26	676	
1983	560	11	498	33	-22	484	
1984	428	12	512	4	8	64	
1985	666	13	530	7	6	36	
1986	577	14	548	31	-17	289	
1987	245	15	560	11	4	16	
1988	386	16	561	10	6	36	
1989	591	17	565	30	-13	169	

1990	752	18	569	38	-20	400	
1991	702	19	577	14	5	25	
1992	647	20	591	17	3	9	
1993	791	21	598	2	19	361	
1994	770	22	625	5	17	289	
1995	636	23	636	23	0	0	
1996	741	24	647	20	4	16	
1997	792	25	666	13	12	144	
1998	737	26	666	8	18	324	
1999	315	27	672	35	-8	64	
2000	468	28	682	29	-1	1	
2001	682	29	702	19	10	100	
2002	565	30	717	34	-4	16	
2003	548	31	737	26	5	25	
2004	436	32	741	24	8	64	
2005	498	33	752	18	15	225	
2006	717	34	770	22	12	144	
2007	672	35	787	9	26	676	
2008	488	36	791	21	15	225	
2009	372	37	792	25	12	144	
2010	569	38	862	3	35	1225	
Mean	590				Sum Di^2	9538	
					Rsp	-0.04366	
					t	-0.2622	
					tcr	-2.02	2.02

Year	Wukro - observed annual rainfall data	**Kxi** - rank of the data as observed	Observed data ascending order	**Kyi** - rank of the same data in ascending order	Di = Kxi - Kyi	Di^2	
1973	272	1	263	12	-11	121	
1974	590	2	272	1	1	1	
1975	625	3	284	20	-17	289	
1976	1358	4	319	7	-3	9	
1977	789	5	358	25	-20	400	
1978	489	6	370	37	-31	961	
1979	319	7	471	31	-24	576	

1980	956	8	482	32	-24	576	
1981	739	9	486	13	-4	16	
1982	601	10	486	23	-13	169	
1983	807	11	489	6	5	25	
1984	263	12	496	33	-21	441	
1985	486	13	503	36	-23	529	
1986	628	14	543	27	-13	169	
1987	840	15	588	30	-15	225	
1988	1134	16	590	2	14	196	
1989	652	17	601	10	7	49	
1990	620	18	613	22	-4	16	
1991	654	19	620	18	1	1	
1992	284	20	625	3	17	289	
1993	719	21	628	14	7	49	
1994	613	22	652	17	5	25	
1995	486	23	654	19	4	16	
1996	928	24	674	34	-10	100	
1997	358	25	692	38	-13	169	
1998	927	26	719	21	5	25	
1999	543	27	739	9	18	324	
2000	812	28	758	35	-7	49	
2001	1112	29	789	5	24	576	
2002	588	30	807	11	19	361	
2003	471	31	812	28	3	9	
2004	482	32	840	15	17	289	
2005	496	33	927	26	7	49	
2006	674	34	928	24	10	100	
2007	758	35	956	8	27	729	
2008	503	36	1112	29	7	49	
2009	370	37	1134	16	21	441	
2010	692	38	1358	4	34	1156	
Mean	648				Sum Di^2	9574	
					Rsp	-0.0476	
					t	-0.28591	
					tcr	-2.02	2.02

Year	Edagahamus - observed annual rainfall data	**Kxi** - rank of the data as observed	Observed data ascending order	**Kyi** - rank of the same data in ascending order	Di = Kxi - Kyi	Di^2	
1973	505	1	401	25	-24	576	
1974	570	2	407	30	-28	784	
1975	769	3	431	38	-35	1225	
1976	546	4	434	37	-33	1089	
1977	731	5	444	7	-2	4	
1978	535	6	449	8	-2	4	
1979	444	7	454	36	-29	841	
1980	449	8	478	35	-27	729	
1981	606	9	498	31	-22	484	
1982	679	10	505	1	9	81	
1983	614	11	512	27	-16	256	
1984	590	12	526	32	-20	400	
1985	1203	13	535	6	7	49	
1986	2731	14	546	4	10	100	
1987	1913	15	570	2	13	169	
1988	1926	16	571	21	-5	25	
1989	723	17	586	34	-17	289	
1990	869	18	589	26	-8	64	
1991	776	19	590	12	7	49	
1992	734	20	606	9	11	121	
1993	571	21	614	11	10	100	
1994	722	22	616	28	-6	36	
1995	618	23	618	23	0	0	
1996	738	24	646	33	-9	81	
1997	401	25	679	10	15	225	
1998	589	26	722	22	4	16	
1999	512	27	723	17	10	100	
2000	616	28	731	5	23	529	
2001	819	29	734	20	9	81	
2002	407	30	738	24	6	36	
2003	498	31	769	3	28	784	
2004	526	32	776	19	13	169	
2005	646	33	819	29	4	16	
2006	586	34	869	18	16	256	
2007	478	35	1203	13	22	484	

2008	454	36	1913	15	21	441	
2009	434	37	1926	16	21	441	
2010	431	38	2731	14	24	576	
Mean	736				Sum Di^2	11710	
					Rsp	-0.28132	
					t	-1.75897	
					tcr	-2.02	2.02

Year	Mekelle - observed annual rainfall data	**Kxi** - rank of the data as observed	Observed data ascending order	**Kyi** - rank of the same data in ascending order	Di = Kxi - Kyi	Di^2	
1973	476	1	287	36	-35	1225	
1974	451	2	304	12	-10	100	
1975	771	3	374	7	-4	16	
1976	532	4	388	32	-28	784	
1977	670	5	417	37	-32	1024	
1978	439	6	439	6	0	0	
1979	374	7	451	2	5	25	
1980	911	8	456	28	-20	400	
1981	618	9	466	30	-21	441	
1982	589	10	476	1	9	81	
1983	706	11	527	20	-9	81	
1984	304	12	532	4	8	64	
1985	536	13	533	31	-18	324	
1986	590	14	536	13	1	1	
1987	739	15	551	25	-10	100	
1988	918	16	589	10	6	36	
1989	607	17	590	14	3	9	
1990	623	18	599	33	-15	225	
1991	632	19	607	17	2	4	
1992	527	20	618	24	-4	16	
1993	722	21	618	9	12	144	
1994	658	22	619	35	-13	169	
1995	692	23	623	18	5	25	
1996	618	24	623	29	-5	25	
1997	551	25	630	38	-13	169	
1998	749	26	632	19	7	49	

1999	717	27	658	22	5	25	
2000	456	28	670	5	23	529	
2001	623	29	692	23	6	36	
2002	466	30	706	11	19	361	
2003	533	31	717	27	4	16	
2004	388	32	722	21	11	121	
2005	599	33	739	15	18	324	
2006	755	34	749	26	8	64	
2007	619	35	755	34	1	1	
2008	287	36	771	3	33	1089	
2009	417	37	911	8	29	841	
2010	630	38	918	16	22	484	
Mean	592				Sum Di^2	9428	
					Rsp	-0.03162	
					t	-0.18983	
					tcr	-2.02	2.02

Year	Hawzen - observed annual rainfall data	**Kxi** - rank of the data as observed	Observed data ascending order	**Kyi** - rank of the same data in ascending order	Di = Kxi - Kyi	Di^2	
1973	602.4	1	320.3	12	-11	121	
1974	360.0	2	340.5	36	-34	1156	
1975	706.5	3	360.0	2	1	1	
1976	623.1	4	372.3	32	-28	784	
1977	656.0	5	390.3	31	-26	676	
1978	451.3	6	412.3	7	-1	1	
1979	412.3	7	428.1	20	-13	169	
1980	502.1	8	440.3	37	-29	841	
1981	666.4	9	448.0	33	-24	576	
1982	525.5	10	451.3	6	4	16	
1983	637.1	11	468.7	13	-2	4	
1984	320.3	12	470.6	30	-18	324	
1985	468.7	13	488.6	25	-12	144	
1986	535.9	14	502.0	23	-9	81	
1987	655.8	15	502.1	8	7	49	
1988	796.5	16	512.5	24	-8	64	
1989	548.8	17	517.9	22	-5	25	

1990	609.7	18	523.1	35	-17	289	
1991	592.6	19	525.5	10	9	81	
1992	428.1	20	535.9	14	6	36	
1993	546.1	21	546.1	21	0	0	
1994	517.9	22	548.8	17	5	25	
1995	502.0	23	568.0	38	-15	225	
1996	512.5	24	580.7	27	-3	9	
1997	488.6	25	592.6	19	6	36	
1998	607.5	26	602.4	1	25	625	
1999	580.7	27	607.5	26	1	1	
2000	763.4	28	609.7	18	10	100	
2001	890.8	29	623.1	4	25	625	
2002	470.6	30	637.1	11	19	361	
2003	390.3	31	655.8	15	16	256	
2004	372.3	32	656.0	5	27	729	
2005	448.0	33	666.4	9	24	576	
2006	750.5	34	706.5	3	31	961	
2007	523.1	35	750.5	34	1	1	
2008	340.5	36	763.4	28	8	64	
2009	440.3	37	796.5	16	21	441	
2010	568.0	38	890.8	29	9	81	
Mean	547.7				Sum Di^2	10554	
					Rsp	-0.15483	
					t	-0.94033	
					tcr	-2.02	2.02

Appendix B: Soil laboratory results

A. Wet sieve analysis example

Sample code	SUL 001							
Sieve size, D (mm)	Sieve No.	Weight of Sieve (g)	Weight of sieve + soil retained	Weight of soil Retained (g)	Cumulative mass of soil retained (g)	% Retained	Cumulative % retained	% finer
4.75	4	451.7	581.2	129.5	129.5	25.9	25.9	74.1
2.00	10	529.6	560.7	31.1	160.6	6.2	32.1	67.9
0.425	40	468.2	514.1	45.9	206.5	9.2	41.3	58.7
0.075	200	416.8	516.9	100.1	306.6	20.0	61.3	38.7
Pan	--	423.8						
Total weight of sample (g)				500				
			finer	193.4				
			%finer	38.68				

B. Dry sieve analysis example

Sample code						
SUL 013						
Sieve size (mm)	Weight of sieve	wt of sieve + retained soil	Mass retained (gm)	Percent retained (%)	Cumulative % retained	Percentage finer (%)
37.50	1705.96	1705.96	0.00	0.00	0.00	100.00
28.00	1727.22	1727.22	0.00	0.00	0.00	100.00
20.00	1617.33	1617.33	0.00	0.00	0.00	100.00
14.00	1356.9	1356.9	0.00	0.00	0.00	100.00
10.00	1324.81	1324.81	0.00	0.00	0.00	100.00
5.00	1372.25	1383.27	11.02	1.10	1.10	98.90
2.36	1245.13	1258.96	13.83	1.38	2.48	97.52
1.18	491.63	537.44	45.81	4.58	7.07	92.93
0.60	492.08	804.29	312.21	31.22	38.29	61.71
0.30	279.03	650.7	371.67	37.17	75.45	24.55
0.15	442.88	637.36	194.48	19.45	94.90	5.10
0.075	414.57	451.44	36.87	3.69	98.59	1.41
pan	314.57	328.14	13.57	1.36	99.95	0.05
			1000.00			

C. Hydrometer analysis (sedimentation method) example

Oven dry mass of soil (g)	**50**
Volume of suspension (cc)	**1000**
Specific gravity of soil	**2.5**
Specific gravity of water	**1**
unit wt of water (g/cc)	**1**

Sample code
SUL 032

Sr. No.	Time of reading	Elapsed time (t) minute	Actual hydrometer reading	T (^{o}c)	Composite correction	Corrected hydrometer reading	Effective depth (mm) from table	L/t	√(L/t)	K, from table	Particle diameter D (mm)	% Finer
1	3:05	0										
2	3:07	2	1.025	22	0.0017	1.0233	9.7	4.85	2.20227155	0.01286	0.028321212	77.66667
3	3:39	4	1.023	22	0.0017	1.0213	10.5	2.625	1.62018517	0.01286	0.020835581	71
4	3:11	6	1.022	22	0.0017	1.0203	10.85	1.80833	1.34474285	0.01286	0.017293393	67.66667
5	3:13	8	1.021	22	0.0017	1.0193	11	1.375	1.17260394	0.01286	0.015079687	64.33333
6	3:15	10	1.02	22	0.0017	1.0183	11.3	1.13	1.06301458	0.01286	0.013670368	61
7	3:25	20	1.019	22	0.0017	1.0173	12.3	0.615	0.78421936	0.01286	0.010085061	57.66667
8	3:35	30	1.017	22	0.0017	1.016	14.2	0.47333	0.68799225	0.01286	0.00884758	53.33333
9	4:05	60	1.016	22	0	1.0153	16	0.26667	0.51639778	0.01286	0.006640875	51
10	5:05	120	1.012	22	0	1.012	16.15	0.13458	0.36685601	0.01272	0.004666408	40
11	7:05	240	1.011	22	0	1.011	16.15	0.06729	0.25940637	0.01272	0.003299649	36.66667
12	11:05	480	1.009	22	0	1.009	16.15	0.03365	0.18342801	0.01286	0.002358884	30
13	3:05	1440	1.007	21	0	1.007	16.15	0.01122	0.10590221	0.01301	0.001377788	23.33333

D. Soil texture for the Suluh basin based on USDA classification

Soil sample code	Geographical coordinate (UTM)			Percent distribution			Soil texture	Specific gravity
	East	North	Elevation (m)	Sand	Clay	Silt		
SUL 001	545060	1574719	3089	47.82	16.96	35.23	Loam	2.69
SUL 002	540000	1570000	2833	16.72	15.42	67.86	Silt loam	2.74
SUL 003	544872	1569964	2860	54.12	14.44	31.44	Sandy loam	2.81
SUL 004	550000	1570000	2778	46.87	18.93	34.20	Loam	2.71
SUL 005	555000	1570963	2549	73.71	11.47	14.83	Sandy Loam	2.71
SUL 006	545000	1565759	2621	36.53	30.22	33.25	Clay Loam	2.66
SUL 007	550000	1565000	2411	22.84	41.57	35.59	Clay	2.60
SUL 008	556041	1565000	2506	96.18	1.92	1.90	Sand	2.58
SUL 009	560000	1565000	2604	57.20	22.41	20.39	Sand Clay Loam	2.69
SUL 010	565000	1565000	2788	76.75	9.42	13.83	Sandy Loam	2.60
SUL 011	550000	1560000	2353	66.65	13.83	19.52	Sandy Loam	2.71
SUL 012	555000	1560000	2390	19.38	35.95	44.67	Silt Clay Loam	2.66
SUL 013	560000	1560000	2507	98.62	0.63	0.74	Sand	2.66
SUL 014	550000	1555000	2318	99.73	0.09	0.18	Sand	2.63
SUL 015	555000	1555000	2354	88.90	5.88	5.22	Sand	2.71
SUL 016	560000	1555000	2369	68.16	16.00	15.84	Sandy Loam	2.50
SUL 017	565000	1555000	2651	98.85	0.50	0.65	Sand	2.58
SUL 018	550000	1550000	2265	62.51	18.90	18.58	Sandy Loam	2.45
SUL 019	555000	1550000	2291	32.44	47.98	19.58	Clay	2.43
SUL 020	560000	1550000	2343	97.94	0.85	1.21	Sand	2.63
SUL 021	550000	1536000	2339	68.92	8.00	23.08	Sandy Loam	2.60
SUL 022	565000	1550000	2456	26.88	25.08	48.04	Loam	2.43
SUL 023	550000	1545000	2292	29.35	44.73	25.92	Clay	2.36
SUL 024	555000	1545000	2296	80.99	6.77	12.24	Loamy Sand	2.60
SUL 025	560000	1545000	2341	6.08	46.30	47.62	Silty Clay	2.40
SUL 026	565000	1545000	2511	92.34	3.53	4.13	Sand	2.66
SUL 027	555000	1540000	2087	71.26	9.39	19.36	Sandy Loam	2.71
SUL 028	560000	1540000	2287	33.51	15.29	51.20	Silty Loam	2.74
SUL 029	565000	1540000	2462	48.70	13.21	38.09	Loam	2.60
SUL 030	551500	1532500	2080	19.33	44.09	36.59	Clay	2.71
SUL 031	555222	153300	2006	95.43	2.62	1.94	Sand	2.58
SUL 032	560000	1535000	2287	47.23	19.03	33.75	Loam	2.50

E. Soil Texture for Suluh basin based on USDA classification (Continued)

Soil sample code	Geographical coordinate (UTM)			Percent distribution			Soil texture	Specific gravity
	East	North	Elevation (m)	Sand	Clay	Silt		
SUL 033	550000	1531134	2125	55.26	19.32	25.42	Sandy Loam	2.55
SUL 034	555000	1530000	1971	56.21	19.91	23.88	Sandy Loam	2.63
SUL 035	560000	1530000	2328	25.56	62.58	11.86	Clay	2.60
SUL 036	545000	1525000	2155	7.97	40.53	51.50	Silty Clay	2.60
SUL 037	550000	1525000	2094	14.97	43.21	41.82	Silty Clay	2.97
SUL 038	555307	1531520	1975	59.46	10.90	29.64	Sandy Loam	2.74
SUL 039	555000	1525000	1964	28.07	46.29	25.64	Clay	2.60
SUL 040	560000	1525000	2112	29.60	33.03	37.37	Clay Loam	2.58
SUL 041	540000	1520000	2263	2.37	56.30	41.33	Silty Clay	2.58
SUL 042	545000	1520000	2118	2.81	49.73	47.46	Silty Clay	2.71
SUL 043	550000	1520000	2012	14.51	59.65	25.85	Clay	2.52
SUL 044	555000	1520000	1929	18.54	53.19	28.28	Clay	2.50
SUL 045	535475	1515087	2280	30.25	43.78	25.97	Clay	2.74
SUL 046	540000	1515000	2076	73.74	8.62	17.64	Sandy Loam	2.71
SUL 047	545000	1515000	1942	71.74	10.62	17.64	Sandy Loam	2.71
SUL 048	550000	1515000	2065	18.78	44.28	36.94	Clay	2.55
SUL 049	555000	1515000	2246				Rock outcrop	
SUL 050	540583	1509726	2189	74.94	11.78	13.28	Sandy Loam	2.66

Appendix C: Morphometric parameters

A. Sub-basin parameters for the gauged Suluh basin

OBJECT ID	GRID CODE	Shape length km	Shape area km^2	Hydro ID	Drain ID	Sub-basin name	Basin slope (%)	Basin lag	Area HMS km^2
2	2	37.98	35.36	22	22	W220	29.8	2.47	35.36
3	3	43.74	39.45	23	23	W230	10.5	2.23	39.45
5	5	58.56	54.90	25	25	W250	26.9	4.24	54.90
8	8	51.78	68.69	28	28	W280	32.8	2.76	68.69
9	9	37.80	25.26	29	29	W290	14.0	1.98	25.26
10	10	35.82	25.66	30	30	W300	8.1	2.34	25.66
11	11	32.94	20.78	31	31	W310	11.1	2.12	20.78
12	12	35.82	20.60	32	32	W320	9.8	2.07	20.60
13	13	34.62	12.68	33	33	W330	7.3	2.11	12.68
15	15	19.62	7.53	35	35	W350	8.0	1.28	7.53
17	17	55.62	39.03	37	37	W370	8.2	3.15	39.03
18	18	14.34	4.40	38	38	W380	9.3	1.04	4.40
19	19	18.48	4.21	39	39	W390	6.8	1.30	4.21

B. Suluh river parameters for the gauged Suluh basin

ARC ID	GRID CODE	FROM NODE	TO NODE	Hydro ID	Next down ID	Drain ID	Slope (%)	ElevUP HMS (m)	ElevDS HMS (m)	RivLen HMS (m)
1	1	1	2	2	5	28	0.02	2584	2399	8.69
4	7	2	3	5	6	28	0.01	2399	2392	0.51
5	8	3	4	6	10	28	0.01	2392	2355	3.12
6	5	5	4	7	10	25	0.02	2661	2355	18.80
7	2	6	7	8	12	22	0.01	2528	2417	8.62
8	3	8	7	9	12	23	0.02	2588	2417	7.56
9	9	4	9	10	16	29	0.01	2355	2314	6.61
10	11	10	9	11	16	31	0.01	2360	2314	3.76
11	10	7	11	12	17	30	0.01	2417	2318	10.58
12	13	12	11	13	17	33	0.01	2363	2318	3.59
13	14	13	14	14	19	37	0.01	2359	2348	1.47
15	12	9	15	16	18	32	0.01	2314	2261	5.74
16	15	11	15	17	18	35	0.02	2318	2261	3.57
17	18	15	16	18	20	38	0.01	2261	2248	2.53
18	16	14	16	19	20	37	0.01	2348	2248	10.44
19	19	16	17	20	-1	39	0.00	2248	2248	1.67

C. Tsenkanet Test site morphometric parameters

Morphometric parameters	Formula	Reference	Result
Area (km^2)			15.4
Perimeter (km)			19
Basin order	Hierarchical order	Strahler, 1964	4
Basin length (Lb) (km)			7.23
Bifurcation ratio (Rb)	Rb = Nu/ Nu+1; where: Nu = total number of stream segment of order's', Nu+1 = number of segment of next higher order	Schumm, 1956	2.6
Drainage density(Dd) (km/ km^2)	Dd = L/A; where: L = total length of streams, A = area of watershed	Horton, 1945	2
Stream frequency (Fs) (km^{-2})	Fs = N/A; where: N = total number of streams, A = area of watershed	Horton, 1945	3.77
Texture ratio (T) (km^{-1})	T = N1/P; where: N1 = total number of first order streams, P = perimeter of watershed	Horton, 1945	1.53
Form factor (Rf)	Rf = A/(Lb)2; where: A = area of watershed, Lb = basin length	Horton, 1932	0.30
Circulatory ratio (Rc)	Rc = 4πA/P2; where: A = area of watershed, π = 3.14, P = perimeter of watershed	Strahler, 1964	0.54
Elongation ratio (Re)	Re = 2√(A/π)/Lb; where: A = area of watershed, π = 3.14, Lb = basin length	Schumm, 1956	0.61
Relif ratio (%)	RLR = HD/HL, height difference between the outlet and the highest point in the catchment (HD, m) and Horizontal length between the outlet and the remotest point in the catchment divide (HL, m)		3

D. Bati'akor Test site morphometric parameters

Morphometric parameters	Formula	Reference	Result
Area (km^2)			12.2
Perimeter (km)			23.46
Basin order	Hierarchical order	Strahler, 1964	4
Basin length (Lb) (km)			4.4
Bifurcation ratio (Rb)	Rb = Nu/ Nu+1; where: Nu = total number of stream segment of order's', Nu+1 = number of segment of next higher order	Schumm,1956	4.2
Drainage density (Dd) (km/ km^2)	Dd = L/A; where: L=otal length of streams, A = area of watershed	Horton, 1945	2.4
Stream frequency (Fs) (km^{-2})	Fs = N/A where, N = total nu mber of streams, A = area of watershed	Horton, 1945	4.18
Texture ratio (T) (km^{-1})	T = N1/P; where: N1 = total number of first order streams, P = perimeter of watershed	Horton, 1945	1.19
Form factor (Rf)	Rf = A/(Lb)2; where: A = Area of watershed, Lb = basin length	Horton, 1932	0.63
Circulatory ratio (Rc)	Rc = 4πA/P2; where: A = area of watershed, π = 3.14, P = perimeter of watershed	Strahler, 1964	0.28
Elongation ratio (Re)	Re = 2√(A/π)/Lb; where: A = area of watershed, π = 3.14, Lb = basin length	Schumm,1956	0.90

Relif ratio (%)	RLR = HD/HL, height difference between the outlet and the highest point in the catchment (HD, m) and Horizontal length between the outlet and the remotest point in the catchment divide (HL, m)		3.3

E. Abraha-we-Atsbeha Test site morphometric parameters

Morphometric parameters	Formula	Reference	Result
Area (km^2)			5.4
Perimeter (km)			12.8
Stream order	Hierarchical order	Strahler, 1964	3
Basin length(Lb) (km)			4.3
Bifurcation ratio (Rb)	Rb = Nu/ Nu+1; where: Nu = total number of stream segment of order's', Nu+1 = Number of segment of next higher order	Schumm,1956	3.12
Drainage density (Dd) (km/ km^2)	Dd = L/A; where: L = total length of streams, A = area of watershed	Horton, 1945	3
Stream frequency (Fs) (km^{-2})	Fs = N/A; where: N = total nu mber of streams, A = area of watershed	Horton, 1945	7.22
Texture ratio (T) (km^{-1})	T = N1/P; where: N1 = total number of first order streams, P = perimeter of watershed	Horton, 1945	1.72
Form factor (Rf)	Rf = A/(Lb)2; where: A = area of watershed, Lb = basin length	Horton, 1932	0.29
Circulatory ratio (Rc)	Rc = 4πA/P2; where: A = area of watershed ,π = 3.14, P = perimeter of watershed	Strahler, 1964	0.41
Elongation ratio (Re)	Re = 2√(A/π)/Lb; where: A = area of watershed, π = 3.14, Lb = basin length	Schumm,1956	0.20
Relif ratio(%)	RLR = HD/HL, height difference between the outlet and the highest point in the catchment (HD, m) and Horizontal length between the outlet and the remotest point in the catchment divide (HL, m)		12

Appendix D: Details of Soil Moisture Accounting module

Storage	Minimum time step[1]
Canopy interception storage	$TimeStep = \frac{1}{4} * \frac{CunCanStore}{PotEvapTrans}$ Calculated only if evapotranspiration losses can occur and when the current canopy interception storage at the beginning of the time step exceeds the nominal storage volume.
Surface interception storage	$TimeStep = \frac{1}{4} * \frac{CunSurftore}{PotSoilInfl + PotEvapTrans}$ Calculated when potential evapotranspiration or infiltration losses > 0, and *CurSurfStore* > 0.
Soil profile storage	$TimeStep = \frac{1}{4} * \frac{CunSoilStore}{PotSoilIPerc + PotEvapTrans}$ Calculated when percolation or evapotranspiration can occur from the soil profile and *CurSoilStore* > 0.0001 inches.
Groundwater storage	$TimeStep = \frac{1}{4} * \frac{CunGwl1Store}{PotGwl1Perc}$ Calculated when percolation (loss) can occur from a groundwater layer, and the current volume in a groundwater layer > 0 $TimeStep = \frac{1}{16} * RoutGwlStore$ Calculated when the groundwater storage volume divided by the linear reservoir routing coefficient > 0.
Precipitation intensity	$TimeStep = \frac{1}{4} * \frac{MaxCanStore + MaxSurfStore + MaxSoilStore}{\Pr ecipTimeStep}$ Calculated when *PrecipTimeStep* > 0.

[1] *TimeStep* = time step for storage; *CurCanStore* = current canopy interception storage; *CurSurfStore* = current surface interception storage; *CurSoilStore* = current soil profile storage; *MaxCanStore* = maximum canopy interception storage; *MaxSurfStore* = maximum surface interception storage; *MaxSoilStore* = maximum soil profile storage; *CurGw1Store* = current groundwater storage; *PotEvapTrans* = potential ET; *PotSoilInf* = potential infiltration; *PotSoilPerc* = potential

percolation from soil profile; *PotGw1Perc* = potential percolation from groundwater layer; *RoutGw1Store* = coefficient for groundwater linear reservoir model; *PrecipTimeStep* = time step for specification of precipitation data

Appendix E: HEC-HMS objective functions formulae

Objective function	Equation[1]
Sum of absolute error (Stephenson, 1979)	$Z = \sum_{i=1}^{NQ} \left| q_o(i) - q_s(i) \right|$
Sum of squared residuals (Diskin and Simon, 1977)	$Z = \sum_{i=1}^{NQ} \left[q_o(i) - q_s(i) \right]^2$
Percent error in peak	$Z = 100 \left| \frac{q_s(peak) - q_o(peak)}{q_o(peak)} \right|$
Peak-weighted root mean square error objective function (USACE, 1998)	$Z = \left\{ \left[\sum_{i=1}^{NQ} \left[q_o(i) - q_s(i) \right]^2 \left(\frac{q_o(i) + q_o(mean)}{2 q_o(mean)} \right) \right] \right\}^{1/2}$

[1] Z = objective function; NQ = number of computed hydrograph ordinates; $q_O(t)$ = observed flows; $q_S(t)$ = calculated flows, computed with a selected set of model parameters; $q_O(peak)$ = observed peak; $q_O(mean)$ = mean of observed flows; and $q_S(peak)$ = calculated peak

Appendix F: Student t-distribution tables

- Student t-distribution

Percentile points of Student t-distribution for a 5% level of significance

$p = P(t \leq t_p)$:	0.025	0.975
v		
4	-2.78	2.78
5	-2.57	2.57
6	-2.54	2.54
7	-2.36	2.36
8	-2.31	2.31
9	-2.26	2.26
10	-2.23	2.23
11	-2.20	2.20
12	-2.18	2.18
14	-2.14	2.14
16	-2.12	2.12
18	-2.10	2.10
20	-2.09	2.09
24	-2.06	2.06
30	-2.04	2.04
40	-2.02	2.02
60	-2.00	2.00
100	-1.98	1.98
160	-1.97	1.97
	-1.96	1.96

Remark: Take the next higher value for *v* if the required number of degrees of freedom is not listed.

ERKLÄRUNG

Hiermit erkläre ich, dass ich die Dissertation ‘Modeling the Effect of Climate and Land Use Change on the Water Resources in Northern Ethiopia: the Case of the Suluh River Basin’ selbständig angefertigt und keine anderen als die von mir angegebenen Quellen und Hilfsmittel verwendet habe.

Ich erkläre weiterhin, dass die Dissertation bisher nicht in dieser oder anderer Form in einem anderen Prüfungsverfahren vorgelegen hat.

Berlin, 28. Oktober 2013 _____

(Bizuneh Asfaw Abebe)